


November 2019

## Fabrication and Characterization of Electrical Energy Storage and Harvesting Energy Devices Using Gel Electrolytes

Belqasem Aljafari  
*University of South Florida*

Follow this and additional works at: <https://scholarcommons.usf.edu/etd>

 Part of the [Electrical and Computer Engineering Commons](#), [Materials Science and Engineering Commons](#), and the [Oil, Gas, and Energy Commons](#)

---

### Scholar Commons Citation

Aljafari, Belqasem, "Fabrication and Characterization of Electrical Energy Storage and Harvesting Energy Devices Using Gel Electrolytes" (2019). *Graduate Theses and Dissertations*.  
<https://scholarcommons.usf.edu/etd/8615>

This Dissertation is brought to you for free and open access by the Graduate School at Scholar Commons. It has been accepted for inclusion in Graduate Theses and Dissertations by an authorized administrator of Scholar Commons. For more information, please contact [scholarcommons@usf.edu](mailto:scholarcommons@usf.edu).

Fabrication and Characterization of Electrical Energy Storage and Harvesting  
Energy Devices Using Gel Electrolytes

by

Belqasem Aljafari

A dissertation submitted in partial fulfillment  
of the requirements for the degree of  
Doctor of Philosophy  
Department of Electrical Engineering  
College of Engineering  
University of South Florida

Major Professor: Arash Takshi, Ph.D.  
Manoj Ram, Ph.D.  
Elias Stefanakos, Ph.D.  
Sylvia Thomas, Ph.D.  
Ryan Toomey, Ph.D.  
Humberto Gutierrez, Ph.D.

Date of Approval:  
October 30, 2019

Keywords: Supercapacitor, Polyvinyl Alcohol, Dye Sensitized Solar Cell,  
Conducting Polymers, Hybrid Device

Copyright © 2019, Belqasem Aljafari

## **Dedication**

To my parents, wife, brothers, and sisters for their absolute love, support, and motivation.

## **Acknowledgments**

Primarily, I would like to express my sincere gratitude to my advisor Dr. Arash Takshi, for believing in me and giving me this opportunity to pursue my Ph.D. degree. I am thankful to Dr. Takshi for his invaluable support, professional guidance, and constant encouragement for all these years, and for his ever-ready attitude to render help. I am very honored to be one of his graduate students.

Also, I am thankful to the Ph.D. committee members Dr. Manoj Ram, Dr. Lee Stefanakos, Dr. Sylvia Thomas, Dr. Ryan Toomey, and Dr. Humberto Gutierrez for reading this dissertation and their valuable suggestions. A special appreciate and thank goes to Dr. Ram for his precious support, motivation, and help through my research.

From the bottom of my heart, I would like to express my deepest gratitude to my parents, brothers, sisters, and my entire family for their precious time and everlasting support to help me in completing this dissertation. I would like to thank whole-heartedly my beloved wife, HANEEN, for her support and patient. She has listened to, reflected on, and supported me in every possible way for the past three years. This dissertation would not have been possible to accomplish without her.

At last but not least, I would like to thank the almighty God for every beautiful moment happened in my life. It would be impossible for me to have completed any educational success without the help of God. I would like to thank God for conferring this blessed opportunity on me to pursue my Ph.D. degree.

## Table of Contents

List of Tables .....	iv
List of Figures .....	v
Abstract .....	x
Chapter 1: Introduction .....	1
1.1 Motivation of the Work .....	3
1.2 Research Objectives.....	4
1.3 Scope of the Dissertation .....	5
Chapter 2: Background .....	7
2.1 Types of Electrical and Electrochemical Energy Storage Devices.....	7
2.1.1 Dielectric Capacitors.....	8
2.1.2 Electrochemical Capacitors .....	9
2.1.2.1 EDLCs.....	9
2.1.2.2 Pseudocapacitors.....	14
2.1.3 Batteries .....	19
2.2 Solar Energy Harvesting .....	21
2.2.1 Current State of Technology .....	21
2.2.2 Principle Work of Dye-Sensitized Solar Cell .....	24
2.2.3 Performance of Dye Sensitized Solar Cell.....	26
2.3 Electrolyte Materials.....	27
2.3.1 ECs Based Gel Electrolyte.....	29
2.3.2 Dye Sensitized Solar Cell Based on Gel Electrolyte .....	31
2.3.3 Integrated Solar Energy Harvesting and Storage Based on Gel Electrolyte .....	33
Chapter 3: Electrochemical Materials and Methods Used for Fabrication and Characterization of Devices .....	36
3.1 Materials .....	36
3.2 Methods.....	37
3.2.1 Preparation of Electrodes.....	37
3.2.1.1 Conducting Polymer Composites Chemical Deposition Method .....	38
3.2.1.2 Conducting Polymer Composites Electrochemical Deposition Method.....	40
3.2.2 Preparation of Electrolyte .....	41
3.2.3 Electrochemical Setup .....	43

3.3 Characterization .....	44
3.3.1 Cyclic Voltammetry .....	44
3.3.2 Galvanostatic (Chronopotentiometry) .....	47
3.3.3 Electrochemical Impedance Spectroscopy .....	48
3.3.4 Open Circuit Voltage .....	49
3.3.5 Short Circuit Current.....	50
3.3.6 Scanning Electron Microscopy .....	51
3.3.7 Raman Spectroscopy and Fourier Transform Infrared Spectroscopy.....	51
3.3.8 UV-visible Spectroscopy .....	52
3.2 Instruments.....	52
3.2.1 Potentiostat.....	52
3.2.2 Solar Simulator .....	53
3.2.3 Keithley.....	54
3.2.4 Dicing Saw.....	55
3.3 Conclusion .....	56
 Chapter 4: Gel Electrolyte Based Supercapacitors with Higher Capacitance and Lower Resistance than Devices with a Liquid Electrolyte.....	57
4.1 Abstract.....	57
4.2 Introduction.....	58
4.3 Experimental Details.....	59
4.4 Discussion .....	60
4.4.1 Cyclic Voltammetry .....	60
4.4.2 Charging-Discharging.....	61
4.4.3 Electrochemical Impedance Spectroscopy (EIS).....	64
4.4.4 Leakage Study.....	65
4.5 Conclusion .....	65
 Chapter 5: Polyvinyl Alcohol-Acid Redox Active Gel Electrolytes for Electrical Double Layer Capacitor Devices.....	66
5.1 Abstract.....	66
5.2 Introduction.....	67
5.3 Experimental Section .....	69
5.3.1 Materials .....	69
5.3.2 Preparation of Gel and Liquid Electrolytes .....	69
5.3.3 Device Fabrication and Characterization.....	69
5.4 Results.....	71
5.4.1 Electrode Characterization.....	71
5.4.2 Capacitance Study in Porous Electrodes with Liquid and Gel Electrolytes .....	72
5.4.3 Capacitive Behavior Study in Gels with Non-Porous Electrodes.....	74
5.4.4 Gel Based Supercapacitors .....	76
5.5 Discussion .....	81
5.6 Conclusion .....	83
 Chapter 6: Integrated Electrochemical Energy Storage and Photovoltaic Device with a Gel Electrolyte .....	85

6.1 Abstract .....	85
6.2 Introduction .....	86
6.3 Experimental Section .....	88
6.3.1 Materials and Instrumentation .....	88
6.3.2 Electrode Fabrication .....	89
6.3.3 Preparation of Electrolytes .....	90
6.4 Results and Discussion .....	91
6.5 Conclusion .....	95
Chapter 7: Photo-Electric Properties of Polypyrrole Based Gel Electrolyte for Hybrid Photoactive Supercapacitors .....	97
7.1 Abstract .....	97
7.2 Introduction .....	98
7.3 Experimental Section .....	100
7.3.1 Materials and Instrumentation .....	100
7.3.2 Electrode Fabrication .....	101
7.3.3 Preparation of Electrolytes .....	102
7.4 Result and Discussion .....	102
7.5 Conclusion .....	106
Chapter 8: A Polyaniline-Based Redox-Active Composite Gel Electrolyte with Photo- Electric and Electrochromic Properties .....	108
8.1 Abstract .....	108
8.2 Introduction .....	109
8.3 Experimental Section .....	110
8.3.1 Materials .....	110
8.3.2 Electrode Preparation .....	111
8.3.3 Composite Gel Preparation .....	111
8.3.4 Device Fabrication .....	112
8.3.5 Electrical and Electrochemical Measurements .....	112
8.4 Results and Discussion .....	113
8.5 Conclusion .....	128
Chapter 9: Conclusion and Suggestions for Future Work .....	130
9.1 Conclusion .....	130
9.2 Suggestions for Future Work .....	132
References .....	135
Appendix A: Copyright and Permissions .....	148
Appendix B: Supplementary Materials for Chapter 5 .....	156
Appendix C: Supplementary Information for Chapter 8 .....	164
About the Author .....	End Page

## List of Tables

Table 1: Relative Permittivity Values of Common Used Materials [16].....	9
Table 2: Comparison of Electrical and Electrochemical Energy Storage Appliances [44].....	20
Table 3: Comparison of All Three Generations of Solar Cell Technology.....	23
Table 4: Literature Review of ECs with PVA-Based Gel Electrolytes.....	30
Table 5: Literature Review of ECs with PVA-Based Gel Electrolytes with Additive Materials.....	31
Table 6: Literature Review of DSSCs Based Gel Electrolyte.....	33
Table 7: Capacitance and ESR Values of the Devices Based on Liquid and Gel Electrolyte at Different Acid Concentrations.....	63
Table 8: Examples of Reported Supercapacitors with Gel Electrolytes.....	68
Table 9: Parameters of the Equivalent Electric Circuit Model.....	78
Table 10: Capacitance of Integrated Devices Based on Different Nanocomposite Working Electrode and the Same CNT as Counter Electrode.....	92
Table 11: Small Signal Parameters of Equivalent Electric Circuit Model.....	103



## List of Figures

Figure 1: Number of Populations by 2040 [1].	1
Figure 2: Chart Diagram of Electricity Generation Sources by 2040 [3].	2
Figure 3: Basic Structure of Dielectric Capacitor.	8
Figure 4: Electrochemical Capacitors Based on Symmetric Porous Electrodes.	10
Figure 5: Three EDL Models on the Potential Distribution in the Electrolyte (a) Helmholtz Model in which $d$ is the Thickness of the Double Layer, (b) Gouy-Chapman Model, and (c) Stern Model which Represents Stern Layer that Includes Inner Helmholtz Layer (IHL) and Outer Helmholtz Layer (OHL) [22].	12
Figure 6: RC Equivalent Circuit Exemplification Clarifies the Basic Operation of a Single Cell Supercapacitor [17, 18].	13
Figure 7: Ragone Plot Illustrates a Comparison of Power Density and Energy Density of Different Energy Storage Devices [16].	15
Figure 8: Schematic Diagram of Different Redox Reactions Result a Pseudocapacitor (a) Under Potential Deposition (Adsorption Pseudocapacitance), (b) Redox Pseudocapacitor, (c) Intercalation Pseudocapacitance [33, 34].	17
Figure 9: Electron Charge Storage on Conducting Polymers (a) Under Potential Effect (Charging Process), (b) Discharge Process [38].	18
Figure 10: Redox Reaction of PANI During (a) Charging Process Representing by Green Color which is the Most Conductive State and (b) Discharging Process Representing by Blue Color which is the Less Conducting or Insulator.	19
Figure 11: Photovoltaics Solar Cell Technology with Three Different Generations of Technologies Based on the Essential Active Materials [49-51].	22
Figure 12: Principle Work and Energy Level Diagram of Dye Sensitized Solar Cell [55].	25
Figure 13: Current Density vs. Voltage (J vs. V) Characteristics of Dye Sensitized Solar Cell.	27
Figure 14: Three Different Categorizes of Electrolyte Materials [62].	28

Figure 15: Chemical Structure of PVA Material. ....	29
Figure 16: Redox State in a Conducting Polymer Material From Monomer to Oxidized State (Polymer) During Polymerization Process. ....	39
Figure 17: Chemical Deposition Process of PANI Film.....	40
Figure 18: Electrochemical Deposition Process of PANI Film (a) no Potential Effect and (b) Under Potential Effect. ....	41
Figure 19: Process of Making PANI Composite Gel Electrolyte. ....	42
Figure 20: Concentration-Distance Profile at Different Stages of Cyclic Voltammogram. ....	45
Figure 21: Cyclic Voltammogram Shape of Electrochemical Reaction. ....	47
Figure 22: Randle Circuit Model of Electrochemical Cell [114]. ....	49
Figure 23: VersaSTAT 4 Potentiostat Instrument. ....	53
Figure 24: Solar Simulator Instrument. ....	54
Figure 25: Keithley 2602A Device. ....	54
Figure 26: 4-Point Probe Instrument.....	55
Figure 27: Dicing Saw Machine. ....	55
Figure 28: Structural Form for PVA: (a) Fully Hydrolyzed; (b) Partially Hydrolyzed [125]and (c) Gel Polymer Electrolyte.....	59
Figure 29: Cyclic Voltammetry (CV) Results of Devices with (a) H <sub>2</sub> SO <sub>4</sub> Liquid, (b) H <sub>3</sub> PO <sub>4</sub> Liquid, (c) H <sub>2</sub> SO <sub>4</sub> Gel, and (d) H <sub>3</sub> PO <sub>4</sub> Gel Electrolytes with Different Concentrations of the Acids. ....	61
Figure 30: Charging and Discharging Results of Devices with (a) H <sub>2</sub> SO <sub>4</sub> Liquid, (b) H <sub>3</sub> PO <sub>4</sub> Liquid, (c) H <sub>2</sub> SO <sub>4</sub> Gel, and (d) H <sub>3</sub> PO <sub>4</sub> Gel Electrolytes with Different Concentrations of the Acids. ....	62
Figure 31: Nyquist Plots of the EIS Results From Devices with (a) H <sub>2</sub> SO <sub>4</sub> Liquid, (b) H <sub>3</sub> PO <sub>4</sub> Liquid, (c) H <sub>2</sub> SO <sub>4</sub> Gel, and (d) H <sub>3</sub> PO <sub>4</sub> Gel Electrolytes with Different Concentrations of the Acids. ....	63
Figure 32: Open Circuit Voltage After Charging Devices with (a) H <sub>2</sub> SO <sub>4</sub> Liquid, (b) H <sub>3</sub> PO <sub>4</sub> Liquid, (c) H <sub>2</sub> SO <sub>4</sub> Gel, and (d) H <sub>3</sub> PO <sub>4</sub> Gel Electrolytes with Different Concentrations of the Acids to 1.0V. ....	64
Figure 33: Schematic Diagram of the Electrical Double Layer Capacitor (a) EDLC Liquid-Based Electrolyte (b) EDLC Gel-Based Electrolyte.....	71

Figure 34: Characterization of the Electrode Material (MW-CNT) (a, b) SEM Micrograph of CNT/Paper (c) Raman Spectra of CNT Paper (d) FTIR Spectra of CNT/Paper.....	72
Figure 35: Cyclic Voltammetry of the Supercapacitors Based on (a) Sulfuric Acid as gel and Liquid Electrolytes and (b) Phosphoric Acid as Gel and Liquid Electrolytes. ....	74
Figure 36: Cyclic Voltammetry of the Glassy Carbon-Based Supercapacitors with One Layer and Five Layers of the Spacer Made From (a) H <sub>2</sub> SO <sub>4</sub> -PVA and (b) H <sub>3</sub> PO <sub>4</sub> -PVA Gels. ....	75
Figure 37: Galvanostatic Charge-Discharge of CNT-Based Supercapacitors with H <sub>2</sub> SO <sub>4</sub> -PVA and H <sub>3</sub> PO <sub>4</sub> -PVA Gel Electrolytes. ....	77
Figure 38: Nyquist Impedance of CNT-Based Supercapacitors with (a) H <sub>2</sub> SO <sub>4</sub> -PVA and (b) H <sub>3</sub> PO <sub>4</sub> -PVA Electrolytes. (Inset) Electrical Equivalent Circuit Model.....	78
Figure 39: (a) Normalized Capacitance of Devices with H <sub>2</sub> SO <sub>4</sub> -PVA and H <sub>3</sub> PO <sub>4</sub> -PVA Electrolytes to the Initial Capacitance of Each Device Before 1000 Cycles of Charging and Discharging and (b) Bending Test of Supercapacitor Based on H <sub>2</sub> SO <sub>4</sub> -PVA and H <sub>3</sub> PO <sub>4</sub> -PVA at Different Curvatures Flat-to-Bent and Bent-to-Flat. (Inset) a Picture of Bended Device. ....	80
Figure 40: Specific Capacitance of Devices with Acid-PVA Gel Electrolytes at Various Concentrations of the Acids.....	81
Figure 41: Schematic of the Proposed Mechanism of Charge Storage in the Acid-PVA Gel Electrolytes for (a) Sulfuric and (b) Phosphoric Anion-Based Gels.....	83
Figure 42: Schematic Diagram of DSSC and SC Based on HCl-PVA Gel Electrolyte. ....	88
Figure 43: UV-Vis Results for (a) FTO Substrate Coated with PANI, PANI+MB, PANI+MO, and PANI+PB and (b) Dies Solutions Only. ....	91
Figure 44: Cyclic Voltammetry (CV) Results of Devices with (a) PANI, (b) PANI+MB, (c) PANI+MO, and (d) PANI+PB Based on HCl-PVA Gel Electrolyte.....	93
Figure 45: Nyquist Impedance Results of Devices with (a) PANI, (b) PANI+MB, (c) PANI+MO, and (d) PANI+PB Based on HCl-PVA Gel Electrolyte.....	94
Figure 46: Open Circuit Voltage Results of Devices with (a) PANI+MB, (b) PANI+MO, and (dc PANI+PB Based on HCl-PVA Gel Electrolyte.....	94
Figure 47: Short Circuit Current Results of Devices with (a) PANI+MB, (b) PANI+MO, and (dc PANI+PB Based on HCl-PVA Gel Electrolyte.....	95

Figure 48: (a) Schematic Diagram of the Hybrid Device and (b) Electrical Circuit of Solar Cell with Supercapacitor. ....	100
Figure 49: (a) Cyclic Voltammetry, (b) Nyquist Impedance of the Hybrid Device Based Ppy+MB Under the Dark Conditions, and (c) (Inset) Electrical Equivalent Circuit Model. ....	102
Figure 50: UV-Visible Spectroscopy for Ppy Thin Film and Ppy Composite with MB.....	104
Figure 51: Open Circuit Voltage for a Device with Ppy Coated on Photoactive Electrode.....	105
Figure 52: (a) Open Circuit Voltage for a Device with Ppy+MB Coated on Photoactive Electrode and (b) Short Circuit Current of a Device Under Pulses of Solar Simulated Light.....	106
Figure 53: (a) UV-Vis Absorption Spectrum, (b) FTIR Spectrum, and (c) Raman Spectrum of the Composite Gel of PVA-HCl-APS-PANI, PVA, PVA-HC, and PVA-HCl-APS. (d) CV Result and (e) Nyquist Plot From the EIS Study of a Thin Composite Gel Layer Sandwiched Between Two Glassy Carbon Electrodes and (f) Equivalent Electrical Circuit Model of the Complex Impedance in the Gel. The Inset Figure in Plot (d) Shows the Transition of PANI From ES to LS Form. ....	117
Figure 54: (a) Schematic Diagram, (b) A Picture of the Fabricated Supercapacitor with CNT Based Porous Electrodes and a Thin Layer of the Composite Gel as the Electrolyte and Active Redox Material and (c) CV Results From Devices with Two Different Gels: PVA-HCl and PVA-HCl-APS-PANI.....	119
Figure 55: (a) Schematic Diagram, (b) A Picture of the Fabricated Solar Cell with the Composite Gel and (c) J-V Characteristics of the Solar Cell Device in Dark and Light. ....	121
Figure 56: (a) Schematic Diagram, (b) A Picture of the Hybrid Photoactive Supercapacitor for Energy Harvesting and Storage, (c) CV of the Hybrid Device, (d) Open Circuit Voltage and (e) Short Circuit Current Versus Time Under Light and Dark Pulses. ....	122
Figure 57: (a) Schematic Diagram, (b) Pictures of the Fabricated Electrochromic Device at Three Different Modes, (c) CV Result Showing the Redox Peaks, (d,e) Electric Current Through the Device in Response to the Applied Voltage Pulses and (f) Transmittance of the Device in Two Different Biasing Conditions.....	125
Figure 58: (a) 3 Steps of Fabricating the PANI Composite Gel: The Gelling Process of PVA in HCl and the Interactions with APS and PANI, (b) Chemical Reactions in Three Different Oxidation States of PANI, (c) Energy Level Diagram in the Solar Cell and the Hybrid Photoactive Supercapacitor for Energy Harvesting. The Energy Levels are Versus the Vacuum Level. To	

Explain the Process, the Interaction Between PANI and the Ionic Charges are Shown as Two Different Layers; However, that Interaction Occurs in the Bulk Gel Electrolyte and (d) Loss of Electron in Emeraldine and Conversion to Pernigraniline with Stored Energy in the Polymer..... 126

Figure 59: Hybrid Photoactive Supercapacitor Device Based on PVA+HCl Gel Electrolyte..... 132

Figure 60: Schematic Diagram of Photoactive Supercapacitor Based on PANI Composite Gel Electrolyte..... 133

## Abstract

Redox-active materials in the bulk of gel electrolytes are unquestionably holding the primary roles in developing energy harvesting and storage technology. Both technologies are necessary in order to cope with the current challenges of the environmental crises of global warming and finite non-renewable sources while the demand for energy modern societies have been speedily increased. One of the most challenges of making a hybrid device of energy conversion and storage is the cost of the fabrication process. Therefore, gel electrolyte-based materials with redox-active properties can potentially be a promising solution to improve the performance of electrochemical and photoelectrochemical devices for low-cost applications by using abundant and low-cost materials such as polyvinyl alcohol, polyaniline, and polypyrrole. The essential target of this dissertation was to make a gel electrolyte with redox-active properties that can be applied with an electrical double layer capacitor, photoactive supercapacitor, dye-sensitized solar cell, and electrochromic windows. Two different types of gel electrolyte based polyvinyl alcohol as host polymer have been examined with several electrochemical cells. The first type was polyvinyl alcohol mixed with acids in deionized water to form the gel electrolyte. The second type was a composite gel electrolyte of polyvinyl alcohol, acid, conducting polymer (i.e., polyaniline), and oxidized material (i.e., ammonium persulfate).

To address the issues and advantages of using these types of gel electrolytes, several approaches to making electrochemical and photoelectrochemical devices based on redox-active gel electrolytes have been addressed in this dissertation. The first approach was to examine a redox activity of polyvinyl alcohol with acids solutions by a comparison study of making electrical

double-layer capacitors based on liquid and gel electrolytes. The results showed the superiority of the electrical double layer capacitor-based gel electrolyte to the concurrent based liquid electrolyte due to the redox activity of the PVA and its capability of storing charges in addition to the effect of a double-layer capacitor.

The second approach was to make photoactive supercapacitor devices based on conducting polymer materials, synthetic dyes, and redox-active gel electrolyte. Harvesting energy is taking place at the anode electrode by electrochemically deposited a nanocomposite thin film of conducting polymer (i.e., Polyaniline or Polypyrrole)/Dyes. Energy storage occurs at both electrodes' anode and the cathode (i.e., CNT) in addition to the bulk gel electrolyte. Even though the results represented the photovoltaic and storage effect of the device, the results of the photovoltaic effect mainly were relatively weak and needed further improvement. From this point of view, the movement of ionic charges and electronic charges to reach the electrode/ electrolyte interface in the gel medium is slow, leading to affect the performance of the device.

The third approach presented in this dissertation was to develop the gel mentioned above by adding polyaniline, a conducting polymer, and ammonium persulfate, oxidizer material, to form PANI composite gel electrolyte. To test the validation of this composite gel electrolyte, different electrochemical and photoelectrochemical devices were fabricated, which are an electrical double later capacitor, a photoactive supercapacitor, a dye-sensitized solar cell, and an electrochromic window. The results showed improvement in terms of energy storage and photovoltaic effect due to the present of polyaniline and ammonium persulfate intercalated with polyvinyl alcohol. Not only that but also this composite gel was workable with electrochromic applications.

In the end, low cost, abundant, and non-toxic materials such as polyvinyl alcohol, polyaniline, and ammonium persulfate are promising due to their redox-active properties that can

substantially reinforce the total performance of electrochemical and photoelectrochemical devices.



## Chapter 1: Introduction

The rapid growth of industries, population, and economy in recent years has increased the utilization of nonrenewable sources, which lead to tremendous consuming of coal, oil, and gas, which are facilely attainable. Total energy demand from fossil fuels would increase by taking into consideration the significant growth of the population from 7.4 billion presently to be exceeded 9 billion by 2040, as shown in Figure 1 [1]. Not only that, but also the fuel economy of vehicles will increase by 60% during the period time from 2018-2050 [2].

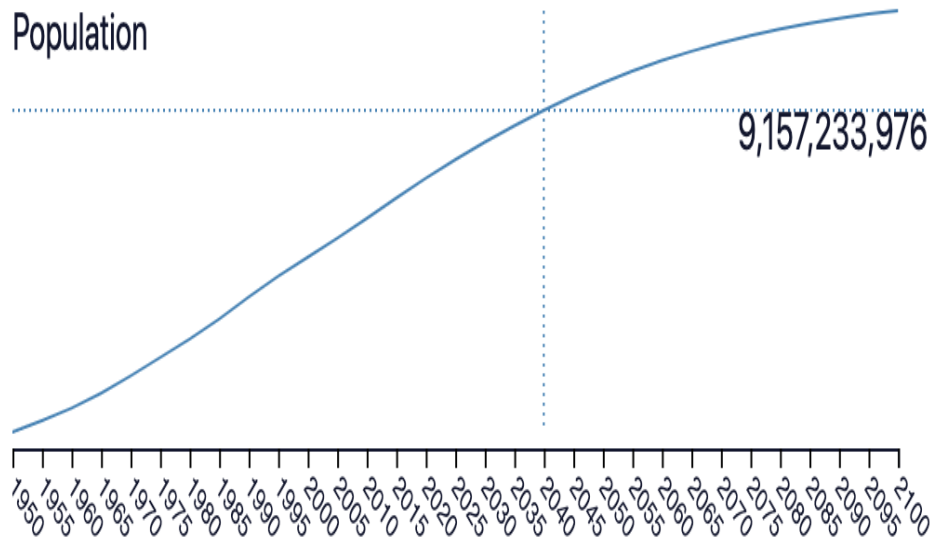


Figure 1: Number of Populations by 2040 [1].

Regarding the negative side effects of using fossil resources, developing clean and renewable energy sources have been widely studied by industry and scientific communities to overcome the issues of energy crisis. Renewable resources are one primary factor of world electricity generation sources that are expected to increase by 40% from 2019 to 2040 as shown in

Figure 2. However, naturally, the availability of renewable resources such as solar, wind, and tidal energies varies during a day and is different at different locations. Consequently, unsettled power generation from the renewable sources is taking place.

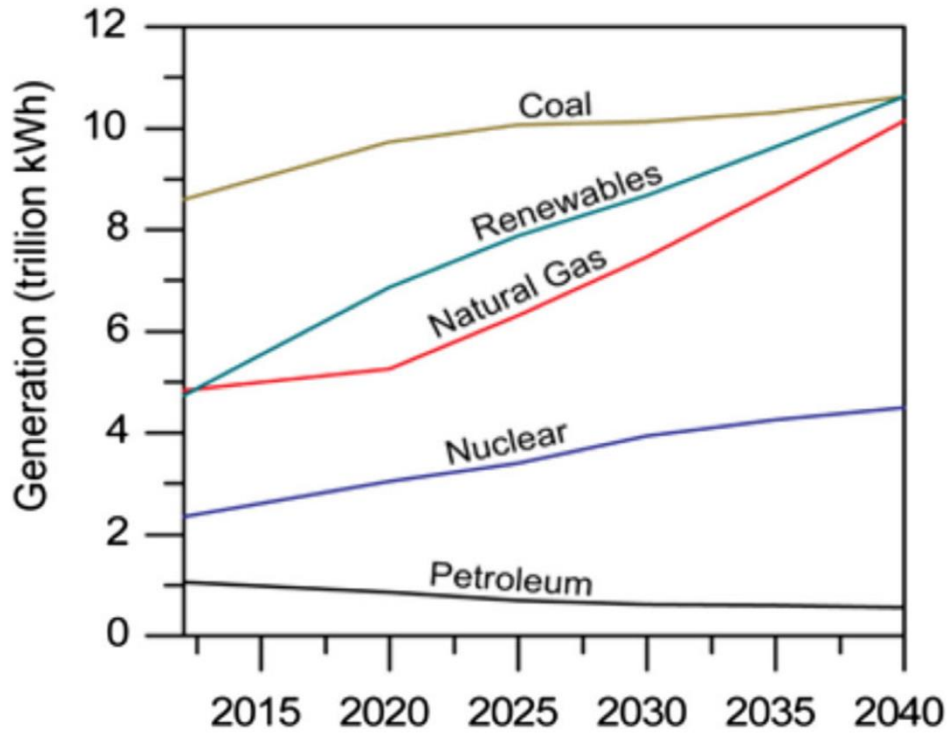


Figure 2: Chart Diagram of Electricity Generation Sources by 2040 [3].

From this point of view, electrochemical energy storage devices such as electrochemical capacitors and batteries are critical apparatuses to ensure the continuity and efficiency of power system generation, especially during the cycles of the high demand of energy from consumers [4]. Among them, electrochemical capacitors (ECs) are promising due to their fast charging cycle, long cycle lifetime, a wide range of operational temperatures (i.e., cold and hot environment), higher power density than batteries, and higher energy density than dielectric capacitors. Even though there are still some challenges in EC devices such as relatively low energy density and high cost of fabrication, in fact, they can narrow the gap between dielectric capacitors and batteries [5]. ECs

can be used in a variety of practical applications such as electric vehicles (EVs), electric buses, portable power supplies, energy backups, memories, smart grids, and renewable energy systems (e.g., storage for photovoltaic device) applications [6].

## 1.1 Motivation of the Work

The augmented demand for energy storage devices, specifically supercapacitors, has drawn attention from industries and universities to keep researching and developing EC technology. In that regard, a significant part of the research is focused on materials for fabricating more efficient ECs. Nowadays, ECs are utilized in many practical applications, including electronic devices, power tools, wireless sensors, and in the transportation industry [7]. Concerning the global market of ECs, the profit is anticipated to reach up to 6.3 billion dollars by 2022, and the compound annual growth rate (CAGR) is rising to 28.7% by 2022 [8, 9].

Despite the advantages of using supercapacitors in considerable practical applications, leakage current, which causes self-discharge [10] and mechanical stability [11], are the pressing issues that limit their implementation in some practical applications. Therefore, there is an ample scope of research to find new solutions and advancements for the drawbacks.

Additionally, integrating solar energy harvesting with electrochemical energy storage in a single device is a hot topic of research today. Traditionally, the power pack system is costly, dense, complicated, and extensive due to its structure that is mainly consisted of silicon solar cells and solid-state lithium-ion batteries. ECs are suitable alternatives to Li-ion batteries because of their long lifetime and fast response to a current change due to the intermittent and fluctuation of the incident light. Hence, crossbreeding both ECs and harvesting energy in one device is essential not only to capture, convert and store energy efficiently but also to fulfill the particular demands of

reducing the cost and size [12, 13]. Furthermore, packaging and sealing an electrochemical device are still the main issue that increases the cost of fabrication. Thus replacing the conventional liquid electrolyte by gel electrolyte is getting more attention from many research groups to enhance mechanical stability and safety, also to reduce the fabrication cost [14].

## 1.2 Research Objectives

Through this dissertation work, three objectives were followed. The first objective was to study energy storage in the gel electrolyte of ECs made of polyvinyl alcohol (PVA) incorporated with different acids such as sulfuric acid ( $H_2SO_4$ ), phosphoric acid ( $H_3PO_4$ ), and hydrochloric acid (HCl). Generally, such devices are easier to fabricate, have a lower cost, and have more limited electrolyte leakage problem compare to the conventional devices with liquid electrolytes.

The second objective was to fabricate and investigate a hybrid device with an integrated structure of a solar energy harvesting device such as a dye-sensitized solar cell (DSSC) and a supercapacitor device. The hybrid device was made by using a novel technique of electrochemically deposited conducting polymer materials (i.e. polyaniline, PANI and polypyrrole, Ppy) composite with synthetic dyes (i.e. methylene blue, MB, prussian blue, PB, and methyl orange, MO) that were synthesized by in-situ self-assembled method on the fluorine-doped tin oxide (FTO) conductive transparent glass with a gel electrolyte.

The third objective was to study and investigate a composite gel polymer electrolyte for various applications such as supercapacitors, photoactive supercapacitors, DSSC, and electrochromic windows.

The results presented in this dissertation are encouraging to implement gel electrolytes in various electrochemical devices. While gel type of electrolytes is preferred over the liquid

electrolytes because of their lower cost and improved safety in practical devices, our founding shows that the composite gel can also enhance the capacitance storage and provide a unique capability of concurrent solar energy harvesting and charge storage. Additionally, in this dissertation, the behavior of nanocomposite conducting polymer with dyes materials from an electrochemical point of view to evaluate their applicability as photoactive materials in an electrochemical cell has been studied, showing a promising approach for making the hybrid devices.

### **1.3 Scope of the Dissertation**

The focus of this research is on electrochemical energy storage and harvesting devices based on the gel electrolyte. The potential of this work is to apply the gel type of electrolyte with different types of electrochemical devices such as supercapacitors, photoactive supercapacitors, DSSCs, and electrochromic windows while observing the fabrication cost. The layout of the dissertation is as following.

A brief background of ECs (i.e., dielectric capacitors, electrical double-layer capacitors, EDLCs, pseudocapacitors, and batteries) and solar energy harvesting is explained in chapter 2. Also, a literature review of gel electrolyte materials based on EDLCs, photoactive supercapacitors, and DSSC are presented in chapter 2. Chapter 3 exhibits the instruments, electrochemical materials, and methods that were used to fabricate and test devices. Chapter 4 discusses the experimental results of comparing gel and liquid electrolyte based EDLCs devices. Using gel electrolyte as an active redox material with EDLCs devices was deeply studied and investigated in chapter 5. In chapter 6, reports on the application of a gel for making a hybrid device of supercapacitors and DSSC based nanocomposite thin film of PANI+dyes as photoactive materials.

Different type of conducting polymer materials (i.e., Ppy) was incorporated with MB dye to make a hybrid device that can harvest and store energy with applying gel electrolyte was accomplished in chapter 7. A new composite gel electrolyte was made and applied for different electrochemical devices is reported in chapter 8. Chapter 9 includes the conclusion and suggestions for future works.

## **Chapter 2: Background**

This chapter illustrates the principle work and mechanism of energy storage and harvesting devices briefly. Since a major part of the studies in this dissertation is on the hybrid devices of solar energy harvesting and storage, it is necessary to review the key electrochemical parameters of supercapacitors (i.e., EDLCs and pseudocapacitors) and dye-sensitized solar cells as the background for the presented research work. Hence, a brief overview of the basics of electrochemistry is addressed in this chapter. The performance of an integrated device is typically relying on the type of electrodes and electrolyte materials. A literature review of electrode and electrolyte materials is presented in this chapter. More specifically, previous works related to the usage of polyaniline and polypyrrole that were used to fabricate devices are reviewed. Besides, both EDLCs and hybrid devices were fabricated with applying a gel electrolyte with the host polymer polyvinyl alcohol (PVA), which is the focus electrolyte type on this dissertation.

### **2.1 Types of Electrical and Electrochemical Energy Storage Devices**

There are numerous fundamental differences between electrical and electrochemical energy storage devices (i.e., dielectric capacitors, electrochemical capacitors, pseudocapacitors, and batteries) when it comes to the principle work and mechanism of charges storage. These energy storage devices are the most commercially available energy storage devices for electronic and electrical applications.

### 2.1.1 Dielectric Capacitors

A dielectric capacitor is constructed of a layer of a dielectric material (i.e., ceramic, plastic, glass, and paper) that is used as an insulator between two electrically conductive electrodes. An electrostatic field is established in the dielectric medium to store energy when a potential difference is applied across the two electrodes, as shown in Figure 3. The electric field exists with the same number of charges on the two electrodes with different polarities. The flow of charges will stop completely when the capacitor's voltage matches the applied voltage. So, the capacitance ( $C$ ) of the capacitor can be measured in Farad (F) based on Gauss's law by calculating the number of charges that remain on the two terminals divided by the voltage across the dielectric [15].

$$C = \frac{Q}{V} \quad (1)$$

where  $Q$  is the total charges,  $V$  is the voltage across the dielectric medium.

Capacitance for typical parallel plate capacitor is:

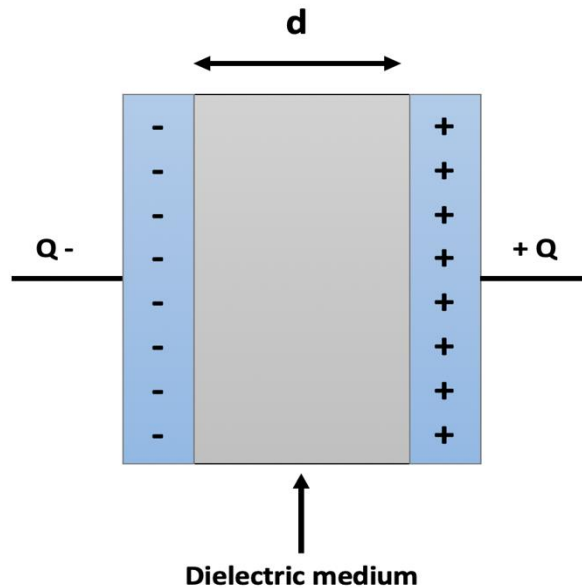


Figure 3: Basic Structure of Dielectric Capacitor.



Table 1: Relative Permittivity Values of Common Used Materials [16].

Dielectric materials	Dielectric constant
Vacuum	1
Helium	1.00065
Argon	1.00052
Air	1.00054
Paper	1.2-2.6
Polypropylene	2.2
Polyethylene	2.2-2.4
Polystyrene	2.5-2.7
Sulfur	2-4.2
Diamond	5.7
Salt	5.9
Aluminum Oxide	9.3-11.5
Silicon	11.8
Titanium Dioxide	16-100
Acetonitril	37.5
Water	80
Barium Titanate	> 10,000

### 2.1.2 Electrochemical Capacitors

In contrast to parallel plate capacitors, ECs or supercapacitors are mainly evaluated due to their capability of storing charges at the electrode-electrolyte interface. Two primary forms of ECs are electrical double-layer capacitors (EDLCs) and pseudocapacitors. Since the energy storage mechanism is different in EDLCs and pseudocapacitors, a short review of the charge storage mechanism and the species of electrode materials used for both devices are discussed in this section.

#### 2.1.2.1 EDLCs

In account of the charging process of EDLCs, the electrostatic separation of electronic and ionic charges takes place at the interface between electrolytes and electrodes, as seen in Figure 4.

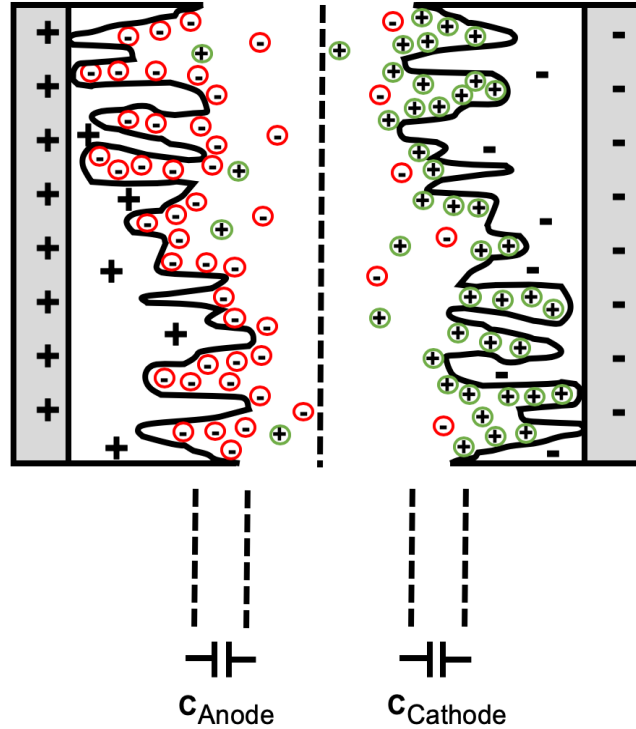


Figure 4: Electrochemical Capacitors Based on Symmetric Porous Electrodes.

After applying a potential across an EDLC, the migration process would immediately start due to the changes in the electrode's polarity. Thus, the positively charged cations (solvated ions) are accumulated near the negative electrode, whereas the negatively charged anions are stacked up at the positive electrode, actively mimicking two capacitors in series [17, 18]. So, each electrode can be addressed as a single capacitor of capacitance value that is proportional to the surface area of the electrode-electrolyte interface and the electrolyte permittivity  $\epsilon$  [19]. A feature that distinguishes EDLCs from pseudocapacitors is that no chemical reaction is taking place between the electrolyte and electrode in EDLCs.

Since  $C = \frac{q}{V}$ , the capacitance of an EDLC capacitor ( $C_d$ ) can be estimated by measuring the variation of voltage with respect to time ( $t$ ) when the device is charged/discharged at a constant current ( $I$ ):

$$C_{dl} = \frac{I}{\left(\frac{dV}{dt}\right)} \quad (2)$$

To explain the effect of charge arrangement at a double-layer structure on the potential distribution in the electrolyte, three models (i.e., Helmholtz, Gouy-Chapman, and Stern) are suggested. Here is a short review of the models. It is worth mentioning that the steady-state potential in all three models can be described by Poisson's equation [20]:

$$\frac{\partial^2 \varphi(x)}{\partial x^2} = -\frac{\rho(x)}{\varepsilon_r \varepsilon_0} \quad (3)$$

where  $x$  is the distance from the electrode,  $\varphi(x)$  is the electric potential as a function of  $x$ ,  $\rho$  is the charge density,  $\varepsilon_0$  is the permittivity of vacuum, and  $\varepsilon_r$  is the relative permittivity of the electrolyte.

EDL theory was the first time revealed in 1853 by the Helmholtz to explain the mechanism of charge storage in EDLCs. He proposed that the electrostatic interaction between electrons and ions with opposite charges across the electrode-electrolyte interface forms a double layer structure similar to parallel plate capacitors with a thickness of an atomic distance between the two layers (Figure 5 (a)) [7]. This model was ineffective to take into account any further interactions that would happen beyond the condensed layer that adsorbed species [21]. Accordingly, the Helmholtz model was improved simultaneously by Gouy-Chapman. Their model is mainly focused on the diffusion process through the electrolyte solution based on the natural thermal motion of ions. The distance ( $d$ ) or (Debye length  $<1\text{nm}$ ) of the diffuse layer between the electrode surface and accumulation charges near to the surface inversely affects the potential near to the surface electrode, as shown in Figure 5 (b). Meaning that, when the distance increases, the potential decreases [22]. It is worth considering that, unlike the Helmholtz model, in the Gouy-Chapman model, there is no compact layer of ions, and it is assumed that the ions (modeled as point charges)

are being free to move. However, this theory resulted in an excessively high estimation of EDL capacitance [23].

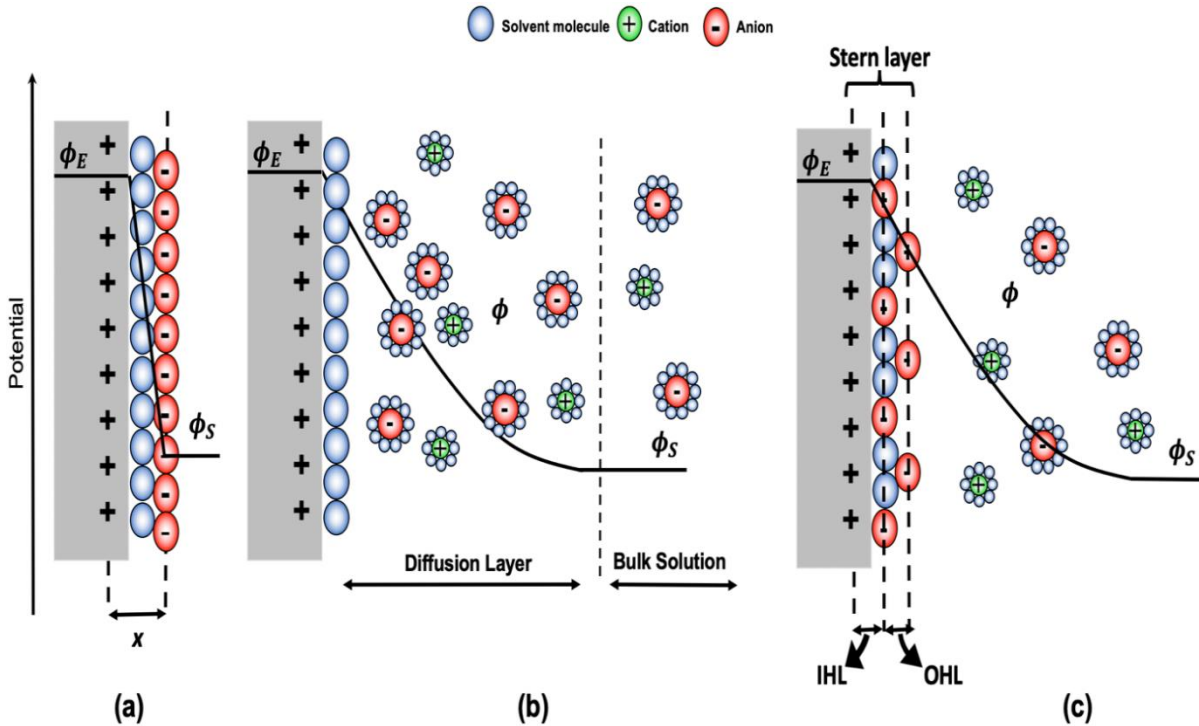


Figure 5: Three EDL Models on the Potential Distribution in the Electrolyte (a) Helmholtz Model in which  $d$  is the Thickness of the Double Layer, (b) Gouy-Chapman Model, and (c) Stern Model which Represents Stern Layer that Includes Inner Helmholtz Layer (IHL) and Outer Helmholtz Layer (OHL) [22].

The  $\varphi(x)$  is the electrode potential,  $\varphi$  the electrical potential, and  $\phi_S$  the electrolyte potential. In order to develop the Gouy–Chapman model for the diffuse layer, Stern model proposed the incorporation of both Helmholtz and Gouy-Chapman models to overcome the divergence and give an internal Stern layer and an outer diffuse layer in the range 10-100 nm from the electrode surface, respectively as illustrated in Figure 5 (c) [22, 24]. Stern model assumes that ions are mightily absorbed by the electrode surface. The Inner Helmholtz Plane (IHP) and the Outer Helmholtz Plane (OHP) are existing within the stern plane.

The equivalent RC circuit of a pure EDLC can be model by having a double layer capacitor ( $C_{anode}$ ) and leakage resistance ( $R_{b,anode}$ ) at the anode electrode, a double layer capacitor ( $C_{cathode}$ ) and leakage resistance ( $R_{b,cathode}$ ) at the cathode electrode, and the electrolyte resistance ( $R_s$ ) as shown in Figure 6 [17, 18].

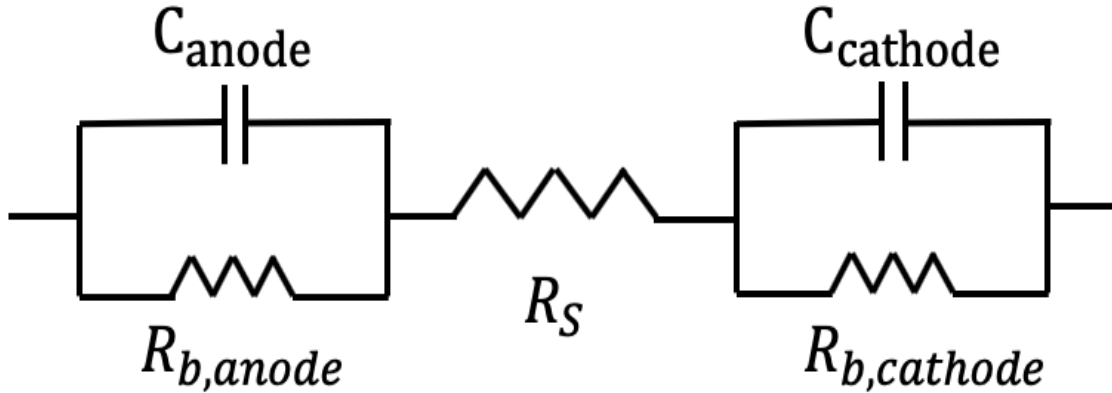


Figure 6: RC Equivalent Circuit Exemplification Clarifies the Basic Operation of a Single Cell Supercapacitor [17, 18].

Overall specific capacitance ( $C_{sp}$ ), which is measured by (F/g), of ECs can be found by taking into account the total mass of the active materials. Thus, the specific capacitance can be calculated by the following equation:

$$C_{sp} = \frac{I}{\left(\frac{dV}{dt}\right) \times m} \quad (4)$$

where  $m$  is the overall mass of the electrodes.

Basically, to evaluate any EC cell, there are two paramount parameters that play essential roles in the performance of ECs namely power density,  $P$ , with the unit of W/kg and energy density,  $E$ , with the unit of Wh/kg as described by the following equations when the device is charged to voltage  $V$  [7].

$$P = \frac{V^2}{4mR_s} \quad (5)$$

$$E = \frac{1}{2} C_{sp} V^2 \quad (6)$$

Massive efforts have been carried out on the expansion of advanced electrode materials in order to enhance the specific capacitance, power density, and energy density of EC devices. Since the mechanism of charge storage in EDLCs is non-faradic reaction, carbonaceous group materials such as carbon nanotubes, activated carbons, and graphene have been used widely for making EDLCs. In EDLCs, the specific capacitance, power density, and energy density mainly depend on electrode surface area, pore size distribution, and the porosity level in the electrode materials. Even though considerable research activities have been addressed to enhance the specific energy of EDLCs by matching ion size in electrolyte with the pore sizes of the carbonaceous group materials, EDLCs still have not reached the requirement of high energy density due to the intrinsic limitations. From this point of view, increasing the power and energy density have taken into account by incorporating redox active materials (faradic reaction) with carbonaceous group materials (non-faradic reaction) in pseudocapacitor devices.

Focusing on ECs as a viable technology to store energy, their power density is higher than batteries, while they present higher energy density than dielectric capacitors as shown in Figure 7. From the plot in Figure 7, ECs can be a transitional state between dielectric capacitors and batteries.

#### *2.1.2.2 Pseudocapacitors*

Pseudocapacitors employ both the double layer and redox reactions for charge storage. Importantly, the charges transfer mechanism is associated with the electrochemical Faradaic and non-Faradic reactions in this sort of capacitor. In that regard, the mechanism of charge storage is analogous to that in batteries. It should be recognized that the specific capacitance and energy

density of a pseudocapacitor can be approximately (10 to 100) times higher than that of an EDLCs. Hence, combining carbon materials with redox-active materials, such as RuO<sub>2</sub>, IrO<sub>2</sub>, Co<sub>3</sub>O<sub>4</sub>, MnO<sub>2</sub> or conducting polymers to frame composite electrodes yield pseudocapacitors [25].

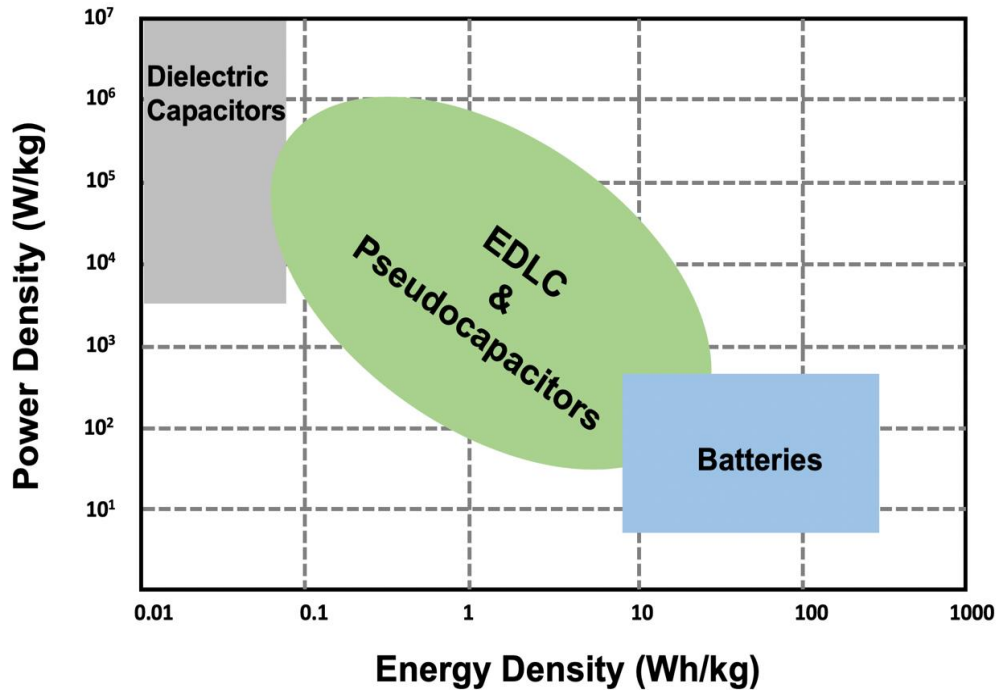


Figure 7: Ragone Plot Illustrates a Comparison of Power Density and Energy Density of Different Energy Storage Devices [16].

Manganese oxide (MnO<sub>2</sub>) is one of the best materials that recently are drawing research interests because of mechanical stability. So, the device that based on MnO<sub>2</sub> and carbon nanotubes composites has lately presented high specific capacitance roughly up to ~950 F/g [26]. J. Yan et al. have reported high specific capacitance (944 F/g), power (45.4K W/kg), and energy (25.2 Wh/kg) for supercapacitor devices based on MnO<sub>2</sub>/CNT composite electrode [27]. Yan al. have shown a high specific capacitance by employing graphene sheets composites with a conducting polymer (PANI) via electrochemical polymerization. The obtained specific capacitance was 1046 F/g [28]. Zhang et al. have studied a supercapacitor device based on a composite electrode of graphene with (Ppy) that has shown 504.5 F/g as specific capacitance [29]. Mini, P. A., et al.

synthesized a supercapacitor device with composite electrodes of graphene/Ppy, obtaining a high specific capacitance of 1510 F/g [30].

In spite of that, the power density of EDLCs is ordinarily higher than pseudocapacitors because of the tardy faradic processes that implicated the pseudocapacitor's performance. Moreover, swelling and shrinking of the electrodes may occur during the redox reactions which is a drawback, resulting in a poor cyclability and mechanical stability in some pseudocapacitors [31, 32]

The electrochemical pseudocapacitor devices were studied deeply by Conway, who identified all the faradic mechanisms that result in the pseudocapacitor, which are underpotential deposition (adsorption pseudocapacitor), redox pseudocapacitor, and intercalation pseudocapacitor. Figure 8 shows all the faradic mechanisms based on different materials. All three types occur under different physical processes, but they are similar electrochemically. It should be noted that all the three faradic reactions are governed by the Nernst equation [33, 34].

$$E = E_o - \frac{RT}{nF} \ln \frac{(C_{Re})}{(C_{Ox})} \quad (7)$$

where  $E$  is the cell potential (variable),  $E_o$  is the standard electrochemical potential (constant),  $R$  is universal gas constant ( $8.3144 \text{ J mol}^{-1}\text{K}^{-1}$ ),  $T$  is absolute temperature (K),  $n$  is number of electrons transferred,  $F$  is Faraday constant ( $\sim 96485 \text{ C mole}^{-1}$ ),  $(C_{Re})$ , and  $(C_{Ox})$  are concentrations of Oxidation and Reduction within the electrolyte ( $\text{mol cm}^{-3}$ ).

Underpotential deposition takes place when the reversibly adsorbed monolayer is created by ions in the electrolyte medium at the surface of the metal electrode (i.e., gold) due to the effect of applied potential. Redox pseudocapacitor happens when the adsorption of ions occurs electrochemically onto or near the electrode surface with a spontaneous faradic charge transfer mechanism. Intercalation pseudocapacitor arises when ions electrochemically insert between the



intercalation redox-active material as host materials accompanied by a spontaneous faradic charge transfer [33, 34].

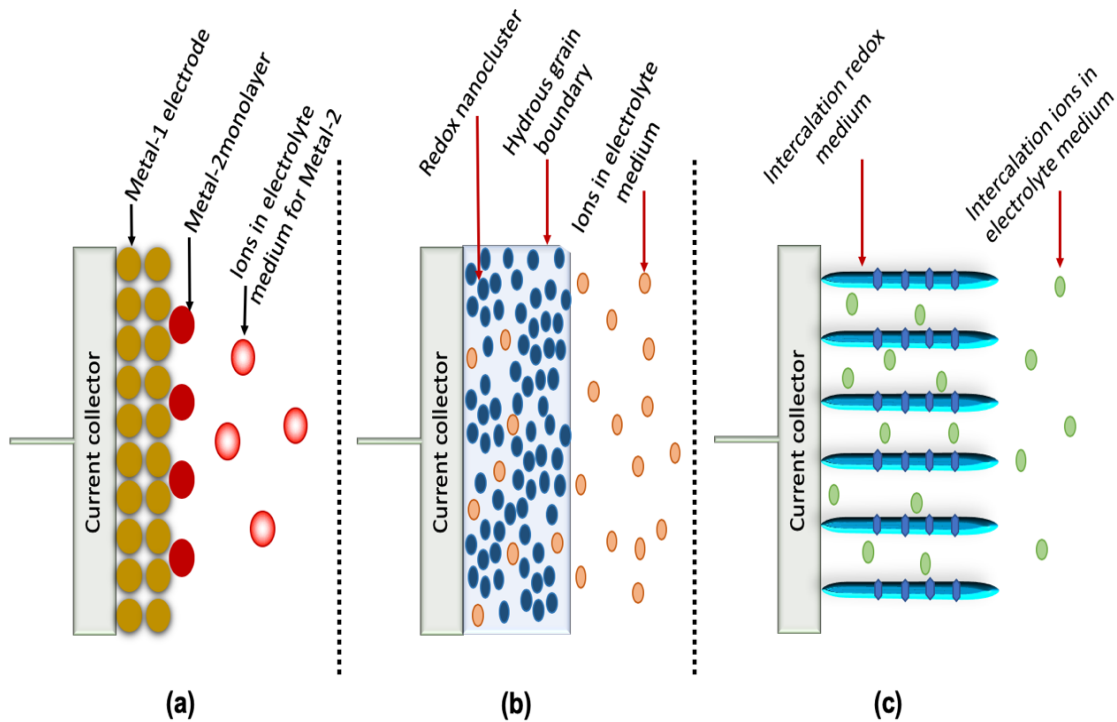


Figure 8: Schematic Diagram of Different Redox Reactions Result a Pseudocapacitor (a) Under Potential Deposition (Adsorption Pseudocapacitance), (b) Redox Pseudocapacitor, (c) Intercalation Pseudocapacitance [33, 34].

Since photoactive supercapacitors made from conducting polymers are one of the main parts of this dissertation, the redox mechanism in conducting polymers is briefly reviewed here. Conducting polymers properties, including multiple oxidation states, being non-toxic, low cost, environmentally friendly, abundance, and photoelectric, have made them promising for both energy storage and solar energy harvesting [35]. Using conducting polymer materials in devices like pseudocapacitors or photoactive supercapacitors, two doping states are playing the primary role in the behavior of a conducting polymer during the charging and discharging process. Therefore, by switching the conducting polymer between these two states, the electron charge storage has existed. During the charging process, conducting polymer undergoes the oxidation

process by losing electrons, as shown in Figure 9 (a). Then, positive charges occupy conducting polymer to become "Polycations," causing in attracting electrolyte ions (anions such as  $\text{Cl}^-$ ) to the backbone of the Polycations chain (doping process). Whereas in a reduction process, which is gaining electrons, the polymer undergoes through the discharge process (de-doping) while the ions released back to the electrolyte medium, as shown in Figure 9 (b) [36].

Among the conducting polymer materials, polyaniline (PANI) and polypyrrole (Ppy) [35] were used in most of the activities research of fabrication of photoactive supercapacitors in this dissertation. They have drawn the most attention because of their multi redox states that are desired for high specific capacitances, good electrical properties, and suitable for energy storage and harvesting applications. The charging and discharging process of Ppy and PANI can be expressed as follow [37]:

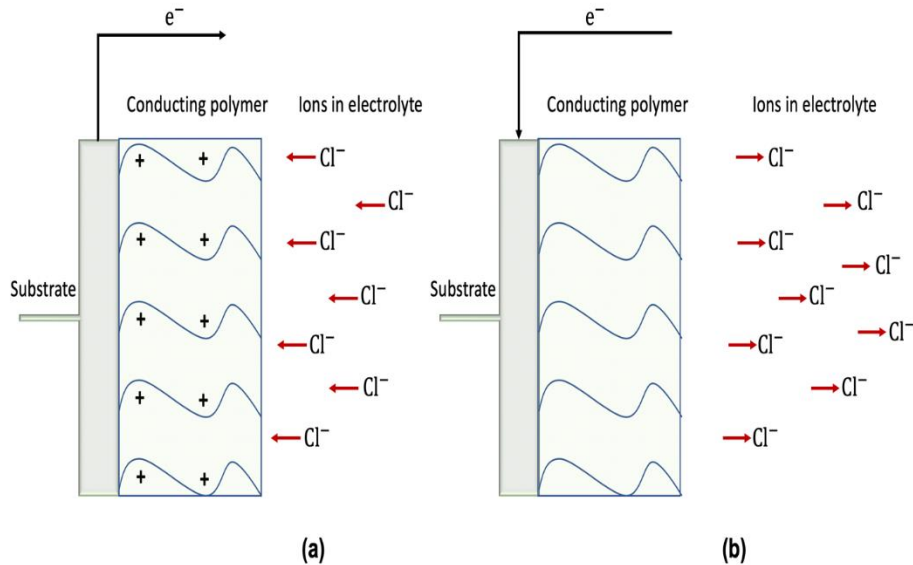
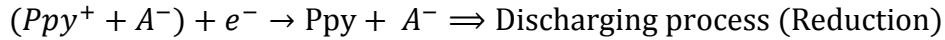
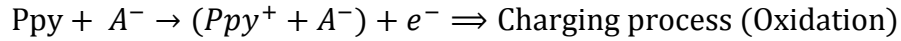


Figure 9: Electron Charge Storage on Conducting Polymers (a) Under Potential Effect (Charging Process), (b) Discharge Process [38].

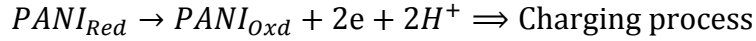


Figure 10 shows the redox reaction of PANI as an active material with electrolyte during charging (a) and discharging (b). An example of charging and discharging process of PANI in acid solution (i.e. sulfuric acid, H<sub>2</sub>SO<sub>4</sub>) is described as follow [39]:

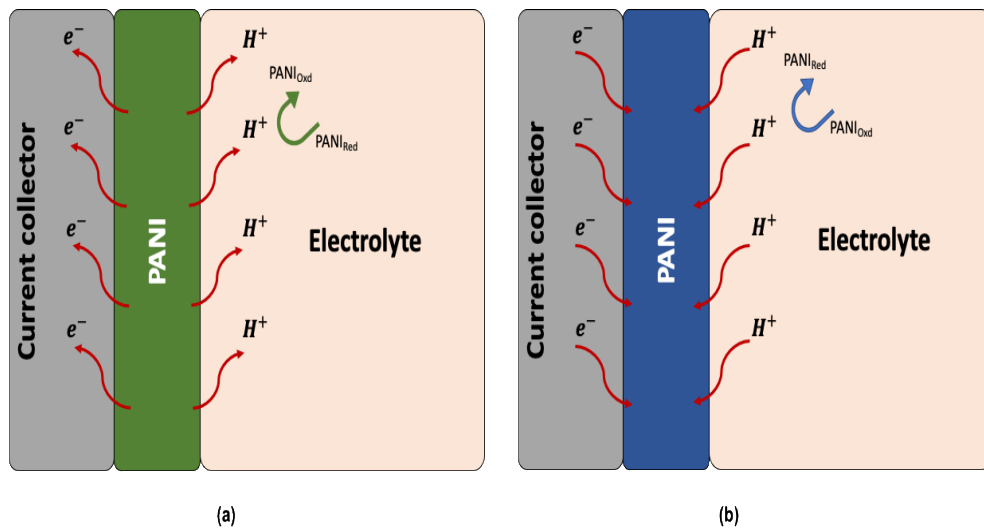
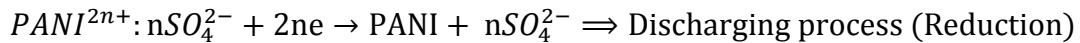
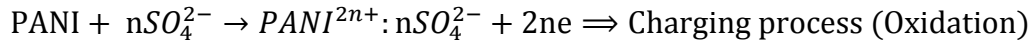


Figure 10: Redox Reaction of PANI During (a) Charging Process Representing by Green Color which is the Most Conductive State and (b) Discharging Process Representing by Blue Color which is the Less Conducting or Insulator.

### 2.1.3 Batteries

Ordinarily, batteries have a relatively high energy density compared to ECs; however, their power density is low. On the other hand, ECs provide better energy density compared to electrolytic capacitors and offer a good alternative for batteries in applications where high-power density (fast charging/discharging capability) is needed. In addition to high power density, ECs

have a large cycle-life (~10<sup>6</sup>), are environmentally friendly, and can be operated at low temperatures [40, 41].

In the battery devices, the mechanism of charge storage is based on electrochemical redox reactions. The most popular form of rechargeable batteries are Li-ion batteries. Basically, a Li-ion battery consists of anode and cathode electrodes that can store lithium ions. The electrolyte is existed between the two electrodes to transport positive charges of lithium ions between the high energy anode (positive electrode) and the low energy cathode (negative electrode) through a membrane (i.e., separator) during the charging and discharging cycles. The transition of the lithium ions between anode and cathode produces free electrons in the anode (redox reaction), resulting to flow current through a load (i.e., computer, cell phone, or any electric device) from one side to another. In case the battery is fully charged, energy is utilized to relocate the lithium ions back to the high-energy anode aggregate [42, 43].

Table 2: Comparison of Electrical and Electrochemical Energy Storage Appliances [44].

Characteristics	Dielectric capacitor	EDLC	Pseudocapacitor	Lithium-ion battery
Specific energy (Wh kg <sup>-1</sup> )	< 0.1	0.1 to 14	0.1 to 20	10 to 500
Specific power (W kg <sup>-1</sup> )	10 <sup>4</sup> – 10 <sup>7</sup>	10 <sup>2</sup> to 10 <sup>6</sup>	10 <sup>2</sup> to 10 <sup>6</sup>	10 <sup>1</sup> to 10 <sup>2.5</sup>
Charging time	10 <sup>-6</sup> – 10 <sup>-3</sup>	0.3 to 30s	NA	1 to 5 hrs
Discharging time	10 <sup>-6</sup> – 10 <sup>-3</sup>	0.3 to 30s	NA	12 to 24 hrs
Cycle life	> 500,000	> 500,000	< 300,000	< 10000
Self-discharge*	days	weeks	months	months
Lifetime*(years)	> 20	5 to 10	5 to 10	3 to 5

\*At room temperature.

Table 2 shows a comparison between all the four electrical and electrochemical energy storage devices in terms of specific energy, specific power, charging time, discharging time, cycle life, self-discharging.

## **2.2 Solar Energy Harvesting**

### **2.2.1 Current State of Technology**

The concern about the energy crisis is rising fast because of the rapid growth of population, economic advancements, and technological development. Therefore, it is necessary to find an alternative source of energy that is safe, cost-effective, and perpetual for future demand. Solar energy harvesting is perhaps the most adaptable and freely obtainable energy [45, 46]. Solar cell technology mainly relies on the radiations from the sun every day. The received solar energy by solar cells is converted to electricity through the photovoltaic (PV) effect. Indeed, numerous factors are influencing the performance of a solar cell and the amount of produced electric power. Some of those factors are the type of active materials, size of the device, and intensity of illumination. In order to produce electrical power from a solar cell, light absorption by the PV material and charge separation are indispensable [47, 48]. Figure 11 shows three different generations of solar cells based on the type of materials used in different solar cell devices.

Further development of fabrication solar cells has been accomplished from generation to another, as shown in Figure 11. More precisely, all three generations are manufactured as wafer and thin film divided into subgroups (i.e., Organic and Inorganic). The first generation of PV solar cells are made on a wafer-based Silicon. In fact, there are different types of wafer-based solar cells, such as polycrystalline silicon solar cells (multiple crystals) and Monocrystalline silicon solar cells (single crystal). Further improvement is taken from the wafer-based solar cell (1st generation) to

a thin-film solar cell (2nd generation) such as Cadmium telluride (CdTe), Copper indium gallium selenide (CIGS), and Amorphous silicon (a-Si). The most recent type is the 3rd generation of solar cells, which is still under the research and development, for example, organic solar cell, polymer solar cell, dye-sensitized solar cell, and perovskite solar cell [49-51].

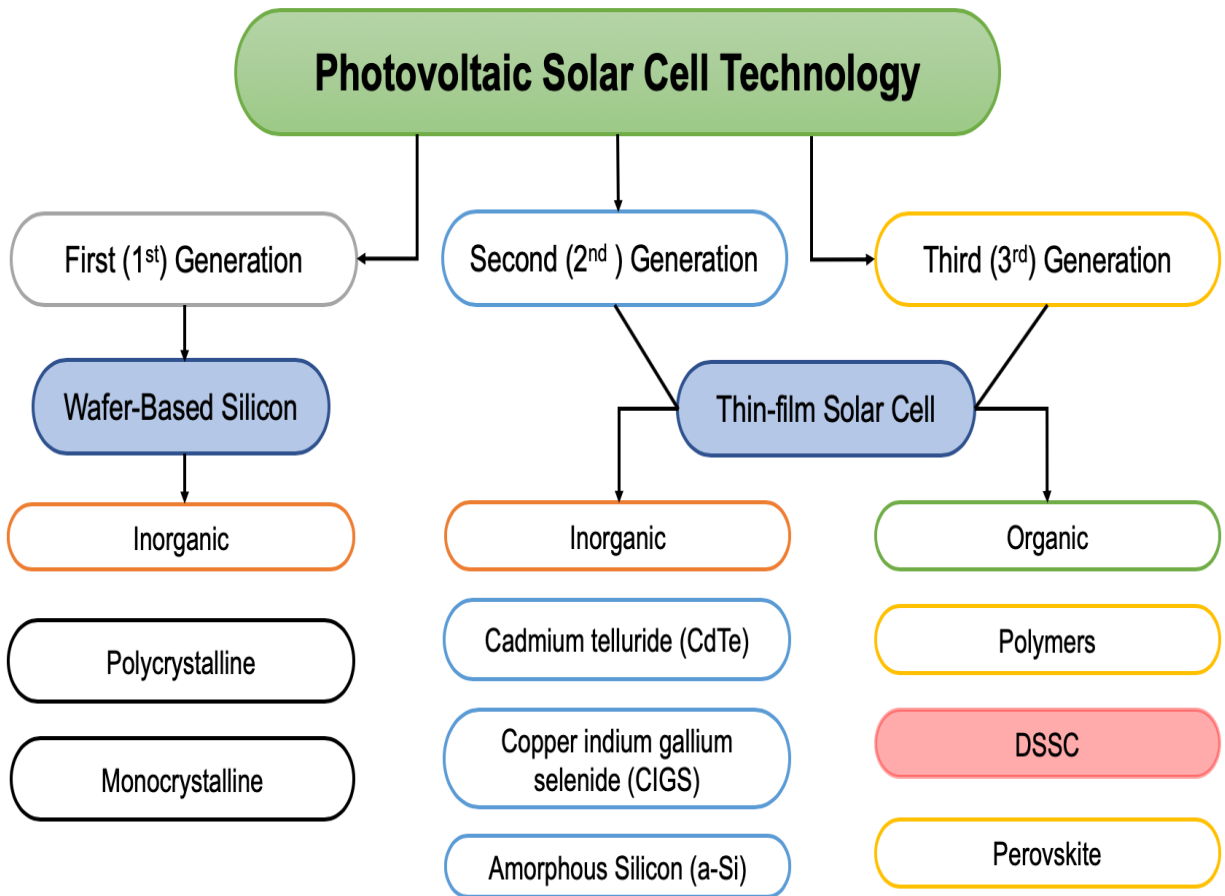


Figure 11: Photovoltaics Solar Cell Technology with Three Different Generations of Technologies Based on the Essential Active Materials [49-51].

In this dissertation, the focus is on the 3rd generation, particularly DSSCs, also known as Gratzel cells [49]. In the last two decades, there has been comprehensive research on thin-film solar cells, more specifically on DSSCs because of their desirable attributes such as a cost-effective method of fabrication, low toxicity, lightweight, everlasting source of energy, and high

performance in diversified light conditions [52]. Moreover, manufacturing DSSCs does not need cleanroom facilities.

All the three generations of photovoltaic solar cell technology based on materials type, efficiency, temperature, size, and cost are listed in Table 3.

Table 3: Comparison of All Three Generations of Solar Cell Technology.

Generations	1st Generation		2nd Generation			3rd Generation			
Cell type	Inorganic/ Wafer-Silicon		Inorganic/ Thin film			Organic/ Thin film			
Material type	Monocrystalline	Polycrystalline	CdTe	CIGS	a-Si	Organic	Polymer	DSSC	Perovskite
Efficiency	14%-17.5%	12%-14%	9%-11%	10%-12%	4%-8%	7%-8%	3%-10%	13%	30%
High temperature	Not good	Not good	Good	Good	Good	Excellent	Not good	Not good	Excellent
Size	Small	Small	Multiple sizes	Multiple sizes	Multiple sizes	Multiple sizes	Multiple sizes	Multiple sizes	Multiple sizes
Cost	Very Expensive	Expensive	Low cost	Low cost	Low cost	Low cost	Low cost	Low cost	Low cost

An advantage of DSSC over other solar cells is the ability of DSSCs to operate at low light intensities with the almost same efficiency as in full sunlight. Efficiency as high as 13% [53] has been reported in a device using porphyrin dye sensitizers, which is still not comparable to the first and second generation, which exhibit ~ 20 to 30% [50]. The extensive utilization of photovoltaic devices to produce electricity is still costly. The electrochemical nature of a DSSC is more compatible with the energy storage devices.

### 2.2.2 Principle Work of Dye-Sensitized Solar Cell

Basically, a DSSC is constructed of five components, namely: FTO glass, semiconductor, dye sensitizer, electrolyte, and a cathode electrode. The combination of the transparent electrode, semiconductor, and dye acts as the photo-anode in the cell. The photo-anode electrode is prepared by, first, depositing a thin layer of a metal oxide (MO) material such as TiO<sub>2</sub>, SnO<sub>2</sub>, and ZnO on the surface of a conductive transparent oxide glass made of fluorine-doped tin oxide (FTO) or indium tin oxide (ITO) [54]. The MO materials possess a wide bandgap of energy from ~ 2.1 to 3.2 eV and are transparent to visible light but can absorb UV region [55]. In the second step, the photo-anode electrode is soaked into a solution containing the dye sensitizer molecules. After immersing the photo-anode electrode into the photosensitizer solution, the dye molecules adsorb to the semiconductor layer on the surface of the conductive transparent oxide glass. Thus, the light absorption is enhanced to a broad spectrum covering from UV to near-infrared region (IR) region. Also, the thin coating layer of dyes on the internal surface of the porous semiconductor layer improves the light absorption when it passes through the photo-anode [56, 57]. When it comes to the conductivity and regeneration of dyes, the redox electrolyte mediator takes part.

Among all various components of electrolyte (i.e., additives, solvents, mediators, inions, and cations), redox couple such as iodide/triiodide ( $I^-/I_3^-$ ) has been extensively studied for DSSC applications due to their efficient charge transport through the electrolyte. Redox electrolyte mediators can adversely influence the total performance of a DSSC through redox couple parts, diffusion of charge carrier, and charge transfer resistance in the electrolyte [58]. The last component of DSSC is the cathode electrode, which is foremost made of FTO conductive glass coated with catalyst materials (i.e., Platinum, Pt) due to the high efficiency attained. However, replacing the Pt electrode by carbon electrodes was in need because of the drawbacks of the Pt



electrode, such as cost and scarcity. The main job of the cathode electrode is to catalyze the reduction of the redox electrolyte and provides electrons for the redox reaction from the external wire [59].

The mechanism of operation in DSSCs is based on the photosensitizer dye materials that have two different orbital states, which are the lowest unoccupied molecular orbital (LUMO) and the highest occupied molecular orbital (HOMO). Noted that the LUMO level should be higher than the conduction band (CB) of the semiconductor material and HOMO level lower than the electrochemical potential of the redox mediator in the electrolyte. The photoexcitation process is started when the photosensitizer absorbs the incident light (photon), and then, the electrons get excited within femtoseconds from the HOMO level (ground state) to the LUMO level (excited state) of inside the dye molecules. Afterward, the excited electrons injected into the conduction band of the semiconductor.

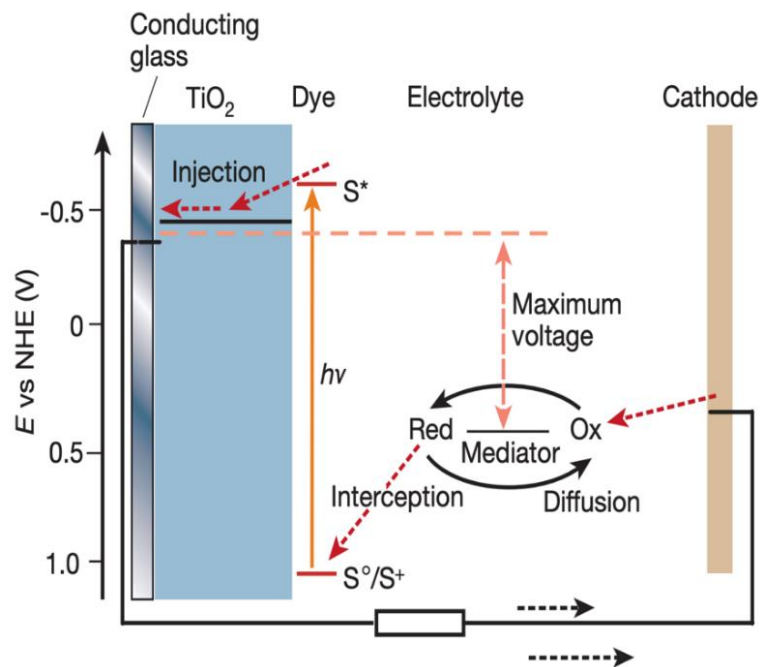


Figure 12: Principle Work and Energy Level Diagram of Dye Sensitized Solar Cell [55].

Then, injected electrons diffuse through the nanoparticles of the semiconductor toward the transparent conductive oxide. After that, in a circuit, electrons will follow the external wiring to reach the counter electrode. After receiving electrons by the counter electrode, redox couple mediator After receiving electrons by the counter electrode, redox couple mediator electrolyte regenerates electrons back to the ground state of the dye by reducing the  $I^{-3}$  to  $I^{-}$  and then oxidize the  $I^{-}$  back to  $I^{-3}$  [60]. The schematic diagram of principle work and operation of DSSC is shown in Figure 12.

### 2.2.3 Performance of Dye Sensitized Solar Cell

To evaluate the performance of DSSC, there are five essential parameters: open circuit voltage ( $V_{oc}$ ), short circuit current ( $J_{sc}$ ,  $mA/cm^2$ ), maximum power output, fill factor, and efficiency ( $\eta$ , %).  $V_{oc}$  is the voltage value across the electrodes under zero current (open circuit).  $J_{sc}$  is calculated based on the apparent surface area of the photo-anode and drifting process of charges under the effect of light and the internal electric field with no exterior potential. Although  $V_{oc}$  and  $J_{sc}$  present the highest voltage and the highest photocurrent that can be achieved from a cell, respectively, the highest output power would be obtained at  $P_{max}$ , as shown in the J-V characteristic of a solar cell in Figure 13. By finding the ratio between the maximum output power ( $J_{max} \times V_{max}$ ) and the product of  $V_{oc}$  and  $J_{sc}$ , the fill factor can be evaluated by calculating  $\left(\frac{\text{Area (a)}}{\text{Area (b)}}\right)$  as it can be seen in Figure 13 [61]. The most critical factor in any solar cell is the energy conversion efficiency, which is the ratio of  $P_{max}$  to the solar radiation power received by the device. Efficiency,  $\eta$ , is usually expressed as a percentage. The highest reported efficiency in DSSC is 13% from a cell made by [53].

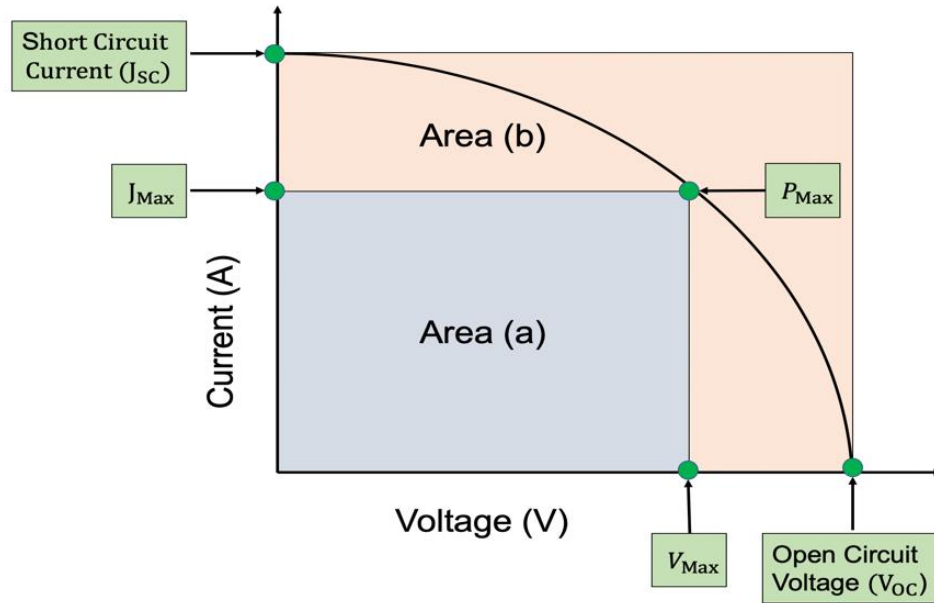


Figure 13: Current Density vs. Voltage (J vs. V) Characteristics of Dye Sensitized Solar Cell.

### 2.3 Electrolyte materials

Great efforts have accomplished in terms of optimizing electrochemical devices components such as electrode and electrolyte materials. Getting high specific power and energy in energy storage cells is not only relying on the electrode materials but also influenced by electrolyte materials. In fact, taking into consideration only the mass of active materials on the electrodes is not an accurate way of measuring the specific capacitance, specifically in the industries. However, the overall weight of the device is necessary, including electrodes, electrolytes, packaging, and the current collector. Consequently, the density ( $\rho$ ) of the electrolytes ( $\text{g/cm}^3$ ) and the volume of the electrolyte material used in supercapacitors are crucial to finding the specific capacitance, power density, and energy density of the device.

In this regard, electrolyte materials have been deliberated more and more because of the highly poignant in the performance of electrochemical devices. The electrolytes have diverse categories, including liquids, solids, and gel polymer electrolytes, as shown in Figure 14 [62]. Each

category of the electrolytes has a different operation regarding the potential window of the cell. For instance, the potential window of ECs based on aqueous electrolyte is about 1.0 V to 1.2 V [63], whereas the potential window of ionic liquids electrolytes is in the range of 3.5 V to 4.0 V [64]. It should be noted that the expansibility of the cell potential window would be more effective in terms of energy density improvement since the energy is proportional to the square potential, as stated in equation (7).

Discussion on electrolyte materials in this section focuses only on gel polymer electrolytes. Gel polymer electrolytes have attracted particular attention because it is perhaps one of the most promising candidates in advanced materials for electrochemical, photoelectrochemical, and electrical applications to tackle issues such as safety (i.e., leakage), corrosion, and poor stability. This type of electrolyte is preferable for several applications such as ECs, PVs, Electrochromic (EC) devices, sensors, and rechargeable batteries [14, 65].

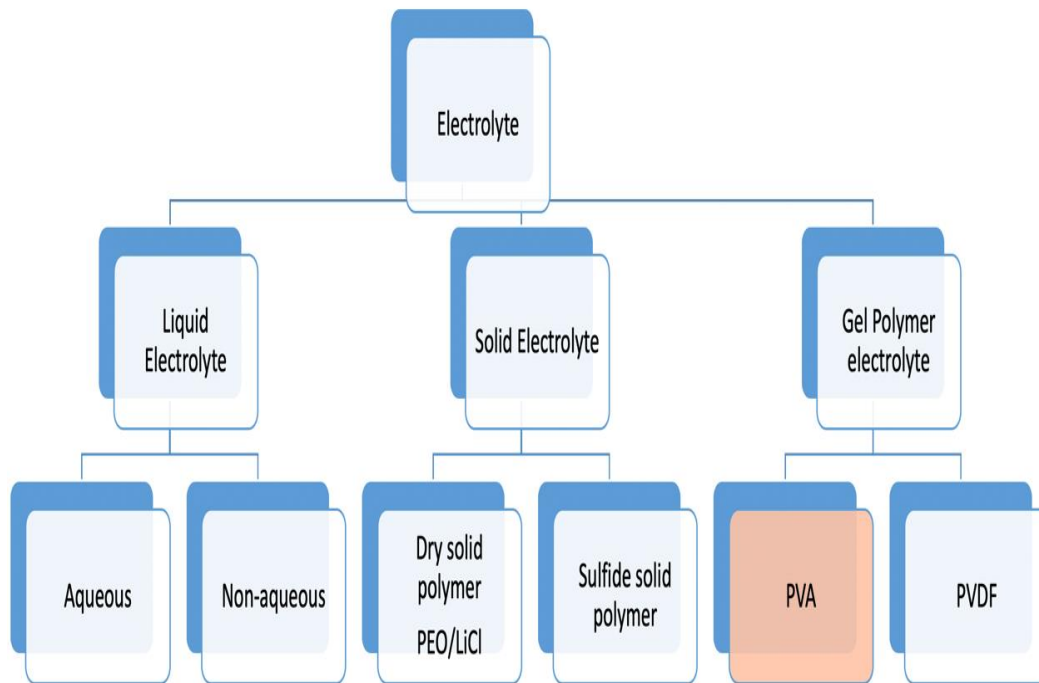


Figure 14: Three Different Categorizes of Electrolyte Materials [62].

Gel electrolyte can be prepared by mixing host polymer materials such as polyvinyl alcohol (PVA), poly(ethyl oxide) (PEO), poly-(methyl methacrylate) (PMMA), and poly(vinylidene fluoride-co-hexafluoropropylene) (PVDF-HFP) with an aqueous electrolyte including H<sub>2</sub>SO<sub>4</sub>, H<sub>3</sub>PO<sub>4</sub>, HCl, or a conducting salt dissolved in organic solvent [66]. In this dissertation, a polymer host (PVA) has been carried out for all the experiments with different materials such as aqueous solutions, conducting polymers, and photosensitizers that employed for different electrochemical applications. Among other host polymers, PVA has been chosen because of its advantages, which are high mechanical strength, non-toxic, hydrophilic, good electronic properties, and low-priced. Figure 15 shows the structure of the PVA polymer, which has hydroxyl and carbonyl groups.

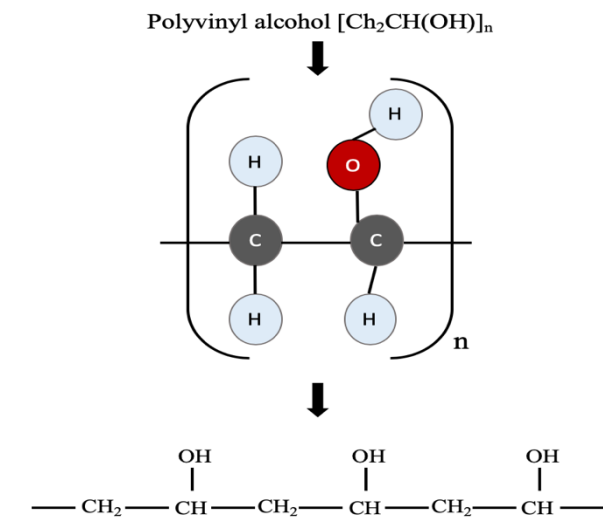


Figure 15: Chemical Structure of PVA Material.

### 2.3.1 ECs based Gel electrolyte

In this section, some of the major works on PVA-based gel electrolytes for ECs have been reviewed. Zhong et al. have reported a quasi-solid-state supercapacitor that was assembled by having active electrodes and PVA/H<sub>2</sub>SO<sub>4</sub> gel electrolyte including two additives redox materials such as hydroquinone (HQ) and methylene blue (MB) that were mixed with the gel electrolyte to

enhance the capacitance of the devices [67]. Meng et al. have studied a solid-state supercapacitor with two nanocomposite thin films of CNT/PANI separated by H<sub>2</sub>SO<sub>4</sub>-PVA gel electrolyte. The results were promising by showing high specific capacitance, good stability, and low self-discharge [68]. Cao et al. have examined the performance of a supercapacitor device based on the H<sub>2</sub>SO<sub>4</sub>/PVA gel electrolyte. The results showed high stability under different bending conditions, low degradation after 5000 cycles, and good electrochemical performance [69]. Kaempgen et al. have demonstrated a supercapacitor device with single-wall carbon nanotube (SWCNT) based electrodes and H<sub>3</sub>PO<sub>4</sub>/PVA as gel electrolyte to make a flexible device. High energy and power densities were obtained [70]. Xu et al. have obtained unprecedented results for the areal specific capacitance of 372 mF/cm<sup>2</sup>, low leakage current, high stability, and good flexibility by sandwiching two graphene hydrogel electrodes and placing H<sub>2</sub>SO<sub>4</sub>-PVA gel electrolyte in between [71]. Lu et al. have elucidated the effect of employing PVA/KOH as a gel electrolyte on the performance of supercapacitor with TiN nanowires-based electrodes. PVA/KOH gel electrolyte quells the oxidation reaction on the surface of TiN nanowires electrodes without any degradation in its electrochemical performance. The electrochemical tests showed the stability of the supercapacitor up to 15000 cycles [72]. More examples of ECs based gel electrolytes without and with additives materials are presented in Tables 4 and 5.

Table 4: Literature Review of ECs with PVA-Based Gel Electrolytes.

Polymer electrolyte	Type of electrode	Type of ECs	Specific capacitance (F/g)	Power density (W/kg)	Energy density (Wh/kg)	Ref.
PVA+H <sub>2</sub> SO <sub>4</sub>	Carbon	EDLC	245	5.97K	8.01	[73]
PVA+KOH	Carbon	EDLC	69	400	24.6	[74]
PVA+KOH	Conducting polymer /metal oxide	Pseudocap.	308.1	2019.1	26.6	[75]

Table 4: (Continued)

PVA+H <sub>3</sub> PO <sub>4</sub>	Carbon/metal oxide	Pseudocap.	138	96K	18.8	[76]
PVA+H <sub>2</sub> SO <sub>4</sub>	Conducting polymer	Pseudocap.	350	2.189K	7.1	[68]
PVA+H <sub>2</sub> SO <sub>4</sub>	Carbon coated with Silver nanoparticles	EDLC	115.6	16.64K	4.65	[77]
PVA+H <sub>2</sub> SO <sub>4</sub>	Metal oxides	Pseudocap.	404	500	14	[69]
PVA+H <sub>3</sub> PO <sub>4</sub>	Carbon	EDLC	12.4 ( $\mu\text{F cm}^{-2}$ )	438.6K	2.94	[78]
PVA+H <sub>3</sub> PO <sub>4</sub>	Carbon	EDLC	312	7000	36	[79]
PVA+H <sub>3</sub> PO <sub>4</sub>	Carbon	EDLC	47	Na	Na	[80]
PVA+LiClO <sub>4</sub>	Metal oxide	Pseudocap.	112	3.8K	15	[81]

Table 5: Literature Review of ECs with PVA-Based Gel Electrolytes with Additive Materials.

Polymer electrolyte with additive	Type of electrode	Type of ECs	Specific capacitance (F/g)	Power density (W/kg)	Energy density (Wh/kg)	Ref.
PVA+H <sub>2</sub> SO <sub>4</sub> +HQ/MB	Carbon	EDLC	563	NA	18.7	[67]
PVA+H <sub>2</sub> SO <sub>4</sub> +PB	Carbon	EDLC	474.29	1000	11.31	[82]
PVA+KOH+KI	Carbon	EDLC	236.90	15.34K	7.8	[83]

### 2.3.2 Dye Sensitized Solar Cell Based on Gel Electrolyte

Fabrication DSSCs devices based liquid electrolyte is still questionable due to the limited shapes, stability, and sealing requirement in order to avoid the electrolyte leakage issue. Therefore,

the substitution of the liquid electrolyte by solid or gel electrolytes is drawing the attention of researchers. More specifically, gel polymer electrolyte aids in reducing the cost and fabrication time due to the easier assembly of DSSC devices [49, 55]. Nath et al. have investigated a high performance of dye-sensitized solar cell (DSSC) fabricated based on PVA/MWCN/PANI gel electrolyte. The process of making a gel electrolyte was carried out by soaking 0.5 g of PVA/MWCNT/PANI powder in 0.1 M lithium iodide (LiI), 0.6 M I<sub>2</sub>, 0.5 M tert-butylpyridine (TBP), 0.05 M 1-methyl-3propyl imidazolium iodide (NMP) in a mixed solvent of N-methyl 2-pyrrolidone (NMP) and acetonitrile. The results showed amelioration for ionic conductivity, device efficiency, and charge transport [84]. Wang et al. have made an analogy study of DSSC based on two electrolytes, e.g., fluorine polymer, poly (vinylidene fluoride-co-hexafluoropropylene (PVDF-HFP) polymer with 3-methoxypropionitrile (MPN) as a quasi-solid-state gel electrolyte combined with polypyridyl ruthenium dye and only MPN combined with polypyridyl ruthenium dye as a liquid electrolyte. The results of conversion efficiency and stabilities of DSSC based on gel and liquid were comparable [85]. Aziz et al. have reported a DSSC based PVA with mixed iodide salts (K<sup>+</sup>I<sup>-</sup> and Bu<sub>4</sub>N<sup>+</sup>I<sup>-</sup>) as gel polymer electrolyte sandwiched between the photoanode electrode and FTO conductive glass coated with platinum as a counter electrode. The device obtained  $J_{sc}=12.56 \text{ mA cm}^{-2}$ ,  $V_{oc}=0.71 \text{ V}$ , and  $\eta=5.8 \%$  with the mixture salts of 30% of K<sup>+</sup>I<sup>-</sup> and 70 % of Bu<sub>4</sub>N<sup>+</sup>I<sup>-</sup> [86]. Wang et al. have investigated a solid state DSSC based on PVDF–HFP polymer blended with MPEI ionic liquid as a gel polymer electrolyte sandwiched between coated nanocrystalline TiO<sub>2</sub> electrode and Pt foil-based counter electrode. They presented that gel polymer electrolyte not only was exhibited the same advantages as liquid electrolytes but also had the flexibility feature [87]. The list in Table 6 summarizes some DSSCs devices with gel electrolytes.



Table 6: Literature Review of DSSCs Based Gel Electrolyte.

Polymer electrolyte	Dye	V <sub>oc</sub> (V)	J <sub>sc</sub> (mA/cm <sup>2</sup> )	FF	Efficiency %	Ref.
PVDF-HFP	Z907	0.665	11.29	0.712	5.3	[87]
PVA+KI	N719	0.51	11.03	0.68	3.83	[88]
Phthaloylchitosan (PhCh)	N3	0.71	19.68	0.69	9.61	[89]
Polyacrylonitrile (PAN)	D35	0.61	4.64	0.62	1.71	[90]
PVDF+KI+I <sub>2</sub>	N719	0.66	5.24	0.53	1.8	[91]
PVA+PEO+TBAI+LiI	N3	0.63	16.41	0.60	6.26	[92]
PVA+PEO+TBAI+BMII	N3	0.79	14.25	0.67	7.49	[93]

### 2.3.3 Integrated Solar Energy Harvesting and Storage Based on Gel Electrolyte

Solar energy harvesting and storage technologies are developed independently, but also they are used with each other ordinarily as a power pack system to reduce the vexatious mismatch between demand and supply. A myriad of suggested approaches to combine solar energy harvesting (i.e., DSSC, OPV, etc.) and storage (i.e., ECs and Lithium-ion batteries) were clearly addressed in [94]. Among these sorts of devices, DSSCs and ECs were mostly investigated. Hybridizing both electrochemical energy storage and conversion in one device is not only important to efficiently capture, convert, and store energy but also to fulfill the demands of reducing the cost and size. Due to the limited lifetime of batteries, ECs have been chosen to be connected directly with the DSSCs in a power pack system for further improvement. ECs are preferable because of the long lifetime and the speedy response to current change since the source (i.e., light) is typically changed with the climate changes [95]. DSSCs are certainly the most type of organic photovoltaic (OPV) devices that use chemical reaction to absorb the light (photons) and

convert them to electric charges without the necessity for intermolecular carriers of electronic excitation. It is also the unique solar cell that detaches the two functions of light-harvesting and charge-carrier, whereas conventional and all of the other of OPV devices perform both features simultaneously [56].

Yang et al. have developed an integrated device based on three electrode configurations. MWCNT electrode was shared between the supercapacitor and the dye-sensitized solar cell as the first phase and MWCNT composite with PANI as the second phase to improve the performance. PVA-H<sub>3</sub>PO<sub>4</sub> was sandwiched between the two MWCNT electrodes as the gel electrolyte for the energy storage part. Different gel electrolytes were used for the conversion energy part that prepared by mixing poly (vinylidene fluoride-co-hexafluoropropylene) (10 wt.%) and 3-methoxypropionitrile solution containing 0.1 M LiI, 0.05 M I<sub>2</sub>, 0.5 M 4-tert-butylpyridine and 0.5 M 1-propyl-2,3 dimethyl imidazolium iodide. The results exhibited a 6.10% conversion efficiency [96]. Wen et al. have made a hybrid device of DSSC and supercapacitor by using H<sub>3</sub>PO<sub>4</sub>/PVA as a gel electrolyte. The open circuit voltage and the specific capacitance of the supercapacitor were obtained to be 1.2 V and 1.9 mF cm<sup>-1</sup>, respectively [97]. Harankahawa et al. have fabricated photoelectric conversion (DSSC) and energy storage (Supercapacitor) devices based on gel electrolyte. The gel electrolyte was synthesized by mixing Polyacrylonitrile (PAN) which is also called polyvinyl cyanide, ethylene carbonate (EC), propylene carbonate (PC), and sodium iodide (NaI). A DSSC exhibited 0.68 V open circuit voltage, 0.33 mA cm<sup>2</sup> short current density, 0.64 fill factor, and the efficiency was 0.05%. The result of the redox capacitor was 26.70 Fg<sup>-1</sup> [98, 99]. Scalia et al. have reported for the first time a flexible integrated energy harvesting and storage device, which was invented by integrating a DSSC (TiO<sub>2</sub>) and a supercapacitor (graphene). A gel photo polymer electrolyte was used as a membrane soaking in two different liquid electrolytes.

They obtained the highest efficiency for energy conversion and storage, which was 1.02%, based on DSSC and non-wired photo capacitor devices. The results showed high cyclability and light degradation for a supercapacitor device even after 10000 cycles [100].

This chapter briefly addressed most of the background of the electrochemical devices that have been studied in this dissertation. Moreover, the principal work of each device has been mentioned herein. In the following chapter, the materials, instruments, and methods that were used for the fabrication and characterization of devices will be discussed.

### **Chapter 3: Electrochemical Materials and Methods Used for Fabrication and Characterization of Devices**

Even though different research activities with different types of electrochemical devices (i.e., EDLCs, pseudocapacitors, and DSSCs) have been fabricated and characterized in this dissertation, the device performance has been evaluated by employing certain electrochemical materials, methods, and instruments.

This chapter exhibits briefly the materials and methods that were used for the fabrication of all the studied electrochemical cells. It should be noted that the materials and methods of fabrication are included as an experimental part of published manuscripts in each of the following chapters.

Electrical and electrochemical measurements, such as cyclic voltammetry (CV), galvanostatic, electrochemical impedance spectroscopy (EIS), open circuit voltage ( $V_{oc}$ ), and short circuit current ( $I_{sc}$ ) measurements, and spectroscopy methods are presented in this chapter under characterization section. Also, the instruments that were used in the research activities are addressed herein.

#### **3.1 Materials**

All chemical materials that were used in the experiments of this dissertation were purchased from Sigma Aldrich and Alfa Aesar. The materials are classified to acid solutions (i.e., hydrochloric acid, HCl, phosphoric acid,  $H_3PO_4$  with 85wt. % in  $H_2O$ , sulfuric acid,  $H_2SO_4$  with 95.0-98.0%  $H_2SO_4$ , and P-toluene sulfonic, PTS ( $CH_3C_6H_4SO_3H$ )), carbon materials (i.e. multi-

wall carbon nanotube), surfactants materials (i.e. sodium dodecyl benzenesulfonate, SDBS ( $C_{18}H_{29}NaO_3S$ )), polymer materials (i.e. polyvinyl alcohol, PVA ( $C_2H_4O$ )<sub>x</sub>), conducting polymer materials (i.e. aniline ( $C_6H_5NH_2$ ) and pyrrole monomer ( $C_4H_4NCH_3$ )), synthetic dyes materials (i.e. methylene blue, MB ( $C_{16}H_{18}ClN_3S \cdot xH_2O$ ), methyl orange, MO ( $C_{14}H_{14}N_3NaO_3S$ ), and prussian blue, PB ( $C_{18}Fe_7N_{18}$ ), and oxidizing agents (i.e. ammonium persulfate, APS ( $(NH_4)_2S_2O_8$ ) and iron(III) chloride ( $FeCl_3$ )). The paper substrates used for making the electrodes were from Office Depot (8.5 in.  $\times$  11 in.). All chemical materials were used as received without any further purification. Fluorine doped tin oxide conductive substrate (FTO) was purchased from Huanyu Instrument (China) with 1.66 mm and  $12 \Omega \text{ cm}^{-2}$  sheet resistance. Another Fluorine doped tin oxide conductive substrate (FTO) coated with titanium dioxide ( $TiO_2$ ) was purchased from Solaronix with a size 20 x 20 mm and active area 6 x 6 mm. Two pieces of glassy carbons (GC) ( $25 \times 25 \times 3 \text{ mm}^3$ ) were purchased from SPI Supplies.

## 3.2 Methods

### 3.2.1 Preparation of Electrodes

All the experiments were based on two electrodes configurations with a counter electrode (CE) and the working electrode (WE). Since a few devices were made during the research (i.e. EDLC, Photoactive supercapacitor, and DSSC), different WEs were fabricated. However, a carbon nanotube (CNT) based CE was used in the majority of devices made in this work. The electrodes were prepared using multiwall CNTs (MWCNTs). To fabricate the electrodes, the process explained by Hu et al. was followed [101]. At the first step, MWCNT based ink was made by mixing 300 mg of MWCNT and 150 mg of SDBS into 30 mL of DI water. A homogeneous solution was made by sonicating the solution for 30 min using a probe sonicator at 30 W and 40 J

average power and energy, respectively. The ink was used for making the electrodes by spreading 1 mL of the ink on each side of a piece of a copy paper (4 cm x 7 cm) and then dry it in a vacuum furnace for 30 minutes at 120 °C. The coating and drying processes were repeating three times. At the end, strips of (1 cm × 4 cm) were cut and used as the electrodes. For fabrication of SC devices, symmetric electrodes were made based on MWCNT/paper.

Different methods of making photoactive electrodes have been used in this dissertation for designing photoactive supercapacitor and DSSC devices. FTO and FTO/TiO<sub>2</sub> glasses were used as WEs (photoanode).

The active area that used for testing a photoactive supercapacitor device was designated to be a (0.6 cm×0.6 cm). The rest of the surface area was covered using Kapton tape. Conducting polymers (i.e., PANI, and Ppy) were incorporated with synthetic dyes (i.e., MB, MO, and PB) as nanocomposite materials coated on the active surface area by the in-situ self-assembled technique that carried out via chemical or electrochemical deposition methods.

### *3.2.1.1 Conducting Polymer Composites Chemical Deposition Method*

To make a chemical polymerization on the surface of a targeted electrode, the polymerization reaction can be limited by using an oxidant material such as ammonium persulfate (APS) in the solution containing the monomers and the electrodes. Oxidant materials are able to remove electrons from the monomers and link them for the polymerization. As soon as oxidant materials remove the electrons from the monomers, the dimer starts forming going to the oligomer form and finally gets completely oxidized, forming the polymer as shown in Figure 16.

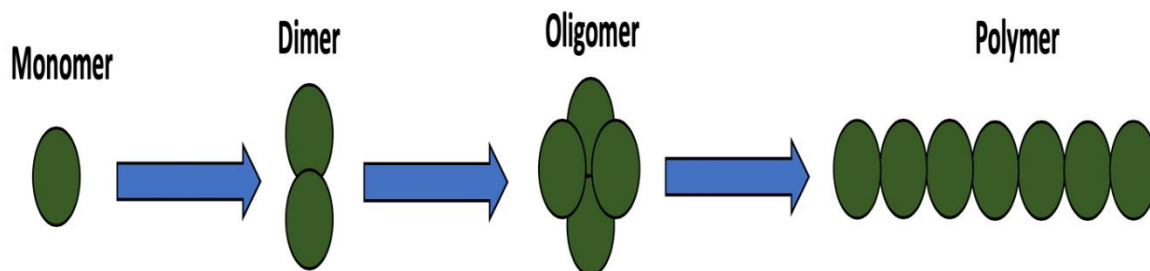


Figure 16: Redox State in a Conducting Polymer Material From Monomer to Oxidized State (Polymer) During Polymerization Process.

In order to make a chemical polymerization to deposit a thin film on the surface of an electrode, four steps of composite materials are needed, which are shown in figure 17. Prior to following these four steps, a very high negatively charged surface is needed. As suggested by Ram et al., the process of making the surface of electrode negatively charged is to take the substrate electrode and deep it in Poly(styrenesulfonate) (PSS) for 24– 48 hours to give a thin one layer of polyelectrolyte (-) negatively charged [102, 103]. Then, through step 1, the monomers of aniline were mixed with HCl under continuous stirring for 30 minutes. After 30 minutes, MB dye was added to the mixture solution for 20 minutes, as shown in Figure 17 step 2. In step 3, APS oxidant material was mixed with the same concentration of HCl in a different beaker. Finally, step 2 and 3 were mixed together to make the polymerization process. After step 4, the treated FTO glass with PSS material was inserted in the beaker, so any positive charge inside the homogenous solution gets attracted to the negative charged FTO glass electrode, and then the polymerization is taking place on the surface of treated FTO substrate to form PANI thin film.

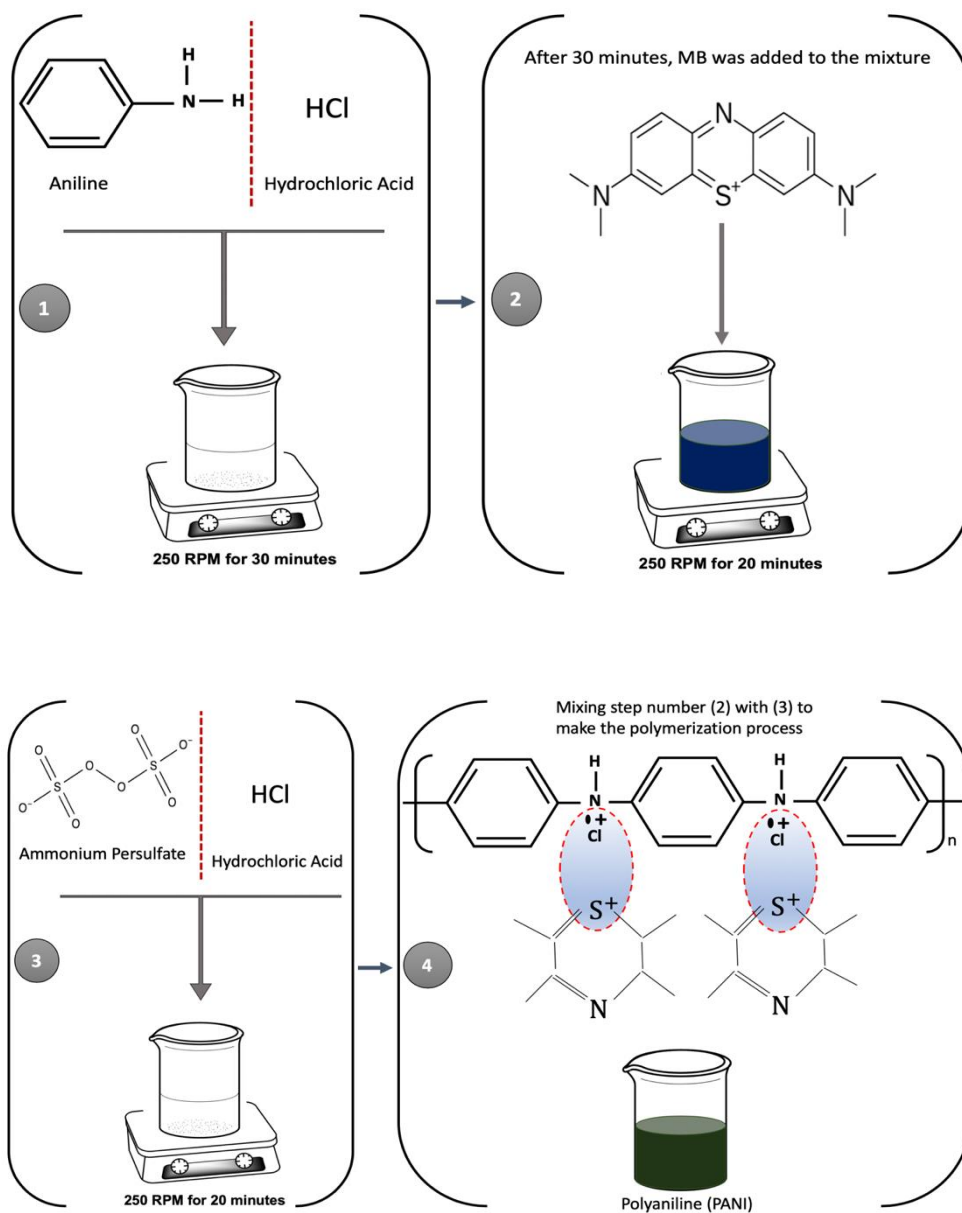


Figure 17: Chemical Deposition Process of PANI Film.

### 3.2.1.2 Conducting Polymer Composites Electrochemical Deposition Method

Electrochemical deposition is another way to oxidize monomers. This technique localized because it can be controlled near the electrode-electrolyte interface. When the potential is applied, the monomers get oxidized, and then two oxidized monomers come together to become dimer and



then take them oxidized to become oligomer and then change the propagation to make the polymer. The oligomer is a combination of few monomers which are not yet oxidized because polymerization needs at least 50,100 or 200 monomers of aniline come together, which called the degree of polymerization. So, when the potential is applied, we are able to oxidize monomers, as shown in Figure 18.

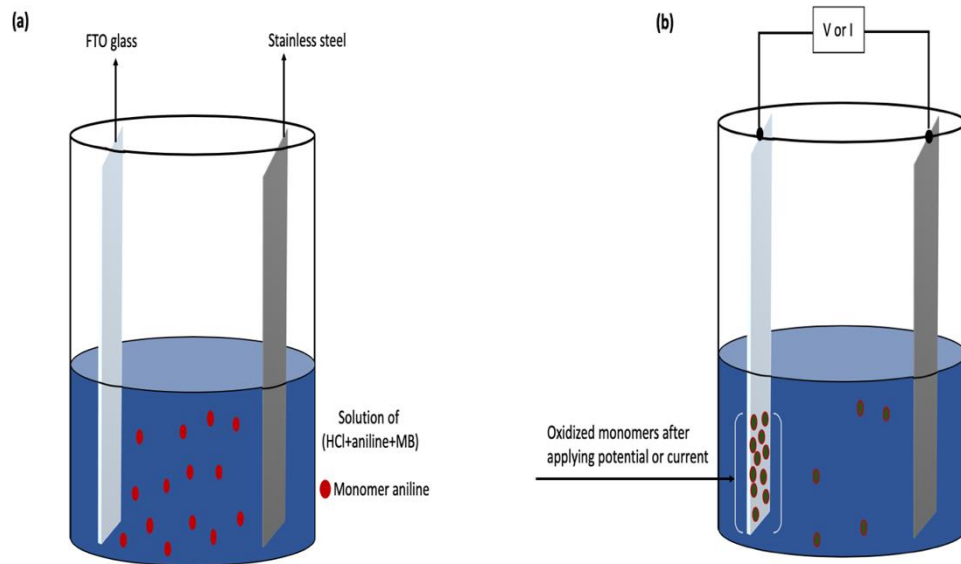


Figure 18: Electrochemical Deposition Process of PANI Film (a) no Potential Effect and (b) Under Potential Effect.

The FTO/ TiO<sub>2</sub> glass coated with titanium dioxide with a size (20 mm × 20 mm) and active area (6 mm × 6 mm) was used for fabrication a photoactive supercapacitor and DSSC as received without cleaning processes. The photoactive electrode of photoactive supercapacitor cell was assembled by following the same techniques as mentioned above.

### 3.2.2 Preparation of Electrolyte

Two types of electrolytes were made for testing the devices, which are liquid electrolyte and gel electrolyte. The liquid electrolytes H<sub>2</sub>SO<sub>4</sub>, H<sub>3</sub>PO<sub>4</sub>, and HCl with different molarity

concentrations have been characterized at room temperature by simply mixing the acid solution with DI water.

Two types of gel electrolytes were made in this dissertation. The first type was made by adding a polymer material (i.e., PVA) with different grams to different acid concentrations in different volumes of DI water. Then, the solution was stirred on hot plate (70°C - 80°C) for 4 hours at different speeds ranging from 250 rpm to 400 rpm. The product was transparent and glue-like gel, followed by cooling down to room temperature. The second type is a composite gel electrolyte made by dissolving PVA polymer in 100 mL of 1 M HCl. Then, the solution was stirred continuously and heated at 75 °C for 6 hrs at a speed of 400 rpm. After that, a 30 ml solution of 0.1 M APS in 1 M HCl was added to the PVA-HCl solution at room temperature and stirred for 30 min at 600 rpm. At last, the composite gel was made by adding 3 ml of aniline to the PVA-HCl-APS at room temperature and stirred for 12 hrs., as shown in Figure 19. The composite gel polymer electrolyte PVA-HCl-PANI-APS was kept in a beaker (covered by a piece of Parafilm) at room temperature for at least a week before the fabrication of the devices.

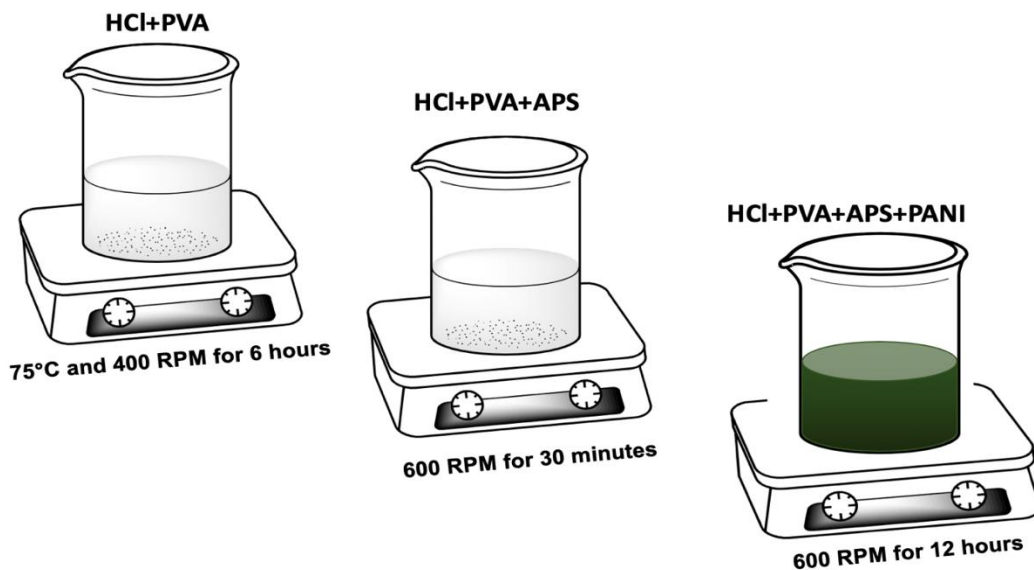


Figure 19: Process of Making PANI Composite Gel Electrolyte.

### 3.2.3 Electrochemical Setup

An electrochemical cell is a sealed container that is designed to block the ingress of air. In general, electrochemical cell is tested in a three-electrode configuration in an electrolyte solution. For fabricating electrochemical cells of EC device based on liquid and gel electrolyte, two-electrodes configurations technique was used. A plastic cuvette ( $1 \times 1 \times 4 \text{ cm}^3$ ) was used to contain 1 mL of the liquid electrolyte solution and then placing the two symmetric MWCNT/paper electrodes inside the cuvette. However, for fabricating the EC device based on gel electrolyte, the first one electrode was laid down on a glass slide. A piece of plastic mesh was soaked into the gel and placed over the electrode. Another glass slide was put over the spacer. The applied gel was covering almost the same area of the electrodes as the wet part of the electrodes in the liquid-based devices. It should be noted that the two-electrodes approach is toward a device study.

All fabricated photoactive supercapacitors cells based on either two or three electrodes were illuminated with the solar simulator (RST300S, Radiant Source Technology), which was equipped with an internal AM 1.0 optical filter, with an incident light intensity of  $80 \text{ mW cm}^{-2}$  at the working electrode's surface. VersaSTAT 4 potentiostat was used to measure the electrochemical and electrical tests, including cyclic voltammetry (CV), electrochemical impedance spectroscopy (EIS), open circuit voltage (OSV) and short circuit current (SCC). The experimental setup, including the dark box and the shutter mechanism, was designed to eliminate the effect of ambient light in the experiment. All devices were placed in the dark box in the beginning to apply electrochemical measurements. Each cell was kept in the dark until the open circuit voltage (OCV) stabilized. For the photocurrent measurements, the same potential was applied to the cell by the potentiostat such that the current in the dark was zero.

When photoactive supercapacitors devices based on three-electrodes were designed, Ag/AgCl electrode was needed as a reference electrode to eliminate the effect of CE and mainly study the reactions only on the surface of the WE by monitoring the potential changes of the working electrode are measured regardless the potential variation that perhaps happens at the counter electrode. Therefore, three-electrodes is mainly for studying the interface between WE and electrolyte. Not only that but also for studying material characterization.

### 3.3 Characterization

#### 3.3.1 Cyclic Voltammetry

Cyclic voltammetry (CV) is the most extremely utilized technique that can deeply investigate the behavior of electrochemical cells by demonstrating the complexity of chemical reactions (i.e., oxidation and reduction) in both forward and reverse directions. The CV is the only method among other voltammetry techniques that is able to obtain physical and chemical properties of electrochemical cells. The CV is an acquiring of beneficial electrochemical analytical information (i.e., redox reactions, adsorption processes, mass transport reactions, and kinetics rate reactions) that is derived from a systematic study by applying constant potential and measuring the current as a function of time [104-106].

The two different mechanisms that occur during the CV measurement are kinetic rate (Butler Volmer) and mass transport. These two mechanisms could happen at the same time, and sometimes one mechanism is stronger than the other. At some point, these two mechanisms get in balance ( $E = E_{peak}$ ), and at that point, the peak has existed, as shown in Figure 20. At  $E = E_{peak}$ , the concentration of the reactant is zero, and the concentration of the product gets to the maximum at the electrode surface.

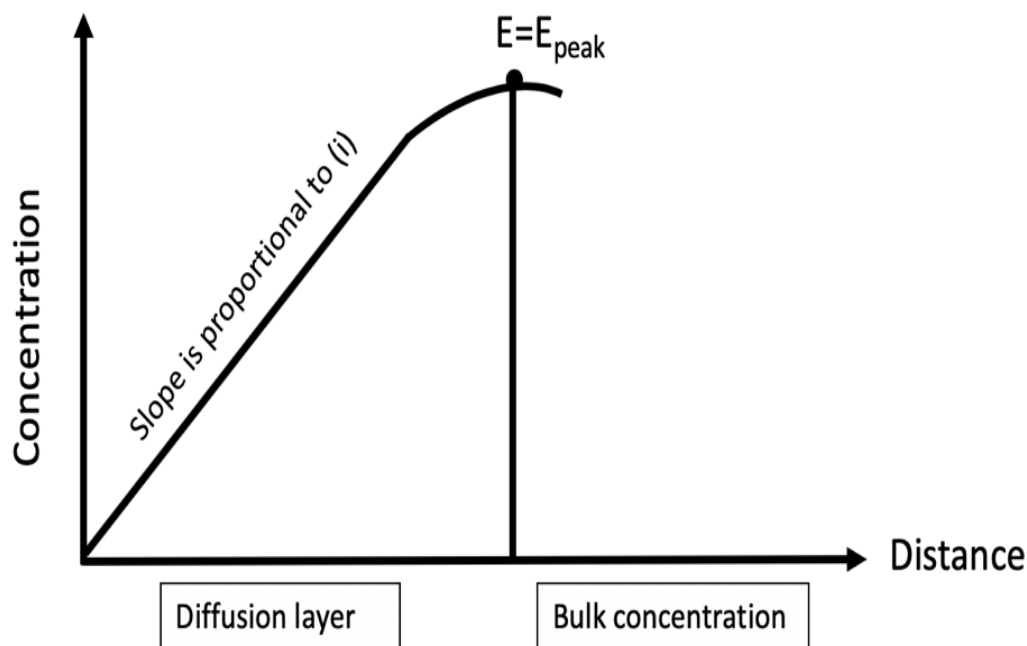


Figure 20: Concentration-Distance Profile at Different Stages of Cyclic Voltammogram.

The slope is proportional to the electric current ( $i$ ) which is equal to:

$$\text{electric current } (i) = \text{rate of ions motion} \times nF \quad (8)$$

$$E = E_{peak} \quad \Rightarrow \quad [O]_{at \ x=0} = \text{Zero}$$

Before reaching the peak, the kinetic rate is dominated, and the current can be calculated by Butler Volmer equation [107]:

$$i = i_o \left( \exp \frac{\alpha n F \eta}{RT} - \exp \frac{(1-\alpha) n F \eta}{RT} \right) \quad (9)$$

$$\eta = E - E_o \quad (10)$$

where  $i$  is the electrode current,  $i_o$  is the exchange current,  $\alpha$  is charge transfer coefficient,  $n$  is number of electrons transferred,  $F$  is Faraday constant ( $\sim 96485 \text{ C mole}^{-1}$ ),  $\eta$  is the overpotential,  $E$  is the cell potential (variable),  $E_o$  is the standard electrochemical potential (constant),  $R$  is universal gas constant ( $8.3144 \text{ J mol}^{-1}\text{K}^{-1}$ ), and  $T$  is absolute temperature (K). So, applying a

potential that is equal to  $E_o$  leads to have zero current based on Butler Volmer equation. It should be noted that the kinetic reaction always happens at the electrode surface at ( $x=0$ ).

When  $E < E_{peak}$ , the kinetic is in control and the current is set by the rate of the reaction. However, when the reaction exists, more agents (oxidant) will be consumed and generated products. Consequently, the diffusion mechanism is needed to supply the consumed agents and keep the current passing through the system. Indeed, diffusion and kinetic rate happen at the same time, but kinetic is in control because diffusion is only following up to whatever kinetic is setting as the rate. The main issue is that when the voltage increases gradually, the current increases exponentially and that corresponded to the consumption of ions per unit of time. Therefore, diffusion cannot follow up anymore because the concentration of ions will be zero and beyond that point, there is no change in terms of concentration. The mass transport (diffusion and migration) is taking place after the peak point, which leads to the drop-down of the slope.

When  $E > E_{peak}$ , more agents will be consumed, and the region of diffusion length will be expanded but consequently, the current will be dropped. The slope will not be sharper, and the current level is dropping down because mass transport process is in control.

When a positive potential ramp is applied to the electrochemical cell, the oxidation reaction at the electrode happens (losing electron). Hence, the oxidation peak at a specific value of potential ( $E_{pa}$ ) is existed due to the raise of anodic peak current ( $i_{pa}$ ). When the applied voltage is switched to a negative direction, cathodic current peak ( $i_{pc}$ ) is observed due to the redox reaction at a given potential ( $E_{pc}$ ). Capacitive current or non-faradic current is not associated with any chemical reaction. Capacitive current is related to the electrical charges on the electrode/electrolyte interface. Faradic current is the current caused by the chemical reactions (i.e., oxidation or reduction) at the electrode surface, as shown in Figure 21. This substantial characteristic makes

this method to be the most adequate technique for studying electroactive substance (i.e., oxidation or reduction).

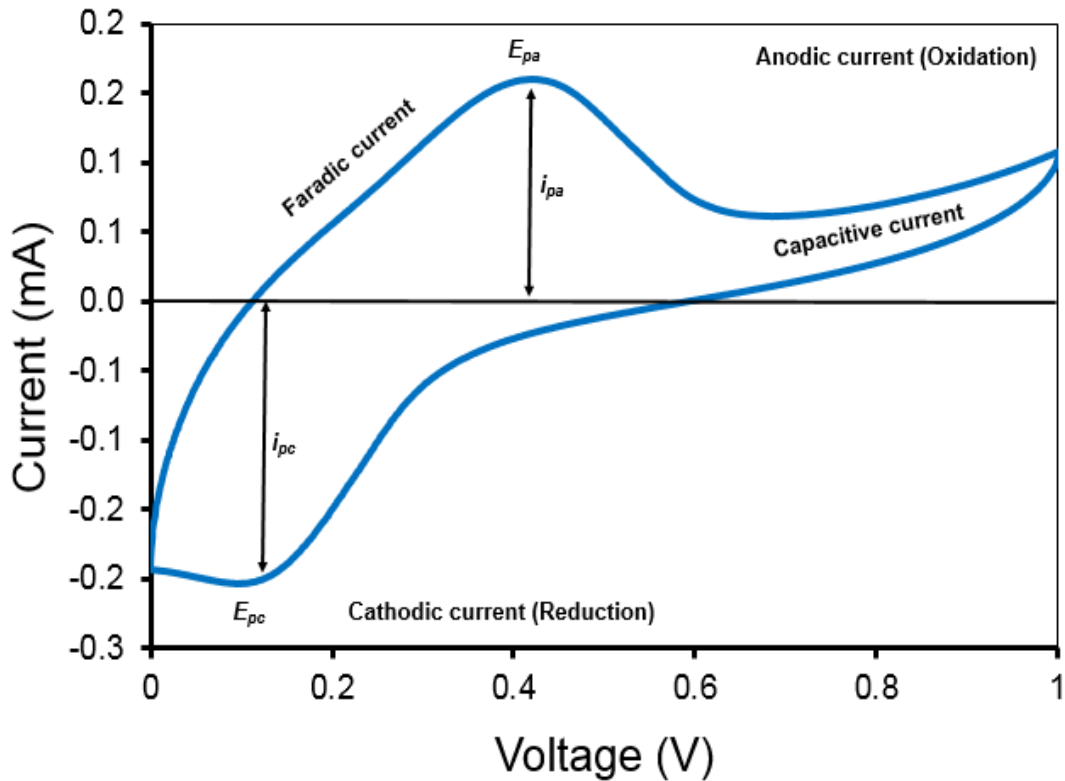


Figure 21: Cyclic Voltammogram Shape of Electrochemical Reaction.

### 3.3.2 Galvanostatic (Chronopotentiometry)

The persistence variation of electrode potential through a CV measurement causes a complicated response of the substantial quantities (i.e., Voltage, V and Current, I), more specifically current intensity. Therefore, to ease the study to be more efficient, it is preferable to rectify one of the electrical parameters such as V and I [108]. There are two studies associated with the interpretation of the V and I, which are chronoamperometry and Galvanostatic or chronopotentiometry. Chronoamperometry is controlling the potential and measuring the spontaneous variation of the faradic flow current over time. In fact, it is a matter of studying the stability over time of the electrochemical device. However, chronopotentiometry is one of the

electrochemical techniques that used to control the applied current pulses and to monitor the variance voltage as a function of time. Indeed, it is more beneficial for studying the characterization and the breakdown point of voltage. Also, it measures the capacity of the electrochemical system. Chronopotentiometry will give a systematic study on electrode stability [31, 109]. The equivalent series resistance (ESR) can be calculated by Ohm's law via applying the chronopotentiometry measurements on the electrochemical cell which will present the voltage drop in current pulses [110].

$$ESR = \frac{\Delta V}{2 \times I} \quad (11)$$

where  $\Delta V$  is the voltage drop across the cell and  $I$  is the amplitude of the current pulse.

### 3.3.3 Electrochemical Impedance Spectroscopy

Electrochemical impedance spectroscopy (EIS) analysis is performed to identify between more than two electrochemical reactions and understand the nature of the electrode/electrolyte interfaces [111]. EIS can be measured by applying a small AC sinusoidal signal (i.e. Potential or Current) to an electrochemical cell over the frequency range at 0.0 V DC biasing. EIS is a powerful technique that can go with very low frequencies values to investigate deeply any electrochemical system to have a very small perturbation. Hence, all the information of electrochemical cells under EIS test can be gleaned [112, 113]. EIS measurements are usually represented by Nyquist plots to show the imaginary impedance versus the real impedance and Bode plots to represent the magnitude of the impedance and phase angle over the frequency range. In addition, EIS can explain numerous electronic properties of electrochemical cells, for instance, charge transfer resistances, electrolyte resistance, capacitance, diffusion coefficients, electron transfer, and pore sizes [114].



An electrochemical cell can be modeled to estimate the value of each element from the impedance results. The software that has been used called EIS Spectrum Analyzer software (version 1.0). This software has the ability to find the best fit for the experimental data and representing the results in the form of equivalent electrical circuit model (Figure 22), which is called the Randle model. From figure 22, at high frequency, the kinetic rate is in control, and at low frequency diffusion process is in control. Where  $C_{dl}$  is a double layer capacitor,  $Z_w$  is a diffusion,  $R_s$  is the overall series resistance, and  $R_{ct}$  is the charge transfer resistance.

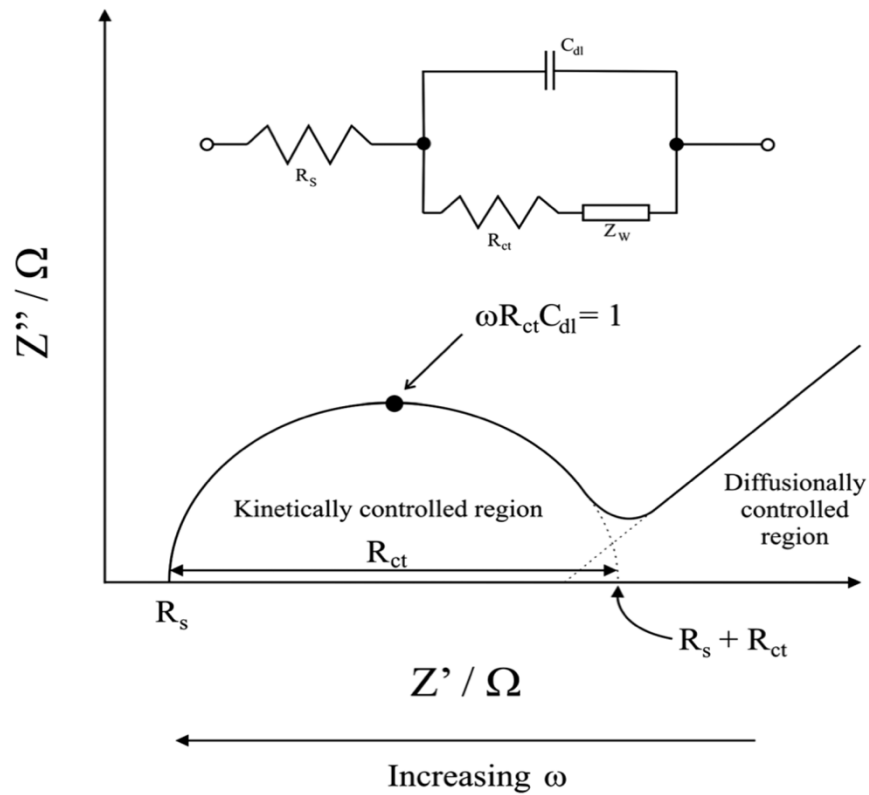


Figure 22: Randle Circuit Model of Electrochemical Cell [114].

### 3.3.4 Open Circuit Voltage

Since a photoactive supercapacitor and solar cell devices were fabricated in this dissertation, open circuit voltage measurement ( $V_{oc}$ ) is needed to evaluate the performance of

photoelectrochemical devices and the capability of the devices for solar energy harvesting.  $V_{oc}$  measurement is reading the voltage over the cell when the current passing through the cell is zero. For photoactive supercapacitor, the  $V_{oc}$  is monitored under dark and light conditions. From Randle circuit (Figure 23),  $V_{oc}$  can be calculated since the total current  $i$  in the circuit is given by:

$$i = I_C + I_{R_{ct}} \quad (12)$$

where  $I_C$  is the current passing via  $C_{dl}$  and  $I_{ct}$  the leakage current passing through  $R_{ct}$ . In open circuit mode, the supercapacitor is self-discharging and  $i = 0$ , since  $(I_C = -C \frac{dv}{dt})$  and  $(I_{R_{ct}} = \frac{V}{R_{ct}})$

the equation becomes:

$$0 = \frac{V}{R_{ct}} - C \frac{dv}{dt} \quad (13)$$

Thus, the voltage can be obtained by:

$$V = R_{ct} \times C \frac{dv}{dt} \quad (14)$$

where  $V$  is the  $V_{oc}$  at a given time and  $\frac{dv}{dt}$  is the slope of the self-discharge curve.

In solar cell devices, there are four fundamental quantities for evaluating the performance of solar cells, which are open circuit voltage ( $V_{oc}$ ), short circuit current ( $I_{sc}$ ), fill factor (FF), and efficiency ( $\eta$ ). The easiest way to find and calculate these parameters is with an I-V curve, as shown in Figure 11.

### 3.3.5 Short Circuit Current

Short circuit current measurement ( $I_{sc}$ ) is a primary study to investigate photoelectrochemical devices.  $I_{sc}$  measurement is monitoring the current passing through the cell when the voltage over the cell is zero.  $I_{sc}$  is completely relying on the light intensity because  $I_{sc}$  is proportionally related to the number of electrons that are generated by the light. Therefore, the

generated current is standing for the  $I_{sc}$ . As a matter of fact,  $I_{sc}$  is an accumulation of both light and dark current. However, due to the minimal value of current under the effect of dark,  $I_{sc}$  is fairly the generated current under light condition.

### 3.3.6 Scanning Electron Microscopy

Scanning electron microscopy (SEM) remains as one of the greatest tools of material characterization to study the topography and morphology of the sample's surface. In this dissertation, SEM images were taken for supercapacitor electrodes (i.e., MWCNT/paper) by scanning the electrode surface with a beam of electrons using SEM S800, Hitachi. The SEM image shows how CNTs have been infused to the fibers of the paper. The porosity and diameter of the CNT were observed as well.

### 3.3.7 Raman Spectroscopy and Fourier Transform Infrared Spectroscopy

Raman spectroscopy and Fourier Transform Infrared (FTIR) are the most widely used characterization techniques for distinguishing the functional groups in the materials by absorbing the beam of infrared (IR) radiation. Both characterizations are totally providing vibrations that are widely utilized for the locating of molecular bonds, and every bond has a different vibrational frequency [115, 116]. In the current dissertation, the FTIR study was done to learn about the interaction of the polymer matrix of PVA with the oxidant materials (i.e., APS and PANI). FTIR results showed several peaks due to functional groups such as hydroxyl, carboxyl, and carbonyl. Raman results showed benzenoid (polaronic and bipolaronic structures in the PANI) and quinoid (a mixed mode of the C=N and CH=CH stretching vibrations) structures of PANI material [107, 117].

### 3.3.8 UV-visible Spectroscopy

UV-vis spectroscopy is a beneficial technique to study the optical and electronic properties of materials and measure the absorption of light when it comes through a substrate. Absorption light is completely relying on the excitation process of the electron from the HOMO level to the LUMO level. Increasing the wavelength of absorption is linked with the energy that is needed for the excitation process. Furthermore, less energy is leading to have a high wavelength of absorption, and extra energy is ended up with a short wavelength of absorption [118]. It can also be used for characterizing the materials with different tests such as absorption, transmission, or reflectiveness.

## 3.2 Instruments

### 3.2.1 Potentiostat

A potentiostat is a powerful electronic instrument that dominates the potential difference between either two or three electrodes of an electrochemical cell. VersaSTAT 4.0 potentiostat (Figure 23) is the instrument that used for all the electrochemical experiments. It works by controlling the potential and monitoring the flowing current between working and counter electrodes. A potentiostat measurement can be carried out with two setups of configuration, namely two-electrodes configuration and three-electrodes configuration. In the two-electrodes configuration, an applied potential is measured between the working and counter electrode, and the output current is measured in either working or counter electrode. The counter electrode in this configuration allows the current to pass to complete the electrochemical cell and spontaneously preserves a constant potential. In the three-electrode configuration, the reference electrode eliminates the effect of the counter electrode and the results mainly focusing on the working

electrode. The counter electrode in this configuration lets the current pass through it to complete the circuit.



Figure 23: VersaSTAT 4 Potentiostat Instrument.

### 3.2.2 Solar Simulator

A solar simulator (RST - Radiant Source Technology) (Figure 24) connected with an external dark box via an optical fiber was utilized as a setup for measuring the performance of the photoelectrochemical devices (i.e., Photoactive supercapacitors and DSSC). The solar simulator provides an output power intensity of  $80 \text{ mW cm}^{-2}$ , which was equipped with an internal AM 1.0 optical filter. The purpose of this instrument is making the indoor test for photoelectrochemical cells.

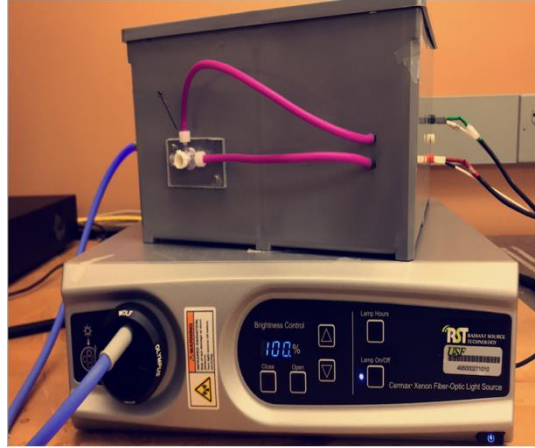


Figure 24: Solar Simulator Instrument.

### 3.2.3 Keithley

Keithley source meter (model 2602) (Figure 25) is used to measure the conductivity with a 4-probe setup (Figure 26). The 4-probe method is one of the best techniques that eliminate the contact resistance to get the sample resistance only by using four aligned probes. 1 mA is the current value that used to run the experiment. The flow current is passing through the outer probes, and the voltage is recorded between the two inner probes. Then, the conductivity of the sample calculated, and the resistivity is the reciprocal of conductivity [119].



Figure 25: Keithley 2602A Device.

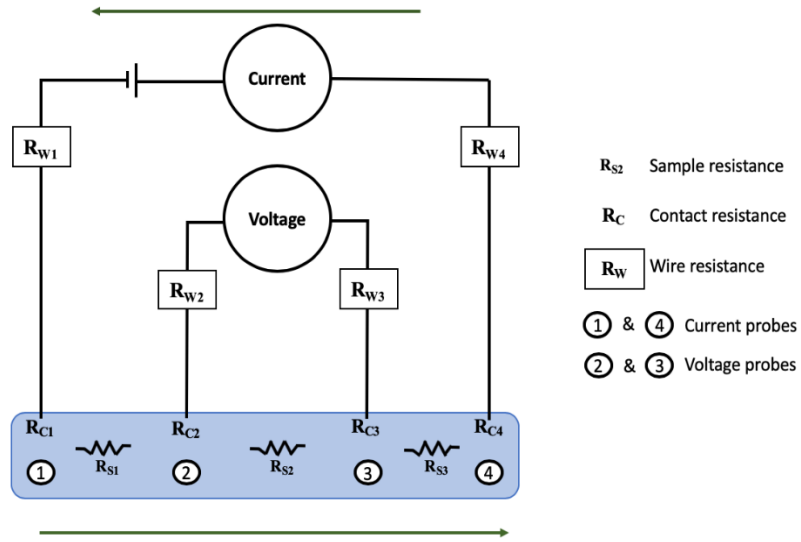


Figure 26: 4-Point Probe Instrument.

### 3.2.4 Dicing Saw

Dicing Saw Machine (MA1006) (Figure 27) was used for cutting the FTO glasses with a high-speed spindle-shaped with a very thin diamond blade to dice, cut, or groove numerous of substrates such as silicon wafers, glass, ceramic, crystal, and etc. For cutting the FTO glasses, the program was set with 1.9 mm thickness, 90 angle, 1 mm/sec feed speed, 142 mm diameter, and 30000 RPM spindle speed.

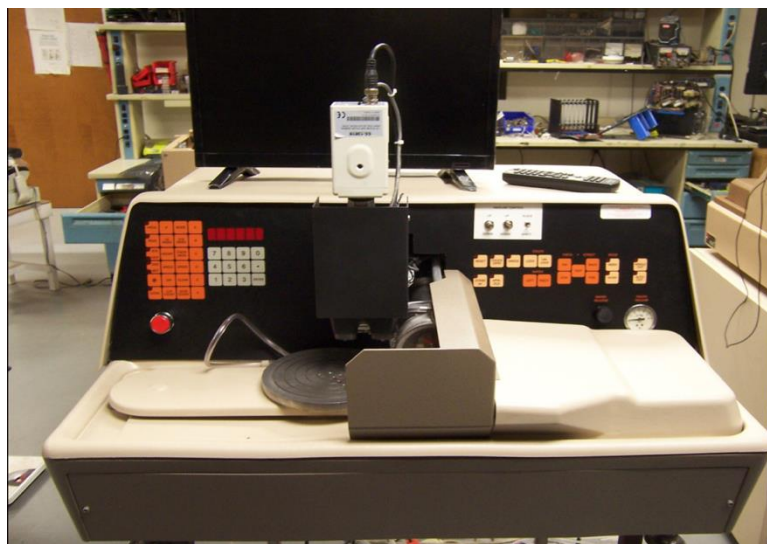


Figure 27: Dicing Saw Machine.

### 3.3 Conclusion

In this chapter, concisely all the chemical materials, methods, electrochemical techniques, and instruments that were used for the fabrication of all the studied electrochemical and photoelectrochemical cells are addressed. In the following chapters, the electrochemical materials and methods are presented in detail in the experimental section of each chapter.



## Chapter 4: Gel Electrolyte Based Supercapacitors with Higher Capacitance and Lower Resistance than Devices with a Liquid Electrolyte<sup>1</sup>

### 4.1 Abstract

Recently, gel polymer electrolytes (GPEs) have been drawn noteworthy attention for different applications, specifically, for supercapacitors. GPEs could become an excellent substitute to liquid electrolytes (LEs) for making flexible and more durable devices. The performance of two different electrolytes (GPEs and LEs) in multi-wall carbon nanotube based supercapacitors were investigated. In spite of significantly lower conductivity of GPEs than LEs, devices with the gel electrolyte presented a superior performance. More focused has been given in this work on demonstrating the performance of supercapacitors based on GPEs and LEs at different concentrations of the acids ranging from 1M to 3M. Both electrolytes have been characterized at room temperature by making supercapacitors and using cyclic voltammetry, charging-discharging, electrochemical impedance spectroscopy, and leakage tests. The experimental results showed that GPE devices had much better capacitances and resistances compare to the LE based devices. Moreover, the capacitances of all devices were increased proportionally with the increase in the concentration from 1M to 3M, and the resistances were increased inversely with the decreased of concentration. The promising results from the gel electrolytes is encouraging for further development of flexible and high capacitance energy storage devices.

---

<sup>1</sup>This chapter was before published in MRS proceedings (Aljafari, B., & Takshi, A. (2018). Gel electrolyte based supercapacitors with higher capacitances and lower resistances than devices with a liquid electrolyte. MRS Advances, 3(22), 1261-1267). Permission is included in Appendix A.

## 4.2 Introduction

Electrical double layer capacitors (EDLCs) are one type of many important energy storage devices with good features such as high-power density, long life time, high specific capacitance, environmentally friendly and fast charging-discharging [120]. The true challenge is to design and develop reliable, safer, and high performance GPEs for flexible supercapacitors without leakage problem. Up to date, liquid electrolytes have been used in making supercapacitors. However, due to the imperfections of using liquid electrolytes, replacing them with gel polymer electrolytes, which have been developed rapidly, will stop corrosion and leakage of electrolytes and will boost the reliability of the supercapacitor devices [62]. Gel polymers composed of a polymer network and solvents that wrap the liquid and block it from leakage. In fact, it plays the role of a vessel that can hold a significant amount of trapped solvent and possesses the characteristics of both liquids and solids [121]. Polyvinyl alcohol (PVA) is a synthesized water-soluble polymer, and a candidate for water-based PGEs due to relatively low cost, environmental-friendliness and safety [122]. Many PVA based PGE systems have been developed and shown promising results. The chemical structure of the PVA as (partially hydrolyzed and fully hydrolyzed) is shown in Figure 28. Most the researches and results show the superiority of using gel electrolytes comparing with liquid electrolytes. The articles from [81, 123, 124] demonstrated the high rate of cyclability and the high ionic conductivity of using gel electrolytes based on PVA. In this work, four devices have been made with the same type of electrodes using multiwall carbon nanotubes (MW-CNTs) but with different types of electrolytes such as  $H_2SO_4$ -PVA and  $H_3PO_4$ -PVA gel electrolytes;  $H_2SO_4$  and  $H_3PO_4$  liquid electrolytes. In fact, more attention in this experiment has been taking toward the concentration of acid electrolyte on both devices that based on liquid and gel electrolytes. To understand the relationship between the acid electrolytes and the electrochemical performance of

all devices based liquid and gel electrolytes, electrolytes with acid concentrations from 1M to 3M were studied.

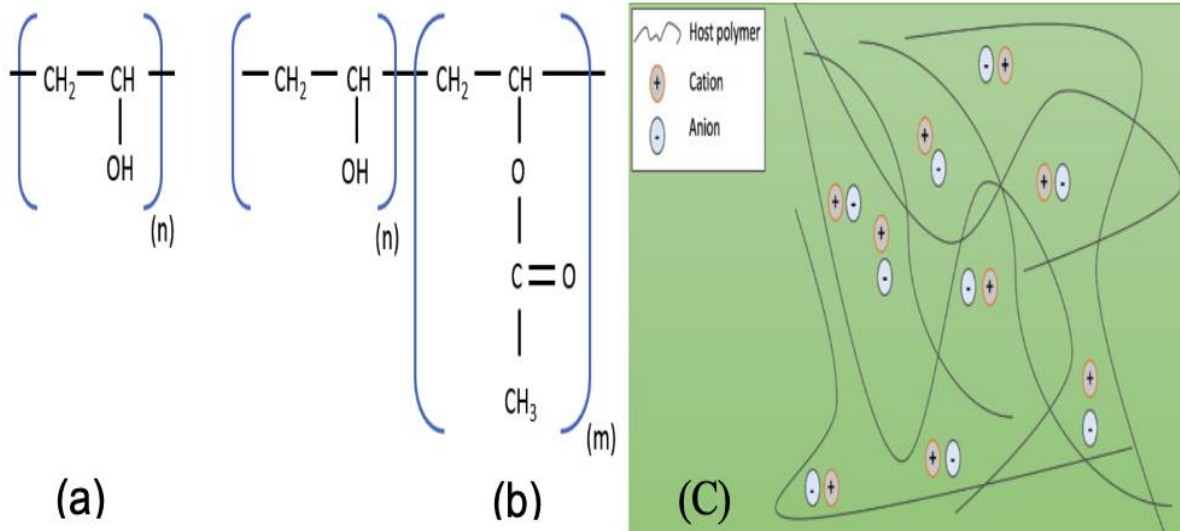


Figure 28: Structural Formal for PVA: (a) Fully Hydrolyzed; (b) Partially Hydrolyzed [125]and (c) Gel Polymer Electrolyte.

### 4.3 Experimental Details

Polyvinyl alcohol (PVA), multi-walled carbon nanotube (MW-CNT), sodium dodecyl benzenesulfonate (SDBS), sulfuric acid ( $H_2SO_4$ ), and phosphoric acid ( $H_3PO_4$ ) were the materials used in the experiments, and they all were purchased from Sigma-Aldrich. The electrodes were fabricated by making a conductive ink and spreading the ink on a piece of paper (Office Depot). The ink was made by adding 300 mg of MW-CNT and 150 mg of SDBS into a tube that contained 30 mL of DI water. Then, the ink was sonicated by the probe sonicator for 35 minutes. Afterward, the ink was spread on a normal sheet of paper and then put it in a furnace for 35 minutes at 120 °C. The concentration of the ink on the paper was 3 mL on both sides.

In a simple way, liquid electrolytes were made by adding acids ( $H_2SO_4$  or  $H_3PO_4$ ) into 15 mL of DI water to make different concentrations ranging from 1.0 M to 3.0M. For the gel electrolytes, 2 grams of PVA powder was added to 15 mL of DI water with different acid

concentrations ranging from 1M to 3M which was the same molarity as the liquid electrolytes. Then, all the mixtures were continuously agitated along with moderate heating with the same degree (70°C) and the same time (5 hours) at the speed of 250 rpm so that uniform gels were made.

#### 4.4 Discussion

Electrochemical performance of the devices was studied by cyclic voltammetry (CV), charge/discharge tests and electrochemical impedance spectroscopy (EIS). All of the measurements were carried out in a two-electrode configuration.

##### 4.4.1 Cyclic Voltammetry

The effect of acid concentration was studied over all the devices with the potential range from +1.0 V to -1.0 V and 50 mV.s<sup>-1</sup> scan rate by the measurements of cyclic voltammetry (CV). As can be seen in Figure 29.a and 29.b the width of the loops at 0.0 V for both devices with H<sub>2</sub>SO<sub>4</sub> and H<sub>3</sub>PO<sub>4</sub> liquid electrolytes were decreasing drastically by lowering the acid concentration as shown in Figure 29. This indicates larger double layer capacitances in the devices that had higher concentration of acids. Also, there was no visible redox peak in their CV results. The maximum capacitance was observed at 3M concentration with the supercapacitors that based on H<sub>2</sub>SO<sub>4</sub>, which was C=26.95 mF calculated from C=current width at zero voltage/ (2\*scan rate). The concentration of greater than 3M of the acid electrolytes was obviated by reason of the peel off of the electrode material from the substrate paper. Unlike the liquid electrolytes, the effect of acid concentration on the capacitance was significant in the devices with the gel electrolytes. Particularly, the H<sub>2</sub>SO<sub>4</sub>-PVA based device with 2 M acid concentration showed the highest capacitance, while both higher and lower H<sub>2</sub>SO<sub>4</sub> concentrations. The reason for reaching the

maximum capacitance at a specific concentration is not known. Such a local maximum was not observed in the device with  $\text{H}_3\text{PO}_4$ -PVA electrolyte, but the capacitance showed significantly higher value (62.41 mF) when the acid concentration was 3M. The capacitance values for all devices are listed in Table 7.

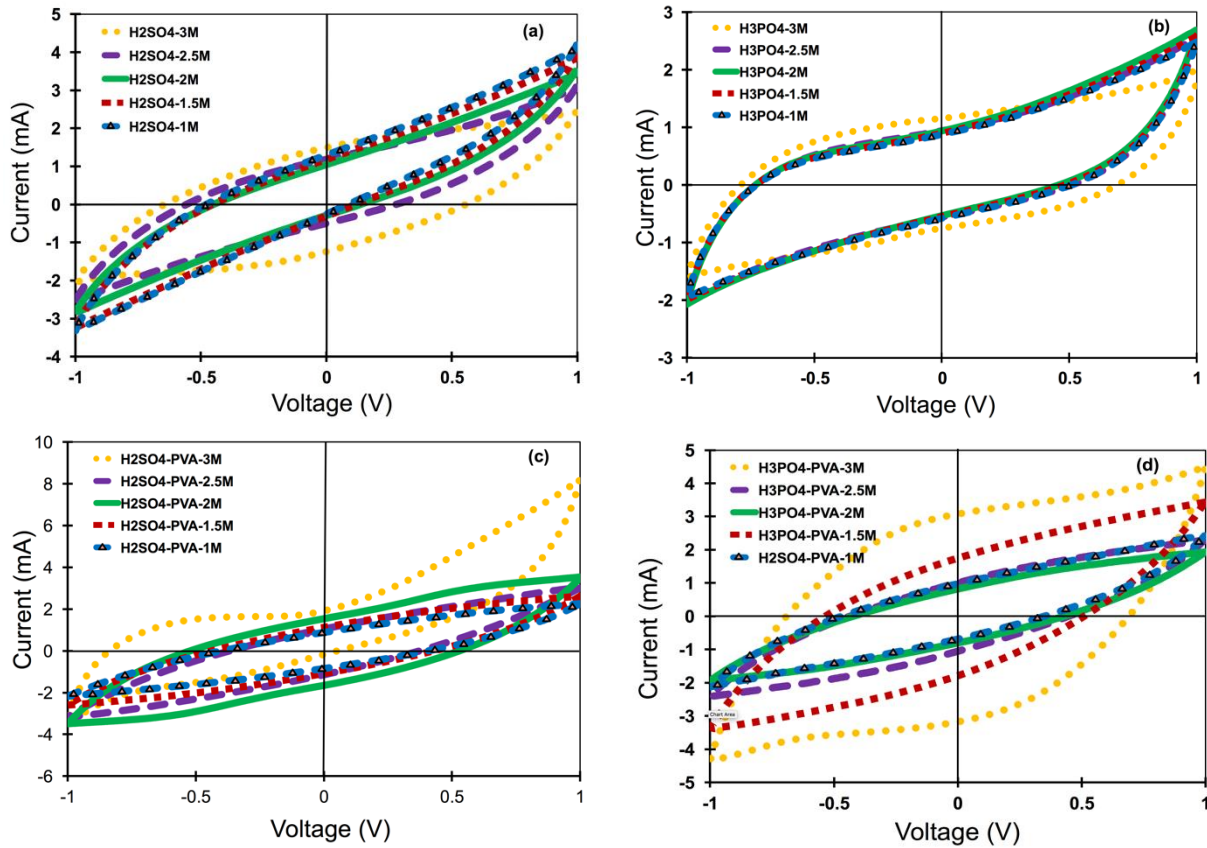


Figure 29: Cyclic Voltammetry (CV) Results of Devices with (a)  $\text{H}_2\text{SO}_4$  Liquid, (b)  $\text{H}_3\text{PO}_4$  Liquid, (c)  $\text{H}_2\text{SO}_4$  Gel, and (d)  $\text{H}_3\text{PO}_4$  Gel Electrolytes with Different Concentrations of the Acids.

#### 4.4.2 Charging-Discharging

The charging-discharging cycling was applied to examine the performance of the fabricated supercapacitors. The devices were charged by applying an alternative pulse current  $I=1$  mA for 10 seconds' duration to charge and  $-1$  mA for the same time to discharge them. The results of charging-discharging experiment represented non-linear curves voltage profile during the

charging and discharging cycles as seen in Figure 30. Meanwhile, the curves of the charging and discharging process were nearly symmetric in the potential range, which represented a high reversibility. The voltage drop ( $\Delta V$ ) in the initial voltage atop discharge is due to the equivalent series resistance (ESR) of the supercapacitors that is calculated from  $ESR = \Delta V / (2 * I)$ . The ESR values are listed in Table 7. As expected, ESR was increased with the acid concentration decrease, due to lower conductivity of the electrolyte at lower concentrations.

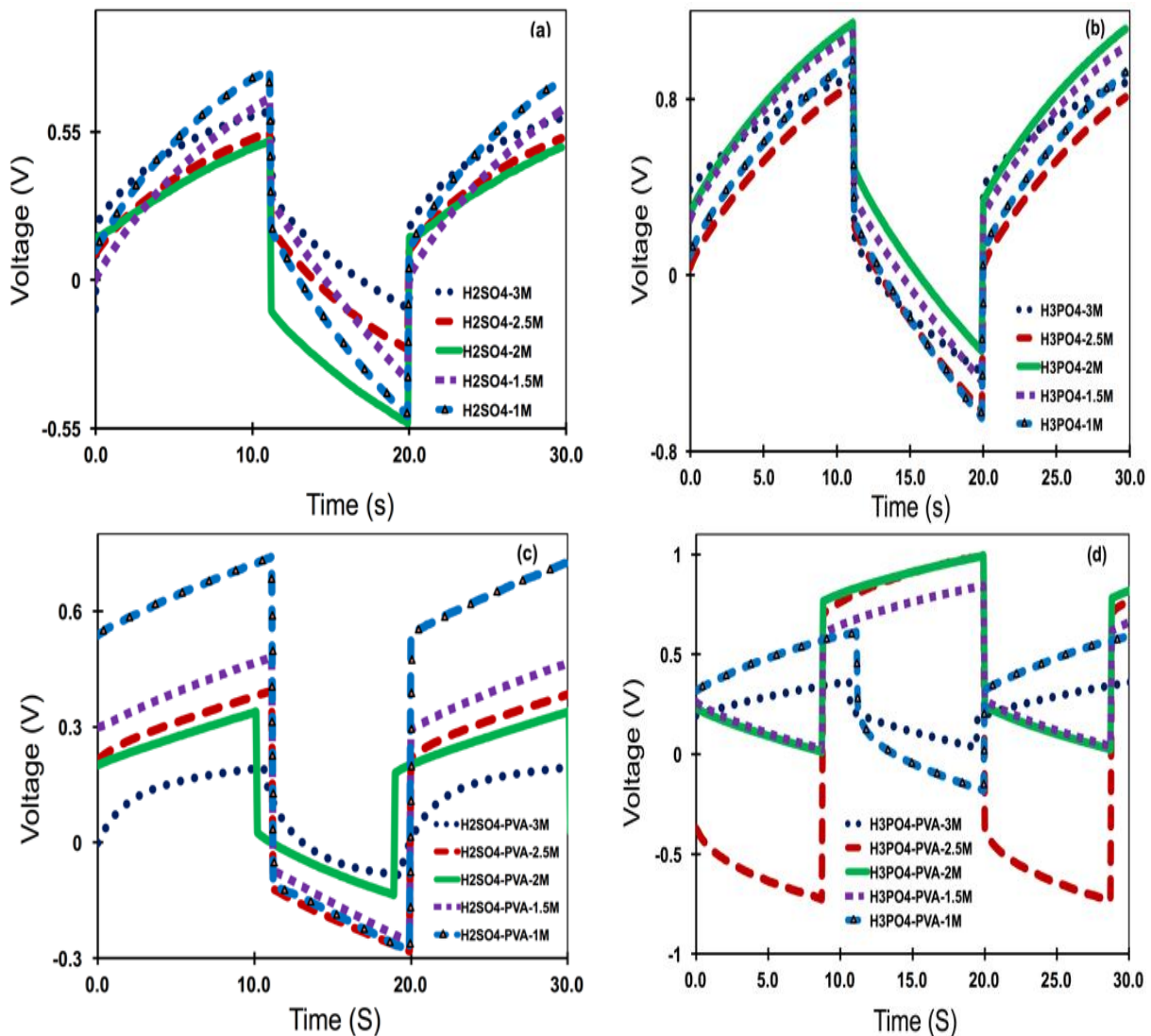


Figure 30: Charging and Discharging Results of Devices with (a) H<sub>2</sub>SO<sub>4</sub> Liquid, (b) H<sub>3</sub>PO<sub>4</sub> Liquid, (c) H<sub>2</sub>SO<sub>4</sub> Gel, and (d) H<sub>3</sub>PO<sub>4</sub> Gel Electrolytes with Different Concentrations of the Acids.

Table 7: Capacitance and ESR Values of the Devices Based on Liquid and Gel Electrolyte at Different Acid Concentrations.

	Liquid				Gel			
	H <sub>2</sub> SO <sub>4</sub>		H <sub>3</sub> PO <sub>4</sub>		H <sub>2</sub> SO <sub>4</sub>		H <sub>3</sub> PO <sub>4</sub>	
Molarity	(mF)	ESR(Ω)	C (mF)	ESR(Ω)	C (mF)	ESR(Ω)	C (mF)	ESR(Ω)
3.0	26.95	157	19.13	330.5	20.86	14.7	62.41	74.2
2.5	16.93	178.8	14.99	335	22	256.7	20.42	712.4
2.0	13.72	179.64	14.67	338.5	31.75	158.3	16.31	376.1
1.5	14.99	181.25	14.42	374	22	277.8	35.75	273.2
1.0	15.66	297.5	14.42	379	17.25	427.3	16.59	184.5

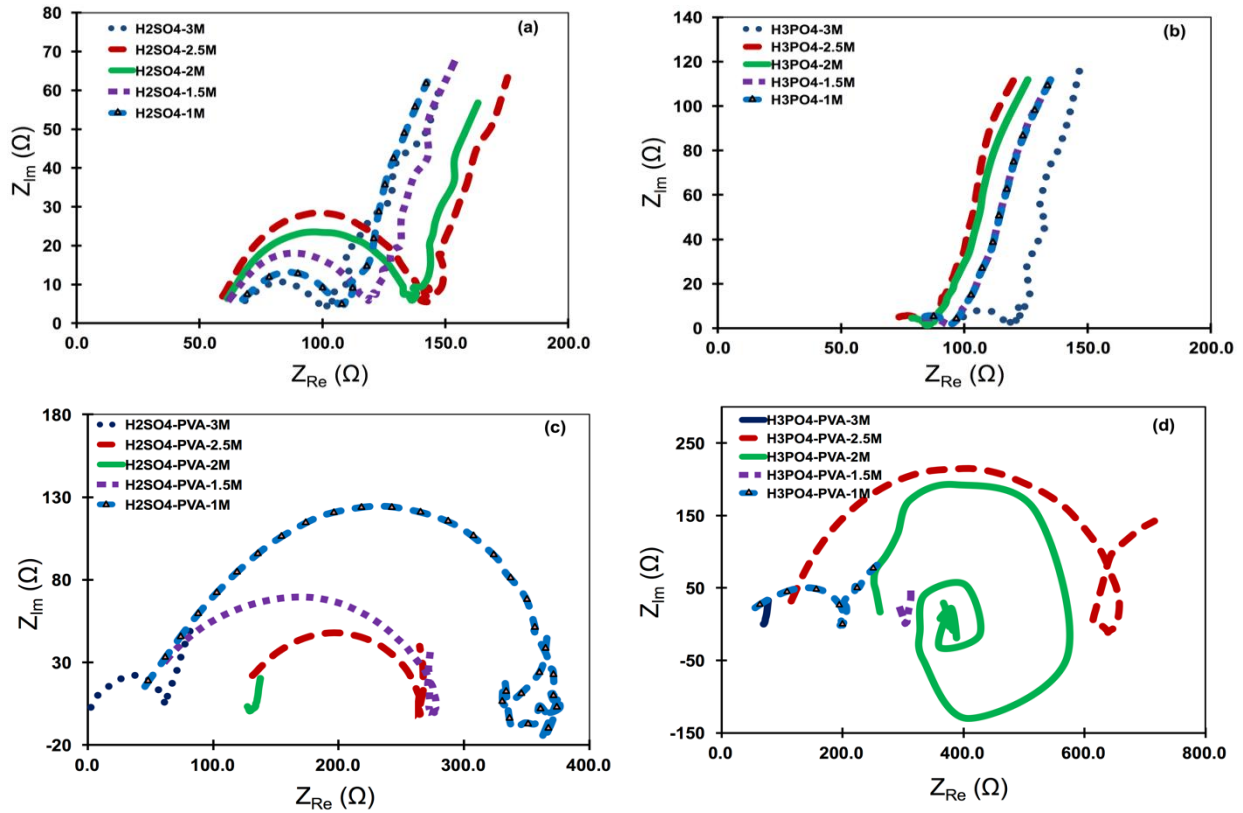


Figure 31: Nyquist Plots of the EIS Results From Devices with (a) H<sub>2</sub>SO<sub>4</sub> Liquid, (b) H<sub>3</sub>PO<sub>4</sub> Liquid, (c) H<sub>2</sub>SO<sub>4</sub> Gel, and (d) H<sub>3</sub>PO<sub>4</sub> Gel Electrolytes with Different Concentrations of the Acids.

#### 4.4.3 Electrochemical Impedance Spectroscopy (EIS)

EIS analysis of EDLCs was performed to reveal the effect of acid concentration on the small signal model of the devices. As shown in Figure 31, for the devices with the liquid electrolyte the standard semi-circle with a tail is observed at the different acid concentration, but the gel based devices showed different responses which implies that the acid concentration affects the gel properties significantly. This calls for further study of the electrical properties of the gels at different acid concentrations.

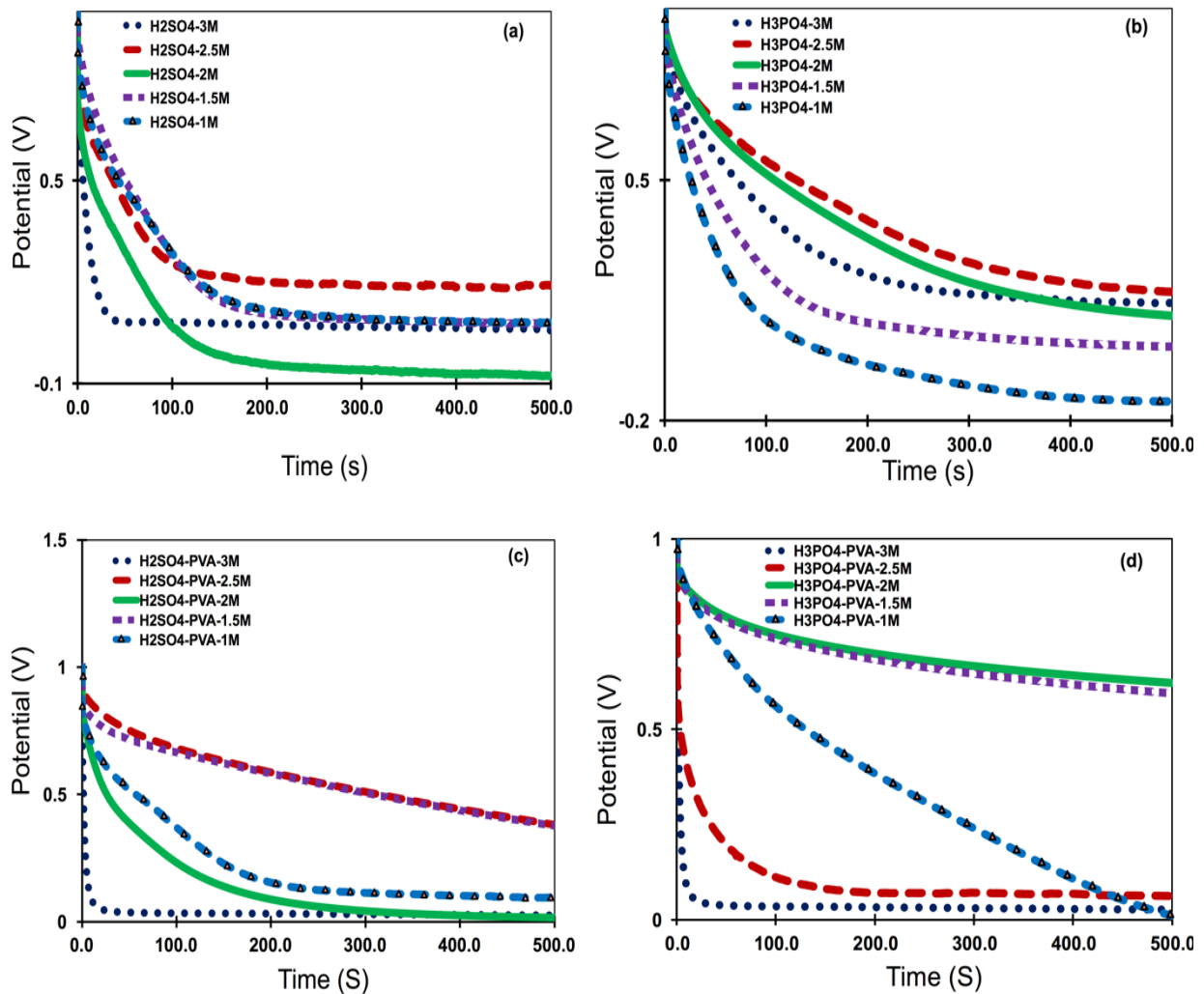


Figure 32: Open Circuit Voltage After Charging Devices with (a) H<sub>2</sub>SO<sub>4</sub> Liquid, (b) H<sub>3</sub>PO<sub>4</sub> Liquid, (c) H<sub>2</sub>SO<sub>4</sub> Gel, and (d) H<sub>3</sub>PO<sub>4</sub> Gel Electrolytes with Different Concentrations of the Acids to 1.0V.



#### 4.4.4 Leakage Study

The leakage in the devices were studied by applying 1.0 V to each device until the current reached to a stable value. Then the open circuit voltage drop was recorded. The results in Figure 32 shows the open circuit voltage of the devices. Among all, it is found that H<sub>3</sub>PO<sub>4</sub>-PVA with 1.5 M and 2.0 M acid was the best. In the other hand, 3M acid in both gel device presented the worst leakage situation, reflecting the importance of the acid concentration in the PVA based gel electrical properties.

#### 4.5 Conclusion

In conclusion, the different acid concentrations of both gel and liquid electrolytes based EDLCs have been demonstrated. By addressing the electrochemical performance of the EDLCs with symmetric MW-CNT electrodes and different acids, the H<sub>2</sub>SO<sub>4</sub>-PVA and H<sub>3</sub>PO<sub>4</sub>-PVA gel electrolytes stand out as operating better than the H<sub>2</sub>SO<sub>4</sub> and H<sub>3</sub>PO<sub>4</sub> liquid electrolytes. However, the highest capacitance for the H<sub>2</sub>SO<sub>4</sub>-PVA device showed a local maximum for the 2.0 M H<sub>2</sub>SO<sub>4</sub> concentration. Additionally, 3M concentration of acids in the gel devices showed very high leakage current. These results reflect the benefits of using the gel type electrolytes and suggests further study of the electrical properties of the gel electrolytes at different acid concentrations.

## Chapter 5: Polyvinyl Alcohol-Acid Redox Active Gel Electrolytes for Electrical Double Layer Capacitor Devices<sup>2</sup>

### 5.1 Abstract

Since the mechanism of charge storage in electrical double layer capacitors (EDLCs) relies on diffusion of ions into the pores of the electrodes, in general, a much lower capacitance is expected for gel based electrolytes than liquid electrolytes. However, in this work, we have found that the specific capacitance in gel based electrolytes made of polyvinyl alcohol (PVA) and an acid ( $\text{H}_2\text{SO}_4$  or  $\text{H}_3\text{PO}_4$ ) is even higher than the specific capacitances of similar devices with liquid acid-based electrolytes. We have discovered that the reason is due to the gel being a redox active material with the capability of charge storage in the volume of the electrolyte. In this work, solid-state and flexible devices with both  $\text{H}_2\text{SO}_4$ -PVA and  $\text{H}_3\text{PO}_4$ -PVA electrolytes were fabricated and characterized. The cyclic voltammetry (CV) and electrochemical impedance spectroscopy (EIS) methods were applied to estimate the capacitance associated to the gel electrolytes. Also, a relatively high cycling stability of 97.5% for  $\text{H}_2\text{SO}_4$ -PVA and 95% for  $\text{H}_3\text{PO}_4$ -PVA was obtained after 1000 charging-discharging cycles. A mechanism of charge storage is proposed to explain the redox active behavior of the gel electrolyte. The presented results are promising for employment of PVA gel electrolytes in some low-cost applications.

---

<sup>2</sup>This chapter was prior published in Solid State Electrochemistry Journal (Aljafari, B., Alamro, T., Ram, M. K., & Takshi, A. (2019). Polyvinyl alcohol-acid redox active gel electrolytes for electrical double-layer capacitor devices. Journal of Solid State Electrochemistry, 23(1), 125-133). Permission is included in Appendix A.

## 5.2 Introduction

The call for energy storage devices has been increasing day by day with the rapid increase in usage of portable and wireless electronics. Particularly, the rapid growth in employing renewable energies, such as winds and solar energies, is deriving the batteries and supercapacitors' market to a higher level [126, 127]. Among different technologies, EDLCs are promising candidates for energy storage due to their unique features. Besides being environmentally friendly products, EDLCs are more preferred over conventional capacitors and batteries when high power density, fast charging-discharging, and long lifetime is needed. The device construction of EDLCs consists of two porous electrodes in an electrolyte media and a membrane between the two electrodes. Mainly, electrolyte plays a significant role in EDLCs performance due to its ionic conductivity and potential range [128]. While the majority of the research on supercapacitors are based on liquid electrolytes, for practical applications, special packaging is required for such devices to avoid the electrolyte leakage. This makes the devices to be bulky and mechanically less flexible. More recently, there have been tremendous efforts to overcome these challenges and enhance capacitance and energy density in supercapacitors by developing new and cost-effective electrode and electrolyte materials [22, 127].

To address the challenge in liquid electrolytes, gel electrolytes have been studied before by other research groups [71, 72, 129-134]. A common formula for making a gel is to mix an acid with polyvinyl alcohol (PVA). Liu et al. reported  $H_3PO_4$ -PVA based devices with a simple method of fabrication [134]. Also,  $H_2SO_4$ -PVA was used to make devices with specific capacitance of 135 F/g [133]. Different types of electrodes including graphene, carbon cloth, and composite materials have been used with gel electrolytes for fabricating flexible and solid state devices. A list of some

gel based devices is presented in Table 8 which shows that the specific capacitance drops significantly when bases (i.e. KOH) are used instead of acids with PVA [72].

Table 8: Examples of Reported Supercapacitors with Gel Electrolytes.

Gel materials	Electrode materials	Specific capacitance	Ref
H <sub>3</sub> PO <sub>4</sub> -PVA	PANI-CNT	16 F/g	[134]
H <sub>2</sub> SO <sub>4</sub> -PVA	CNT	135 F/g	[133]
H <sub>3</sub> PO <sub>4</sub> -PVA	Carbon-MnO <sub>2</sub>	2.5 F/cm <sup>3</sup>	[132]
H <sub>2</sub> SO <sub>4</sub> -PVA	Carbon cloth-graphene	11.8 F/g	[130]
H <sub>2</sub> SO <sub>4</sub> -PVA	Graphene	187 F/g	[71]
KOH-PVA	TiN	0.33 F/cm <sup>3</sup>	[72]
H <sub>3</sub> PO <sub>4</sub> -PVA	Carbon fiber-graphene oxide	43.8 F/g	[129]
H <sub>3</sub> PO <sub>4</sub> -PVA	CNT fiber	13.31 F/g	[131]

Despite the potential advantages of gel electrolytes, a major drawback is in the nature of gel materials not being able to penetrate deep into porous structure of an electrode, specifically structures with nano-size pores. This can limit the effective surface area between the electrode and a gel electrolyte and consequently limiting the double layer capacitance of an electrode. In this work, we have tested both gel and liquid electrolytes containing 3 M concentration of H<sub>2</sub>SO<sub>4</sub> or H<sub>3</sub>PO<sub>4</sub> acids on CNT-based electrodes with a porous structure. While much lower capacitance was expected in devices with the gel electrolytes, surprisingly, the results show even higher specific capacitance for the gel based devices than those with the liquid electrolytes. Further study of the gel material has revealed that the gel itself is acting as a media for storing electric charges. This effect of charge storage in PVA-acid gels has not been reported before. Our results about the ability of charge storage in the electrolyte (in addition to the double-layer) and advantages of gels to liquids for fabricating flexible and solid-state devices are promising for practical applications where low-cost energy storage is needed.

## 5.3 Experimental Section

### 5.3.1 Materials

Two pieces of glassy carbons (GC) ( $25 \times 25 \times 3 \text{ mm}^3$ ) were purchased from SPI Supplies. The rest of the materials that used in the experiments were purchased from Sigma-Aldrich, namely multi-walled carbon nanotube (MW-CNT), sodium dodecyl benzenesulfonate (SDBS) ( $\text{C}_{18}\text{H}_{29}\text{NaO}_3\text{S}$ ), PVA ( $\text{C}_2\text{H}_4\text{O}$ )<sub>x</sub>,  $\text{H}_3\text{PO}_4$  with solution of 85 wt.% in  $\text{H}_2\text{O}$ ,  $\text{H}_2\text{SO}_4$  solution of 95.0-98.0% containing  $\text{H}_2\text{SO}_4$ . The paper substrates used for making the electrodes were from Office Depot (8.5 in  $\times$  11 in).

### 5.3.2 Preparation of Gel and Liquid Electrolytes

The gel electrolytes were made by adding 3 grams of PVA to 15 mL of 3 M acid solutions ( $\text{H}_2\text{SO}_4$  or  $\text{H}_3\text{PO}_4$ ) in deionized (DI) water. Then, the solution was stirred on a hot plate ( $70^\circ\text{C}$ ) for 7 hours at the speed of 250 rpm. There was condensation reaction with acid ( $\text{H}_2\text{SO}_4$  or  $\text{H}_3\text{PO}_4$ ) to PVA incorporating the acid group in PVA polymer chain. The  $\text{H}_3\text{PO}_4$ -PVA as well as  $\text{H}_2\text{SO}_4$ -PVA became conducting, transparent and gel based electrolyte. The gel was brought to room temperature before fabrication of any supercapacitor device. For the liquid electrolytes, 3 M concentration of  $\text{H}_2\text{SO}_4$  or  $\text{H}_3\text{PO}_4$  in DI water was used at room temperature.

### 5.3.3 Device Fabrication and Characterization

Devices with the GC electrodes were made by coating the entire surface of one GC electrode with the gel electrolyte (i.e.  $\text{H}_2\text{SO}_4$ -PVA or  $\text{H}_3\text{PO}_4$ -PVA), putting one or five layers of a plastic mesh (mesh thickness of  $272 \mu\text{m}$ ) as separators, and putting the second GC electrode on the mesh and pressing them together. Copper tape was attached on the back of the GC electrodes

and used as electric connection for electrochemical experiments. A picture of the fabricated device is shown in the supplementary material in Appendix B (Figure S1). MW-CNT based electrodes were fabricated as explained by Hu et al. [101]. Briefly, MW-CNT based ink was made by adding 300 mg of MW-CNT and 150 mg of SDBS into 30 mL of DI water. To make a homogeneous solution of the MW-CNT ink, the solution was sonicated for 30 min using a probe sonicator at 30 W and 40 J average power and energy, respectively.

The MW-CNT ink was used to make the electrodes by spreading the ink on both sides of a (4 cm × 7 cm) paper and then put it in a vacuum furnace for 30 minutes at 120 °C to make the ink completely dry. The process was repeated three times by adding 1 mL of the ink on each side to make it conductive enough. Strips of 1 cm × 4 cm were cut from the conductive paper and used as the electrodes to make devices. The thickness of the MW-CNT based electrodes was 15 μm. The liquid based devices were fabricated by placing two electrodes in a plastic cuvette (1 × 1 × 4 cm<sup>3</sup>) and pour 1 mL of the electrolyte into the cuvette (Figure 33.a). In this configuration, no metal contact was used as the current collector. To fabricate the gel based devices, first one electrode was laid down on a piece of transparency with a piece of aluminum tape on it as the support and the current collector. A piece of the plastic mesh (i.e. separator) was soaked into the gel and placed over the electrode. The second electrode with its current collector and support (i.e. another piece of aluminum tape and transparency) was put over the plastic mesh. Office clips were used to press the electrodes to each other. After a few minutes the clips were removed, and the gel glued the device together. The applied gel was covering almost the same area of the electrodes as the wet part of the electrodes in the liquid based devices (Figure 33.b). All the electrochemical experiments were carried out using VersaStat 4.0 potentiostat in the two-electrode configuration.

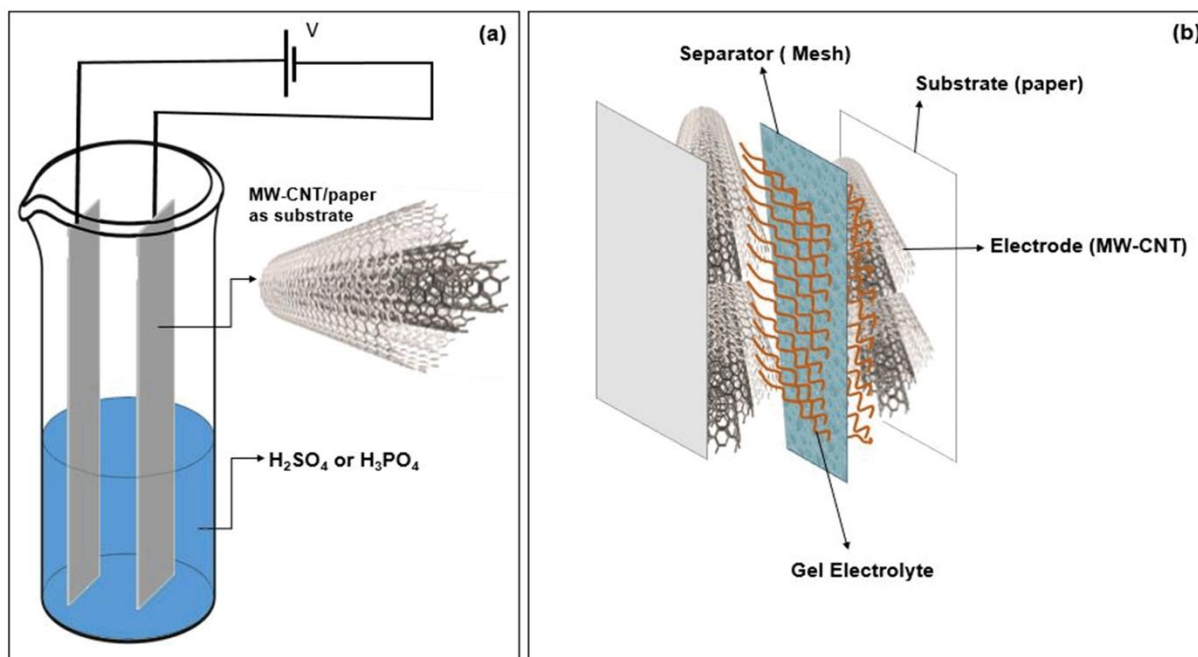


Figure 33: Schematic Diagram of the Electrical Double Layer Capacitor (a) EDLC Liquid-Based Electrolyte (b) EDLC Gel-Based Electrolyte.

## 5.4 Results

### 5.4.1 Electrode Characterization

The CNT based electrodes were studied using scanning electron microscopy (SEM), Fourier transform infrared (FTIR) spectroscopy, Raman spectroscopy, and four-probe method. The SEM images of MW-CNT samples were taken using FE-SEM, S-800, Hitachi (Figure 34. a and b). The SEM image in Figure 34.a shows how CNTs have been infused to the fibers of the paper. The porous structure of the paper provides large internal surface area for the double layer charges in a device. Also, it was observed that the diameter of the CNTs was between 10 and 20 nm while the majority of pores had sizes higher than 20 nm (Figure 34.b). The result of Raman spectra Figure 34.c is similar to the data presented for CNT based electrodes [135]. These bands are related to the lattice vibration of all carbon materials with  $sp^2$  bonds. FTIR spectra of CNT/paper was carried out in a range  $500-4000\text{ cm}^{-1}$ . FTIR of CNT showed dominant

characteristics peaks at 970, 1506, 1621, 1724, 2351, 3739, 3844  $\text{cm}^{-1}$  (Figure 34.d). Additionally, the conductivity of the electrodes was estimated to be  $98 \text{ S}\cdot\text{cm}^{-1}$  after being measured by a custom made four-probe setup connected to a Keithley (2602) source-meter unit. The electrode study confirms the carbon structure of the electrode with dominated macro ( $> 50 \text{ nm}$ ) and meso size pores ( $> 2 \text{ nm}$ ) [136, 137].

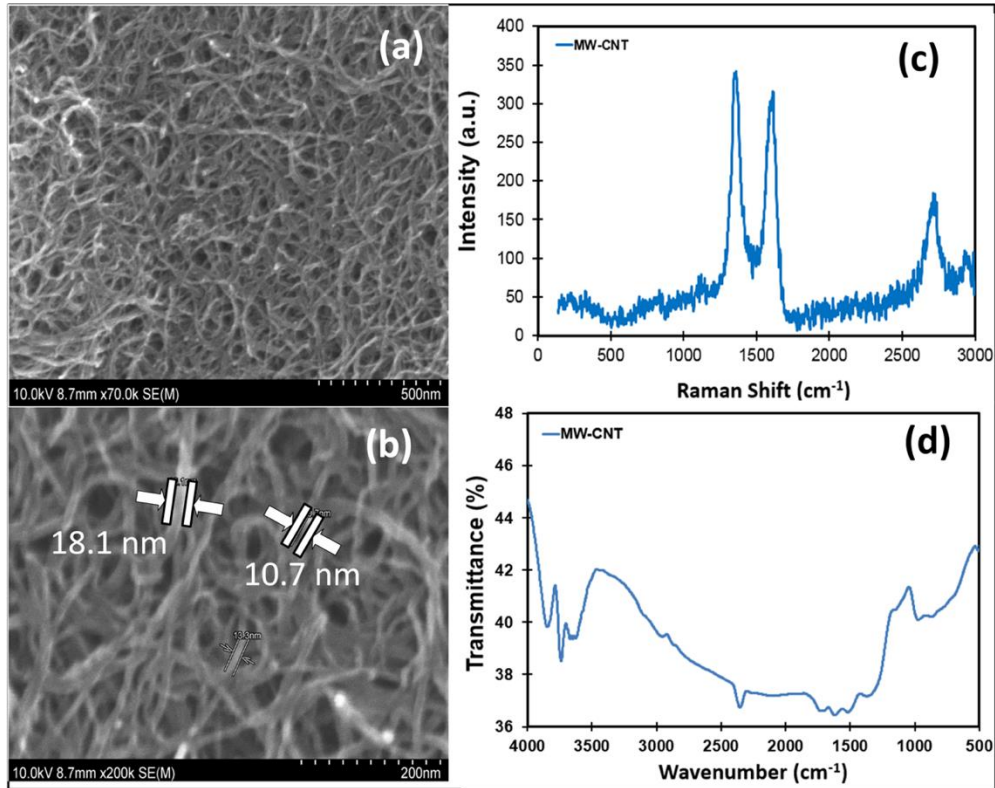


Figure 34: Characterization of the Electrode Material (MW-CNT) (a, b) SEM Micrograph of CNT/Paper (c) Raman Spectra of CNT Paper (d) FTIR Spectra of CNT/Paper.

#### 5.4.2 Capacitance Study in Porous Electrodes with Liquid and Gel Electrolytes

To study both liquid and gel electrolytes, EDLCs were fabricated and tested with the CNT electrodes and different electrolytes including  $\text{H}_2\text{SO}_4$ -PVA,  $\text{H}_3\text{PO}_4$ -PVA,  $\text{H}_2\text{SO}_4$  and  $\text{H}_3\text{PO}_4$ , respectively.



Cyclic voltammetry (CV) measurements were carried out for all four devices within the potential range from -1.0 V to +1.0 V with 50 mV.s<sup>-1</sup> scan rate. The results are presented in Figure 3. The capacitance,  $C_s$ , value of each device can be calculated from the CV measurements [138, 139] using:

$$C_s = \frac{\int_{T1}^{T2} i(t) dt}{(E2 - E1) \times m} \quad (15)$$

where  $\int_{T1}^{T2} i(t) dt$  is equal to the voltammetric charge during either scan up or scan down of the voltage. E1 (lower limit) and E2 (upper limit) are the switching potentials in the cyclic voltammetry test. Dividing the capacitance to the mass ( $m$ ), the specific capacitance,  $C_s$ , in devices with liquid H<sub>2</sub>SO<sub>4</sub> and H<sub>3</sub>PO<sub>4</sub> was 3.29 F/g and 3.91 F/g, respectively. In gel devices, the  $C_s$  value was 3.84 F/g and 4.39 F/g for PVA-H<sub>2</sub>SO<sub>4</sub> and PVA-H<sub>3</sub>PO<sub>4</sub> based devices. Considering the mechanism of charge storage in EDLCs (formation of the double-layer at the electrode-electrolyte interface), a much higher capacitance is expected for devices with liquid electrolytes where the ions can easily penetrate into the nano-pores in the depth of the electrodes. However, comparing the loop areas in the cyclic voltammetry results (Figure 35), it is clear that the specific capacitance is larger in the gel-based devices than the liquid ones. Also, it can be seen that the CV curves were not ideal rectangular shapes. Specifically, the gel devices showed small peaks of redox activities. Since CNT is not an electrochemically active material, it is likely that a redox reaction in the gel electrolytes is responsible for the higher capacitance. It should be noted that many composite materials have been developed for the electrodes to achieve specific capacitances much higher than the reported values in this work [140]. However, the purpose of this work was to study the electrolyte properties. To ensure, no pseudocapacitive effect on the electrode of devices we have used the CNT based electrodes, and not any composite. The comparative results from devices with

liquid and gel electrolytes in Figure 35 suggest the possibility of some sort of charge storage in the gel materials in addition to the double layer.

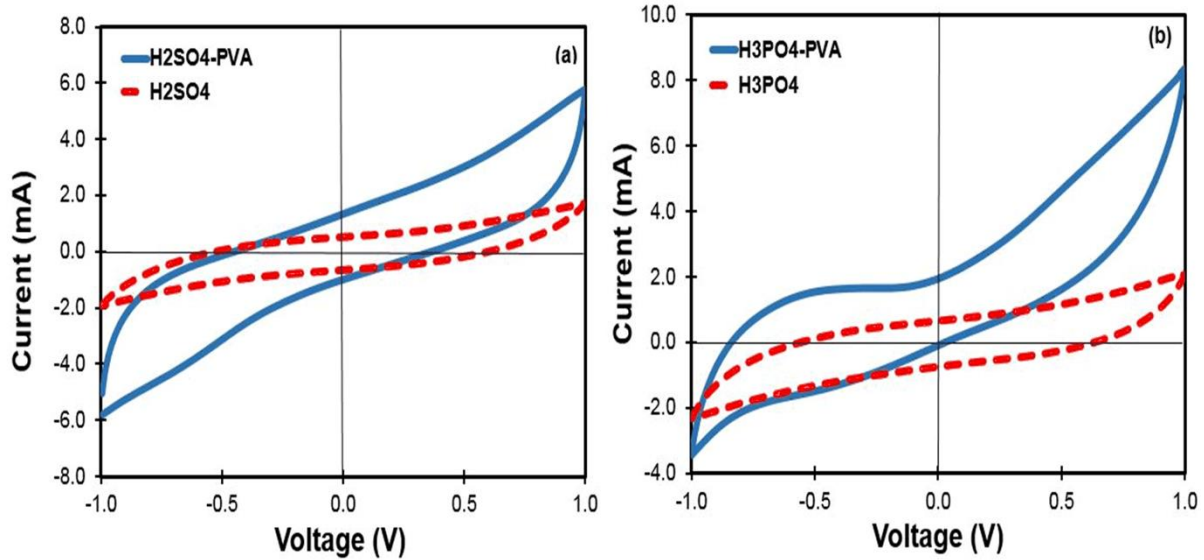


Figure 35: Cyclic Voltammetry of the Supercapacitors Based on (a) Sulfuric Acid as gel and Liquid Electrolytes and (b) Phosphoric Acid as Gel and Liquid Electrolytes.

#### 5.4.3 Capacitive Behavior Study in Gels with Non-Porous Electrodes

To learn more about the charge storage in the electrolyte, devices were fabricated with GC electrodes and various volumes of the gel between the two electrodes (Figure S1.a) in Appendix B. Due to the non-porous structure of the GC, the area of the electrode-electrolyte interface was the same as the electrode area (25 mm×25 mm) in all the devices. Two devices were made for each gel electrolyte: one with the one layer and another one with five layers of the mesh separator (five times higher volume/mass of the gel than that in one layer). Figure 36 shows their CV results when the voltage was scanned back and forth with a rate of 50 mV.s<sup>-1</sup>. For both gel materials, the width of the CV loops at 0.0 V was exactly five times higher in the devices with five layers of the separator than that in the devices with one layer. This clearly implies that the charge somehow has

to be stored in the volume of the gel. Considering the density of the gels ( $\rho = 0.942 \text{ g/cm}^3$ ) and the volume of the gel used in the devices, the specific capacitance ( $C_{\text{gel}}$ ) of the gels was calculated and found to be  $2.705 \text{ mF/g}$  for  $\text{H}_2\text{SO}_4\text{-PVA}$  and  $2.516 \text{ mF/g}$  for  $\text{H}_3\text{PO}_4\text{-PVA}$ . It should be noted that for calculating  $C_s$ , the measured capacitance was divided by the mass of the electrode, but  $C_{\text{gel}}$  was estimated by dividing the measured capacitance in a non-porous electrode structure to the mass of the gel.

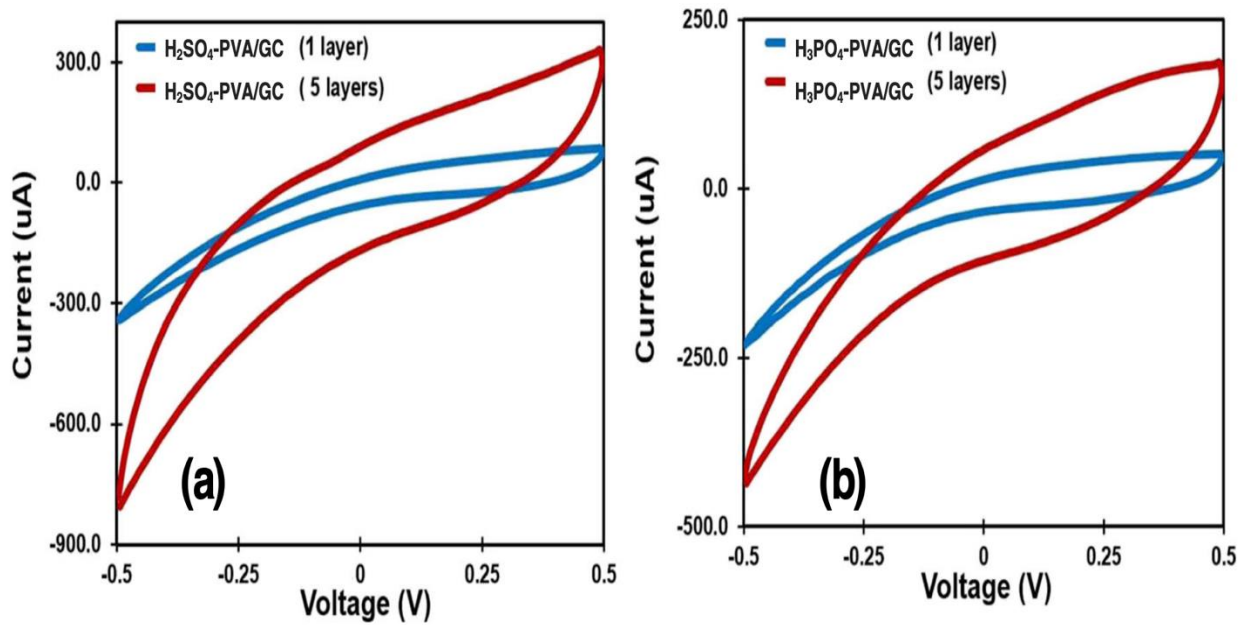


Figure 36: Cyclic Voltammetry of the Glassy Carbon-Based Supercapacitors with One Layer and Five Layers of the Spacer Made From (a)  $\text{H}_2\text{SO}_4\text{-PVA}$  and (b)  $\text{H}_3\text{PO}_4\text{-PVA}$  Gels.

In Figure 36, the voltage range was limited to  $\pm 0.5 \text{ V}$ , but the responses are not symmetrical. This can be due to nonuniform distribution of the charges inside the gels after the first cycle of charging, resulting in accumulation of positive charges near one electrode and negative charges near the other electrode. The effect is more significant in the thicker layer of gels when a larger spatial charge separation is possible. When the voltage range was increased above  $\pm 1.0 \text{ V}$ , the gel start showing bubbles and a large anodic current was recorded (Figures S1.b and

S2) in Appendix B. The bubbles are most likely due to water hydrolysis. However, no bubble was observed in the devices with the porous electrode, maybe because of trapping the bubbles inside the pores.

#### 5.4.4 Gel Based Supercapacitors

The combination of the CNT based electrodes and the gel electrolytes showed better results than the devices with the liquid electrolyte. Therefore, the gel based devices were further characterized. The effect of the gel resistance on the performance of the supercapacitors with the porous electrodes was studied using the galvanostatic cycling method. The experiment was performed by applying alternative 1 mA pulse current for 10 s to charge the devices and -1 mA (10 s duration) to discharge them [16]. The curves that seen in Figure 37 exhibit non-linear shapes voltage profile during the charging and discharging cycles. However, the charge curves were nearly symmetric to their corresponding discharge curves in the potential range, which indicated a high reversibility between charge and discharge processes. The sharp voltage drop,  $\Delta V$ , in the initial voltage upon discharge is due to the equivalent series resistance (ESR) of the supercapacitor [141]. The ESR value was calculated from the voltage drop at the transition by the following equation [16]:

$$\text{ESR} = \frac{\Delta V}{2 \times I} \quad (16)$$

where  $I$  is the amplitude of the current pulse. The ESR values were found to be 33  $\Omega$  and 28  $\Omega$  for the CNT based devices with the sulfuric and phosphoric based gel electrolytes, respectively. The effect of the liquid resistance on the performance of the EDLCs based CNT electrode has also been studied using the galvanostatic cycling method as presented in the supplementary material

Appendix B (Figure S3). The lower ESR in the gel based devices is mainly due to the aluminum current collector that was employed only in the solid-state devices.

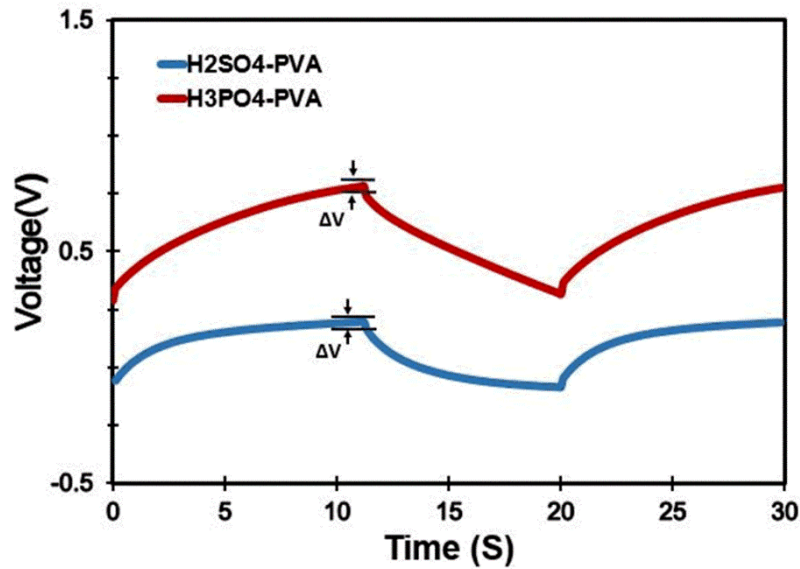


Figure 37: Galvanostatic Charge-Discharge of CNT-Based Supercapacitors with H<sub>2</sub>SO<sub>4</sub>-PVA and H<sub>3</sub>PO<sub>4</sub>-PVA Gel Electrolytes.

The electrochemical impedance spectroscopy (EIS) analysis of EDLCs was performed to understand the nature of the electrode-electrolyte interfaces and the role of charge storage in the gels. The impedance measurements were made over a frequency from 0.1 Hz to 10 kHz at 0.0 V DC biasing using VersaSTAT 4.0 Potentiostat with sinusoidal signal of 10 mV over the frequency range and the results of Nyquist impedance plots are presented in Figure 38. Devices with the liquid electrolytes have also been studied as seen in the supplementary material Appendix B (Figure S4 and S5). As expected, the impedance results for devices with the liquid electrolyte could be easily modeled with the standard EDLC models including resistors, one double layer capacitor and one Warburg element, *W* (Figure S6). However, the Nyquist results in Figure 38 shows almost

two semicircles, suggesting two stages of charge storage (inset Figure 38).

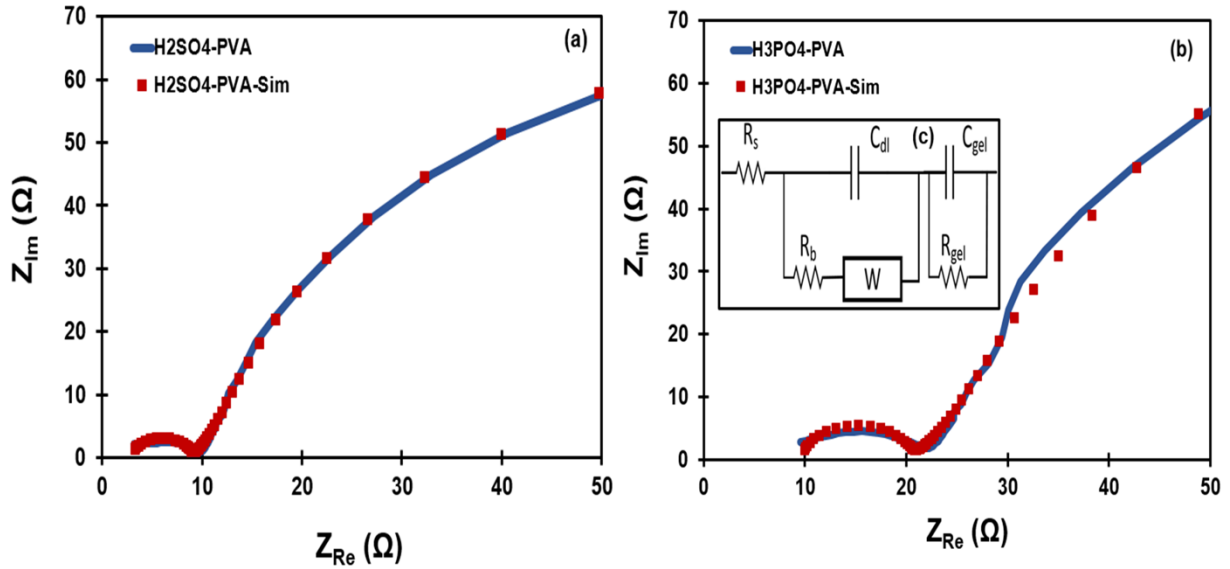


Figure 38: Nyquist Impedance of CNT-Based Supercapacitors with (a) H<sub>2</sub>SO<sub>4</sub>-PVA and (b) H<sub>3</sub>PO<sub>4</sub>-PVA Electrolytes. (Inset) Electrical Equivalent Circuit Model.

The first stage with the  $C_{dl}$  and  $W$  represents the energy storage at the interface between the porous electrode and the electrolyte, while the second stage with  $C_{gel}$  and  $R_{gel}$  are added to include the storage property of the gels which explains the second semicircle in the EIS results. To estimate the value of each element, the experimental data was analyzed using EIS Spectrum Analyzer software (version 1.0). For the given model the software found the best fit to the experimental data for which the value of each component was estimated. The small signal parameters are all listed in Table 9. While  $C_{dl}$  and  $W$  acted as elements for storing charges at the interface of the electrolyte and the porous electrode, the capacitance of the gel itself was substantial in both H<sub>2</sub>SO<sub>4</sub>-PVA and H<sub>3</sub>PO<sub>4</sub>-PVA.

Table 9: Parameters of the Equivalent Electric Circuit Model.

Devices	$R_s$ ( $\Omega$ )	$R_b$ ( $\Omega$ )	$C_{dl}$ ( $\mu\text{F}$ )	$W(S.s)^{0.5}$	$C_{gel}$ (mF)	$R_{gel}$ ( $\Omega$ )
H <sub>2</sub> SO <sub>4</sub> -PVA	3.01	5.75	12.59	10.81	19.84	100.95
H <sub>3</sub> PO <sub>4</sub> -PVA	9.87	10.44	11.26	0.01	23.48	134.07

Considering the higher capacitance in the gel based devices, the stability of the capacitors with H<sub>2</sub>SO<sub>4</sub>-PVA and H<sub>3</sub>PO<sub>4</sub>-PVA and CNT porous electrodes were further studied by using the CV method for 1000 cycles at the scan rate of 50 mV.s<sup>-1</sup>. Equation (1) was used to estimate the capacitance at each cycle. The example of the CV loops and estimated value of the capacitances are presented in Figure S7 and S8 and Table S1 and S2 in the supplementary material Appendix B. To demonstrate the capacitance retention, the normalized value of the capacitances to the capacitance of the first cycle (*C*<sub>0</sub>) versus the number of charging-discharging cycles is plotted in Figure 39.a. The results showed good stability for the continuous use of both electrolytes and with negligible performance degradation. In fact, no obvious lassitude in the devices was observed and the capacitance decreased slightly by less than 2.5 % for H<sub>2</sub>SO<sub>4</sub>-PVA and 5.0 % for H<sub>3</sub>PO<sub>4</sub>-PVA. Nevertheless, the size and shape of the CV curves were identical (see Figure S7 and S8) even after 1,000 cycles which confirm the electrochemical stability of the interface between the MW-CNTs/paper and the gel electrolytes. Overall, the result expresses a good cycling stability of both devices that based gel electrolytes, confirming the stability of the gels.

In some applications, flexibility and the mechanical strength of the supercapacitor devices are extremely important [124, 133]. To characterize the devices under bending conditions, the capacitance of the devices was measured using the CV method while the device was bended to different curvatures. Cylindrical shape objects were used for applying a uniform bending to the tested devices. The reported curvatures are equal to 1/radius of the cylindrical objects. To investigate the full flexibility of the devices, each capacitor was tested first with an increasing curvature from 0 to 0.16 mm<sup>-1</sup> and then measuring it again for curvatures from 0.16 to 0 mm<sup>-1</sup> (data are presented in Table S3 and S4). As shown in Figure 39.b, the original capacitance of the EDLCs was retained to about 93.57 % for H<sub>2</sub>SO<sub>4</sub>-PVA and 98.16 % for H<sub>3</sub>PO<sub>4</sub>-PVA after bending.

The reason behind recovering the capacitance is the characteristics of H<sub>2</sub>SO<sub>4</sub>-PVA and H<sub>3</sub>PO<sub>4</sub>-PVA that make them docile to elastic deformation. Also, the good capacitance and cycle's stability observed during the bending test implies a reliable contact between the electrodes and PVA gel electrolytes. Furthermore, the test indicates the stability of CNT coatings on the paper substrates under mechanical deformation.

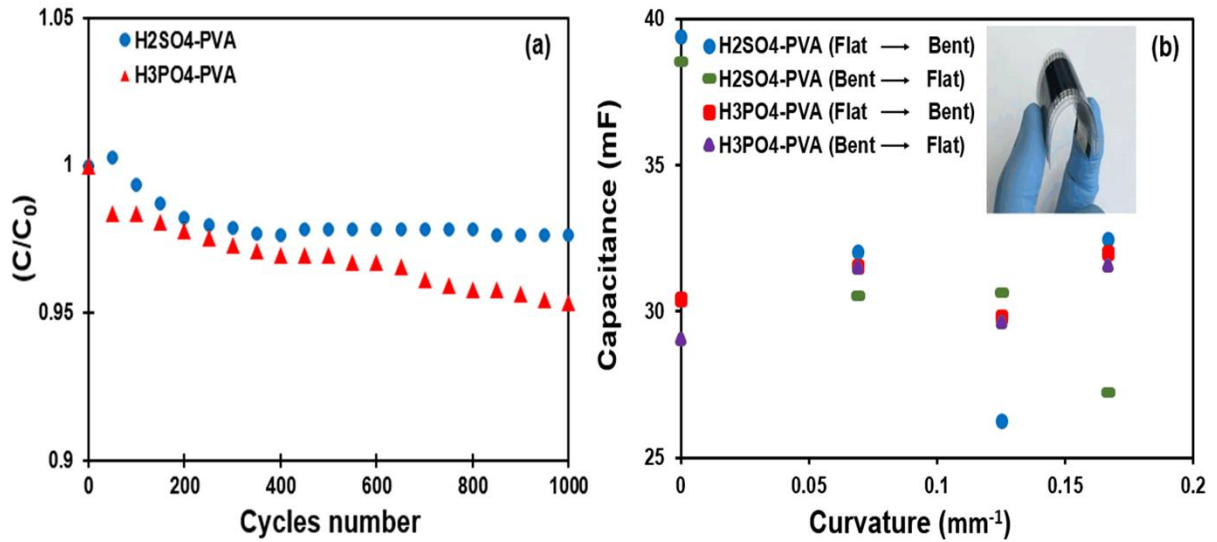


Figure 39: (a) Normalized Capacitance of Devices with H<sub>2</sub>SO<sub>4</sub>-PVA and H<sub>3</sub>PO<sub>4</sub>-PVA Electrolytes to the Initial Capacitance of Each Device Before 1000 Cycles of Charging and Discharging and (b) Bending Test of Supercapacitor Based on H<sub>2</sub>SO<sub>4</sub>-PVA and H<sub>3</sub>PO<sub>4</sub>-PVA at Different Curvatures Flat-to-Bent and Bent-to-Flat. (Inset) a Picture of Bended Device.

In order to study the effect of acid concentration on the charge storage capability in devices, PVA-H<sub>2</sub>SO<sub>4</sub> and PVA-H<sub>3</sub>PO<sub>4</sub> gels were made with acid concentrations of 1 M to 3 M. The CV results of each device was studied and presented in our previous publication [142]. As shown in Figure 40, the highest specific capacitance was obtained at 3 M concentration of acids. We noticed that the gel viscosity was higher at higher concentrations of acids. For concentrations higher than 3 M, the viscosity was too high to even make a uniform film of gel.



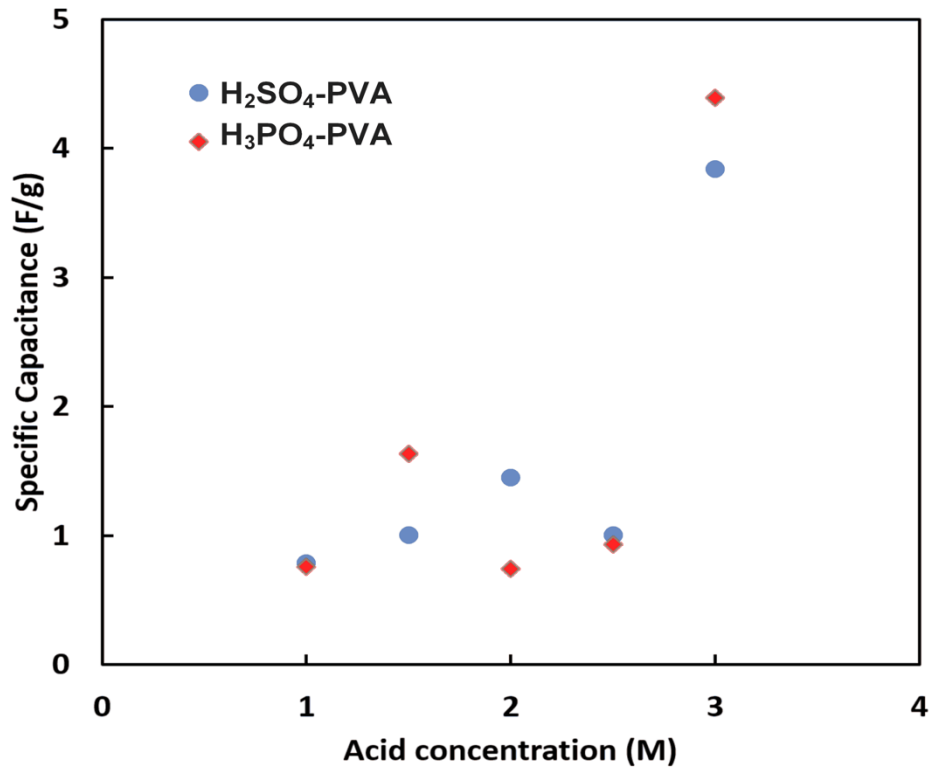


Figure 40: Specific Capacitance of Devices with Acid-PVA Gel Electrolytes at Various Concentrations of the Acids.

## 5.5 Discussion

The presented results, particularly from the device with glassy carbon electrodes, suggest that there should be a mechanism for storing charges in the PVA-acid gel. This property of PVA gel has not been reported before. The previously reported devices with the capability of storing charges in electrolyte have employed certain redox active materials such as I<sup>-</sup>/I<sub>2</sub>, P-phenylenediamine (PPD), hydroquinone (HQ), methylene blue (MB) or p-benzenediol (PB) as additives to the electrolyte [67, 82, 83]. The charge storage mechanism in the electrolytes with the redox active additives relies on the change of the oxidation state of the added materials when electric charges are pumped into the electrolyte during a charging process. This is more like a pseudocapacitive charge storage, but in the volume of the electrolyte instead of on the electrodes.

A reversible reaction is expected during the discharge cycle through which the released charges from the redox materials return back to the electrodes. However, the gel electrolytes used in this study lack any bi-stable redox mediator. Since the gel materials were made of only PVA, water, and an acid ( $\text{H}_2\text{SO}_4$  or  $\text{H}_3\text{PO}_4$ ), it is likely that the observed pseudocapacitive effect is due to the change in the bonds between OH groups on PVA and the anions from the acids. The gel fabrication process is as simple as mixing an acid with an aqueous solution containing PVA and stir the mixture on a hotplate.

During this process, some of the OH branches on the PVA backbone react with the acid molecules to release  $\text{H}_2\text{O}$  which results in bonding the anions to PVA and formation of the gel after some water evaporation. However, the gel would still contain substantial amount of water. As shown in Figure 41, the sulfate and phosphate based anions can link to PVA through one or two oxygen atoms. Pumping a negative and a positive charge to the gel with the structures shown at the left side of Figure 41, PVA loses the second  $\text{OH}^-$  and the anion loses a proton ( $\text{H}^+$ ) to reach the structure shown at the right side of the reaction with two oxygen bonds to PVA. The reverse process returns the charges back to the system.

Regarding the application of gel electrolytes, it is important to notice that in this study we used CNT based electrodes with relatively large pores (Figure 34.b). In a structure with large size pores, the surface area for formation of double layer charges is almost the same for gel and liquid electrolytes. Therefore, the charge storage in the volume of the gel can add to the overall capacitance of a device. This advantage can be undermined in electrodes with high density of nano-size pores where only liquid electrolyte can diffuse and form much larger double layer charge than that at a gel-electrode interface.

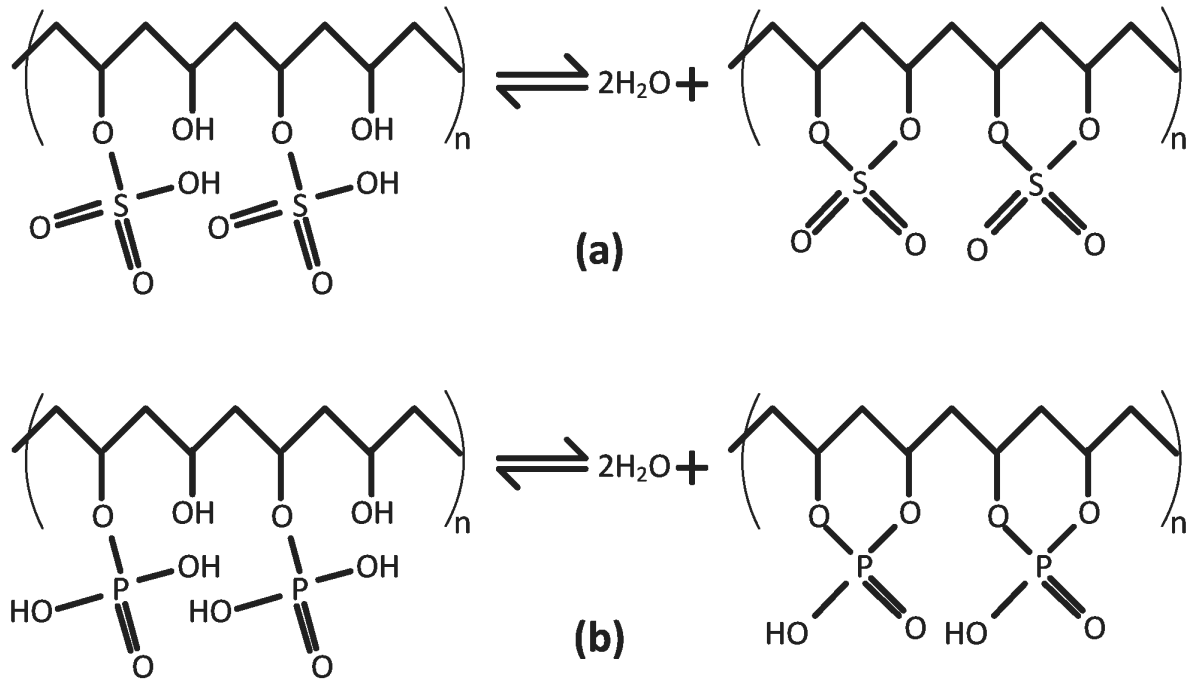


Figure 41: Schematic of the Proposed Mechanism of Charge Storage in the Acid-PVA Gel Electrolytes for (a) Sulfuric and (b) Phosphoric Anion-Based Gels.

Since a high density of small pores is required for making high capacitance devices, generally gel electrolytes are not viable candidates for real applications. Additionally, the observed bubbles in the gel electrolyte when the scan voltage window was expanded beyond  $\pm 1.0$  V (Figure S1.b) is another challenge for using the gel electrolytes in real applications. Nevertheless, the results of our study encourage the usage of gel electrolytes in combination with electrodes with high density of large pores for making low-cost, flexible energy storage devices operating at a limited voltage range.

## 5.6 Conclusion

In conclusion, the cyclic voltammetry and electrochemical impedance spectroscopy methods have shown higher specific capacitances in the gel-based EDLCs than those in liquid-based devices. Further study of the gel electrolytes with glassy carbon electrodes revealed that the

capacitance of devices is proportional to the volume of the gel electrolytes, suggesting a mechanism of charge storage in the volume of the gel. Also, the two-semicircle shape of the Nyquist plots from the EIS studies confirmed the storage capability of the gels. The proposed mechanism to explain the redox activity in the gel includes a bi-stable formation of bonds between PVA and anions of the acids. With this feature of the gel and the simplicity in fabrication of the gel and the CNT electrodes with large size pores, flexible and low-cost supercapacitors can be made for energy storage in low-voltage applications.

## Chapter 6: Integrated Electrochemical Energy Storage and Photovoltaic Device with a Gel Electrolyte<sup>3</sup>

### 6.1 Abstract

Integrating both electrochemical devices solar cell (harvesting energy) and supercapacitor (energy storage) into a single device is unquestionably one of the great challenges nowadays. There has been an extended research in the design and construction of integrated solar energy harvesting and storage systems that can simultaneously capture and store various forms of energies from nature. Here, we successfully designed, fabricated and characterized a compact and monolithically photoelectrochemical device combining a polyvinyl alcohol (PVA)/hydrochloric acid (HCl)-based gel electrolyte, multi-walled carbon nanotube (MWCNTs), and fluorine tin oxide (FTO) as counter and working electrodes, respectively. The combination device can act either as an independent solar cell, a supercapacitor, or as a solar cell/supercapacitor device. In this work, energy harvesting takes place only at the working electrode (WE) made of a thin film composite of a conducting polymer (i.e. Polyaniline, PANI) and synthetic dyes materials that coat on the FTO surface by electrochemical deposition technique. The energy storage occurs in both (WE) and counter electrode (CE) that made of (MWCNTs) in addition to the gel electrolyte materials. Different synthetic dyes have been used such as Methylene Blue (MB), Methyl Orange, and

---

<sup>3</sup>This chapter was before published in SPIE proceeding (Aljafari, B., Ram, M. K., & Takshi, A. (2019, February). Integrated electrochemical energy storage and photovoltaic device with a gel electrolyte. In Physics, Simulation, and Photonic Engineering of Photovoltaic Devices VIII (Vol. 10913, p. 1091318). International Society for Optics and Photonics). Permission is included in Appendix A.

Prussian Blue. However, MB has shown the strongest photoelectrochemical reaction in HCl-PVA gel electrolyte. The cyclic voltammetry was used to show the effect of PANI/synthetic dyes on the cell, and impedance spectroscopy demonstrated the effect of surface modification of MWCNTs on the performance of the CE and dye-sensitized solar cell.

## 6.2 Introduction

The call for utilizing renewable energy sources is increasing persistently due to the destructive impact factors of fossil fuels and emission of greenhouse gases toward the environment. The copious free energy sources (e.g. solar and wind energy) that exist in our world need a technology that can develop and convert them to electrical energies. These kinds of energies are predominantly available free of charge, but the stumbling block is the continuous availability during both day and night. Solar energy as one of the diversified forms of renewable energies is widely the most promising alternative to fossil fuels. Since solar energy is available only during day, so beside using solar cell to harvest energy, an additional device is needed to store that energy, for instance, supercapacitor or battery. Therefore, the harvested energy would be stored and used by the load at any time [143-149]. The conventional approach is to integrate a solar cell with a supercapacitor in power pack system. This method has been considered by certain research groups. More focusing has been giving, particularly, to the dye-sensitized solar cell, more than other types of solar cells, integrated with a supercapacitor because both are essentially electrochemical paradigms. A thin film of supercapacitor can be agglutinant to the back of a solar cell. However, a cost-effective approach is to build two devices in one package [12, 150-153]. Various structures have been proposed for devices with the dual properties of energy harvesting and charge storage. The majority of the structures are essentially a DSSC and a supercapacitor with three-electrodes

configurations. In those structures, an electrode is shared between the DSSC and the energy storage cell. Therefore, an external switching mechanism is needed for practical applications to switch between the solar cell and the storage cell upon the availability of the solar energy [12, 13, 75, 154, 155].

To overcome the issue of cost, size and complexity of having two devices connected together, an integrated device that has dual properties of storage and conversion energy simultaneously is established. This device can work as solar cell to harvest the sunlight energy, and supercapacitor to store the electrical energy that converted from solar energy in the form of mobile charges in one device. Therefore, a switch is not needed to toggle the operation of the device between photo charging and electrical discharging, as would be the case where a thin film of supercapacitor can be agglutinant to the back of a solar cell. Recently, our group has invented an integrated device based on two-electrodes configuration of photoactive supercapacitor. The ingenuity of the device is the nanocomposite thin film of a dye-conducting polymer (i.e. poly 3,4-ethylenedioxythiophene: polystyrene sulfonate, PEDOT:PSS) at the working electrode (i.e. Indium Tin Oxide, ITO) [156-160].

In this study, a new technique of energy storage in a DSSC as two-electrodes configurations with the dual properties of energy harvesting and storage has been addressed as shown in Figure 42. simply by having PANI/Dye nanocomposite layer on a transparent electrode (i.e. Fluorine doped tin oxide, FTO) and CNT/paper at counter electrode to offer the double layer functionality of a supercapacitor in addition to its main catalytic performance upon its insertion inside the electrolyte. Because of high porosity of PANI and the MWCNT electrodes the device is as might be expected a photoactive supercapacitor. However, the existence of dye molecules that embedded in the PANI can absorb the light and generate photogenerated charges. Therefore, the

supercapacitor can be charged when the working electrode is exposed to the light. Sundry other probabilities have been looking thoughtfully to store energy in composite dye sensitized with a conducting polymer. The results of electrochemical and electrical characterization techniques such as Cyclic Voltammetry (CV), Electrochemical Impedance Spectroscopy (EIS), Open Circuit Voltage (OSV), and Short Circuit Current (SCC) on the integrated cell have been discussed in this paper.

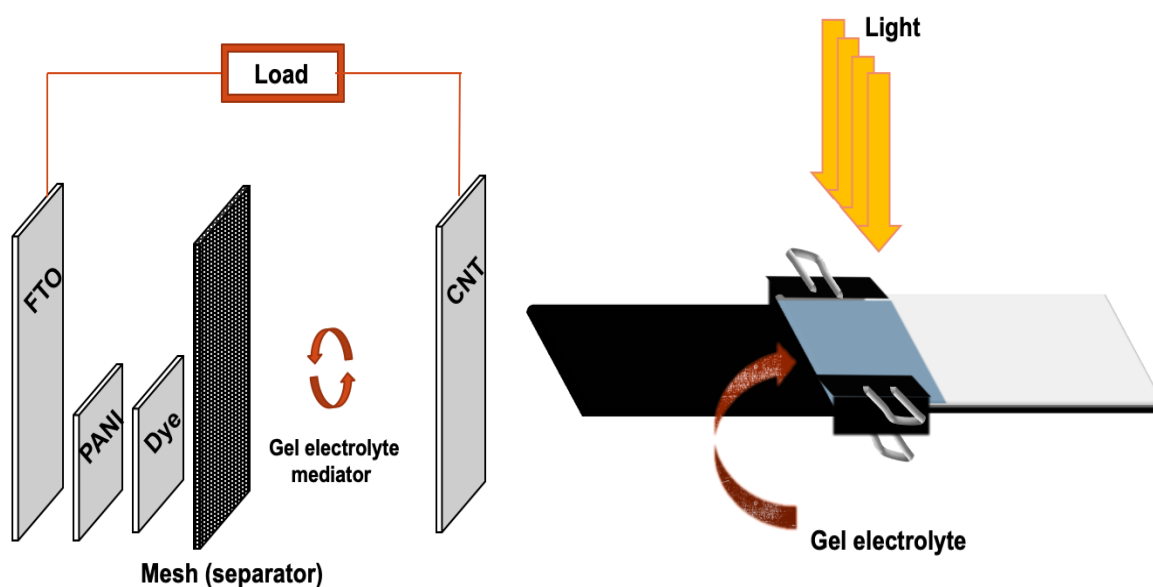


Figure 42: Schematic Diagram of DSSC and SC Based on HCl-PVA Gel Electrolyte.

## 6.3 Experimental Section

### 6.3.1 Materials and Instrumentation

All chemical materials, which are multi-walled carbon nanotube (MWCNTs), sodium dodecyl benzenesulfonate (SDBS) ( $C_{18}H_{29}NaO_3S$ ), polyvinyl alcohol (PVA) ( $(C_2H_4O)_x$ ), hydrochloric acid solution (HCl), aniline ( $C_6H_5NH_2$ ), and methylene blue ( $C_{16}H_{18}ClN_3S \cdot xH_2O$ ) used in this paper were purchased from Sigma Aldrich. The paper substrates used for



making the electrodes were from Office Depot (8.5 in. × 11 in.). VersaSTAT 4 potentiostat with two-electrodes configuration was used to measure the electrochemical and electrical tests, including cyclic voltammetry (CV), electrochemical impedance spectroscopy (EIS), open circuit voltage (OSV) and short circuit current (SCC). The devices were placed in a dark box connected via an optical fiber to a solar simulator (RST, Radiant Source Technology) with an output power intensity of 80 mW /cm<sup>2</sup>, which was equipped with an internal AM 1.0 optical filter. For testing the devices, the illumination time was controlled via the serial port of the desktop computer connected to the solar simulator. The experimental setup, including the dark box and the shutter mechanism, was designed to eliminate the effect of ambient light in the experiment. UV-Vis spectra were recorded on Thermo Scientific Evolution 201/220 UV-Visible Spectrophotometers.

### 6.3.2 Electrode Fabrication

MWCNTs-based paper was made by having an aqueous mixture of 300 mg of MWCNTs, 150 mg of SDBS, which was working as surfactant and 30 mL of DI water. After MWCNTs and SDBS materials were disseminated in the distilled water, the solution was sonicated for 30 min using a probe sonicator at 30 W and 40 J average power and energy, respectively. The conductive ink of MWCNTs solution was used to make the electrodes by drop casted the ink on the surface of a (4 cm × 7 cm) paper and then cured in a vacuum oven for 30 min at 120 °C to make the ink completely dry. The process was repeated three-times to make it conductive enough. The conductive paper sheet was cut in rectangular pieces with the surface area of 4.0 cm<sup>2</sup>~1.0 cm, as functional counter electrodes. The thickness of the MWCNTs based electrodes was 15 μm. For working electrode, 1 M of HCl solution, 0.9m M of dyes materials, and 50m M of aniline in 10 mL of DI water were mixed together. Then, the mixture solution was sonicated for 10 minutes to

make a homogenous solution. After that, fluorine doped tin oxide substrate (FTO) with a thickness of 1.65 mm and conductive layer resistance of  $12 \Omega/\square$  was cut ( $1 \text{ cm} \times 4 \text{ cm}$ ) and subjected to several cleaning processes, which were (i) rinsed with deionized water (DI), (ii) sonicated in DI water for 5 minutes, and (iii) sonicated in methanol and ethanol for 5 minutes respectively to remove all possible contaminations. Then, the cleaned FTO substrate was dried out using nitrogen flow. Then, electrochemical polymerization technique took place by applying a constant voltage (1.5 V) for 10 minutes to the electrochemical cell that has the FTO as working electrode and stainless steel as the counter electrode. Electrochemical polymerization technique was carried out because it is localizing since we are controlling the localization that near electrode-electrolyte interface, which means the charges are moving in the whole solution but more concentration near the electrode-electrolyte interface.

Once the potential is applied, the monomers get oxidized and then two oxidized monomers come together to become dimer and then take them oxidized to become trimer then tetramer and then change the propagation to make the Oligomer. Then, the composite PANI/dye film deposited on the surface of FTO. The film was washed with DI water to obtain a uniform PANI/dye composite film on the FTO glass substrate. The FTO substrate was designated to have a ( $1\text{cm} \times 4\text{cm}$ ) active area, the rest of the surface area were covered using Kapton tape.

### 6.3.3 Preparation of Electrolytes

The gel electrolytes were made by adding 1 g of PVA to 10 mL of 2 M hydrochloric acid (HCl) solution in deionized (DI) water. Then, the solution was stirred on a hot plate ( $75 \text{ }^\circ\text{C}$ ) for 3 h at the speed of 350 rpm. The HCl-PVA solution became conducting, transparent, and gel-based

electrolyte. The gel was cool down to room temperature before fabrication of any integrated device.

## 6.4 Results and Discussion

The optical absorption of a PANI film and PANI composite with three different dyes were studied using the UV-Vis spectroscopy method as shown in Figure 43. The high energy photons are more absorbed by the dye and the polymer. To increase the photo absorption, we synthesized nanocomposites of PANI with different synthetic dyes.

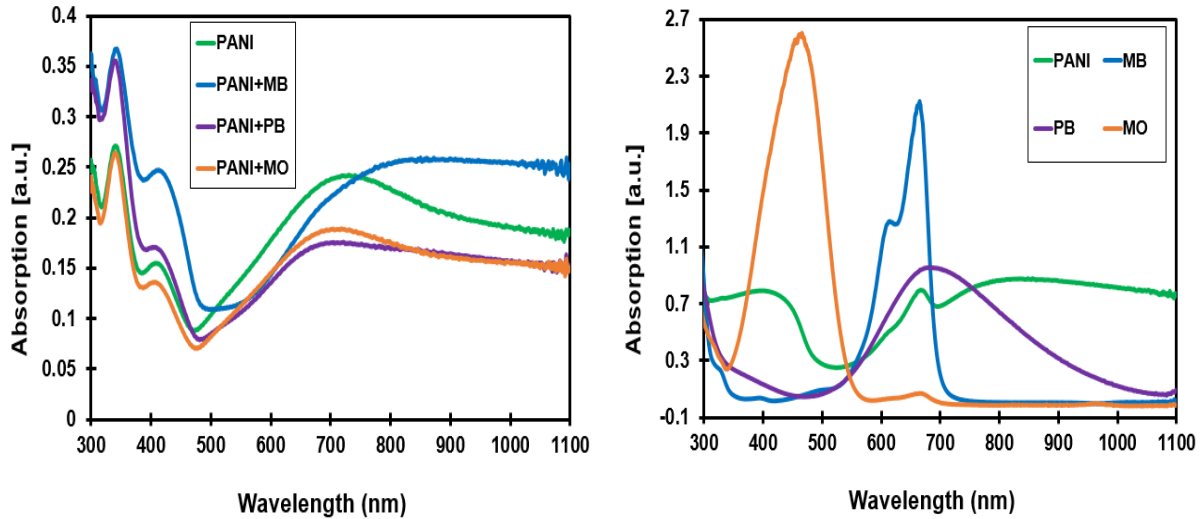


Figure 43: UV-Vis Results for (a) FTO Substrate Coated with PANI, PANI+MB, PANI+MO, and PANI+PB and (b) Dies Solutions Only.

Cyclic voltammetry (CV) method was carried out for all devices to study the storage capacitance within the potential window from  $-0.8$  V to  $+1.0$  V with  $50$  mV/s scan rate. The experiments were performed in dark box to eliminate the effect of ambient light. All the devices were placed horizontally in a glass slide with a path length of  $10$  cm from the light. Figure 44 shows the CV results for four different working electrodes of the integrated cell, which are based

on FTO substrate coated with (a) PANI, (b) PANI+MB, (c) PANI+MO, and (d) PANI+PB. The experiments were carried out in the dark at the beginning and then repeated when the working electrode was under the effect of solar irradiation. After illumination, the experiments were repeated in dark again to see the effect of the light on the performance of the device. In Figure 44 (a), a difference between the dark and light results was observed. Also, the amplitudes of the redox peaks were obvious, which indicate photo-redox reaction in the PANI without dye molecules. The experiment after illumination represented the same features of solar irradiation effect which indicated the stability of the charge in the polymer after storing the photogenerated charges.

Moreover, the CV results in Figure 44 show almost three redox peaks in the range of -0.8 V to +1.0 V. In addition, we have found that the magnitude of the peaks changed when the composite PANI/dye was exposed to light. This clearly shows the photoelectrochemical reaction of the PANI/dye. The capacitance in the four devices is listed in Table 10 and was estimated from the width of the CV loop at 0.0 V by the following equation:

$$\text{Capacitance (c)} = \frac{\Delta I}{2 \times v} \quad (17)$$

where  $\Delta I$  is the width of the loop at 0.0 V and  $v$  is the scan rate.

Table 10: Capacitance of Integrated Devices Based on Different Nanocomposite Working Electrode and the Same CNT as Counter Electrode.

Device based on working electrode	Capacitance (mF) at dark	Capacitance (mF) at light
PANI	20.37	21.08
PANI+MB	24.78	24.92
PANI+MO	22.12	23.83
PANI+PB	22.12	23.13

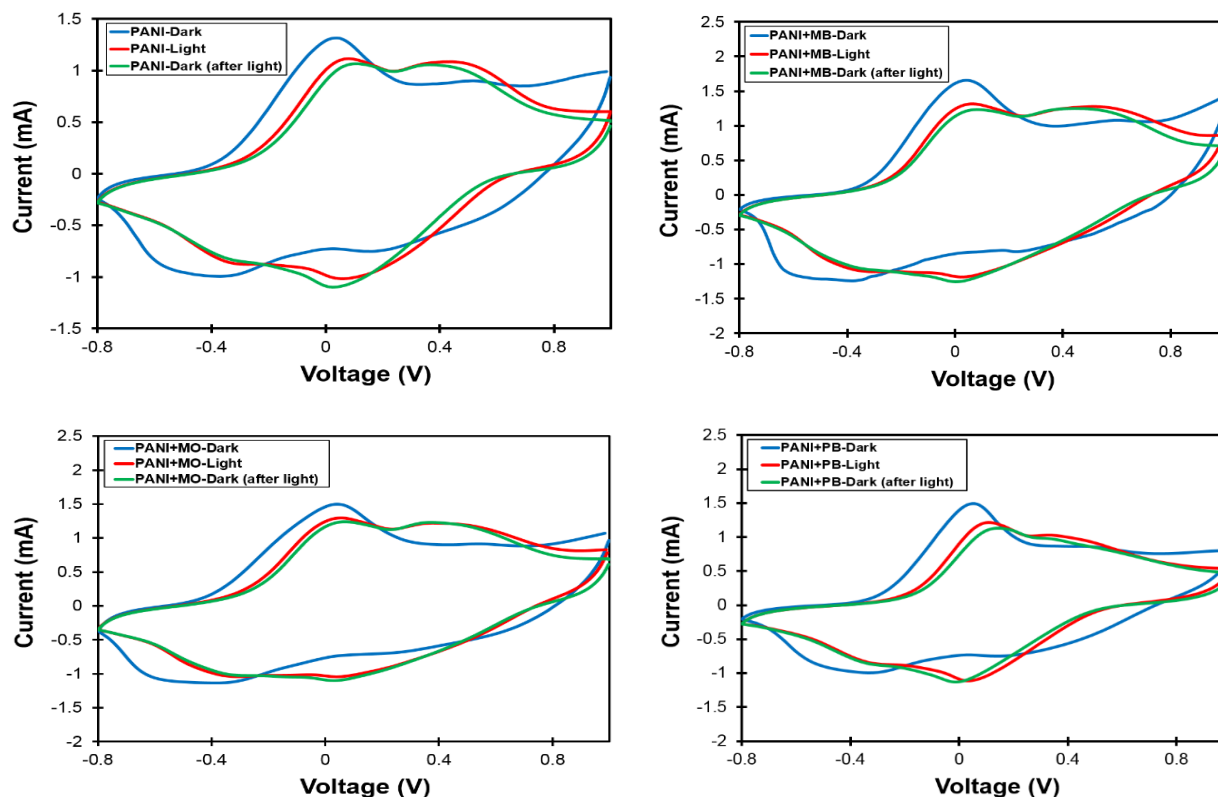


Figure 44: Cyclic Voltammetry (CV) Results of Devices with (a) PANI, (b) PANI+MB, (c) PANI+MO, and (d) PANI+PB Based on HCl-PVA Gel Electrolyte.

The CV results from PANI-MB under the dark and light conditions are shown in Figure 44 (b) is showing the high capacitance. Also, the change in the oxidation peaks is more pronounced in the PANI-MB than the other devices. A notable fact is that the composite film showed a significant increase in the double layer capacitance.

The electrochemical impedance spectroscopy (EIS) analysis of the integrated devices was performed to understand the nature of the electrode-electrolyte interfaces and the role of charge storage in nanocomposite film PANI/dye while keeping them in the dark box. The impedance measurements were made over a frequency from 0.1 Hz to 10 kHz at 0.0 V DC biasing using VersaSTAT 4.0 Potentiostat with sinusoidal signal of 15 mV over the frequency range and the results of Nyquist impedance plots are presented in Figure 45.

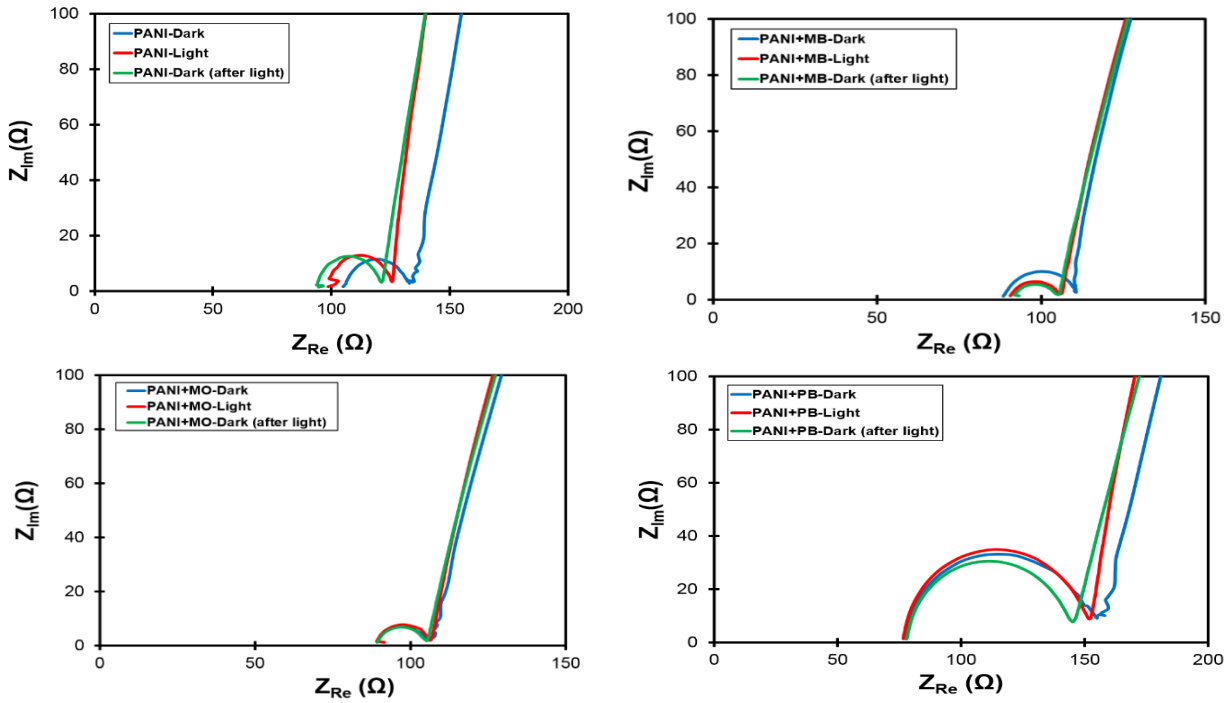


Figure 45: Nyquist Impedance Results of Devices with (a) PANI, (b) PANI+MB, (c) PANI+MO, and (d) PANI+PB Based on HCl-PVA Gel Electrolyte.

The profile of the impedance for all the cells suggests similar response, including a double layer capacitance, a series resistance and a constant phase element. Also, the phase change for all devices showed phases as large as  $45^\circ$  which represents a strong double layer storage effect. The results are showing that despite using similar counter electrodes, the photoactive and energy storage properties of the cell largely depend on the material of the working electrode.

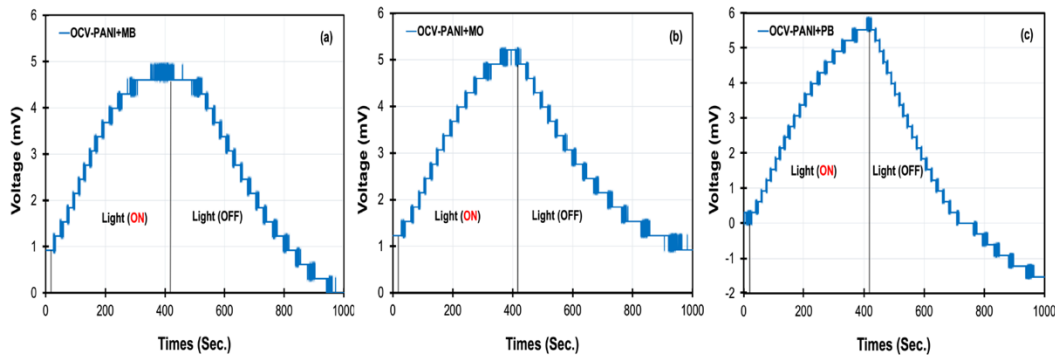


Figure 46: Open Circuit Voltage Results of Devices with (a) PANI+MB, (b) PANI+MO, and (c) PANI+PB Based on HCl-PVA Gel Electrolyte.

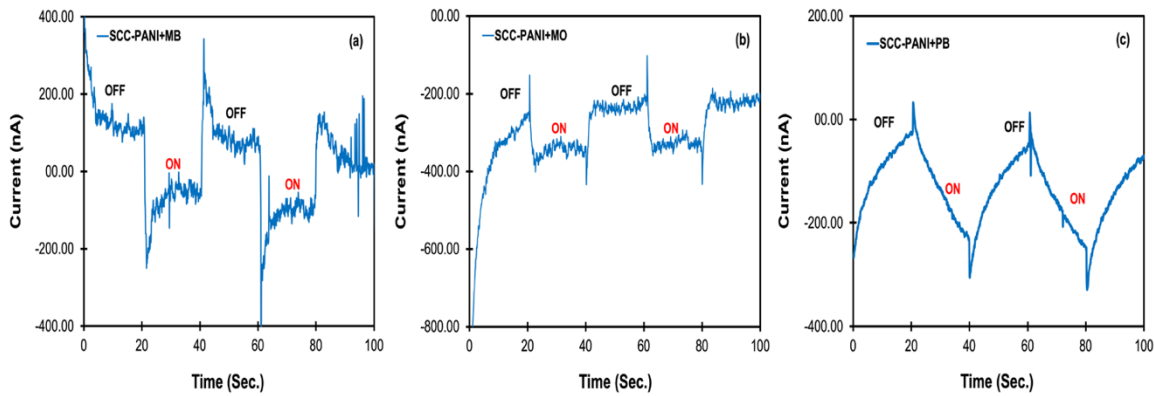


Figure 47: Short Circuit Current Results of Devices with (a) PANI+MB, (b) PANI+MO, and (c) PANI+PB Based on HCl-PVA Gel Electrolyte.

The photovoltaic effect in different working electrodes was studied by monitoring the change in the open circuit voltages and short circuit current in the dark and light as seen in Figure 46 and 47. After the electrochemical tests, which are CV and EIS, the cell was kept in the dark box for about one hour until a stable open circuit voltage was achieved. Then the cell was illuminated for 400 s, using the solar simulator. As shown in Figure 46 (a), the open circuit voltage across the cell in the dark was 0.92 mV. Then, the cell voltage was increased gradually from 0.92 mV to 4.9 mV in 400 s of illumination. After turning off the light, the voltage was dropped to the dark value immediately. For Figure 46 (b and c), the open circuit voltage across the cells in the dark was 1.22 mV and 0.305 mV. Then, the cells voltage was increased gradually from 1.22 mV and 0.305 mV to 4.97 mV and 5.83 mV, respectively.

## 6.5 Conclusion

Applying nanocomposite materials of a conducting polymer (PANI) and three different synthetic dyes materials on the working electrode of photoelectrochemical device was introduced which demonstrated both harvesting energy and internal energy storage capability. The effect of embedded dyes to the conducting polymer on the energy storage and photovoltaic effects were

addressed. It was observed that the addition of the dye molecules enhances the capacitance in the conducting polymer and enhances the photovoltage in the device. The results are encouraging for application of PANI/dye composite for photoactive supercapacitor devices to harvest solar energy and store charges in a single device with two-electrodes configuration.



## Chapter 7: Photo-Electric Properties of Polypyrrole Based Gel Electrolyte for Hybrid Photoactive Supercapacitors<sup>4</sup>

### 7.1 Abstract

The nature of solar radiation is not steady, therefore having a solar-capacitor device that can simultaneously capture, convert and store solar energy can promote the technologies using solar energy. A self-charging photoactive supercapacitor is designed and fabricated as a functional solar energy storage device, which is accomplished in situ self-assembled storage technique. The solar-capacitor device is assembled on a multilayered photo-electrode including cationic dye and conducting polymer. The supercapacitor can be charged when the photo-electrode is illuminated. The voltage of the Ppy and Ppy+MB photo-electrodes based devices was increased under illumination effect by 5.22 mV and 23 mV, respectively. The presented results on the hybrid device based Ppy+MB are encouraging for solar-capacitor devices with dual properties of harvesting solar energy and store charges in a single device with two-terminals. With the simplicity of fabrication nanocomposite thin film Ppy+MB, low-cost solar capacitor device can be made for small integrated electronic devices for harvesting and storage energy.

---

<sup>4</sup>This chapter was before published in ECS transaction (Aljafari, Belqasem, Fatemeh Khorramshahi, Manoj K. Ram, and Arash Takshi. "Photo-Electric Properties of Polypyrrole Based Gel Electrolyte for Hybrid Photoactive Supercapacitors." ECS Transactions 92, no. 9 (2019): 7-14. Permission is included in Appendix A.

## 7.2 Introduction

Worldwide concerns on the environmental deterioration as well as energy deficiency markedly spur the technological endeavor of renewable energy sources. Therefore, the demand of energy has been growing intensively due to the drastically dwindling of non-renewable resources. There are numerous clean energy sources among them solar energy is the most popular alternative to the non-renewable resources (i.e. fossil fuel). The performance of solar energy technology is associated with the most two important factors which are generated energy and storage [12]. Therefore, solar energy can be used efficiently by coupling the harvesting energy cell with the energy storage device to recompense for the sporadic power supply when energy is not being produced [161].

Several amalgamations of solar cells technology and energy storage devices have been suggested for devices with dual properties such as dye-sensitized solar cells (DSSCs) with redox flow batteries, supercapacitors (SCs), or lithium-ion batteries. However, high performance would be accomplished by the integration of DSSCs with SCs devices among other energy storage devices because of their extraordinary power density, long cycle life, and safety. The majority research of this combination is based on three-electrodes configurations [13, 75] and liquid electrolyte [12, 154]. Therefore, an exterior switching mechanism is in demand for functional applications to toggle the operation of the device between photo charging and electrical discharging upon the availability of solar radiation. In fact, liquid electrolytes play a prime role in electrochemical cells. However, due to their safety issues and poor stability, gel polymer electrolyte has been prepared and investigated herein to increase the rate of safety and improve stability [14].

A device that combines both harvesting properties and energy storing provides lower fabrication cost. In a recent study, we have reported a cell that unified both a solar cell and a supercapacitor in one unit based two-electrodes configuration. The recency of the device is the nanocomposite thin film of a dye/conducting polymer (i.e. Polyaniline, PANI and Poly 3,4-ethylenedioxythiophene: polystyrene sulfonate, PEDOT:PSS) at the working electrode (i.e. Fluorine Doped Tin Oxide, FTO and Indium Tin Oxide, ITO) [157, 159, 160, 162].

Conducting polymer materials have been implemented in many research scopes as advanced materials such as energy storage, harvesting, and electronic applications. The most commonly conducting polymer materials are PANI, PEDOT:PSS, and Ppy. Conducting Ppy is particularly the utmost conducting polymer material studied due to stability on several substrates, high conductivity, ease of coating and fabrication, and low cost [163-165].

In this study, a two terminal hybrid photoactive supercapacitor is presented that has a multilayer structure with the electrodes made of Ppy/MB coated (photo-electrode); and MWCNT/paper to offer the double layer functionality of a supercapacitor in addition to its main catalytic performance, and a gel electrolyte which is shown in Figure 48 (a). Our proposed structure operates independently as a solar-capacitor device (Figure 48 (b)). Conducting Ppy film containing methylene blue were electrochemically deposited on the surface of FTO using polymerized P-Toluenesulfonic acid (PTS) as an electrolyte anion. The results of electrochemical and electrical measurements such as Cyclic Voltammetry (CV), Electrochemical Impedance Spectroscopy (EIS), Open Circuit Voltage ( $V_{OC}$ ), and Short Circuit Current ( $I_{sc}$ ) on the integrated cell have been discussed in this paper.

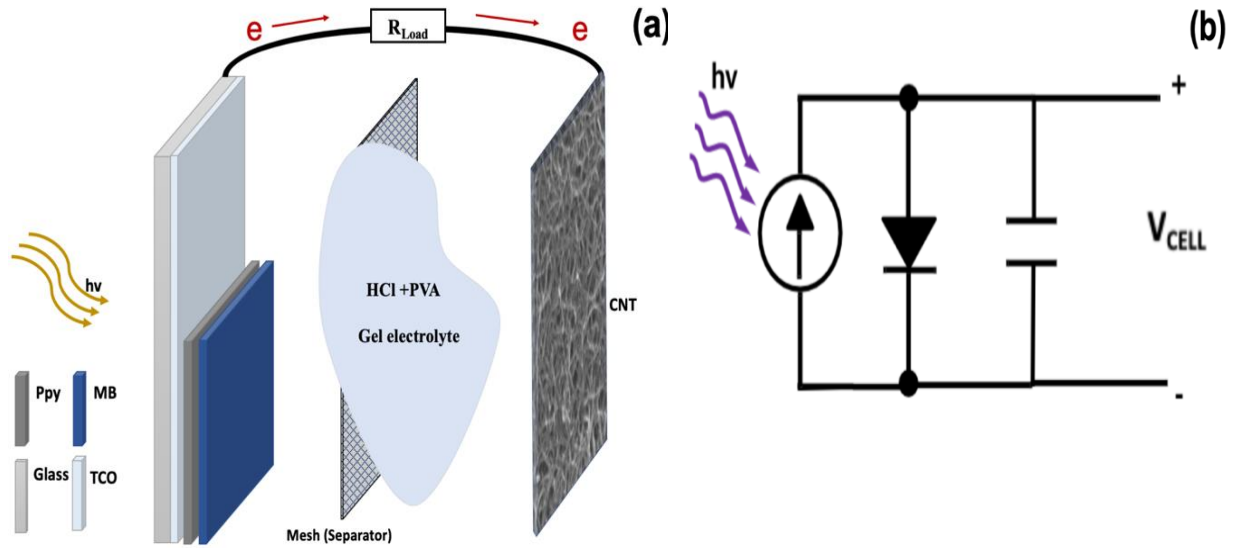


Figure 48: (a) Schematic Diagram of the Hybrid Device and (b) Electrical Circuit of Solar Cell with Supercapacitor.

## 7.3 Experimental Section

### 7.3.1 Materials and Instrumentation

P-Toluenesulfonic acid ( $\text{CH}_3\text{C}_6\text{H}_4\text{SO}_3\text{H}$ ) (PTS), multi-walled carbon nanotubes (MWCNT<sub>s</sub>), sodium dodecyl benzenesulfonate (SDBS) ( $\text{C}_{18}\text{H}_{29}\text{NaO}_3\text{S}$ ), polyvinyl alcohol (PVA) ( $\text{C}_2\text{H}_4\text{O}$ )<sub>x</sub>, hydrochloric acid solution (HCl), pyrrole monomer ( $\text{C}_4\text{H}_4\text{NCH}_3$ ), and methylene blue (MB) were procured from Sigma Aldrich. The paper substrates used for fabricating the electrodes were from Office Depot (8.5 in.  $\times$  11 in.). VersaSTAT 4.0 potentiostat with two-electrodes configuration was applied to measure the electrochemical and electrical tests. The devices were placed in a dark box connected via an optical fiber to a solar simulator (RST, Radiant Source Technology). The output power intensity of solar simulator was  $80 \text{ mW}/\text{cm}^2$ , which possessed an internal AM 1.0 optical filter. To eliminate the effect of ambient light in the experiment, a dark box and the shutter mechanism were designed.

### 7.3.2 Electrode Fabrication

MWCNT/paper electrode was prepared by mixing a 300 mg of MWCNT powder, 150 mg of a surfactant material SDBS [166], and 30 mL of DI water. The mixture solution of MWCNT and SDBS was placed in a beaker that contains an ice to reduce the heat of the probe sonicator. Then, the solution was sonicated for 30 min using a probe sonicator at 30 W. A drop casting technique was used to make the electrodes by dropping the conductive ink of MWCNTs solution on the surface of a (4 cm × 7 cm) paper and then cured in a vacuum oven for 30 min at 120 °C to make the electrodes completely dry. The procedure was reiterated three times to make it quite conductive. The conductive paper sheet was cut in rectangular pieces with the surface area of 4.0 cm x 1.0 cm, as functional counter electrodes. The thickness of the MWCNTs based electrodes was 15 μm.

For fabricating the working electrode, 0.9m M of MB dye material (only for fabricating electrodes with MB in the polymer), 0.05 M of pyrrole, and 0.05 M of PTS acid in 10 mL of DI water were mixed together. Then, the medley solution was sonicated for 10 minutes to make a homogenous solution. Afterward, fluorine doped tin oxide substrate (FTO) with a thickness of 1.65 mm and conductive layer resistance of 12 Ω/□ was cut (1 cm × 4 cm) and clean under several steps such as rinsed with DI water, sonicated in DI water for 5 minutes, and sonicated in methanol and ethanol for 5 minutes respectively to remove all possible contaminations. Monomer pyrrole was used for the growth of polymer film deposited under galvanostatic conditions by applying constant current density (0.15 mA.cm<sup>-2</sup>) for 200s to the electrochemical cell that has the FTO as working electrode and stainless steel as the counter electrode. The MB stands as one of the photonic and optical materials and works as cationic dye interacts with Ppy. Once the current is applied, the monomers get oxidized. After depositing the composite of Ppy and MB dye, the film

was washed with DI water. The FTO substrate was designated to have a (1cm×1cm) active area, the rest of the surface were covered using Kapton tape.

### 7.3.3 Preparation of Electrolytes

The gel polymer electrolyte was made by adding 1 g of PVA to 10 mL of DI water mixed with 2 M hydrochloric acid (HCl) solution. Later on, the electrolyte solution was placed on a hot plate of (75 °C) for 3 h with continuous stirring at the speed of 350 rpm. The HCl+PVA solution became conducting, transparent, and gel-based material. The gel was cooled down to room temperature before fabrication of any integrated devices.

## 7.4 Result and Discussion

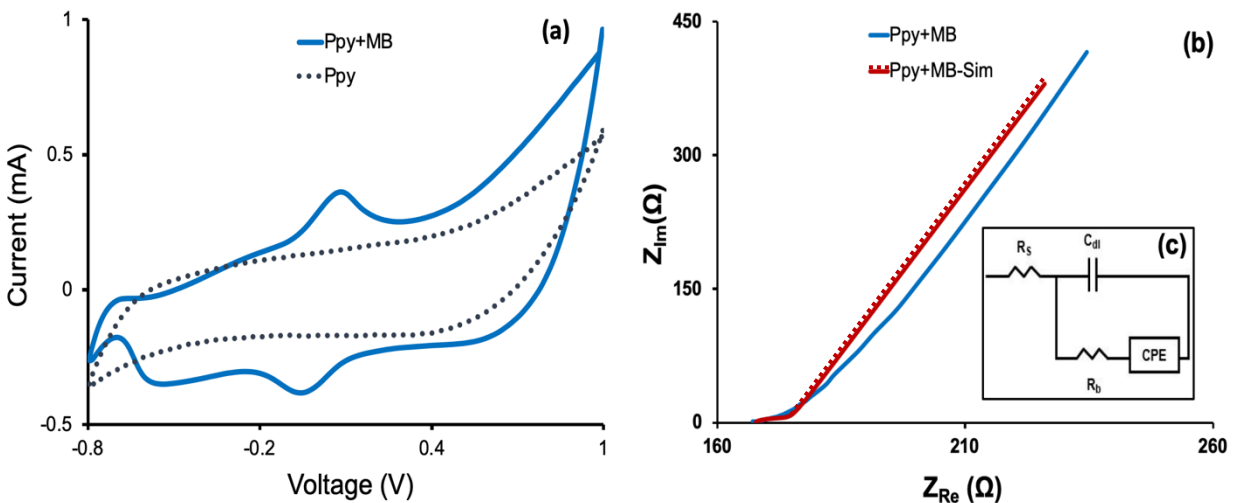


Figure 49: (a) Cyclic Voltammetry, (b) Nyquist Impedance of the Hybrid Device Based Ppy+MB Under the Dark Conditions, and (c) (Inset) Electrical Equivalent Circuit Model.

To evaluate the performance of the hybrid device for charge storage, cyclic voltammetry (CV) measurement was performed within the potential window from  $-0.8$  V to  $+1.0$  V and scan

rate at 50 mV/s. The CV measurements were carried out in a dark box to revoke the impact of ambient light. Figure 49 (a) represents the CV results of the hybrid cell that is based on Ppy and Ppy+MB coated on the photoactive electrode. A non-rectangular shape of the CV results based on both devices was achieved as depicted in Figure 49 (a). However, a couple of redox peaks were appeared on the CV result of the hybrid device based on Ppy+MB due the redox reactions of the embedded MB molecules to the conducting Ppy. Consequently, the capacitance of the cell based on nanocomposite thin film Ppy+MB is obviously higher than the cell based on Ppy only.

To understand the nature of the electrode-electrolyte interfaces and the role of charge storage of the nanocomposite thin film Ppy+MB in the integrated device, the electrochemical impedance spectroscopy (EIS) analysis is performed. Figure 49 (b) shows the results of the Nyquist impedance measurements for the experimental and simulation data with sinusoidal signal of 15 mV over the frequency range from 0.1 Hz to 10 kHz at 0.0 V DC biasing using VersaSTAT 4.0 Potentiostat. The nearly 45° slope in the low frequencies suggests a diffusion limited response being modeled as a constant phase element. The experimental result of Nyquist impedance was analyzed to estimate the value of each component by utilizing EIS Spectrum Analyzer software (version 1.0). The EIS Spectrum got the preferable fit to the experimental data. The small signal parameters of the electrical equivalent circuit as shown in Figure 49 (c) were estimated and listed in Table 11.

Table 11: Small Signal Parameters of Equivalent Electric Circuit Model.

Device	$R_s \Omega$	$R_b \Omega$	C (uF)	n	P (S.sec)
Hybride Device based Ppy+MB photoactive electrode	9.61	167.66	500	0.9035	0.0035

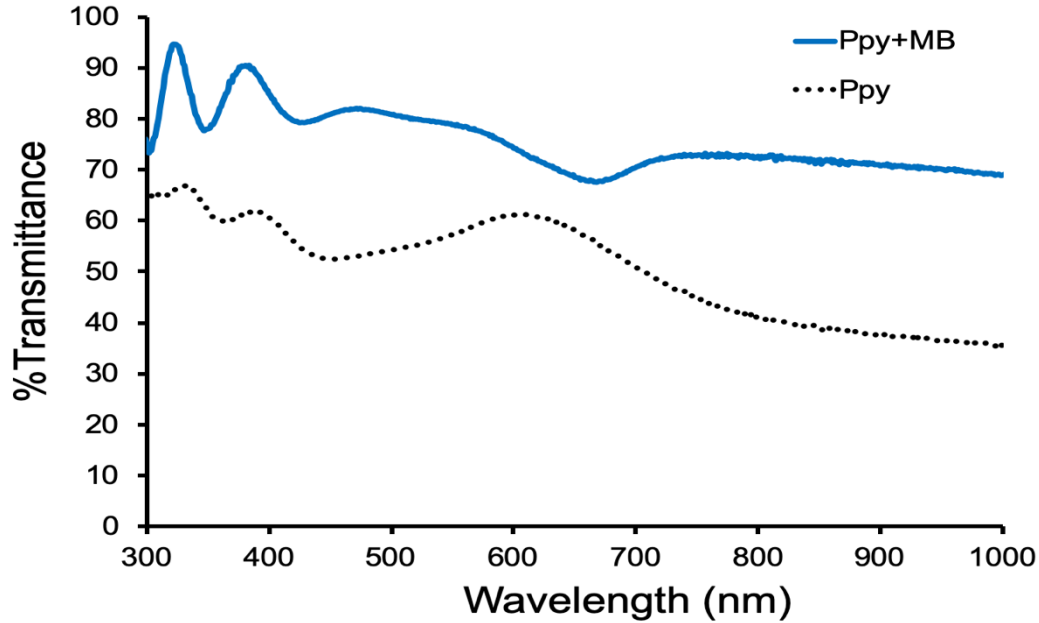


Figure 50: UV-Visible Spectroscopy for Ppy Thin Film and Ppy Composite with MB.

The optical properties of Ppy film and nanocomposite thin film of Ppy+MB that deposited onto FTO glass were measured using the UV-visible spectroscopy as shown in Figure 50. MB dye can be easily blended with conducting Ppy to enhance the photo-redox properties. The high energy photons are more absorbed by the composite of MB dye and the conducting Ppy as shown in Figure 50. Therefore, photo absorption can be raised by incorporating nanocomposites of Ppy with MB dye.

The photovoltaic effects were studied by monitoring the change in the open circuit voltage ( $V_{OC}$ ) and short circuit current ( $I_{SC}$ ) in the dark and light conditions as shown in Figure 51 and 52. The position of the cell was horizontal in a glass slide with a path length of 10 cm from the Radiant Source. After the electrochemical experiments (i.e. CV and EIS) the hybrid cell was kept in the dark box for about one hour until a stable OCV was achieved. Then the cell was exposed to the light for 100 s, using the solar simulator. The  $V_{OC}$  across the cell based Ppy film (Working



electrode) as shown in Figure 51 was 5 mV in the dark, but the cell voltage was increased gradually from 5 mV to 10 mV in 100 s of illumination. After turning off the light, the voltage dropped immediately to the initial dark value. The photocurrent result was neglected due to its very small value.

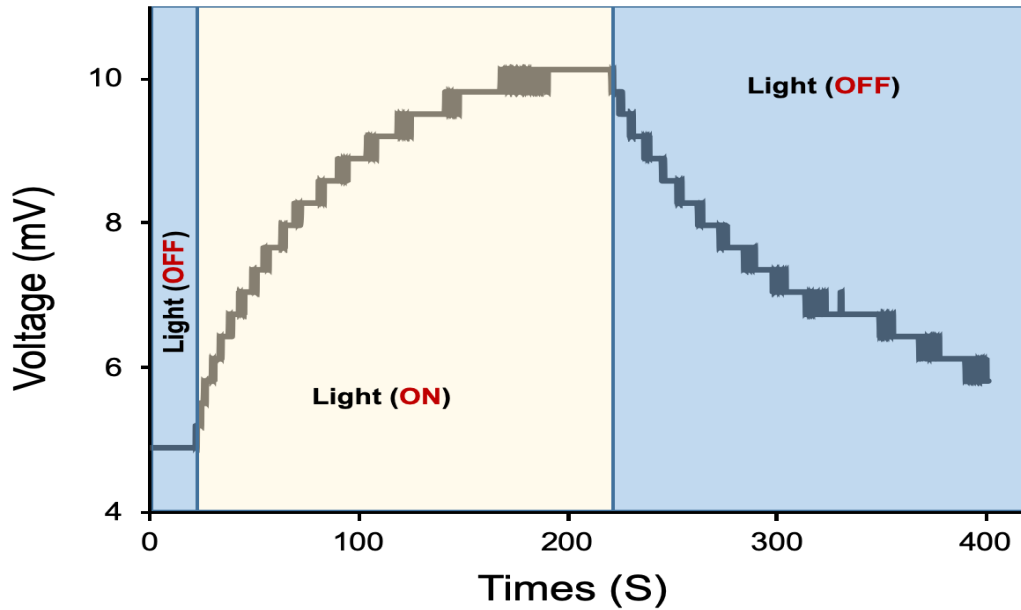


Figure 51: Open Circuit Voltage for a Device with Ppy Coated on Photoactive Electrode.

However, for the second hybrid device based on Ppy+MB thin film as shown in Figure 52 (a), the  $V_{oc}$  across the cell in the dark was 52 mV. But, under the effect of light the cell voltage was increased gradually from 52 mV to 75 mV in 100 s. After severance the light, the voltage did not drop to the initial dark value, and only 10 mV voltage drop in 300 s was recorded. The slow reduction in the voltage was likely due to the leakage current across of the double layer capacitor. Hence, the cell voltage of the hybrid device increased by the blend of MB dye with Ppy film.

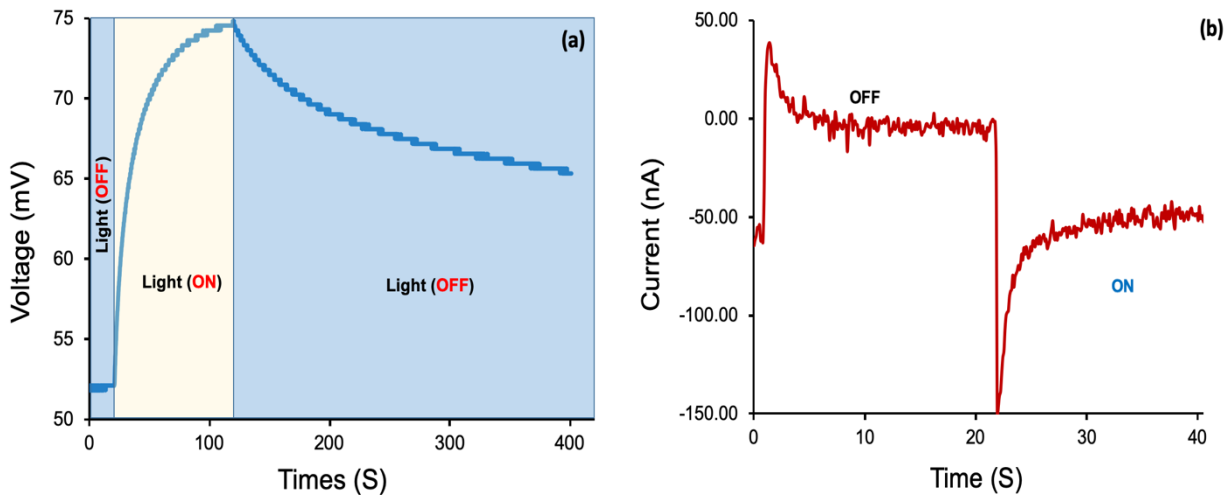


Figure 52: (a) Open Circuit Voltage for a Device with Ppy+MB Coated on Photoactive Electrode and (b) Short Circuit Current of a Device Under Pulses of Solar Simulated Light.

Not only that but also the photocurrent result, which was measured at (0 V), was accomplished as shown in Figure 52 (b). The response of the photocurrent was under the effect of dark and light conditions. The change in the photocurrent was due to the existence of dye molecules that embedded in the conducting polymer (i.e. Ppy) and the photo effect properties of the Ppy. A current fluctuation that appears in the photocurrent result is due to the parasitic effects.

## 7.5 Conclusion

A photoactive supercapacitor device with two-electrode type based on a nanocomposite thin film Ppy+MB photo-electrode and a MWCNT/paper to display the double layer capacitor functionality was fabricated by employing in situ self-assembled deposition technique. The efficiency of the device was not measured due to the low photocurrent result and relatively large storage effect. The results manifested the potential of consolidating harvesting energy and storage in a single device with two-electrodes configuration. Electrical and optical properties of thin film Ppy and nanocomposite Ppy+MB have been achieved herein. Additional study is needed to

investigate the effect of adding metal oxides materials such Titanium Dioxide ( $\text{TiO}_2$ ) or Zinc Oxide ( $\text{ZnO}$ ) on the performance of photovoltaic and energy storage via studying the energy structure of the proposed device. Furthermore, there are still some technical problems for practical applications e.g. sealing and packaging the device, which must be considered in accordance with device evolution.

## Chapter 8: A Polyaniline-Based Redox-Active Composite Gel Electrolyte with Photo-Electric and Electrochromic Properties<sup>5</sup>

### 8.1 Abstract

A polyaniline (PANI)-based gel material with a redox-active nature has demonstrated unique charge storage, photovoltaic, and electrochromic properties in the bulk of the gel. The specific capacitance in the volume of the gel was measured to be  $428.9 \text{ mF g}^{-1}$ . Also, a hybrid device for concurrent solar energy harvesting and charge storage was made simply by placing a layer of the gel between a  $\text{TiO}_2$  coated electrode and a carbon electrode. The hybrid device showed 137 mV open circuit voltage under the light condition with only 10 mV voltage drop in 600 s after cessation of light. The electrochromic property of the composite gel was also studied in a device made of two transparent electrodes. The results showed 64% transmittance at 564 nm and zero transmittance when the cell was biased at 0.0 V and 2.0 V, respectively. The photoelectric property and the redox-active nature of the gel suggest existence of both ionic and electronic conductions through the electrolytes. The results are encouraging to further customize the composite gel for various applications, including supercapacitors, solar cells, photoactive supercapacitors, and electrochromic windows.

---

<sup>5</sup>This chapter is accepted for publication in ChemElectroChem Journal as an online copy (not published one) (Aljafari, Belqasem, Sharan Kumar Indrakar, Manoj K. Ram, Prasanta Kumar Biswas, Elias Stefanakos, and Arash Takshi. "A Polyaniline-Based Redox-Active Composite Gel Electrolyte with Photo-Electric and Electrochromic Properties." In Appendix C.

## 8.2 Introduction

To endure the evolution of green energy sources, harvesting, storage, and delivering energy is paramount to limit the dependence on nonrenewable sources. Electrochemical devices are exemplary applications to achieve this demand and cope with the intermittent nature of renewable energy sources. Some examples of such devices are supercapacitors, dye sensitized solar cells (DSSCs), and electrochromic windows [43, 167-171]. Great efforts have been made to improve the performance and durability of the materials used as electrodes and electrolyte of such devices. As low-cost and flexible materials, conducting polymer (particularly polyaniline, PVA) based composite gels have received great attention to be used as the electrode material in supercapacitors [172-182].

Li et al. have reported the supramolecular assembly of polyvinyl alcohol (PVA) and PANI for fabrication of flexible supercapacitors with  $13.6 \text{ Whkg}^{-1}$  energy density [175]. In another work, graphene oxide was mixed with a composite gel to make supercapacitor electrodes with the specific capacitance of  $438.8 \text{ Fg}^{-1}$  [173]. Also, in a device made by researchers at the National Center for Nanoscience and Technology Beijing, PANI was embedded in a hydrogel film of PVA– $\text{H}_2\text{SO}_4$  for making a flexible supercapacitor that presented  $488 \text{ mF cm}^{-2}$  capacitance [178].

In addition to the applications of the gels as the electrode material, due to their low volatility, high thermal stability, and safety, gels are one of the most promising candidate materials as the electrolyte in various electrochemical devices [179, 183-185]. Deka et al. have found a significant enhancement of the ionic conductivity and interfacial stability in a composite gel electrolyte by incorporating dedoped (insulating form) PANI nanofibers to the gel [181]. Nath et al. have reported a solid-state DSSC with 2.18% efficiency using a composite hydrogel electrolyte containing PANI, PVA, and carbon nanotubes [179].

While in the most reported works, the gel materials were used as either the electrode or electrolyte of devices, we have found that that due to the ability of conducting both ionic and electronic charges, a single layer of PVA-PANI composite gel can be employed as a functional material to serve as the redox-active electrode and electrolyte. This simplifies the fabrication process and converts the electrolyte to an active part of the electrochemical cells. More importantly, it is found that the redox nature and the photoelectric properties of a PVA-PANI gel can be used to fabricate electrochromic devices [186], supercapacitors, solar cells, and even a hybrid photoactive supercapacitor by simply sandwiching a single layer of the gel between different electrodes.

## 8.3 Experimental Section

### 8.3.1 Materials

All chemical materials, including multi-walled carbon nanotubes (MWCNTs), sodium dodecyl benzenesulfonate (SDBS), polyvinyl alcohol (PVA), hydrochloric acid (HCl), aniline, and ammonium persulfate (APS) were purchased from Sigma-Aldrich and used as received without any further purification. FTO electrodes were purchased from Huanyu Instrument (China) with 1.66 mm thickness and  $12 \Omega \text{ cm}^{-2}$  sheet resistance. Pt-coated FTO conductive electrodes (2.0 cm  $\times$  2.0 cm) and TiO<sub>2</sub> coated FTO electrodes (2.0 cm  $\times$  2.0 cm with 6 mm  $\times$  6 mm active area - TiO<sub>2</sub> coated part) were purchased from Solaronix. Two pieces of glassy carbons (25  $\times$  25  $\times$  3 mm<sup>3</sup>) were purchased from SPI Supplies. The paper substrates used for making the electrodes were standard letter-size copy paper from Office Depot.

### 8.3.2 Electrode Preparation

Porous carbon electrodes were made using in-house prepared MWCNT-based ink on the copy papers. Following the instruction developed by Hu et al., [101] the ink was made by first mixing 300 mg of CNTs and 150 mg of SDBS in 30 mL of deionized (DI) water. Then, the solution was sonicated for 30 min using a probe sonicator at 30 W and 40 J average power and energy, respectively. The conductive ink solution was used to make the electrodes by drop casting 1 mL on the surface of a piece of a paper (4.0 cm × 7.0 cm) and drying in a vacuum oven for 30 min at 120 °C. The process was repeated three times to make the electrodes conductive enough. The conductive paper sheet was cut in rectangular pieces with the surface area of 4.0 cm × 0.8 cm or 4.0 cm × 0.6 cm, as electrodes for supercapacitors and photoactive supercapacitor devices. The thickness of the CNTs based electrodes was 150 μm. Additionally, the conductivity of the electrodes was measured to be 98 S cm<sup>-1</sup> using a custom made four-probe setup connected to a Keithley (2602) source-meter unit.

Before using, FTO, Pt, FTO-TiO<sub>2</sub> and glassy carbon electrodes were cleaned by rinsing with DI water, sonicating in DI water for 5 min, and sonicating in methanol and then in ethanol each for 5 min. The cleaned electrodes were dried under hot air flow.

### 8.3.3 Composite Gel Preparation

First, PVA-HCl gel electrolyte was made by dissolving 5 g of PVA in 100 mL of 1 M HCl in a beaker. Then, the solution was stirred continuously and heated at 75 °C for 6 hrs at a speed of 400 rpm. After that, 30 ml solution of 0.1 M APS in 1 M HCl was added to the PVA-HCl solution at room temperature and stirred for 30 min at 600 rpm. At last, the composite gel was made by adding 3 ml of aniline to the PVA-HCl-AP at room temperature and stirred for 12 h. The composite

gel polymer electrolyte was kept in a beaker (covered by a piece of Parafilm) at room temperature for at least a week before fabrication of the devices.

#### 8.3.4 Device Fabrication

Devices were made by coating the entire surface of one of the electrodes with the composite gel, putting one layer of a fiberglass mesh (mesh thickness of 270  $\mu\text{m}$ ) or a Parafilm frame (130  $\mu\text{m}$  thick) as separator, and putting the second electrode on the mesh and pressing them together with binder clips. Mesh separators were used for the device with the glassy carbon electrodes and the supercapacitor (CNT based electrodes). In the supercapacitor, the gel covered only 8 mm  $\times$  8 mm of each electrode. Frames were cut from a Parafilm and used between the two electrodes in the solar cell, hybrid photoactive supercapacitor, and electrochromic devices. The effective area covered by the gel in the solar cell and the hybrid device was only 6 mm  $\times$  6 mm (i.e.,  $\text{TiO}_2$  coated area on FTO). The gel covered area in the electrochromic device was 2.0 cm  $\times$  1.5 cm.

#### 8.3.5 Electrical and Electrochemical Measurements

VersaSTAT 4 potentiostat with two-terminals configuration was used to measure the electrochemical and electrical tests, including CV, EIS, galvanostatic method, open circuit voltage, and short circuit current all in the two-probe configuration. All CVs were conducted at 50  $\text{mV s}^{-1}$  scan rate. Multiple cycles were tested, and the last cycle of each experiment is reported in this work, except for the device with the glassy carbon electrodes that both the first and last cycle data is reported. All EIS studies were done at 0.0 V DC bias with an AC voltage amplitude of 20 mV for a frequency range of 0.1 Hz to 10 kHz. All the electrochemical measurements were carried out at room temperature. More specifically, the measurements for the supercapacitor and



electrochromic devices were performed at ambient light in the lab. However, the hybrid photoactive supercapacitor and the solar cell were placed in a dark box connected via an optical fiber to a solar simulator (RST, Radiant Source Technology) with an output power intensity of  $80 \text{ mW cm}^{-2}$ , which was equipped with an internal AM 1.0 optical filter. The experimental setup, including the dark box and the shutter mechanism, was designed to eliminate the effect of ambient light in the experiment. UV-Vis spectra and the transmittance data were recorded by a Thermo Scientific Evolution 201/220 UV-Visible Spectrophotometer. FTIR and Raman analysis were done by using PerkinElmer Spectrum 100 FT-IR and LabRAM HR Evolution, respectively.

#### 8.4 Results and Discussion

The composite gel material was synthesized by first mixing polyvinyl alcohol (PVA) and hydrochloric acid (HCl) in water. In two steps, ammonium persulfate (APS) and monomer ‘aniline’ were added. APS and HCl reacted with aniline to polymerize it to PANI, forming a uniformly distributed conducting polymer in the PVA gel. Chemically synthesizing PANI in the presence of APS in HCl containing composite gel produces emeraldine salt (ES) which is naturally green in color [187].

The optical absorption of the composite gel with PANI was studied and compared with the gels made from only PVA, PVA-HCl, and PVA-HCl-APS. As shown in Figure 1.a, the gels without PANI were all transparent, but the absorption spectrum of the gel containing PANI confirmed the formation of the ES form of the polymer. The relatively broad absorption peak around 775 nm corresponds to the energy gap between the valence and polaron bands, and the peak at 350 nm is attributed to the transition from the valence band to the conduction band. Also, the shoulder at 440 nm is ascribed to the polaron to the conduction band transition, as shown in

inset Figure 53.a [187, 188]. The FTIR study was done to learn about the interaction of the PVA polymer matrix with APS and PANI. After normalization in the range of 650-4000  $\text{cm}^{-1}$ , the FTIR spectra (Figure 1.b) showed several transmittance peaks for PVA, PVA-HCl, PVA-HCl-APS, and PVA-HCl-APS-PANI. The wide absorption at the wavenumber from 3700–3000  $\text{cm}^{-1}$  is due to the symmetry of the stretching vibration of hydroxyl in PVA. Also, NH stretching vibration of the -C<sub>6</sub>H<sub>4</sub>NHC<sub>6</sub>H<sub>4</sub>- groups of PANI is present in this region [189]. The band at 2950-2660  $\text{cm}^{-1}$  is related to C-H stretching in the alkyl group [190, 191].

The above broad band nature is extended up to nearly 2500  $\text{cm}^{-1}$  in presence of PANI. In the wavenumber range, 2950-2600  $\text{cm}^{-1}$  only one shoulder was observed in the FTIR spectrum of PVA while in presence of PANI, two shoulders appeared in this region with relatively high prominent feature. These well-defined shoulders at around 2950 and 2637  $\text{cm}^{-1}$  are possibly due to the strong H-bonding of hydroxyl group of PVA with PANI in addition to the stretching vibrations related to C-H. To understand the interaction of PVA with PANI during the reaction progress, the band at around 1000-1150  $\text{cm}^{-1}$  of PVA should be precisely noted in presence of acid, APS and PANI. The band at 1100  $\text{cm}^{-1}$  may be attributed to O-H deformation and C-O stretching vibration of secondary alcohol of PVA in PVA [192] as well as in PVA + HCl. In the presence of APS this band apparently splits, and a new band appears at around 1050  $\text{cm}^{-1}$  which is possibly due to the start of oxidation of PVA. Intensity of this band decreases in presence of PANI. During oxidation the stretching vibration of C=C becomes more symmetric and it shows at ~1650  $\text{cm}^{-1}$ . The bands at 1283  $\text{cm}^{-1}$  (assigned as C-N stretching due to the linkage of APS with PVA), 1105  $\text{cm}^{-1}$  (C-O stretching) and 820  $\text{cm}^{-1}$  (C-S stretching) are for PVA-APS gel-based electrolyte [193, 194]. Two main peaks at around 1450  $\text{cm}^{-1}$  and 1283  $\text{cm}^{-1}$  occur for C-C and C-N stretching modes, their shapes differ along with intensity ratio being opposite in presence of PANI. Broadening of

these bands usually occur due to differentiation of their bond order [195]. In addition, the expanded intensities of C-O and C-S stretching of PANI composite gel electrolyte in comparison to the other materials are apparent which also verifies the interaction of PANI with PVA and APS materials [196].

For further investigation, Raman spectra were taken for all similar systems to understand the interaction between PVA and PANI. The band at  $1080\text{ cm}^{-1}$  of PVA is assigned as O-H bond deformation [192]. In presence of HCl, line broadening occurs possibly for cross linking of PVA [197], which shifts towards lower wavenumber with disappearing nature to support oxidation by APS. On the other hand, in presence of PANI, it shifts to higher wavenumber,  $1130\text{ cm}^{-1}$  along with the development of three characteristic bands due to the stretching of (i) C-N<sup>+</sup> (ii) imine (iii) and partially charged imine groups [198]. The band for C-N<sup>+</sup> appears at around  $1330\text{ cm}^{-1}$  with splitting pattern having peaks at  $1320$  and  $1340\text{ cm}^{-1}$  which are possibly for polaron and bipolaron effects. The stretching vibration of C-O of PVA after interaction with PANI may also contribute to this  $1340\text{ cm}^{-1}$  band. The Raman spectrum of PVA shows a band at around  $1360\text{ cm}^{-1}$  which appears at lower wavenumber,  $1340\text{ cm}^{-1}$  for interaction with PANI. The contribution of benzenoid and quinoid structures of PANI was studied by Raman spectra (Figure 1.c). Band shift (a mixed mode of the C=N and CH=CH stretching vibrations) due to the quinoid structure appears around  $1485\text{-}1471\text{ cm}^{-1}$  [199, 200]. In addition, other band shifts at  $1150, 950, 870$  due to C-H in-plane bending and C-N-C of the benzene ring are related to both polaronic and bipolaronic structures in the PANI in the presence of HCl and PVA [201].

To study the electrical properties, a layer of the PVA-PANI gel (thickness=  $\sim 270\text{ }\mu\text{m}$ ) was sandwiched between two glassy carbon (GC) electrodes with an area of  $25\times 25\text{ mm}^2$ . The cell was then tested via the cyclic voltammetry (CV) and electrochemical impedance spectroscopy (EIS)

methods. The redox peaks in the CV result (Figure 1.d) and nature complex impedance (Figure 1.e) show that the PANI composite gel electrolyte has a charge storage property like a pseudocapacitor. The magnitude of the capacitance was estimated from the CV data to be 38.6 mF, which is two orders of magnitude higher than the estimated double layer capacitance in a device with non-porous electrodes and surface area of  $25 \times 25 \text{ mm}^2$  [110].

While the glassy carbon is not a redox active material and the storage capacitance in a gel without the conducting polymer is negligible (Figure S1 in the supporting information), the symmetric redox peaks in the CV loop suggest a pseudocapacitive charge storage mechanism in the bulk gel electrolyte due to the presence of PANI. Considering the mass of the gel, the specific capacitance ( $C_{\text{gel}}$ ) of the composite gel has been calculated to be  $428.9 \text{ mF g}^{-1}$ . The mechanism of charge storage in the volume of the gel can be explained through the change in the oxidation state of PANI (inset Figure 1.d) between leucoemeraldine salt (LS) and ES by removing/adding electron and proton ( $\text{H}^+$ ) pairs in a reversible redox reaction:



The reversibility of the reactions and the stability of the gel in a non-sealed device was confirmed after 1000 cycles in the CV with <1% change in the capacitance (Figure S2). Since the conducting polymer is dispersed inside the bulk gel, the occurrence of the redox reaction implies the capability of the composite gel to conduct both electronic and ionic charge. The profile of the Nyquist response from the EIS result (Figure 53.e) confirms this feature by showing a pure constant phase element response that can be modeled as distributed elemental capacitances and resistors in the bulk gel (Figure 53.f). In this model, each monomer mimics a capacitor,  $C$ , that can be charged or discharged by receiving/donating an electron- $\text{H}^+$  pair.  $R_{\text{ion}}$  and

$R_{ele}$  represent the elemental resistors for ionic and electronic charge transport through the composite gel, respectively.

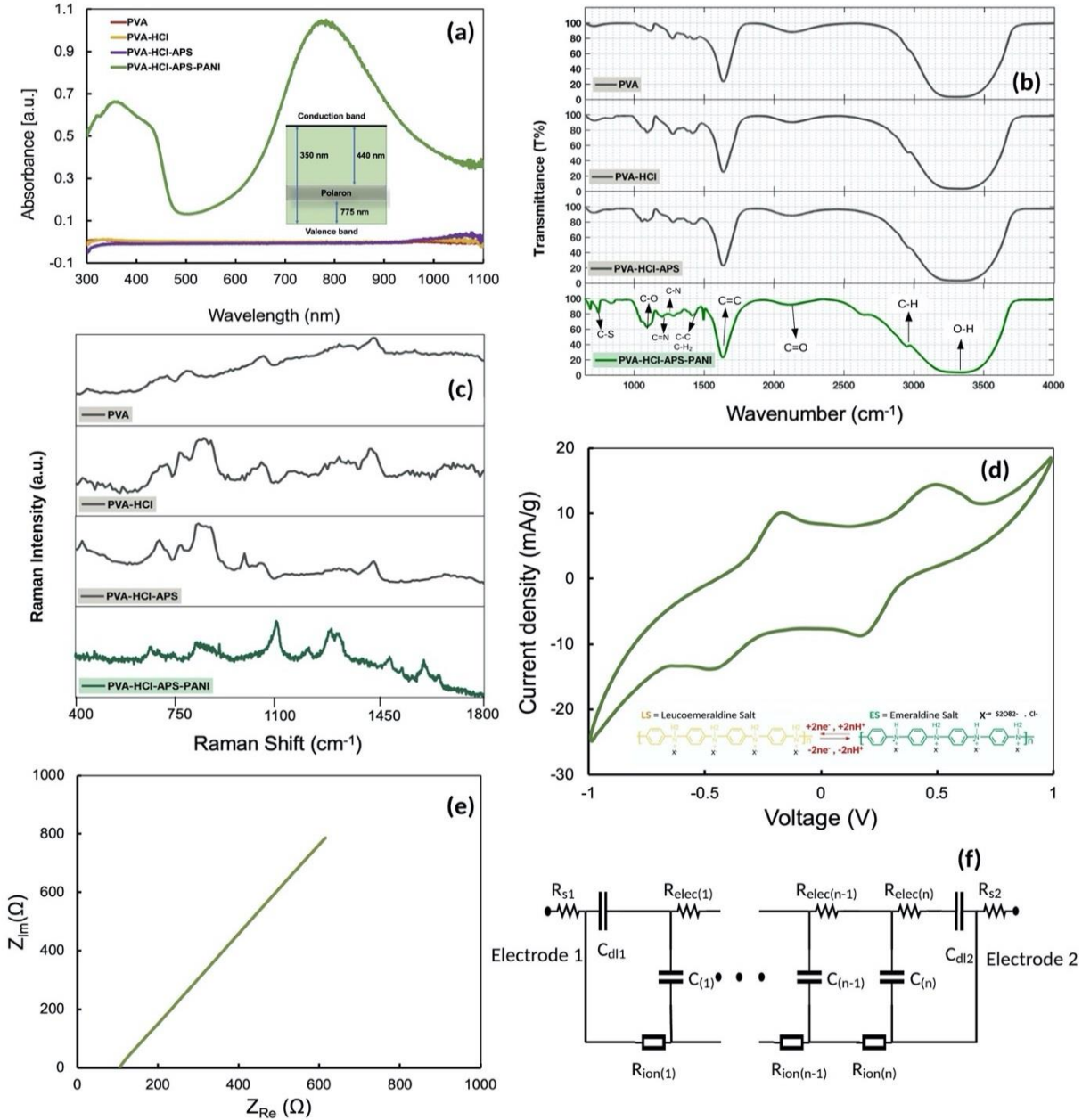


Figure 53: (a) UV-Vis Absorption Spectrum, (b) FTIR Spectrum, and (c) Raman Spectrum of the Composite Gel of PVA-HCl-APS-PANI, PVA, PVA-HC, and PVA-HCl-APS. (d) CV Result and (e) Nyquist Plot From the EIS Study of a Thin Composite Gel Layer Sandwiched Between Two Glassy Carbon Electrodes and (f) Equivalent Electrical Circuit Model of the Complex Impedance in the Gel. The Inset Figure in Plot (d) Shows the Transition of PANI From ES to LS Form.

Since one expects the formation of double layer charges at the interfaces between the gel and the electrodes, two capacitors ( $C_{dl1}$  and  $C_{dl2}$ ) are considered in the model. The resistance of the electrodes is also shown as series resistors  $R_{s1}$  and  $R_{s2}$ . Due to the distributed capacitors in the volume of the gel, when a voltage is applied across the gel layer, a progressive charging process is expected by pumping positive and negative charges from the electrodes until all the elemental capacitances are charged.

Recognizing this unique capability of storing charge in the PANI composite gel, a simple supercapacitor device was fabricated with two carbon nanotubes (CNTs) based porous electrodes and the PANI based composite gel as the electrolyte. Figures 54.a and 54.b show a schematic and a picture of the supercapacitor with the gel layer thickness of  $\sim 270 \mu\text{m}$ . In Figure 54.c, The CV result from the device with the PVA-HCl-APS-PANI gel electrolyte is compared with that in a similar device with an acidic gel of PVA-HCl. The results clearly show the advantage in employing both ionic and electronic conductivity in the composite gel to store charges in the volume of the electrolyte as well as at the double layers.

The absence of the redox peaks in the CV result from the PANI composite gel implies domination of the storage via the double layer charges due to the high porosity of the electrodes. Supercapacitor devices with gel electrolytes with and without the conducting polymer was further studied via the EIS and galvanostatic charging methods. The results presented in Figures S3 and S4. Specifically, the galvanostatic test (Figure S4) showed an equivalent series resistance (ESR) of  $\sim 83 \Omega$ . Considering the poor conductivity of the CNT electrodes, application of more conductive electrodes with current collectors would reduce ESR significantly [202].

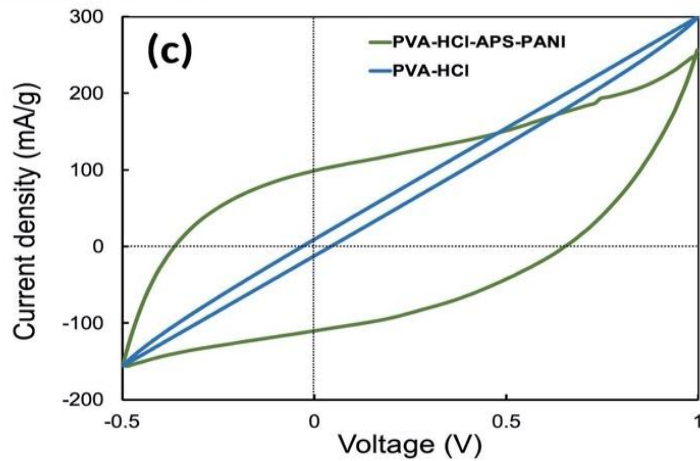
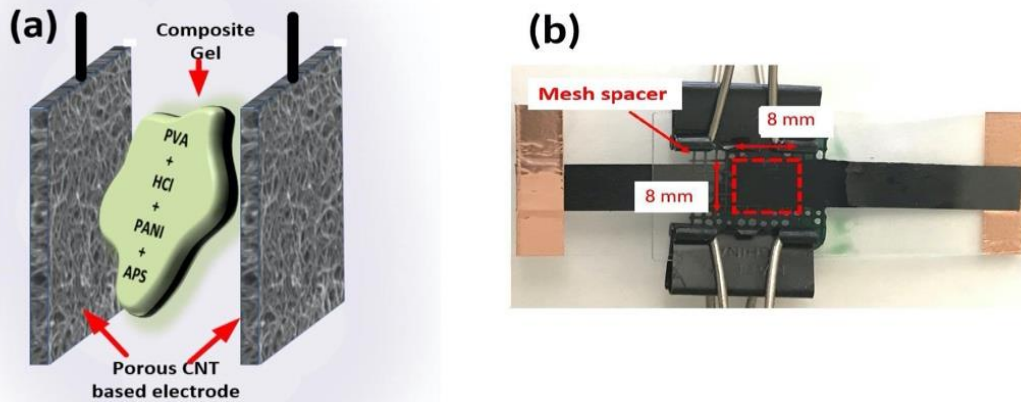


Figure 54: (a) Schematic Diagram, (b) A Picture of the Fabricated Supercapacitor with CNT Based Porous Electrodes and a Thin Layer of the Composite Gel as the Electrolyte and Active Redox Material and (c) CV Results From Devices with Two Different Gels: PVA-HCl and PVA-HCl-APS-PANI.

The overall capacitance of the device with the PANI-based gel was estimated from the CV result to be 48 mF which corresponds to  $3.33 \text{ Fg}^{-1}$  (specific capacitance) based on the mass of CNTs on the electrodes [138]. The specific capacitance can be significantly increased by optimizing the electrode material and structure. For instance, much higher capacitances can be achieved by using composite redox active materials with graphene, conducting polymers, and molybdenum disulfide for the electrodes [203-206]. With the mechanism of charge storage

inside the gel volume, potentially, devices can be fabricated with higher energy and power densities than conventional devices without this feature. The concept of using small-molecule based redox active materials in the electrolyte of a device for partial charge storage has been reported before [67, 82, 83]. In the composite gel, PANI is acting as the redox material and the hydrogenation/dehydrogenation of PVA adds to the storage capacity of the bulk gel [110]. Considering the low cost of the gel material, simplicity in device fabrication, and no need for sealing devices, the PANI composite gel is potentially suitable for fabricating high capacitances, low-cost, and flexible supercapacitors.

The UV-vis study of the PANI composite gel (Figure 53.a) showed light absorption by PANI. Therefore, the feasibility of harvesting solar energy by the composite gel was studied in a DSSC-like device. As shown in Figure 55.a and 55.b, the gel was placed between two electrodes: a TiO<sub>2</sub> coated FTO (Fluorine-doped tin oxide) as the anode and a Pt-coated FTO as the cathode. In this configuration, dye material was not used, and the gel acted both as the electrolyte and photoactive layer in which PANI (ES form) was the photoactive material and PVA mesh with ions served as the electrolyte.

The current-voltage characteristics of the device were measured both under dark and under simulated sunlight conditions. The J-V characteristics in Figure 55.c clearly show the generated power under illumination. From the results, the device was found to have an open circuit voltage ( $V_{oc}$ ) of 0.48 V and a short circuit current density ( $J_{sc}$ ) of 0.12 mA.cm<sup>-2</sup>. However, the fill factor and overall conversion efficiency were relatively low compared to conventional DSSCs with a separate layer of dye materials and liquid electrolytes [207]. This can be further addressed by adding dye materials to the gel.



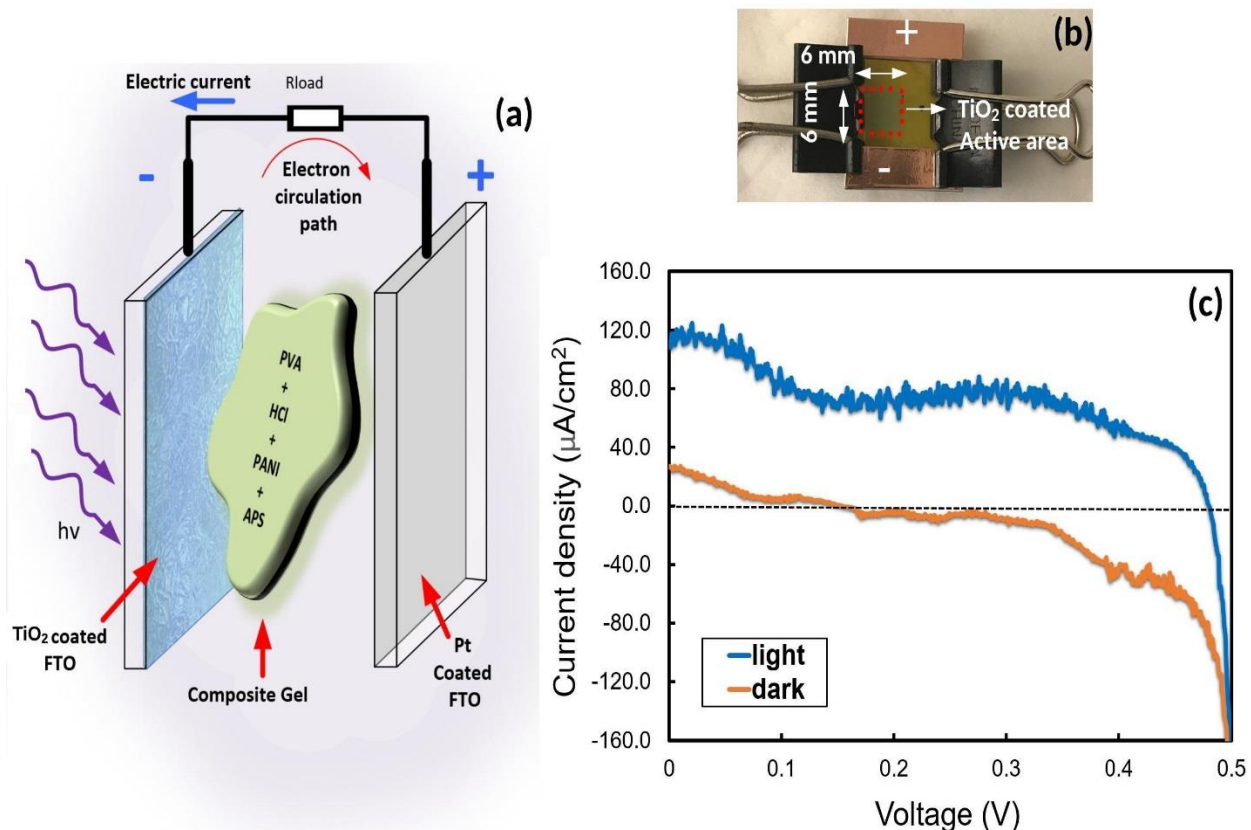


Figure 55: (a) Schematic Diagram, (b) A Picture of the Fabricated Solar Cell with the Composite Gel and (c) J-V Characteristics of the Solar Cell Device in Dark and Light.

Since the composite gel demonstrated both energy storage and solar energy harvesting capabilities, we designed and tested a hybrid device for concurrent harvesting and storage in a single two-terminal device (i.e., photoactive supercapacitor). The hybrid device was made as before with a single layer gel between two electrodes: a FTO-TiO<sub>2</sub> and a porous CNT-based electrode (Figure 56.a and 56.b). Fig. 56c shows the CV measurements under dark conditions. The loop verifies the internal storage capacity. A part of this storage effect is due to the double charges at the electrode-electrolyte interfaces. However, the redox peaks imply additional charge storage in a pseudocapacitive form, occurring inside the volume of the composite gel electrolyte due to the existence of PANI and PVA. From the electrical response of the cell in the dark (Figure 56.c), the specific capacitance of the cell was calculated to be 1.53 Fg<sup>-1</sup>. Additional

characterization of the photoactive supercapacitor through the galvanostatic test (Figure S5) showed an equivalent series resistance (ESR) of  $\sim 120 \Omega$ .

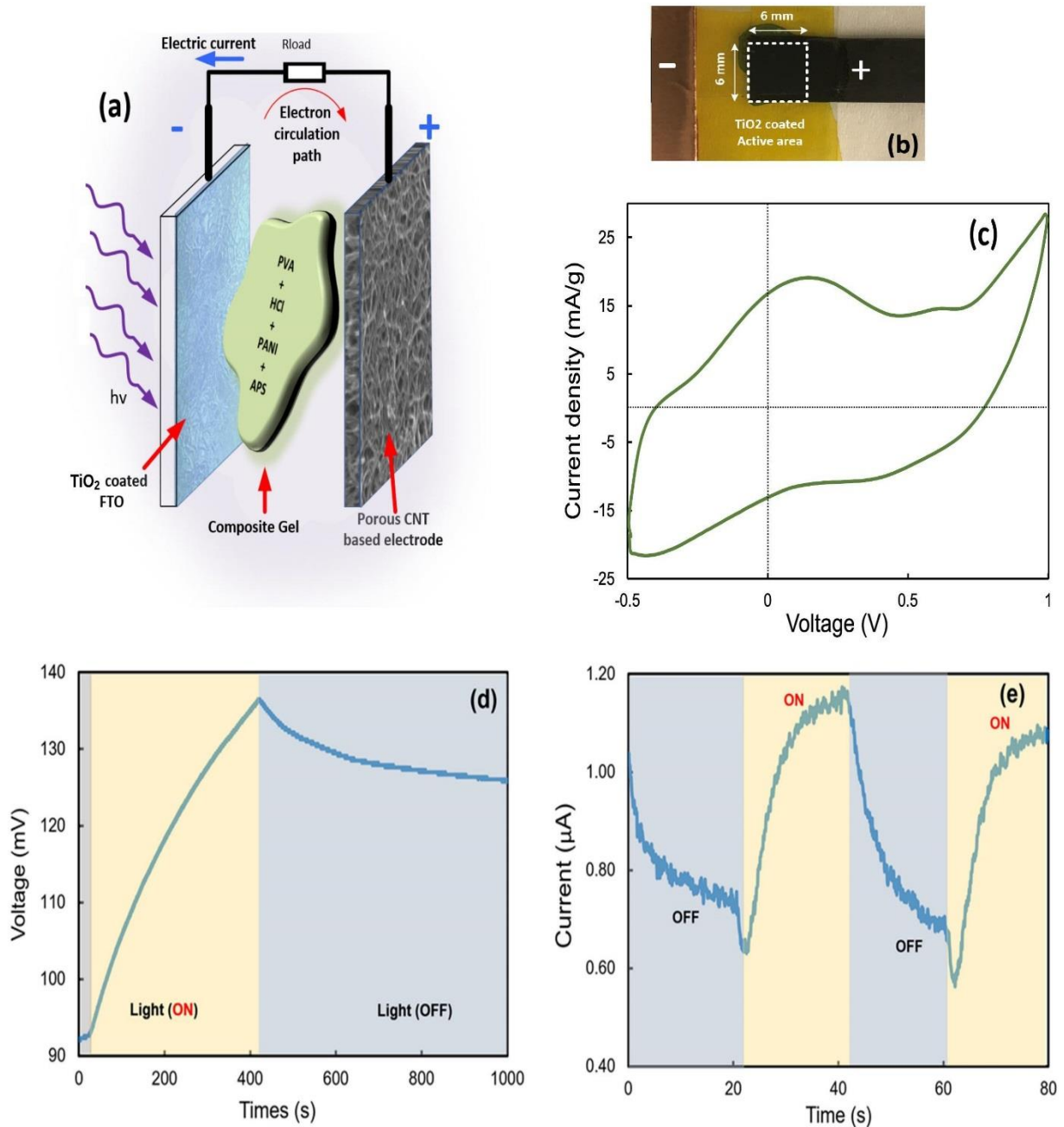


Figure 56: (a) Schematic Diagram, (b) A Picture of the Hybrid Photoactive Supercapacitor for Energy Harvesting and Storage, (c) CV of the Hybrid Device, (d) Open Circuit Voltage and (e) Short Circuit Current Versus Time Under Light and Dark Pulses.

To study the capability of the device for solar energy harvesting, the open circuit voltage of the cell was monitored under dark and light conditions. As shown in Fig. 56d, the voltage across the cell was increased gradually from 92 mV (dark) to 137 mV in 400 s under light conditions. The gradual voltage change is due to the storage property of the device [160]. The trend in the voltage change suggests that longer illumination time could result in a larger voltage increase before reaching a saturated level when the internal capacitor is fully charged. After cessation of the light, the voltage did not return to its initial dark value. Instead, the slow change in the voltage under dark conditions (i.e. 10 mV drop in 600 s) shows the capability of the gel to retain the charge for a relatively long time. This implies low leakage current in the discharge process.

Additionally, the short circuit current in the cell was studied under alternating 20 s of dark and light pulses (Fig. 56e). The non-zero current in the dark is from the stored charges. However, the current showed an increase of  $\sim 0.5 \mu\text{A}$  when the cell was illuminated by the solar simulator. The low current in the dark is because of the large internal resistance. It should be mentioned that the conventional J-V characteristics do not reflect the full capability of the cell due to the large storage effect and the low photocurrent [160].

Therefore, no attempt was made to measure the efficiency and the fill-factor of the device. The majority of hybrid devices were made by integrating a DSSC with a supercapacitor in one package and sharing one of the electrodes of each cell to make a three-terminal hybrid device [12, 143, 151, 152, 208-214]. For practical applications, a two terminal hybrid device is potentially more efficient. Almost all reported two terminal hybrid devices have a multilayer structure for the photoactive layer with an electrolyte and a porous counter electrode [160, 215, 216]. The above described single layer device composed of a gel as the photoactive layer, energy storage media, and electrolyte is more promising for the development of low-cost and dry photoactive

supercapacitors. Additionally, our preliminary results show that adding a dye material to the composite gel can enhance the energy harvesting in the gel [162].

The synthesized gel was also tested for electrochromic applications by fabricating a device with two FTO electrodes and a single active layer of the PANI composite gel in between (Figure 57.a). As shown in Figure 57.b, the gel was semi-transparent when PANI was in its ES form.

The CV study of the cell (Figure 57.c) showed an almost symmetrical response with redox peaks around  $\pm 1.5$  V and around  $\pm 0.38$  V. As the voltage of the cell was changing, we noticed that for applied voltages larger than 1.5 V, ( $|V_{\text{applied}}| > 1.5$  V), the color of the gel changed to dark blue. However, when the voltage was scanned to lower magnitudes, the gel became transparent at  $\sim 0.5$  V.

To study the two modes of operation, the voltage was pulsed between 0.0 V and 2.0 V every 20 s. As shown in Figure 57.d, the current through the cell showed a transient response with a steady state current of  $\sim 50$  mA and 0.0 mA at the dark and transparent modes, respectively. The color change in the sample is clearly seen in Figure 57.b. After applying the last voltage pulse at 2.0 V, the cell was operated under open circuit conditions (Figure 57.e). The gradual voltage change occurred with a slow color change to green, while the color change between the transparent and dark modes under the applied pulses was almost instantaneous (Video 1 in the SI). The transparency test results show 64% transmittance around 564 nm at 0.0 V, while the transmittance was almost zero at 2.0 V for the entire range of the spectrum (Figure 57.f). Further study of the transmittance spectrum for the electrochromic device at different biasing voltages via UV-visible test is shown in Figure S7.

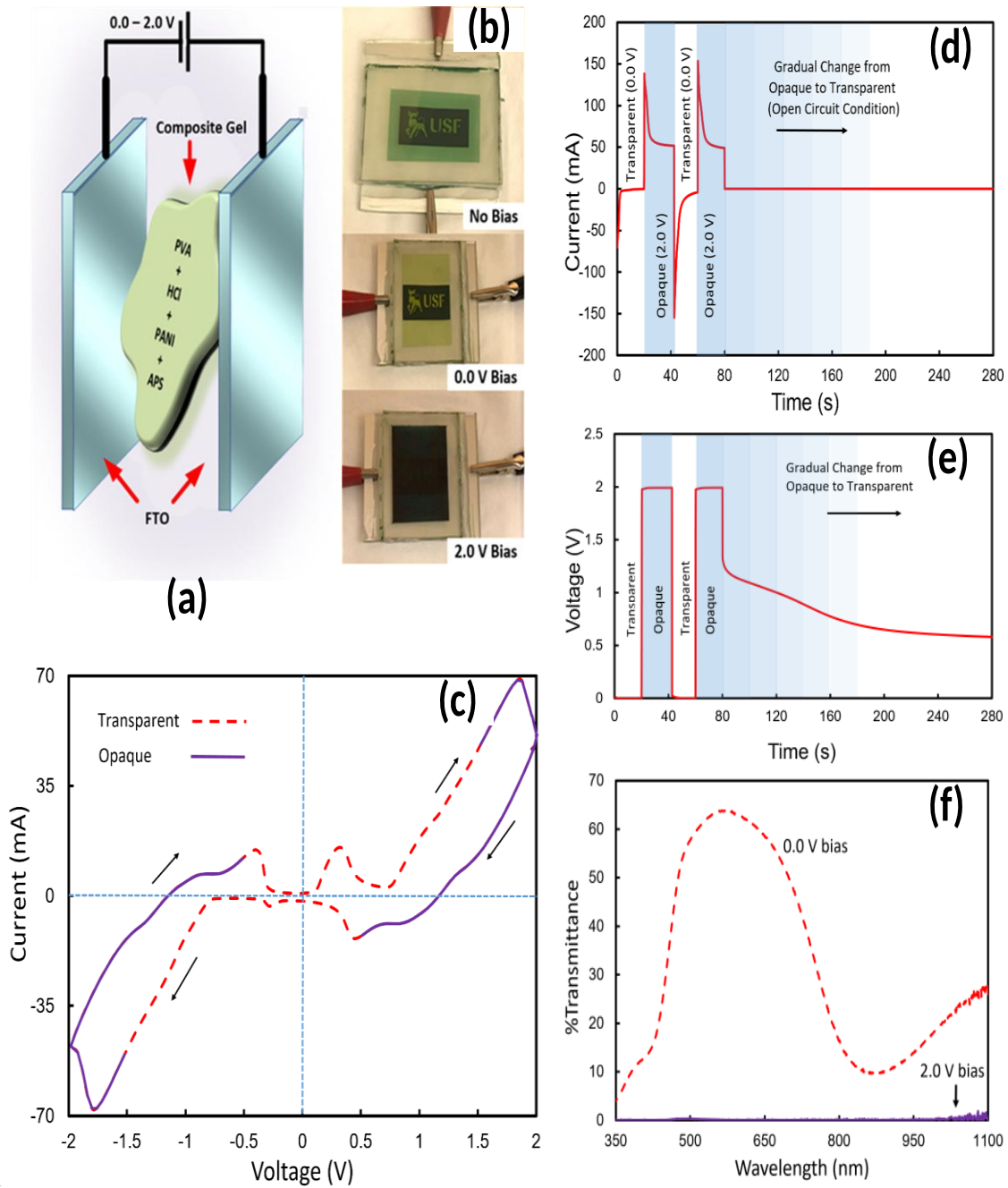


Figure 57: (a) Schematic Diagram, (b) Pictures of the Fabricated Electrochromic Device at Three Different Modes, (c) CV Result Showing the Redox Peaks, (d,e) Electric Current Through the Device in Response to the Applied Voltage Pulses and (f) Transmittance of the Device in Two Different Biasing Conditions.

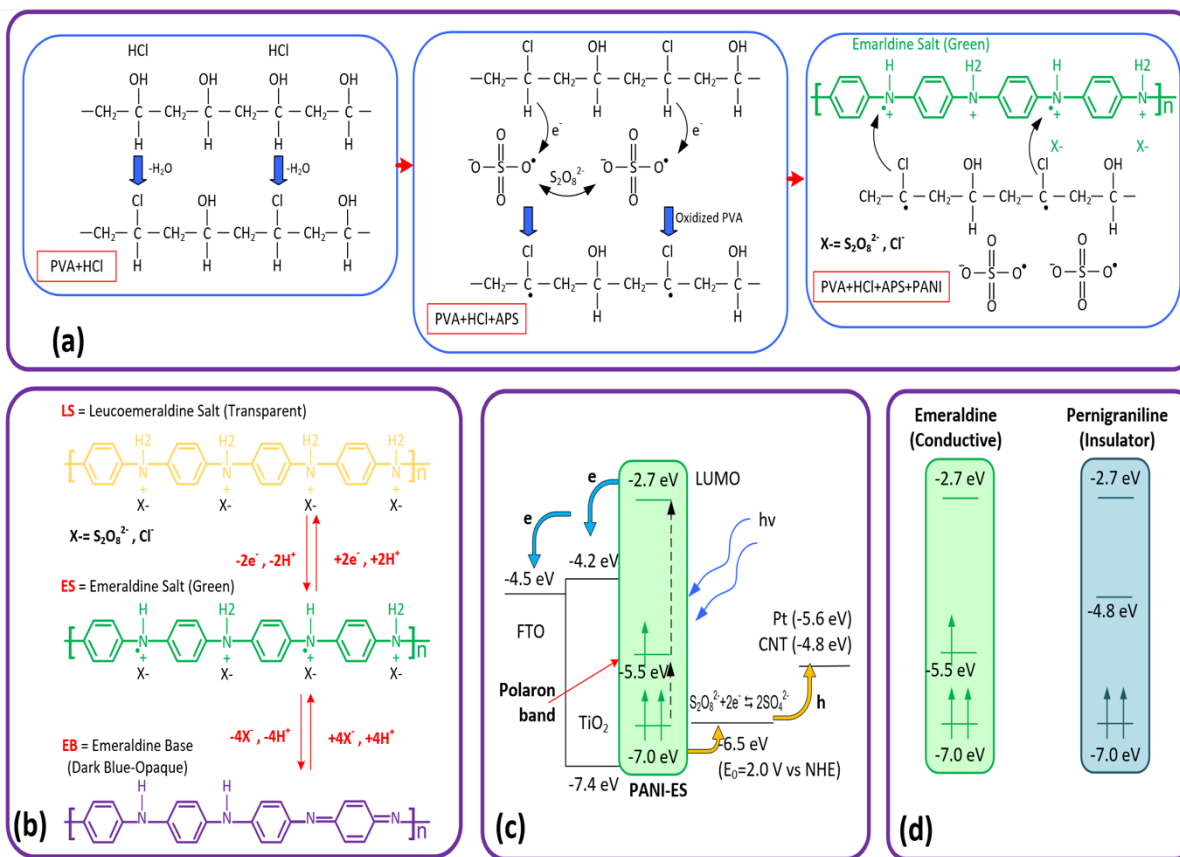
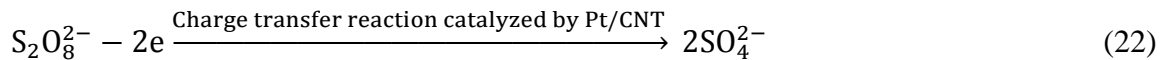
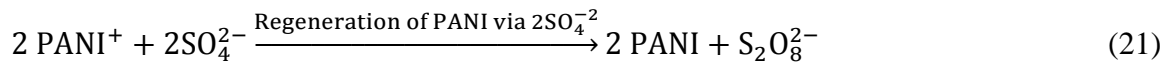
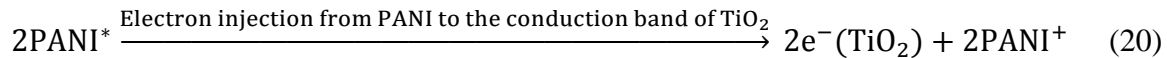
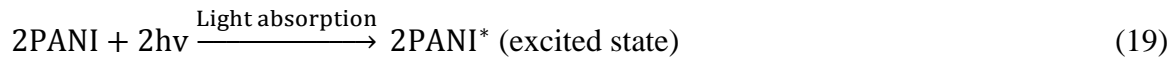


Figure 58: (a) 3 Steps of Fabricating the PANI Composite Gel: The Gelling Process of PVA in HCl and the Interactions with APS and PANI, (b) Chemical Reactions in Three Different Oxidation States of PANI, (c) Energy Level Diagram in the Solar Cell and the Hybrid Photoactive Supercapacitor for Energy Harvesting. The Energy Levels are Versus the Vacuum Level. To Explain the Process, the Interaction Between PANI and the Ionic Charges are Shown as Two Different Layers; However, that Interaction Occurs in the Bulk Gel Electrolyte and (d) Loss of Electron in Emeraldine and Conversion to Pernigraniline with Stored Energy in the Polymer.

As shown in Fig. 58a, the step-by-step adding chemicals have resulted in the formation of PANI-emeraldine salt (ES) which is green in color. As explained, the mechanism of charge storage in the gel is due to the change in the oxidation state of PANI in the bulk gel. In the supercapacitor device, the oxidation state was changed between ES and LS states by adding or removing electron-proton ( $H^+$ ) pairs. However as shown in Figure 6.b, the oxidation state of PANI can also be changed to emeraldine base (EB) by removing protons ( $H^+$ ) and dedoping the polymer [217, 218].

This process is reversible, and the polymer can get back to the ES form through a protonation process. Transition from LS to ES and then EB under sufficiently large voltages across the gel was confirmed in the electrochromic experiments. Not only the CV result (Figure 5.c) implied the change in the oxidation state, but also the color change was a clear evidence as EB has a dark blue color and LS is fade yellow to transparent in color [219].

The fact that the oxidation state of the conducting polymer inside the volume of the gel can be changed suggests existence of both ionic and electronic conductions through the gel. In this regard, the composite gel is different than regular gel electrolytes with only ionic charge transport. This unique property of conducting two different types of charges can also explain the observed photovoltaic effect in the bulk gel. The energy diagram of the solar cell and the hybrid photoactive supercapacitor is shown in Figure 58.c. In the composite gel, ES form of PANI absorbs light and generates an excited state. The photogenerated electrons can be transferred to the conduction band of TiO<sub>2</sub> and a regeneration process by the ionic mediators (S<sub>2</sub>O<sub>8</sub><sup>2-</sup>+2e<sup>-</sup>↔ 2SO<sub>4</sub><sup>2-</sup>) replace the lost electrons in PANI. In the last step, charge exchange occurs between the mediators and the cathode (i.e., Pt or CNT-based electrode). The detail reactions are explained as below:



The device with the Pt cathode responded like a DSSC with a negligible charge storage effect. This can be due to the catalytic property of Pt [220] that facilitates the charge circulation via the mediator for regeneration of PANI into its ES state. However, the weak of catalytic property

in CNTs can affect the regeneration process in PANI and convert it to the pernigraniline form after losing the photoexcited electrons and  $H^+$  ions ( $\text{Emeraldine} + h\nu \rightarrow e^- + H^+ + \text{pernigraniline}$ ). Losing a negative ( $e^-$ ) and a positive ( $H^+$ ) charge results in a higher energy mode in PANI which was observed as gradual increase in the open circuit voltage of the hybrid photoactive supercapacitor. The difference in the energy structure of PANI in the Emeraldine and pernigraniline are shown in Figure 58.d. The change in the oxidation state can also explain the charge stability in the device. Since at the pernigraniline state the electronic conductivity in the polymer is substantially lower than that in the ES form, the recombination rate between electronic and ionic charges would be considerably lower, resulting in a stable form of charge storage in dark as it was observed in Figure 56.d.

Although the results clearly show the feasibility of using the composite gel for fabricating various low-cost devices by simply putting a layer of the gel between two electrodes, the composite can be further customized for different applications. For example, for solar cells or photoactive supercapacitors, a dye material could be added to the gel to enhance the light absorption [221]. This is particularly necessary as PANI in its LS state is semi-transparent. Also, for long operational lifetime of devices appropriate sealing and packaging is required.

## 8.5 Conclusion

A facile and low-cost procedure for preparing a new composite material of gel electrolyte is described. The electrical and electrochemical behavior of the composite gel was investigated for application to electrochromic devices, supercapacitors, solar cells, and hybrid photoactive supercapacitors. While all the devices studied in this work are traditionally electrochemical devices, application of the composite gel with both ionic and electronic conductivity between two



electrodes demonstrates a different type of cell with a single layer material being active in its entire volume. Potentially, low-cost and more efficient devices can be designed and fabricated by customizing the composite gel by adding other elements such as dyes or nanoparticles. An additional study is needed to explore the impact of materials and concentrations on the energy storage and photovoltaic properties of the devices.

## Chapter 9: Conclusion and Suggestions for Future Work

### 9.1 Conclusion

Different projects have been addressed in this dissertation including studying the effect of redox-active materials in the bulk of gel electrolyte on the performance of EDLC devices, obtaining the effect of photoactive electrode-based nanocomposite thin film of PANI or Ppy with synthetic dyes for making a photoactive supercapacitor with a gel electrolyte, and developing a new composite gel electrolyte for fabrication EDLC, photoelectrochemical devices, and electrochromic window. The fundamental study of this work focused on the redox-active gel electrolytes based on comparatively low-cost materials and high safety aspects. Based on the results of the activities research in this dissertation, redox-active gel electrolytes have shown signs of future success in the fabrication of low-cost electrochemical and photoelectrochemical devices for real applications.

The fast-moving activities in fabricating a hybrid device of integrated energy harvesting and storage in a single unit-based gel electrolyte is a promising approach for developing a sustainable energy technology because this idea is mimicking nature. The activities work in this dissertation contributed to a better understanding of integrated two functions in a single device-based redox gel electrolyte and have identified the existed impasses. Specific contributions have been accomplished to the field of solar energy harvesting and storage technology were:

- 1- Discovering the active redox properties in the bulk of the gel electrolyte (PVA+acids) and its effects on the performance of the electrochemical devices such as supercapacitors and

hybrid cell of solar energy harvesting and storage. The presented results have been published as research papers on journal and conference proceedings [110, 142, 162, 222].

2- Developing a redox-active gel electrolyte based PVA+acids by adding a conducting polymer material (i.e., PANI) to form a new composite gel electrolyte that was implemented with different electrochemical devices, namely EC, DSSC, photoactive supercapacitor, and electrochromic window. It has been found with these features of the new composite gel electrolyte and the simplicity in the fabrication of the gel, low-cost and voltage of applications can be made.

3- Making a photoelectrochemical device that can harvest energy and at the same time has the function of energy storage by making a nanocomposite thin film of conducting polymer materials (i.e., PANI and Ppy) with synthetic dyes coated on the surface of TiO<sub>2</sub> via electrochemical deposition technique. The novelty of this work was the simplicity of the device structure of having a photoanode electrode, cathode electrode (i.e., CNT), and a layer of redox-active gel electrolyte, which sandwiched between the two electrodes. The harvesting energy was taking place at the photoanode electrode, and the energy storage participated in both sides of the electrodes in addition to the bulk of the gel electrolyte. The presented results have been published as research papers on conferences proceeding [162, 222].

In the end, low cost, abundant, and non-toxic materials such as polyvinyl alcohol, polyaniline, and ammonium persulfate are promising due to their redox-active properties that can substantially enhance the total performance of electrochemical and photoelectrochemical cells.

## 9.2 Suggestions for Future Work

To continue this work, further study is needed to understand the movement of charges (i.e., ions and electrons) inside the bulk of gel electrolyte in order to enhance the total efficiency of the hybrid device. There is an ample scope of research to find new solutions and advancements for the current limitations of the proposed integrated solar energy harvesting and storage devices based on PVA+HCl gel electrolyte and PVA+HCl+APS+PANI composite gel electrolyte, as shown in Figure 59 and 60, respectively. The suggested solutions are listed below for both photoactive supercapacitor devices.

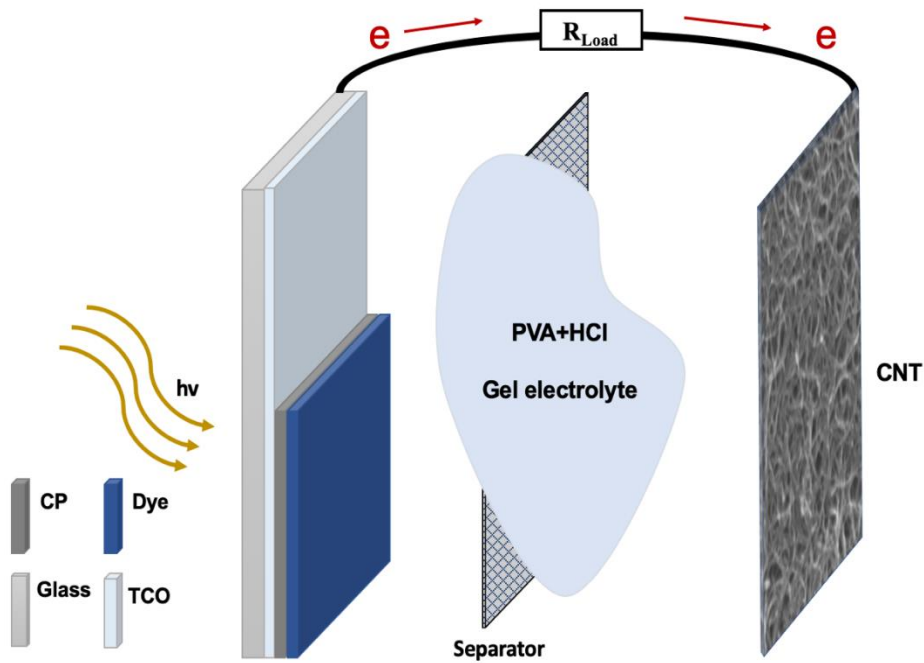


Figure 59: Hybrid Photoactive Supercapacitor Device Based on PVA+HCl Gel Electrolyte.

1. Changing the type of the oxidizer material such as potassium permanganate ( $\text{KMnO}_4$ ), or ferric chloride ( $\text{FeCl}_3$ ) instead of using APS, specifically, for polymerization of Ppy conducting polymer material.

2. Changing the type of the acids solution in case of changing the pH concentration since that will affect the oxidation state of PANI.
3. Replacing the HCl acid by weak acid such as citric acid in order to enhance the power generated by reducing the conductivity of the solution.
4. Adding a redox couple materials such as (iodide/triiodide) to the PVA+HCl gel electrolyte.
5. Mixing a conducting polymer materials or metal oxide materials with CNT will in order of increasing the energy storage part for all devices.

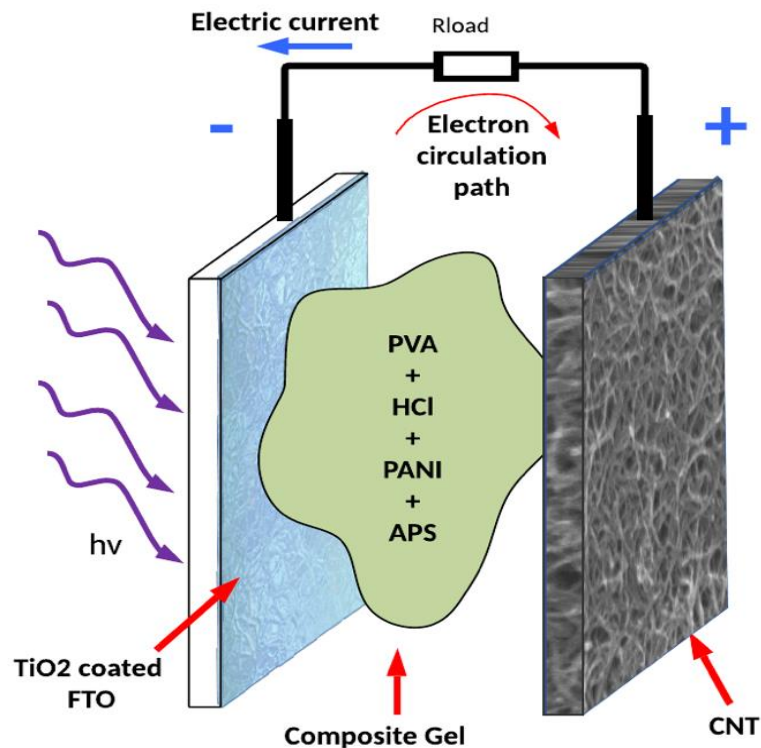


Figure 60: Schematic Diagram of Photoactive Supercapacitor Based on PANI Composite Gel Electrolyte

1. Changing the TiO<sub>2</sub> to another nanoparticles type such as ZnO material.
2. Adding ruthenium dyes to the composite gel electrolyte or coated on the FTO glass instead of adding the synthetic dyes.

3. Choosing different type of the conducting polymer materials, for instance, Ppy or polythiophene instead of the PANI to form the composite gel electrolyte.

## References

- [1] U. EIA, "Annual energy outlook 2019: with projections to 2050," 2019.
- [2] V. Lizunkov, E. Politsinskaya, E. Malushko, A. Kindaev, M. J. I. j. o. e. e. Minin, and policy, "Population of the world and regions as the principal energy consumer," vol. 8, no. 3, pp. 250-257, 2018.
- [3] Y. Y. Smolin, K. K. Lau, and M. J. A. J. Soroush, "First-principles modeling for optimal design, operation, and integration of energy conversion and storage systems," 2019.
- [4] D. P. Dubal, O. Ayyad, V. Ruiz, and P. J. C. S. R. Gomez-Romero, "Hybrid energy storage: the merging of battery and supercapacitor chemistries," vol. 44, no. 7, pp. 1777-1790, 2015.
- [5] W. Liu, M. S. Song, B. Kong, and Y. J. A. m. Cui, "Flexible and stretchable energy storage: recent advances and future perspectives," vol. 29, no. 1, p. 1603436, 2017.
- [6] Y. Wang, Y. Song, and Y. J. C. S. R. Xia, "Electrochemical capacitors: mechanism, materials, systems, characterization and applications," vol. 45, no. 21, pp. 5925-5950, 2016.
- [7] B. E. Conway, *Electrochemical supercapacitors: scientific fundamentals and technological applications*. Springer Science & Business Media, 2013.
- [8] ""Supercapacitor Market by Module Type (Less than 10 Volts Modules, 10-25 Volts Modules, 25-50 Volts Modules, 50-100 Volts Modules, and Above 100 Volts Modules) and Application (Automotive, Industrial, Energy, and Electronics) - Global Opportunities Analysis & Industry Forecast, 2014-2022, Allied Market Research.," Online p. 150, 2017. [Online]. Available: <https://www.alliedmarketresearch.com/supercapacitor-market>.
- [9] ""Supercapacitor - Global Market Outlook (2017-2026)," Research and Market," 2017. [Online]. Available: <https://www.researchandmarkets.com/research/qfjwxm/global?w=5>.
- [10] L. Zhang, X. Hu, Z. Wang, F. Sun, D. G. J. R. Dorrell, and S. E. Reviews, "A review of supercapacitor modeling, estimation, and applications: A control/management perspective," vol. 81, pp. 1868-1878, 2018.
- [11] Y. Zhao *et al.*, "Microgel-enhanced double network hydrogel electrode with high conductivity and stability for intrinsically stretchable and flexible all-gel-state supercapacitor," vol. 10, no. 23, pp. 19323-19330, 2018.
- [12] M. Skunik-Nuckowska *et al.*, "Integration of solid-state dye-sensitized solar cell with metal oxide charge storage material into photoelectrochemical capacitor," vol. 234, pp. 91-99, 2013.
- [13] B. Luo, D. Ye, and L. J. A. S. Wang, "Recent progress on integrated energy conversion and storage systems," vol. 4, no. 9, p. 1700104, 2017.
- [14] K. S. Ngai, S. Ramesh, K. Ramesh, and J. C. J. I. Juan, "A review of polymer electrolytes: fundamental, approaches and applications," vol. 22, no. 8, pp. 1259-1279, 2016.
- [15] A. J. J. o. p. s. Nishino, "Capacitors: operating principles, current market and technical trends," vol. 60, no. 2, pp. 137-147, 1996.
- [16] B. K. Kim, S. Sy, A. Yu, and J. J. H. o. C. E. S. Zhang, "Electrochemical supercapacitors for energy storage and conversion," pp. 1-25, 2015.

- [17] L. L. Zhang and X. J. C. S. R. Zhao, "Carbon-based materials as supercapacitor electrodes," vol. 38, no. 9, pp. 2520-2531, 2009.
- [18] F. Béguin, V. Presser, A. Balducci, and E. J. A. m. Frackowiak, "Carbons and electrolytes for advanced supercapacitors," vol. 26, no. 14, pp. 2219-2251, 2014.
- [19] E. J. P. c. c. p. Frackowiak, "Carbon materials for supercapacitor application," vol. 9, no. 15, pp. 1774-1785, 2007.
- [20] E. Gongadze, S. Petersen, U. Beck, and U. van Rienen, "Classical Models of the Interface between an Electrode and an Electrolyte," in *COMSOL Conference*, 2009, pp. 14-16.
- [21] M. Endo, T. Takeda, Y. Kim, K. Koshiba, and K. J. C. I. Ishii, "High power electric double layer capacitor (EDLC's); from operating principle to pore size control in advanced activated carbons," vol. 1, no. 3\_4, pp. 117-128, 2001.
- [22] A. González, E. Goikolea, J. A. Barrena, R. J. R. Mysyk, and S. E. Reviews, "Review on supercapacitors: technologies and materials," vol. 58, pp. 1189-1206, 2016.
- [23] X. Zhao, B. M. Sánchez, P. J. Dobson, and P. S. J. N. Grant, "The role of nanomaterials in redox-based supercapacitors for next generation energy storage devices," vol. 3, no. 3, pp. 839-855, 2011.
- [24] O. J. Z. f. E. u. a. p. C. Stern, "Zur theorie der elektrolytischen doppelschicht," vol. 30, no. 21-22, pp. 508-516, 1924.
- [25] Z. S. Iro, C. Subramani, and S. Dash, "A brief review on electrode materials for supercapacitor," *Int. J. Electrochem. Sci*, vol. 11, no. 12, pp. 10628-10643, 2016.
- [26] A. Borenstein, O. Hanna, R. Attias, S. Luski, T. Brousse, and D. J. J. o. M. C. A. Aurbach, "Carbon-based composite materials for supercapacitor electrodes: a review," vol. 5, no. 25, pp. 12653-12672, 2017.
- [27] J. Yan *et al.*, "Carbon nanotube/MnO<sub>2</sub> composites synthesized by microwave-assisted method for supercapacitors with high power and energy densities," vol. 194, no. 2, pp. 1202-1207, 2009.
- [28] J. Yan *et al.*, "Preparation of a graphene nanosheet/polyaniline composite with high specific capacitance," vol. 48, no. 2, pp. 487-493, 2010.
- [29] J. Zhang, Y. Yu, L. Liu, and Y. J. N. Wu, "Graphene-hollow PPy sphere 3D-nanoarchitecture with enhanced electrochemical performance," vol. 5, no. 7, pp. 3052-3057, 2013.
- [30] P. Mini, A. Balakrishnan, S. V. Nair, and K. J. C. C. Subramanian, "Highly super capacitive electrodes made of graphene/poly (pyrrole)," vol. 47, no. 20, pp. 5753-5755, 2011.
- [31] V. S. Bagotsky, *Fundamentals of electrochemistry*. John Wiley & Sons, 2005.
- [32] G. Yu, X. Xie, L. Pan, Z. Bao, and Y. J. N. E. Cui, "Hybrid nanostructured materials for high-performance electrochemical capacitors," vol. 2, no. 2, pp. 213-234, 2013.
- [33] V. Augustyn, P. Simon, B. J. E. Dunn, and E. Science, "Pseudocapacitive oxide materials for high-rate electrochemical energy storage," vol. 7, no. 5, pp. 1597-1614, 2014.
- [34] J. Liu *et al.*, "Advanced energy storage devices: basic principles, analytical methods, and rational materials design," vol. 5, no. 1, p. 1700322, 2018.
- [35] Y. J. T. C. R. Xie, "Electrochemical Performance of Transition Metal-coordinated Polypyrrole: A Mini Review," 2019.
- [36] H. Wang, J. Lin, Z. X. J. J. o. s. A. m. Shen, and devices, "Polyaniline (PANi) based electrode materials for energy storage and conversion," vol. 1, no. 3, pp. 225-255, 2016.
- [37] G. Lota, K. Fic, E. J. E. Frackowiak, and E. Science, "Carbon nanotubes and their composites in electrochemical applications," vol. 4, no. 5, pp. 1592-1605, 2011.



- [38] C. Peng, S. Zhang, D. Jewell, and G. Z. J. P. i. N. s. Chen, "Carbon nanotube and conducting polymer composites for supercapacitors," vol. 18, no. 7, pp. 777-788, 2008.
- [39] T.-H. Le, Y. Kim, and H. J. P. Yoon, "Electrical and electrochemical properties of conducting polymers," vol. 9, no. 4, p. 150, 2017.
- [40] P. Simon, Y. Gogotsi, and B. J. S. Dunn, "Where do batteries end and supercapacitors begin?," vol. 343, no. 6176, pp. 1210-1211, 2014.
- [41] W. Zuo, R. Li, C. Zhou, Y. Li, J. Xia, and J. J. A. S. Liu, "Battery-supercapacitor hybrid devices: recent progress and future prospects," vol. 4, no. 7, p. 1600539, 2017.
- [42] B. E. J. J. o. t. E. S. Conway, "Transition from "supercapacitor" to "battery" behavior in electrochemical energy storage," vol. 138, no. 6, pp. 1539-1548, 1991.
- [43] D. Larcher and J.-M. J. N. c. Tarascon, "Towards greener and more sustainable batteries for electrical energy storage," vol. 7, no. 1, p. 19, 2015.
- [44] A. Afif, S. M. Rahman, A. T. Azad, J. Zaini, M. A. Islan, and A. K. J. J. o. E. S. Azad, "Advanced materials and technologies for hybrid supercapacitors for energy storage—A review," vol. 25, p. 100852, 2019.
- [45] N. Kannan, D. J. R. Vakeesan, and S. E. Reviews, "Solar energy for future world:-A review," vol. 62, pp. 1092-1105, 2016.
- [46] J. Khan, M. H. J. R. Arsalan, and S. E. Reviews, "Solar power technologies for sustainable electricity generation—A review," vol. 55, pp. 414-425, 2016.
- [47] K. Solangi, M. Islam, R. Saidur, N. Rahim, H. J. R. Fayaz, and s. e. reviews, "A review on global solar energy policy," vol. 15, no. 4, pp. 2149-2163, 2011.
- [48] T. Ibn-Mohammed *et al.*, "Perovskite solar cells: An integrated hybrid lifecycle assessment and review in comparison with other photovoltaic technologies," vol. 80, pp. 1321-1344, 2017.
- [49] B. O'regan and M. J. n. Grätzel, "A low-cost, high-efficiency solar cell based on dye-sensitized colloidal TiO<sub>2</sub> films," vol. 353, no. 6346, p. 737, 1991.
- [50] P. Choubey, A. Oudhia, R. J. R. R. i. S. Dewangan, and Technology, "A review: Solar cell current scenario and future trends," vol. 4, no. 8, 2012.
- [51] S. Sharma, K. K. Jain, A. J. M. S. Sharma, and Applications, "Solar cells: in research and applications—a review," vol. 6, no. 12, p. 1145, 2015.
- [52] M. J. J. o. p. Grätzel and p. C. P. Reviews, "Dye-sensitized solar cells," vol. 4, no. 2, pp. 145-153, 2003.
- [53] S. Mathew *et al.*, "Dye-sensitized solar cells with 13% efficiency achieved through the molecular engineering of porphyrin sensitizers," vol. 6, no. 3, p. 242, 2014.
- [54] M. Ye *et al.*, "Recent advances in dye-sensitized solar cells: from photoanodes, sensitizers and electrolytes to counter electrodes," vol. 18, no. 3, pp. 155-162, 2015.
- [55] M. J. n. Grätzel, "Photoelectrochemical cells," vol. 414, no. 6861, p. 338, 2001.
- [56] M. J. A. o. c. r. Grätzel, "Recent advances in sensitized mesoscopic solar cells," vol. 42, no. 11, pp. 1788-1798, 2009.
- [57] S. G. Kumar and L. G. J. T. J. o. p. c. A. Devi, "Review on modified TiO<sub>2</sub> photocatalysis under UV/visible light: selected results and related mechanisms on interfacial charge carrier transfer dynamics," vol. 115, no. 46, pp. 13211-13241, 2011.
- [58] J. Wu *et al.*, "Electrolytes in dye-sensitized solar cells," vol. 115, no. 5, pp. 2136-2173, 2015.
- [59] Q. Tai *et al.*, "In situ prepared transparent polyaniline electrode and its application in bifacial dye-sensitized solar cells," vol. 5, no. 5, pp. 3795-3799, 2011.

- [60] M. K. Nazeeruddin, E. Baranoff, and M. J. S. e. Grätzel, "Dye-sensitized solar cells: a brief overview," vol. 85, no. 6, pp. 1172-1178, 2011.
- [61] A. J. J. A. M. Heeger, "25th anniversary article: bulk heterojunction solar cells: understanding the mechanism of operation," vol. 26, no. 1, pp. 10-28, 2014.
- [62] C. Zhong, Y. Deng, W. Hu, J. Qiao, L. Zhang, and J. J. C. S. R. Zhang, "A review of electrolyte materials and compositions for electrochemical supercapacitors," vol. 44, no. 21, pp. 7484-7539, 2015.
- [63] Y. Chen, X. Zhang, D. Zhang, P. Yu, and Y. J. C. Ma, "High performance supercapacitors based on reduced graphene oxide in aqueous and ionic liquid electrolytes," vol. 49, no. 2, pp. 573-580, 2011.
- [64] T. Y. Kim *et al.*, "High-performance supercapacitors based on poly (ionic liquid)-modified graphene electrodes," vol. 5, no. 1, pp. 436-442, 2010.
- [65] S. B. Aziz, T. J. Woo, M. Kadir, H. M. J. J. o. S. A. M. Ahmed, and Devices, "A conceptual review on polymer electrolytes and ion transport models," vol. 3, no. 1, pp. 1-17, 2018.
- [66] X. Cheng, J. Pan, Y. Zhao, M. Liao, and H. J. A. E. M. Peng, "Gel polymer electrolytes for electrochemical energy storage," vol. 8, no. 7, p. 1702184, 2018.
- [67] J. Zhong *et al.*, "Improved energy density of quasi-solid-state supercapacitors using sandwich-type redox-active gel polymer electrolytes," vol. 166, pp. 150-156, 2015.
- [68] C. Meng, C. Liu, L. Chen, C. Hu, and S. J. N. I. Fan, "Highly flexible and all-solid-state paperlike polymer supercapacitors," vol. 10, no. 10, pp. 4025-4031, 2010.
- [69] X. Cao *et al.*, "Reduced Graphene Oxide-Wrapped MoO<sub>3</sub> Composites Prepared by Using Metal–Organic Frameworks as Precursor for All-Solid-State Flexible Supercapacitors," vol. 27, no. 32, pp. 4695-4701, 2015.
- [70] M. Kaempgen, C. K. Chan, J. Ma, Y. Cui, and G. J. N. I. Gruner, "Printable thin film supercapacitors using single-walled carbon nanotubes," vol. 9, no. 5, pp. 1872-1876, 2009.
- [71] Y. Xu, Z. Lin, X. Huang, Y. Liu, Y. Huang, and X. J. A. n. Duan, "Flexible solid-state supercapacitors based on three-dimensional graphene hydrogel films," vol. 7, no. 5, pp. 4042-4049, 2013.
- [72] X. Lu *et al.*, "Stabilized TiN nanowire arrays for high-performance and flexible supercapacitors," vol. 12, no. 10, pp. 5376-5381, 2012.
- [73] P. Du *et al.*, "Self-Powered Electronics by Integration of Flexible Solid-State Graphene-Based Supercapacitors with High Performance Perovskite Hybrid Solar Cells," vol. 25, no. 16, pp. 2420-2427, 2015.
- [74] F. Barzegar, A. Bello, J. K. Dangbegnon, N. Manyala, and X. J. A. e. Xia, "Asymmetric supercapacitor based on activated expanded graphite and pinecone tree activated carbon with excellent stability," vol. 207, pp. 417-426, 2017.
- [75] S. Lau *et al.*, "A three-electrode integrated photo-supercapacitor utilizing graphene-based intermediate bifunctional electrode," vol. 238, pp. 178-184, 2017.
- [76] P. Chen, H. Chen, J. Qiu, and C. J. N. R. Zhou, "Inkjet printing of single-walled carbon nanotube/RuO<sub>2</sub> nanowire supercapacitors on cloth fabrics and flexible substrates," vol. 3, no. 8, pp. 594-603, 2010.
- [77] S. Kim *et al.*, "Facile fabrication of paper-based silver nanostructure electrodes for flexible printed energy storage system," vol. 151, pp. 1-7, 2018.
- [78] Y. Gao *et al.*, "Transparent, flexible, and solid-state supercapacitors based on graphene electrodes," vol. 1, no. 1, p. 012101, 2013.

- [79] L. F. Aval, M. Ghoranneviss, G. B. J. M. f. R. Pour, and S. Energy, "Graphite nanoparticles paper supercapacitor based on gel electrolyte," vol. 7, no. 4, p. 29, 2018.
- [80] J.-Y. Shieh, S.-H. Zhang, C.-H. Wu, and H. H. J. A. S. S. Yu, "A facile method to prepare a high performance solid-state flexible paper-based supercapacitor," vol. 313, pp. 704-710, 2014.
- [81] N. R. Chodankar, D. P. Dubal, A. C. Lokhande, C. D. J. J. o. c. Lokhande, and i. science, "Ionically conducting PVA–LiClO<sub>4</sub> gel electrolyte for high performance flexible solid state supercapacitors," vol. 460, pp. 370-376, 2015.
- [82] H. Yu *et al.*, "A novel redox-mediated gel polymer electrolyte for high-performance supercapacitor," vol. 198, pp. 402-407, 2012.
- [83] H. Yu *et al.*, "Improvement of the performance for quasi-solid-state supercapacitor by using PVA–KOH–KI polymer gel electrolyte," vol. 56, no. 20, pp. 6881-6886, 2011.
- [84] B. C. Nath, B. Gogoi, M. Boruah, M. Khannam, G. A. Ahmed, and S. K. J. E. A. Dolui, "High performance polyvinyl alcohol/multi walled carbon nanotube/polyaniline hydrogel (PVA/MWCNT/PAni) based dye sensitized solar cells," vol. 146, pp. 106-111, 2014.
- [85] P. Wang, S. M. Zakeeruddin, J. E. Moser, M. K. Nazeeruddin, T. Sekiguchi, and M. J. N. m. Grätzel, "A stable quasi-solid-state dye-sensitized solar cell with an amphiphilic ruthenium sensitizer and polymer gel electrolyte," vol. 2, no. 6, p. 402, 2003.
- [86] M. Aziz, M. Buraidah, M. Careem, and A. J. E. A. Arof, "PVA based gel polymer electrolytes with mixed iodide salts (K<sup>+</sup> I<sup>-</sup> and Bu<sub>4</sub>N<sup>+</sup> I<sup>-</sup>) for dye-sensitized solar cell application," vol. 182, pp. 217-223, 2015.
- [87] P. Wang, S. M. Zakeeruddin, I. Exnar, and M. J. C. C. Grätzel, "High efficiency dye-sensitized nanocrystalline solar cells based on ionic liquid polymer gel electrolyte," no. 24, pp. 2972-2973, 2002.
- [88] M. Careem, M. Aziz, and M. J. M. T. P. Buraidah, "Boosting efficiencies of gel polymer electrolyte based dye sensitized solar cells using mixed cations," vol. 4, no. 4, pp. 5092-5099, 2017.
- [89] M. Buraidah *et al.*, "High efficient dye sensitized solar cells using phthaloylchitosan based gel polymer electrolytes," vol. 245, pp. 846-853, 2017.
- [90] O. Bettucci *et al.*, "Organic dye-sensitized solar cells containing alkaline iodide-based gel polymer electrolytes: influence of cation size," vol. 20, no. 2, pp. 1276-1285, 2018.
- [91] T. Azizi, H. Toujeni, M. B. Karoui, and R. Gharbi, "A comprehensive device modeling of solid state dye sensitized solar cell with SCAPS-1D," in *2019 19th International Conference on Sciences and Techniques of Automatic Control and Computer Engineering (STA)*, 2019: IEEE, pp. 336-340.
- [92] L. Teo, T. Tiong, M. H. Buraidah, and A. K. J. O. M. Arof, "Effect of lithium iodide on the performance of dye sensitized solar cells (DSSC) using poly (ethylene oxide)(PEO)/poly (vinyl alcohol)(PVA) based gel polymer electrolytes," vol. 85, pp. 531-537, 2018.
- [93] M. M. Sri, M. Buraidah, and L. J. M. T. P. Teo, "Effect of 1-butyl-3-methylimidazolium iodide on the performance of dye-sensitized solar cell having PEO-PVA based gel polymer electrolyte," vol. 4, no. 4, pp. 5161-5168, 2017.
- [94] W. Guo, X. Xue, S. Wang, C. Lin, and Z. L. Wang, "An integrated power pack of dye-sensitized solar cell and Li battery based on double-sided TiO<sub>2</sub> nanotube arrays," *Nano letters*, vol. 12, no. 5, pp. 2520-2523, 2012.

- [95] B. Luo, D. Ye, and L. Wang, "Recent progress on integrated energy conversion and storage systems," *Advanced Science*, vol. 4, no. 9, p. 1700104, 2017.
- [96] Z. Yang *et al.*, "An integrated device for both photoelectric conversion and energy storage based on free-standing and aligned carbon nanotube film," vol. 1, no. 3, pp. 954-958, 2013.
- [97] Z. Wen *et al.*, "Self-powered textile for wearable electronics by hybridizing fiber-shaped nanogenerators, solar cells, and supercapacitors," vol. 2, no. 10, p. e1600097, 2016.
- [98] C. Bandaranayake, W. WADSS, K. Vidanapathirana, and K. J. S. L. J. o. P. Perera, "A cyclic voltammetry study of a gel polymer electrolyte based redox-capacitor," vol. 16, pp. 19-27, 2015.
- [99] N. Harankahawa, K. Perera, and K. J. J. o. E. S. Vidanapathirana, "Use of gel polymer electrolytes to integrate photoelectric conversion and energy storage," vol. 13, pp. 96-102, 2017.
- [100] A. Scalia *et al.*, "A flexible and portable powerpack by solid-state supercapacitor and dye-sensitized solar cell integration," vol. 359, pp. 311-321, 2017.
- [101] L. Hu *et al.*, "Highly conductive paper for energy-storage devices," vol. 106, no. 51, pp. 21490-21494, 2009.
- [102] M. K. Ram, M. Salerno, M. Adami, P. Faraci, and C. J. L. Nicolini, "Physical properties of polyaniline films: assembled by the layer-by-layer technique," vol. 15, no. 4, pp. 1252-1259, 1999.
- [103] M. K. Ram, M. Adami, S. Paddeu, and C. J. N. Nicolini, "Nano-assembly of glucose oxidase on the in situ self-assembled films of polypyrrole and its optical, surface and electrochemical characterizations," vol. 11, no. 2, p. 112, 2000.
- [104] A. J. Bard, L. R. Faulkner, J. Leddy, and C. G. Zoski, *Electrochemical methods: fundamentals and applications*. Wiley New York, 1980.
- [105] C. Brett and A. M. Oliveira Brett, *Electrochemistry: principles, methods, and applications* (no. 544.6 BRE). 1993.
- [106] A. J. Bard and L. R. J. E. M. Faulkner, "Fundamentals and applications," vol. 2, p. 482, 2001.
- [107] Y. Furukawa, T. Hara, Y. Hyodo, and I. J. S. M. Harada, "Vibrational spectra of polyaniline and its 15N-and 2H-substituted derivatives in as-polymerized, alkali-treated and reduced states," vol. 16, no. 2, pp. 189-198, 1986.
- [108] V. Hacker and S. Mitsushima, *Fuel cells and hydrogen: from fundamentals to applied research*. Elsevier, 2018.
- [109] A. R. Harris, C. Newbold, P. Carter, R. Cowan, and G. G. J. F. i. N. Wallace, "Using Chronopotentiometry to Better Characterize the Charge Injection Mechanisms of Platinum Electrodes Used in Bionic Devices," vol. 13, 2019.
- [110] B. Aljafari, T. Alamro, M. K. Ram, and A. J. J. o. S. S. E. Takshi, "Polyvinyl alcohol-acid redox active gel electrolytes for electrical double-layer capacitor devices," vol. 23, no. 1, pp. 125-133, 2019.
- [111] J. R. J. W.-I. Macdonald, John Wiley and Sons, "Impedance Spectroscopy--Emphasizing Solid Materials and Systems," pp. 1-346, 1987.
- [112] D. D. J. E. A. Macdonald, "Reflections on the history of electrochemical impedance spectroscopy," vol. 51, no. 8-9, pp. 1376-1388, 2006.
- [113] M. E. Orazem and B. Tribollet, *Electrochemical impedance spectroscopy*. John Wiley & Sons, 2017.

- [114] E. P. Randviir and C. E. J. A. M. Banks, "Electrochemical impedance spectroscopy: an overview of bioanalytical applications," vol. 5, no. 5, pp. 1098-1115, 2013.
- [115] P. Larkin, *Infrared and Raman spectroscopy: principles and spectral interpretation*. Elsevier, 2017.
- [116] A. Kumar, M. Khandelwal, S. K. Gupta, V. Kumar, and R. Rani, "Fourier transform infrared spectroscopy: Data interpretation and applications in structure elucidation and analysis of small molecules and nanostructures," in *Data Processing Handbook for Complex Biological Data Sources*: Elsevier, 2019, pp. 77-96.
- [117] M. Trchová, Z. Morávková, M. Bláha, and J. J. E. A. Stejskal, "Raman spectroscopy of polyaniline and oligoaniline thin films," vol. 122, pp. 28-38, 2014.
- [118] T. J. T. S. Spectronic, "Basic UV-Vis theory, concepts and applications," pp. 1-28, 2012.
- [119] K. Krukiewicz and A. J. S. M. Katunin, "The effect of reaction medium on the conductivity and morphology of polyaniline doped with camphorsulfonic acid," vol. 214, pp. 45-49, 2016.
- [120] Q. Chen *et al.*, "Effect of different gel electrolytes on graphene-based solid-state supercapacitors," vol. 4, no. 68, pp. 36253-36256, 2014.
- [121] D. Kalpana, N. Renganathan, and S. J. J. o. p. s. Pitchumani, "A new class of alkaline polymer gel electrolyte for carbon aerogel supercapacitors," vol. 157, no. 1, pp. 621-623, 2006.
- [122] L.-Q. Fan, J. Zhong, J.-H. Wu, J.-M. Lin, and Y.-F. J. J. o. M. C. A. Huang, "Improving the energy density of quasi-solid-state electric double-layer capacitors by introducing redox additives into gel polymer electrolytes," vol. 2, no. 24, pp. 9011-9014, 2014.
- [123] L. Sa'adu, M. Hashim, and M. B. J. J. o. M. S. R. Baharuddin, "Conductivity studies and characterizations of PVA-orthophosphoric electrolytes," vol. 3, no. 3, p. 48, 2014.
- [124] H. Gao and K. J. J. o. M. C. Lian, "Advanced proton conducting membrane for ultra-high rate solid flexible electrochemical capacitors," vol. 22, no. 39, pp. 21272-21278, 2012.
- [125] T. Gaaz, A. Sulong, M. Akhtar, A. Kadhum, A. Mohamad, and A. J. M. Al-Amiery, "Properties and applications of polyvinyl alcohol, halloysite nanotubes and their nanocomposites," vol. 20, no. 12, pp. 22833-22847, 2015.
- [126] N. Choudhary *et al.*, "Asymmetric supercapacitor electrodes and devices," vol. 29, no. 21, p. 1605336, 2017.
- [127] X. Lu, M. Yu, G. Wang, Y. Tong, Y. J. E. Li, and E. Science, "Flexible solid-state supercapacitors: design, fabrication and applications," vol. 7, no. 7, pp. 2160-2181, 2014.
- [128] G. Pandey, S. Hashmi, Y. J. E. Kumar, and Fuels, "Performance studies of activated charcoal based electrical double layer capacitors with ionic liquid gel polymer electrolytes," vol. 24, no. 12, pp. 6644-6652, 2010.
- [129] W. Ma *et al.*, "Bottom-up fabrication of activated carbon fiber for all-solid-state supercapacitor with excellent electrochemical performance," vol. 8, no. 23, pp. 14622-14627, 2016.
- [130] S. Wang, B. Pei, X. Zhao, and R. A. J. N. E. Dryfe, "Highly porous graphene on carbon cloth as advanced electrodes for flexible all-solid-state supercapacitors," vol. 2, no. 4, pp. 530-536, 2013.
- [131] J. Ren *et al.*, "Twisting carbon nanotube fibers for both wire-shaped micro-supercapacitor and micro-battery," vol. 25, no. 8, pp. 1155-1159, 2013.
- [132] X. Xiao *et al.*, "Fiber-based all-solid-state flexible supercapacitors for self-powered systems," vol. 6, no. 10, pp. 9200-9206, 2012.

- [133] Y. J. Kang, H. Chung, C.-H. Han, and W. J. N. Kim, "All-solid-state flexible supercapacitors based on papers coated with carbon nanotubes and ionic-liquid-based gel electrolytes," vol. 23, no. 6, p. 065401, 2012.
- [134] Q. Liu, M. H. Nayfeh, and S.-T. J. J. o. P. S. Yau, "Brushed-on flexible supercapacitor sheets using a nanocomposite of polyaniline and carbon nanotubes," vol. 195, no. 21, pp. 7480-7483, 2010.
- [135] M. Zdrojek, W. Gebicki, C. Jastrzebski, T. Melin, and A. Huczko, "Studies of multiwall carbon nanotubes using Raman spectroscopy and atomic force microscopy," in *Solid State Phenomena*, 2004, vol. 99: Trans Tech Publ, pp. 265-268.
- [136] P. Simon and Y. Gogotsi, "Materials for electrochemical capacitors," in *Nanoscience And Technology: A Collection of Reviews from Nature Journals*: World Scientific, 2010, pp. 320-329.
- [137] P. Simon and A. J. T. e. s. i. Burke, "Nanostructured carbons: double-layer capacitance and more," vol. 17, no. 1, p. 38, 2008.
- [138] H. Li, J. Wang, Q. Chu, Z. Wang, F. Zhang, and S. J. J. o. P. S. Wang, "Theoretical and experimental specific capacitance of polyaniline in sulfuric acid," vol. 190, no. 2, pp. 578-586, 2009.
- [139] C.-C. Hu and T.-W. J. E. C. Tsou, "Ideal capacitive behavior of hydrous manganese oxide prepared by anodic deposition," vol. 4, no. 2, pp. 105-109, 2002.
- [140] S. Senthilkumar, R. K. Selvan, N. Ponpandian, and J. J. R. A. Melo, "Redox additive aqueous polymer gel electrolyte for an electric double layer capacitor," vol. 2, no. 24, pp. 8937-8940, 2012.
- [141] K.-C. Tsay, L. Zhang, and J. J. E. A. Zhang, "Effects of electrode layer composition/thickness and electrolyte concentration on both specific capacitance and energy density of supercapacitor," vol. 60, pp. 428-436, 2012.
- [142] B. Aljafari and A. J. M. A. Takshi, "Gel electrolyte based supercapacitors with higher capacitances and lower resistances than devices with a liquid electrolyte," vol. 3, no. 22, pp. 1261-1267, 2018.
- [143] C.-Y. Hsu, H.-W. Chen, K.-M. Lee, C.-W. Hu, and K.-C. J. J. o. P. S. Ho, "A dye-sensitized photo-supercapacitor based on PProDOT-Et<sub>2</sub> thick films," vol. 195, no. 18, pp. 6232-6238, 2010.
- [144] W. Guo, X. Xue, S. Wang, C. Lin, and Z. L. J. N. l. Wang, "An integrated power pack of dye-sensitized solar cell and Li battery based on double-sided TiO<sub>2</sub> nanotube arrays," vol. 12, no. 5, pp. 2520-2523, 2012.
- [145] X. Zhang, X. Huang, C. Li, and H. J. A. M. Jiang, "Dye-sensitized solar cell with energy storage function through PVDF/ZnO nanocomposite counter electrode," vol. 25, no. 30, pp. 4093-4096, 2013.
- [146] U. Nithiyantham, A. Ramadoss, and S. J. R. A. Kundu, "Supercapacitor and dye-sensitized solar cell (DSSC) applications of shape-selective TiO<sub>2</sub> nanostructures," vol. 4, no. 67, pp. 35659-35672, 2014.
- [147] S. Safshekan, I. Herraiz-Cardona, D. Cardenas-Morcoso, R. Ojani, M. Haro, and S. J. A. E. L. Gimenez, "Solar Energy Storage by a Heterostructured BiVO<sub>4</sub>-PbO<sub>x</sub> Photocapacitive Device," vol. 2, no. 2, pp. 469-475, 2017.
- [148] S. Sharma, B. Siwach, S. Ghoshal, D. J. R. Mohan, and S. E. Reviews, "Dye sensitized solar cells: From genesis to recent drifts," vol. 70, pp. 529-537, 2017.

- [149] N. Roslan *et al.*, "Dye Sensitized Solar Cell (DSSC) greenhouse shading: New insights for solar radiation manipulation," vol. 92, pp. 171-186, 2018.
- [150] N. S. J. s. Lewis, "Toward cost-effective solar energy use," vol. 315, no. 5813, pp. 798-801, 2007.
- [151] Y. Saito, A. Ogawa, S. Uchida, T. Kubo, and H. J. C. I. Segawa, "Energy-storable dye-sensitized solar cells with interdigitated nafion/polypyrrole–Pt comb-like electrodes," vol. 39, no. 5, pp. 488-489, 2010.
- [152] T. Miyasaka, H. Ina, and M. Ikegami, "Dye-sensitized photocapacitors fabricated with ionic liquid electrolytes for power generation and storage," in *Meeting Abstracts*, 2012, no. 38: The Electrochemical Society, pp. 2864-2864.
- [153] J. Kim *et al.*, "A highly efficient self-power pack system integrating supercapacitors and photovoltaics with an area-saving monolithic architecture," vol. 5, no. 5, pp. 1906-1912, 2017.
- [154] T. N. Murakami, N. Kawashima, and T. J. C. C. Miyasaka, "A high-voltage dye-sensitized photocapacitor of a three-electrode system," no. 26, pp. 3346-3348, 2005.
- [155] P. J. Kulesza *et al.*, "Development of solid-state photo-supercapacitor by coupling dye-sensitized solar cell utilizing conducting polymer charge relay with proton-conducting membrane based electrochemical capacitor," vol. 50, no. 43, pp. 235-244, 2013.
- [156] H. D. Tran, J. M. D'Arcy, Y. Wang, P. J. Beltramo, V. A. Strong, and R. B. J. J. o. M. C. Kaner, "The oxidation of aniline to produce "polyaniline": a process yielding many different nanoscale structures," vol. 21, no. 11, pp. 3534-3550, 2011.
- [157] T. M. El-Agez, S. A. Taya, K. S. Elrefi, and M. S. J. O. a. Abdel-Latif, "Dye-sensitized solar cells using some organic dyes as photosensitizers," vol. 44, no. 2, pp. 345--351, 2014.
- [158] S. Hameed, S. A. Kazmi, N. Ahmad, and W. Khan, "Effect of different dyes on TiO<sub>2</sub> based dye sensitized solar cell," in *2015 Annual IEEE India Conference (INDICON)*, 2015: IEEE, pp. 1-6.
- [159] A. Takshi, T. Tevi, and F. Rahimi, "Organic photovoltaic devices with concurrent solar energy harvesting and charge storage capability," in *Next Generation Technologies for Solar Energy Conversion VI*, 2015, vol. 9562: International Society for Optics and Photonics, p. 95620G.
- [160] A. Takshi, H. Yaghoubi, T. Tevi, and S. J. J. o. P. S. Bakhshi, "Photoactive supercapacitors for solar energy harvesting and storage," vol. 275, pp. 621-626, 2015.
- [161] P. Dong *et al.*, "A flexible solar cell/supercapacitor integrated energy device," vol. 42, pp. 181-186, 2017.
- [162] B. Aljafari, M. K. Ram, and A. Takshi, "Integrated electrochemical energy storage and photovoltaic device with a gel electrolyte," in *Physics, Simulation, and Photonic Engineering of Photovoltaic Devices VIII*, 2019, vol. 10913: International Society for Optics and Photonics, p. 1091318.
- [163] M. A. Chougule, S. G. Pawar, P. R. Godse, R. N. Mulik, S. Sen, and V. B. J. S. N. L. Patil, "Synthesis and characterization of polypyrrole (PPy) thin films," vol. 1, no. 01, p. 6, 2011.
- [164] M. Ram, M. Adami, P. Faraci, and C. J. P. Nicolini, "Physical insight in the in-situ self-assembled films of polypyrrole," vol. 41, no. 20, pp. 7499-7509, 2000.
- [165] J. Li, J. Feng, and W. J. A. S. S. Yan, "Excellent adsorption and desorption characteristics of polypyrrole/TiO<sub>2</sub> composite for Methylene Blue," vol. 279, pp. 400-408, 2013.

- [166] M. Islam, E. Rojas, D. Bergey, A. Johnson, and A. J. N. I. Yodh, "High weight fraction surfactant solubilization of single-wall carbon nanotubes in water," vol. 3, no. 2, pp. 269-273, 2003.
- [167] S. Chu and A. J. n. Majumdar, "Opportunities and challenges for a sustainable energy future," vol. 488, no. 7411, p. 294, 2012.
- [168] A. S. Arico, P. Bruce, B. Scrosati, J.-M. Tarascon, and W. Van Schalkwijk, "Nanostructured materials for advanced energy conversion and storage devices," in *Materials for sustainable energy: a collection of peer-reviewed research and review articles from Nature Publishing Group*: World Scientific, 2011, pp. 148-159.
- [169] M. Graetzel, R. A. Janssen, D. B. Mitzi, and E. H. J. N. Sargent, "Materials interface engineering for solution-processed photovoltaics," vol. 488, no. 7411, p. 304, 2012.
- [170] N. Armaroli and V. J. A. C. I. E. Balzani, "The future of energy supply: challenges and opportunities," vol. 46, no. 1-2, pp. 52-66, 2007.
- [171] W. Zeng, L. Shu, Q. Li, S. Chen, F. Wang, and X. M. J. A. m. Tao, "Fiber-based wearable electronics: a review of materials, fabrication, devices, and applications," vol. 26, no. 31, pp. 5310-5336, 2014.
- [172] K. Sharma, K. Pareek, R. Rohan, and P. Kumar, "Flexible supercapacitor based on three-dimensional cellulose/graphite/polyaniline composite," *International Journal of Energy Research*, vol. 43, no. 1, pp. 604-611, 2019.
- [173] A. Rose, K. G. Prasad, T. Sakthivel, V. Gunasekaran, T. Maiyalagan, and T. Vijayakumar, "Electrochemical analysis of graphene oxide/polyaniline/polyvinyl alcohol composite nanofibers for supercapacitor applications," *Applied Surface Science*, vol. 449, pp. 551-557, 2018.
- [174] J. Stejskal *et al.*, "Polyaniline cryogels supported with poly (vinyl alcohol): soft and conducting," *Macromolecules*, vol. 50, no. 3, pp. 972-978, 2017.
- [175] W. Li, F. Gao, X. Wang, N. Zhang, and M. Ma, "Strong and robust polyaniline-based supramolecular hydrogels for flexible supercapacitors," *Angewandte Chemie International Edition*, vol. 55, no. 32, pp. 9196-9201, 2016.
- [176] H. Huang *et al.*, "Reinforced polyaniline/polyvinyl alcohol conducting hydrogel from a freezing–thawing method as self-supported electrode for supercapacitors," *Journal of materials science*, vol. 51, no. 18, pp. 8728-8736, 2016.
- [177] A.-M. Albu, I. Maior, C. A. Nicolae, and F. L. Bocăneală, "Novel PVA proton conducting membranes doped with polyaniline generated by in-situ polymerization," *Electrochimica Acta*, vol. 211, pp. 911-917, 2016.
- [178] K. Wang *et al.*, "Chemically crosslinked hydrogel film leads to integrated flexible supercapacitors with superior performance," *Advanced materials*, vol. 27, no. 45, pp. 7451-7457, 2015.
- [179] B. C. Nath, B. Gogoi, M. Boruah, M. Khannam, G. A. Ahmed, and S. K. Dolui, "High performance polyvinyl alcohol/multi walled carbon nanotube/polyaniline hydrogel (PVA/MWCNT/PAni) based dye sensitized solar cells," *Electrochimica Acta*, vol. 146, pp. 106-111, 2014.
- [180] D. Patil, J. Shaikh, D. Dalavi, S. Kalagi, and P. Patil, "Chemical synthesis of highly stable PVA/PANI films for supercapacitor application," *Materials Chemistry and Physics*, vol. 128, no. 3, pp. 449-455, 2011.
- [181] M. Deka, A. Nath, and A. Kumar, "Effect of dedoped (insulating) polyaniline nanofibers on the ionic transport and interfacial stability of poly (vinylidene fluoride-



- hexafluoropropylene) based composite polymer electrolyte membranes," *Journal of Membrane Science*, vol. 327, no. 1-2, pp. 188-194, 2009.
- [182] A. Bajpai, J. Bajpai, and S. Soni, "Preparation and characterization of electrically conductive composites of poly (vinyl alcohol)-g-poly (acrylic acid) hydrogels impregnated with polyaniline (PANI)," *Express Polymer Lett*, vol. 2, pp. 26-39, 2008.
- [183] K. S. Ngai, S. Ramesh, K. Ramesh, and J. C. Juan, "A review of polymer electrolytes: fundamental, approaches and applications," *Ionics*, vol. 22, no. 8, pp. 1259-1279, 2016.
- [184] S. B. Aziz, T. J. Woo, M. Kadir, and H. M. Ahmed, "A conceptual review on polymer electrolytes and ion transport models," *Journal of Science: Advanced Materials and Devices*, vol. 3, no. 1, pp. 1-17, 2018.
- [185] Z. Tang *et al.*, "Preparation of PAA-g-CTAB/PANI polymer based gel-electrolyte and the application in quasi-solid-state dye-sensitized solar cells," *Electrochimica acta*, vol. 58, pp. 52-57, 2011.
- [186] V. K. Thakur, G. Ding, J. Ma, P. S. Lee, and X. Lu, "Hybrid materials and polymer electrolytes for electrochromic device applications," *Advanced materials*, vol. 24, no. 30, pp. 4071-4096, 2012.
- [187] M. K. Ram, D. Y. Goswami, A. Takshi, and E. J. A. M. Stefanakos, "A new chromic (TouchChromic) thin film," vol. 121, pp. 325-330, 2016.
- [188] P. Ranka, V. Sethi, and A. Q. Contractor, "Characterizing the oxidation level of polyaniline (PANI) at the interface of PANI/TiO<sub>2</sub> nanoparticles under white light illumination," *Thin Solid Films*, vol. 615, pp. 44-55, 2016.
- [189] Y. Furukawa, F. Ueda, Y. Hyodo, I. Harada, T. Nakajima, and T. J. M. Kawagoe, "Vibrational spectra and structure of polyaniline," vol. 21, no. 5, pp. 1297-1305, 1988.
- [190] C. Bao, Y. Guo, L. Song, and Y. J. J. o. M. C. Hu, "Poly (vinyl alcohol) nanocomposites based on graphene and graphite oxide: a comparative investigation of property and mechanism," vol. 21, no. 36, pp. 13942-13950, 2011.
- [191] A. Salunkhe *et al.*, "Polyvinyl alcohol functionalized cobalt ferrite nanoparticles for biomedical applications," vol. 264, pp. 598-604, 2013.
- [192] I. Y. Prosanov and A. Matvienko, "Study of PVA thermal destruction by means of IR and Raman spectroscopy," *Physics of the Solid State*, vol. 52, no. 10, pp. 2203-2206, 2010.
- [193] J. J. E. o. a. c. a. Coates, theory and instrumentation, "Interpretation of infrared spectra, a practical approach," 2006.
- [194] H. S. Mansur, C. M. Sadahira, A. N. Souza, A. A. J. M. S. Mansur, and E. C, "FTIR spectroscopy characterization of poly (vinyl alcohol) hydrogel with different hydrolysis degree and chemically crosslinked with glutaraldehyde," vol. 28, no. 4, pp. 539-548, 2008.
- [195] J. Tokarský, M. Maixner, P. Peikertová, L. Kulhánková, and J. V. Burda, "The IR and Raman spectra of polyaniline adsorbed on the glass surface; comparison of experimental, empirical force field, and quantum chemical results," *European Polymer Journal*, vol. 57, pp. 47-57, 2014.
- [196] S. Honmote, S. V. Ganachari, R. Bhat, H. Kumar, D. S. Huh, and A. Vankataraman, "Studies on polyaniline-polyvinyl alcohol (PANI-PVA) interpenetrating polymer network (IPN) thin films," *International Journal of Science Research*, vol. 1, no. 2, pp. 102-106, 2012.
- [197] J. Gohil, A. Bhattacharya, and P. Ray, "Studies on the crosslinking of poly (vinyl alcohol)," *Journal of polymer research*, vol. 13, no. 2, pp. 161-169, 2006.

- [198] M.-C. Bernard and A. Hugot-Le Goff, "Raman spectroscopy for the study of polyaniline," *Synthetic metals*, vol. 85, no. 1-3, pp. 1145-1146, 1997.
- [199] Y. Furukawa, F. Ueda, Y. Hyodo, I. Harada, T. Nakajima, and T. Kawagoe, "Vibrational spectra and structure of polyaniline," *Macromolecules*, vol. 21, no. 5, pp. 1297-1305, 1988.
- [200] Y. Furukawa, T. Hara, Y. Hyodo, and I. Harada, "Vibrational spectra of polyaniline and its 15N-and 2H-substituted derivatives in as-polymerized, alkali-treated and reduced states," *Synthetic Metals*, vol. 16, no. 2, pp. 189-198, 1986.
- [201] M. Trchová, Z. Morávková, M. Bláha, and J. Stejskal, "Raman spectroscopy of polyaniline and oligoaniline thin films," *Electrochimica Acta*, vol. 122, pp. 28-38, 2014.
- [202] M. Wu, Y. Li, B. Yao, J. Chen, C. Li, and G. J. J. o. M. C. A. Shi, "A high-performance current collector-free flexible in-plane micro-supercapacitor based on a highly conductive reduced graphene oxide film," vol. 4, no. 41, pp. 16213-16218, 2016.
- [203] F. Alvi *et al.*, "Electrochemical supercapacitors based on graphene-conducting polythiophenes nanocomposite," vol. 35, no. 34, pp. 167-174, 2011.
- [204] F. Alvi, M. K. Ram, P. A. Basnayaka, E. Stefanakos, Y. Goswami, and A. J. E. A. Kumar, "Graphene–polyethylenedioxythiophene conducting polymer nanocomposite based supercapacitor," vol. 56, no. 25, pp. 9406-9412, 2011.
- [205] F. M. Abdelmola *et al.*, "Photoelectrochemical Cell Of Hybrid Regioregular Poly (3-Hexylthiophene-2, 5-Diyl) And Molybdenum Disulfide Film," vol. 24, no. 02, p. 1750026, 2017.
- [206] M. Ahmed *et al.*, "A thin film approach for SiC-derived graphene as an on-chip electrode for supercapacitors," vol. 26, no. 43, p. 434005, 2015.
- [207] J. Gong, K. Sumathy, Q. Qiao, Z. J. R. Zhou, and S. E. Reviews, "Review on dye-sensitized solar cells (DSSCs): Advanced techniques and research trends," vol. 68, pp. 234-246, 2017.
- [208] P. Liu, H. Yang, X. Ai, G. Li, and X. J. E. C. Gao, "A solar rechargeable battery based on polymeric charge storage electrodes," vol. 16, no. 1, pp. 69-72, 2012.
- [209] H. Nagai and H. J. C. c. Segawa, "Energy-storable dye-sensitized solar cell with a polypyrrole electrode," no. 8, pp. 974-975, 2004.
- [210] P. A. Mini, S. V. Nair, K. R. J. P. i. P. R. Subramanian, and Applications, "Design and development of an integrated device consisting of an independent solar cell with electrical storage capacity," vol. 21, no. 5, pp. 1153-1157, 2013.
- [211] M. Yu, W. D. McCulloch, D. R. Beauchamp, Z. Huang, X. Ren, and Y. J. J. o. t. A. C. S. Wu, "Aqueous lithium–iodine solar flow battery for the simultaneous conversion and storage of solar energy," vol. 137, no. 26, pp. 8332-8335, 2015.
- [212] W. Wang, X. Liu, and Z. J. J. o. M. R. Shi, "Mechanisms and influences of electro-brush plating micro-force on coatings performances," vol. 31, no. 15, pp. 2337-2346, 2016.
- [213] B. P. Lechene, R. Clerc, A. C. J. S. E. M. Arias, and S. Cells, "Theoretical analysis and characterization of the energy conversion and storage efficiency of photo-supercapacitors," vol. 172, pp. 202-212, 2017.
- [214] R. Singh *et al.*, "Electrical and structural properties of ionic liquid doped polymer gel electrolyte for dual energy storage devices," vol. 42, no. 21, pp. 14602-14607, 2017.
- [215] F. Rahimi and A. Takshi, "Energy storage capability of the dye sensitized solar cells via utilization of highly porous carbon electrodes," in *Next Generation Technologies for Solar Energy Conversion VII*, 2016, vol. 9937: International Society for Optics and Photonics, p. 99370T.

- [216] F. Rahimi, T. Tevi, and A. Takshi, "Photoelectrochemical reaction in conducting polymers for solar energy harvesting and charge storage," in *Next Generation Technologies for Solar Energy Conversion VII*, 2016, vol. 9937: International Society for Optics and Photonics, p. 99370U.
- [217] J. De Albuquerque, L. Mattoso, R. Faria, J. Masters, and A. J. S. M. MacDiarmid, "Study of the interconversion of polyaniline oxidation states by optical absorption spectroscopy," vol. 146, no. 1, pp. 1-10, 2004.
- [218] E. Song and J.-W. Choi, "Conducting polyaniline nanowire and its applications in chemiresistive sensing," *Nanomaterials*, vol. 3, no. 3, pp. 498-523, 2013.
- [219] A. Mohtasebi, T. Chowdhury, L. H. Hsu, M. C. Biesinger, and P. J. T. J. o. P. C. C. Kruse, "Interfacial charge transfer between phenyl-capped aniline tetramer films and iron oxide surfaces," vol. 120, no. 51, pp. 29248-29263, 2016.
- [220] Q. Tai *et al.*, "In situ prepared transparent polyaniline electrode and its application in bifacial dye-sensitized solar cells," *Acs Nano*, vol. 5, no. 5, pp. 3795-3799, 2011.
- [221] B. Aljafari, F. Khorramshahi, M. K. Ram, and A. Takshi, "Photo-Electric Properties of Polypyrrole Based Gel Electrolyte for Hybrid Photoactive Supercapacitors," *ECS Transactions*, vol. 92, no. 9, pp. 7-14, 2019.
- [222] B. Aljafari, F. Khorramshahi, M. K. Ram, and A. Takshi, "Photo-Electric Properties of Polypyrrole Based Gel Electrolyte for Hybrid Photoactive Supercapacitors," 2019, no. 39: The Electrochemical Society, pp. 1778-1778.

## Appendix A: Copyright and Permissions

The permission below is for the use of Figure 2 in this dissertation.



My Orders   My Library   My Profile   Welcome belqasem@mail.usf.edu   [Log out](#) | [Help](#)

My Orders > Orders > All Orders

### License Details

This Agreement between belqasem aljafari ("You") and John Wiley and Sons ("John Wiley and Sons") consists of your license details and the terms and conditions provided by John Wiley and Sons and Copyright Clearance Center.

[Print](#)   [Copy](#)

License Number	4661921391677
License date	Sep 04, 2019
Licensed Content Publisher	John Wiley and Sons
Licensed Content Publication	AIChE Journal
Licensed Content Title	First-principles modeling for optimal design, operation, and integration of energy conversion and storage systems
Licensed Content Author	Yuriy Y. Smolin, Kenneth K. S. Lau, Masoud Soroush
Licensed Content Date	Dec 23, 2018
Licensed Content Volume	65
Licensed Content Issue	7
Licensed Content Pages	16
Type of Use	Dissertation/Thesis
Requestor type	University/Academic
Format	Electronic
Portion	Figure/table
Number of figures/tables	5
Original Wiley figure/table number(s)	Figure 5
Will you be translating?	No
Title of your thesis / dissertation	Fabrication and Characterization of Electrical Energy Storage and Harvesting Energy Devices Using Gel Electrolytes
Expected completion date	Oct 2019
Expected size (number of pages)	
Requestor Location	belqasem aljafari 4202 E Fowler Ave

Publisher Tax ID	
Customer VAT ID	
Total	<b>0.00 USD</b>

The permission below is for the use of Figure 12 in this dissertation.



My Orders   My Library   My Profile   Welcome belqasem@mail.usf.edu   [Log out](#) | [Help](#)

My Orders > Orders > All Orders

## License Details

This Agreement between belqasem aljafari ("You") and Springer Nature ("Springer Nature") consists of your license details and the terms and conditions provided by Springer Nature and Copyright Clearance Center.

[Print](#)   [Copy](#)

License Number	4661930606214
License date	Sep 04, 2019
Licensed Content Publisher	Springer Nature
Licensed Content Publication	Nature
Licensed Content Title	Photoelectrochemical cells
Licensed Content Author	Michael Grätzel
Licensed Content Date	Nov 15, 2001
Type of Use	Thesis/Dissertation
Requestor type	academic/university or research institute
Format	electronic
Portion	figures/tables/illustrations
Number of figures/tables/illustrations	3
Will you be translating?	no
Circulation/distribution	100 - 199
Author of this Springer Nature content	no
Title	Fabrication and Characterization of Electrical Energy Storage and Harvesting Energy Devices Using Gel Electrolytes
Institution name	University of South Florida
Expected presentation date	Oct 2019
Portions	Figure 3
Requestor Location	belqasem aljafari 4202 E Fowler Ave

Customer VAT ID

Total      **0.00 USD**

The two permissions below are for the use of Figure 22 in this dissertation.



RightsLink®

[My Orders](#)

[My Library](#)

[My Profile](#)

Welcome belqasem@mail.usf.edu [Log out](#) | [Help](#)

[My Orders](#) > [Orders](#) > [All Orders](#)

## License Details

This Agreement between belqasem aljafari ("You") and Elsevier ("Elsevier") consists of your license details and the terms and conditions provided by Elsevier and Copyright Clearance Center.

[Print](#) [Copy](#)

License Number	4661931357390
License date	Sep 04, 2019
Licensed Content Publisher	Elsevier
Licensed Content Publication	Electrochimica Acta
Licensed Content Title	Reflections on the history of electrochemical impedance spectroscopy
Licensed Content Author	Digby D. Macdonald
Licensed Content Date	Jan 20, 2006
Licensed Content Volume	51
Licensed Content Issue	8-9
Licensed Content Pages	13
Type of Use	reuse in a thesis/dissertation
Portion	figures/tables/illustrations
Number of figures/tables/illustrations	6
Format	electronic
Are you the author of this Elsevier article?	No
Will you be translating?	No
Original figure numbers	Figure 6 (a and b)
Title of your thesis/dissertation	Fabrication and Characterization of Electrical Energy Storage and Harvesting Energy Devices Using Gel Electrolytes
Publisher of new work	University of South Florida
Expected completion date	Oct 2019
Requestor Location	belqasem aljafari 4202 E Fowler Ave

Publisher Tax ID

Customer VAT ID

Total

**0.00 USD**

Gmail Search mail 6 of 4,484

Compose

**Inbox**

- Starred
- Snoozed
- Sent
- Drafts
- More

**no-reply@rsc.org**  
 Name: BELDAISEN ALJAFARI Address: 4202 E Fowler Ave, Tampa, FL 33620 Tel: 8155551949 Fax: Email: belqasem@mail.usf.edu I am preparing the following work for  
 Oct 20, 2019, 11:40 PM (2 days ago)

**CONTRACTS-COPYRIGHT (shared)**  
 Many thanks for sending the permissions request below. Please send the details of the publication this request is for: Article/Chapter Title - Journal/Book Title  
 Oct 21, 2019, 4:29 AM (2 days ago)

**Belqasem Aljafari** <belqasem@mail.usf.edu>  
 to CONTRACTS-COPYRIGHT +  
 Oct 21, 2019, 9:59 AM (2 days ago)

Greeting,

I need permission for [Eq. 1 Similia Ranges equivalent circuit for an electrochemical cell](#), in the paper below

Article/Chapter Title: Electrochemical impedance spectroscopy: an overview of bioanalytical applications  
 Journal/Book Title: Analytical Methods  
 Editor/Author(s): Edward P. Randvir and Craig E. Banks  
 Publisher: Royal Society of Chemistry

Regards,  
 ...

**CONTRACTS-COPYRIGHT (shared)**  
 Dear Belqasem, We would need the details of the publication this is for (as opposed to the RSC publication this is from). Is this for a thesis or a journal? If  
 Oct 22, 2019, 6:08 AM (1 day ago)

**Belqasem Aljafari**  
 Greeting, Sorry for the misunderstanding. This is going to be published in a dissertation. I would like to reproduce the mentioned Figure in the previous email  
 Oct 22, 2019, 11:07 AM (23 hours ago)

**CONTRACTS-COPYRIGHT (shared)** <Contracts-Copyright@rsc.org>  
 to me +  
 4:43 AM (5 hours ago)

Many thanks for sending the permissions request below. The Royal Society of Chemistry hereby grants permission for the use of the material specified below in your thesis.

Please note that if the material specified below or any part of it appears with credit or acknowledgement to a third party then you must also secure permission from that third party before reproducing that material.

Please ensure that the published article carries a credit to The Royal Society of Chemistry in the following format:

[Original citation] – Reproduced by permission of The Royal Society of Chemistry

and that any electronic version of the work includes a hyperlink to the article on the Royal Society of Chemistry website.

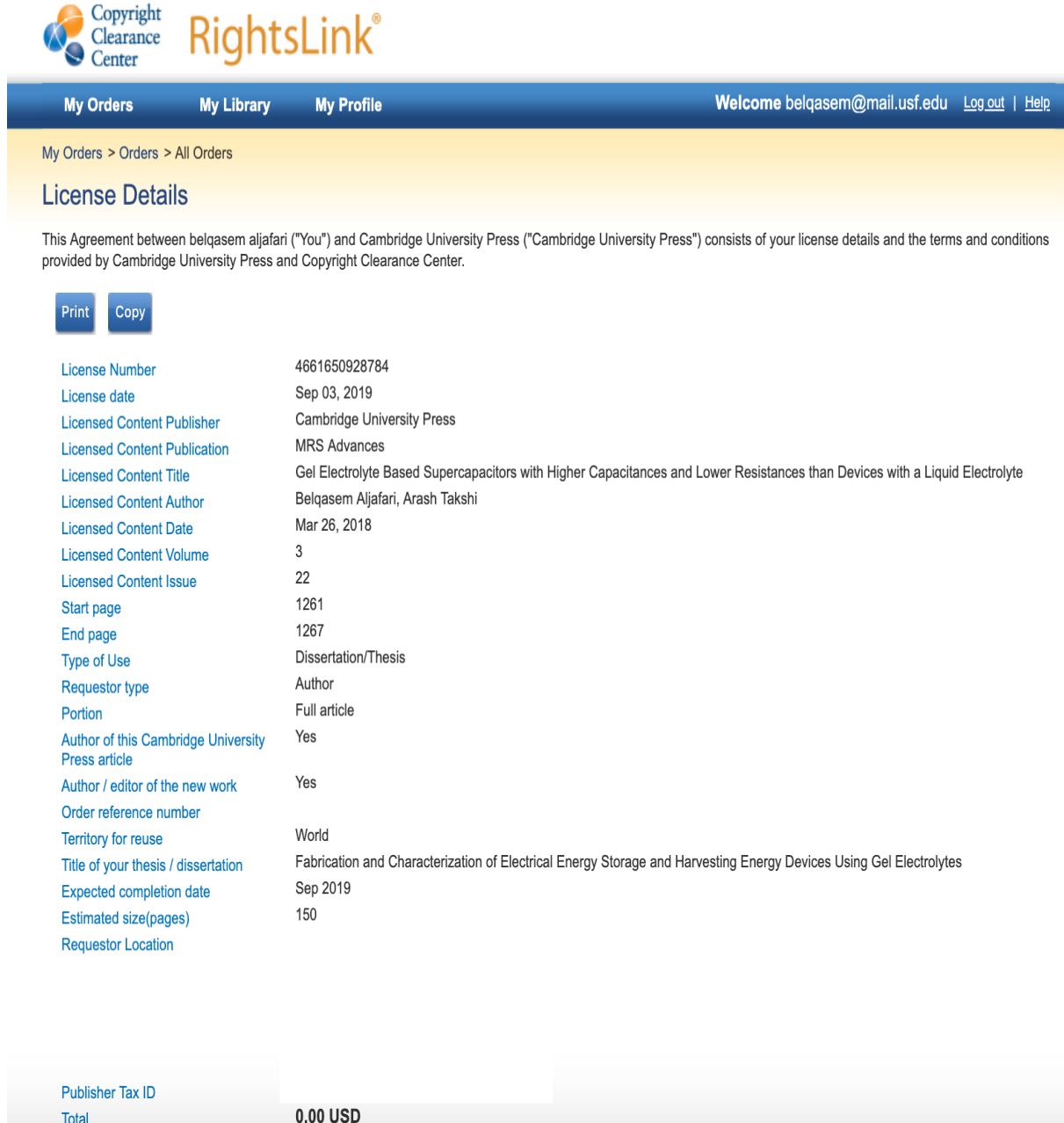
...

Best wishes,

**Chloe Szabrat**  
 Contracts and Copyright Executive  
 Royal Society of Chemistry  
 Thomas Graham House  
 Science Park, Milton Road  
 Cambridge, CB4 0WF, UK  
 Tel: +44 (0) 1223 438329  
[www.rsc.org](http://www.rsc.org)

No recent drafts  
[Start a new one](#)

The permission below is for the use of the published paper entitled “Gel Electrolyte Based Supercapacitors with Higher Capacitances and Lower Resistances than Devices with a Liquid Electrolyte” in chapter 4 of this dissertation.




The screenshot shows the RightsLink interface for a license. At the top, there are navigation links for 'My Orders', 'My Library', and 'My Profile'. A welcome message for 'belqasem@mail.usf.edu' is displayed. The main content area is titled 'License Details' and includes a breadcrumb trail: 'My Orders > Orders > All Orders'. Below the title, there is a brief description of the agreement and two buttons: 'Print' and 'Copy'. The license details are presented in a table format:

License Number	4661650928784
License date	Sep 03, 2019
Licensed Content Publisher	Cambridge University Press
Licensed Content Publication	MRS Advances
Licensed Content Title	Gel Electrolyte Based Supercapacitors with Higher Capacitances and Lower Resistances than Devices with a Liquid Electrolyte
Licensed Content Author	Belqasem Aljafari, Arash Takshi
Licensed Content Date	Mar 26, 2018
Licensed Content Volume	3
Licensed Content Issue	22
Start page	1261
End page	1267
Type of Use	Dissertation/Thesis
Requestor type	Author
Portion	Full article
Author of this Cambridge University Press article	Yes
Author / editor of the new work	Yes
Order reference number	
Territory for reuse	World
Title of your thesis / dissertation	Fabrication and Characterization of Electrical Energy Storage and Harvesting Energy Devices Using Gel Electrolytes
Expected completion date	Sep 2019
Estimated size(pages)	150
Requestor Location	

At the bottom of the page, there is a section for 'Publisher Tax ID' and a 'Total' amount of '0.00 USD'.



The permission below is for the use of the published paper entitled “Polyvinyl alcohol-acid redox active gel electrolytes for electrical double-layer capacitor devices” in chapter 5 of this dissertation.



My Orders   My Library   My Profile   Welcome belqasem@mail.usf.edu   [Log out](#) | [Help](#)

My Orders > Orders > All Orders

### License Details

This Agreement between belqasem aljafari ("You") and Springer Nature ("Springer Nature") consists of your license details and the terms and conditions provided by Springer Nature and Copyright Clearance Center.

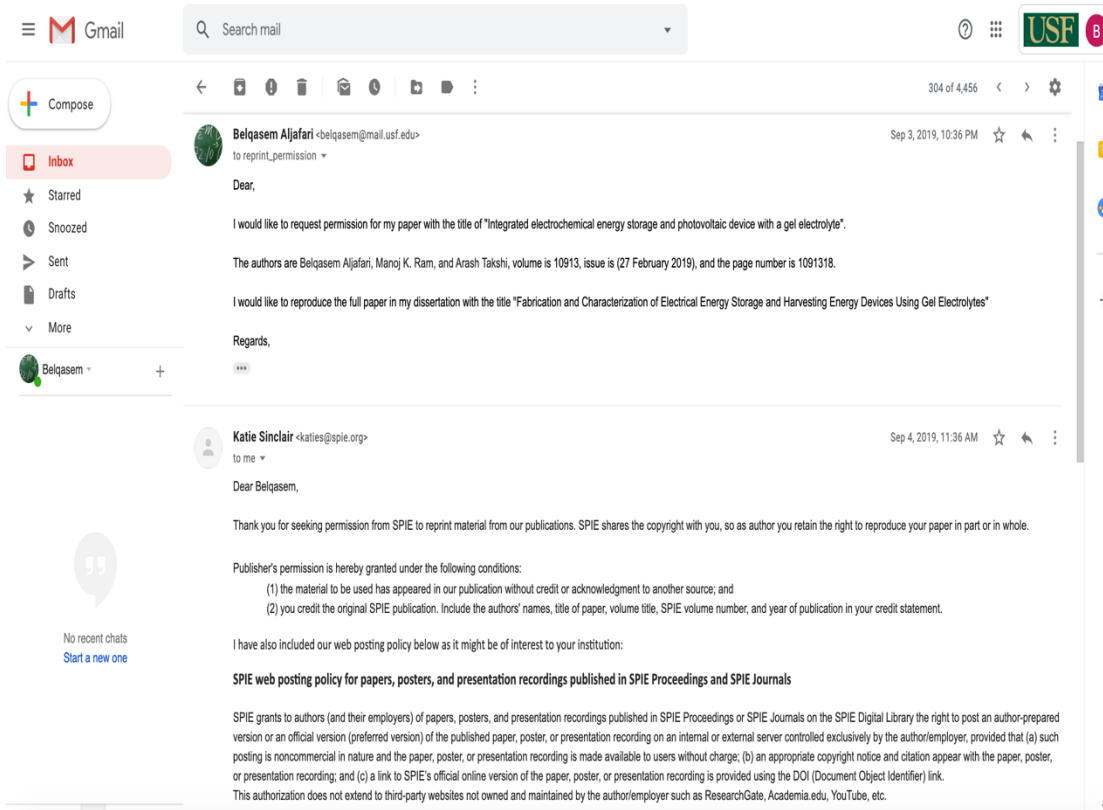
[Print](#)   [Copy](#)

License Number	4661690468909
License date	Sep 03, 2019
Licensed Content Publisher	Springer Nature
Licensed Content Publication	Journal of Solid State Electrochemistry
Licensed Content Title	Polyvinyl alcohol-acid redox active gel electrolytes for electrical double-layer capacitor devices
Licensed Content Author	Belqasem Aljafari, Turki Alamro, Manoj K. Ram et al
Licensed Content Date	Jan 1, 2018
Licensed Content Volume	23
Licensed Content Issue	1
Type of Use	Thesis/Dissertation
Requestor type	academic/university or research institute
Format	print and electronic
Portion	full article/chapter
Will you be translating?	no
Circulation/distribution	100 - 199
Author of this Springer Nature content	yes
Title	Fabrication and Characterization of Electrical Energy Storage and Harvesting Energy Devices Using Gel Electrolytes
Institution name	University of South Florida
Expected presentation date	Oct 2019
Requestor Location	4202 E Fowler Ave

Customer VAT ID	-----
Total	<b>0.00 USD</b>

The permission below is for the use of the published paper entitled “Integrated electrochemical energy storage and photovoltaic device with a gel electrolyte” in chapter 6 of this dissertation.



The permission below is for the use of the published paper entitled “Photo-Electric Properties of Polypyrrole Based Gel Electrolyte for Hybrid Photoactive Supercapacitors” in chapter 5 of this dissertation.



### Electrochemical Society, Inc. - License Terms and Conditions

This is a License Agreement between Belqasem/University of South Florida ("You") and Electrochemical Society, Inc. ("Publisher") provided by Copyright Clearance Center ("CCC"). The license consists of your order details, the terms and conditions provided by Electrochemical Society, Inc., and the CCC terms and conditions.

All payments must be made in full to CCC.

Order Date	23-Oct-2019	Type of Use	Republish in a thesis/dissertation
Order license ID	1000255-1	Publisher	ELECTROCHEMICAL SOCIETY
ISSN	1938-5862	Portion	Chapter/article

#### LICENSED CONTENT

Publication Title	ECS transactions	Country	United States of America
Author/Editor	Electrochemical Society.	Rightsholder	Electrochemical Society, Inc.
Date	01/01/2005	Publication Type	Monographic Series
Language	English		

#### REQUEST DETAILS

Portion Type	Chapter/article	Rights Requested	Main product
Page range(s)	7-14	Distribution	Worldwide
Total number of pages	8	Translation	Original language of publication
Format (select all that apply)	Print, Electronic	Copies for the disabled?	No
Who will republish the content?	Academic institution	Minor editing privileges?	No
Duration of Use	Life of current and all future editions	Incidental promotional use?	No
Lifetime Unit Quantity	More than 2,000,000	Currency	USD

#### NEW WORK DETAILS

Title	Photo-Electric Properties of Polypyrrole Based Gel Electrolyte for Hybrid Photoactive Supercapacitors	Institution name	University of South Florida
Instructor name	Belqasem	Expected presentation date	2019-10-30

#### ADDITIONAL DETAILS

Order reference number	N/A	The requesting person / organization to appear on the license	Belqasem/University of South Florida
------------------------	-----	---	--------------------------------------

#### REUSE CONTENT DETAILS

Title, description or numeric reference of the portion(s)	Fabrication and Characterization of Electrical Energy Storage and Harvesting Energy Devices Using Gel Electrolytes	Title of the article/chapter the portion is from	N/A
Editor of portion(s)	N/A	Author of portion(s)	Electrochemical Society.
Volume of serial or monograph	92	Issue, if republishing an article from a serial	9
Page or page range of portion	7-14	Publication date of portion	2019-10-20

#### CCC Republication Terms and Conditions

1. Description of Service; Defined Terms. This Republication License enables the User to obtain licenses for republishing of one or more copyrighted works as described in detail on the relevant Order Confirmation (the "Work(s)"). Copyright Clearance Center, Inc. ("CCC") grants licenses through the Service on behalf of the rightsholder identified on the Order Confirmation (the "Rightsholder"). "Republishing", as used herein, generally means the inclusion of a Work, in whole or in part, in a new work or works, also as described on the Order Confirmation. "User", as used herein, means the person or entity making such republishing.

## Appendix B: Supplementary Materials for Chapter 5

### Supplementary Material

#### Polyvinyl Alcohol-Acid Redox Active Gel Electrolytes for Electrical Double Layer Capacitor Devices

*Belqasem Aliafari<sup>a</sup>, Turki Alamro<sup>b</sup>, Manoj K. Ram<sup>c</sup> and Arash Takshi<sup>a,d</sup>*

<sup>a</sup>Department of Electrical Engineering, University of South Florida, Tampa, FL, USA

<sup>b</sup>Department of Mechanical Engineering, University of South Florida, Tampa, FL, USA

<sup>c</sup>PolyMaterials APP LLC, Tampa, FL, USA

<sup>d</sup>Clean Energy Research Center, University of South Florida, Tampa, FL, USA

The cyclability and stability of the devices-based gel electrolyte was carried out by shown the consistency of the capacitance results during 1000 cycles as seen in Table S1 and S2. The supercapacitor device based H<sub>2</sub>SO<sub>4</sub>-PVA and H<sub>3</sub>PO<sub>4</sub>-PVA as shown in Figure S6 and S7 showed excellent stability over 1000 cycles with no performance degradation [1,2]. The capacitance,  $C$ , value of each device can be calculated from the CV measurements using:

$$C = \frac{\Delta I}{2 \times v}$$

**Table S1: Capacitance values of H<sub>2</sub>SO<sub>4</sub>-PVA from cycle 1 to 1000.**

Electrolyte	Cycle	Difference Current (mA)	Capacitance (mF)	C/C <sub>0</sub>
H <sub>2</sub> SO <sub>4</sub> -PVA	1	1.9695	39.39	1
	50	1.975	39.5	1.002792587
	100	1.957	39.14	0.993653211
	150	1.944	38.88	0.987052551
	200	1.9345	38.69	0.982289921
	250	1.93	38.6	0.979944148
	300	1.9275	38.55	0.978674790
	350	1.9245	38.49	0.977151561
	400	1.9235	38.47	0.976648504
	450	1.9265	38.53	0.978167047
	500	1.9265	38.53	0.978167047
	550	1.9265	38.53	0.978167047
	600	1.9265	38.53	0.978167047
	650	1.9265	38.53	0.978167047
	700	1.9265	38.53	0.978167047
	750	1.9265	38.53	0.978167047
	800	1.9265	38.53	0.978167047
	850	1.9235	38.47	0.976643818
	900	1.9235	38.47	0.976643818
	950	1.9235	38.47	0.976643818
1000	1.9235	38.47	0.976643818	

**Table S2: Capacitance values of H<sub>3</sub>PO<sub>4</sub>-PVA from cycle 1 to 1000.**

Electrolyte	Cycle	Average Current (mA)	Capacitance (mF)	$C/C_0$
H <sub>3</sub> PO <sub>4</sub> -PVA	1	1.522	30.44	1
	50	1.497	29.94	0.983574244
	100	1.497	29.94	0.983574244
	150	1.493	29.86	0.980946123
	200	1.4885	29.77	0.977989487
	250	1.4845	29.69	0.975361366
	300	1.481	29.62	0.973061760
	350	1.478	29.56	0.971090670
	400	1.4755	29.51	0.969448094
	450	1.4755	29.51	0.969448094
	500	1.4755	29.51	0.969448094
	550	1.472	29.44	0.967148488
	600	1.472	29.44	0.967148488
	650	1.47	29.40	0.965834428
	700	1.463	29.26	0.961235216
	750	1.4605	29.21	0.959592641
	800	1.458	29.16	0.957950065
	850	1.458	29.16	0.957950065
	900	1.456	29.12	0.956636005
	950	1.4525	29.05	0.954336399
1000	1.4515	29.03	0.953679369	

**Table S3: Capacitance values of H<sub>2</sub>SO<sub>4</sub>-PVA and H<sub>3</sub>PO<sub>4</sub>-PVA electrolytes with different radius.**

Electrolyte	Radius (mm)	Curvature (1/Radius)	Capacitance (mF)
H <sub>2</sub> SO <sub>4</sub> -PVA	∞	0	39.39
	14.5	0.166666	32.06
	8	0.125	26.27
	6	0.0689655	32.48
H <sub>3</sub> PO <sub>4</sub> -PVA	∞	0	30.44
	14.5	0.166666	31.54
	8	0.125	29.82
	6	0.0689655	32

**Table S4: Capacitance values of H<sub>2</sub>SO<sub>4</sub>-PVA and H<sub>3</sub>PO<sub>4</sub>-PVA electrolytes with the same radius for reverse.**

Electrolyte	Radius (mm)	Curvature (1/Radius)	Capacitance (mF)
H <sub>2</sub> SO <sub>4</sub> -PVA	6	0.0689655	27.24
	8	0.125	30.65
	14.5	0.166666	30.54
	∞	0	38.56
H <sub>3</sub> PO <sub>4</sub> -PVA	6	0.0689655	31.58
	8	0.125	29.65
	14.5	0.166666	31.5
	∞	0	29.06

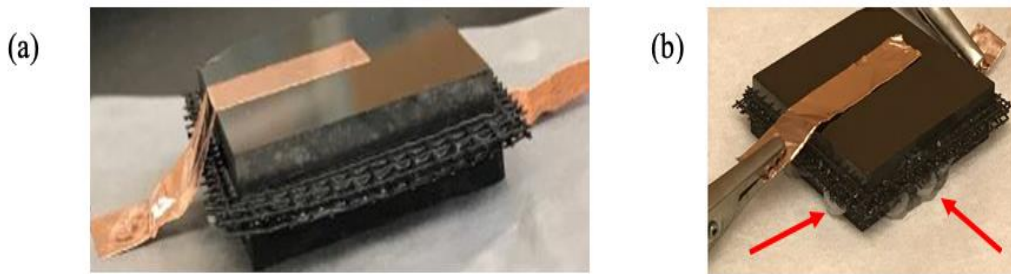


Fig. S1: (a) Fabrication of supercapacitor device based on Glassy Carbon (GC) electrode with the gel electrolyte. (b) Bubbles were observed when the device was charged above 1.0V.

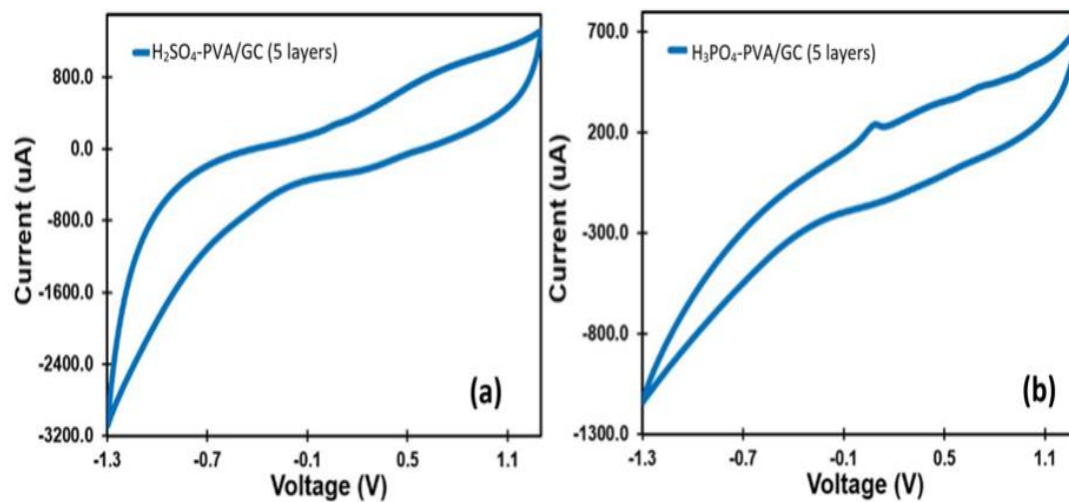


Fig. S2: Cyclic voltammetry of the glassy carbon-based supercapacitors with five layers of the spacer made from (a) H<sub>2</sub>SO<sub>4</sub>-PVA and (b) H<sub>3</sub>PO<sub>4</sub>-PVA gels. A notable feature in the CV results is the asymmetric I-V characteristics. This can be due to non-uniform distribution of the charge inside the gels after the first cycle of charging. The large anodic current can be due to the bubble release, which is most likely because of the water hydrolysis.



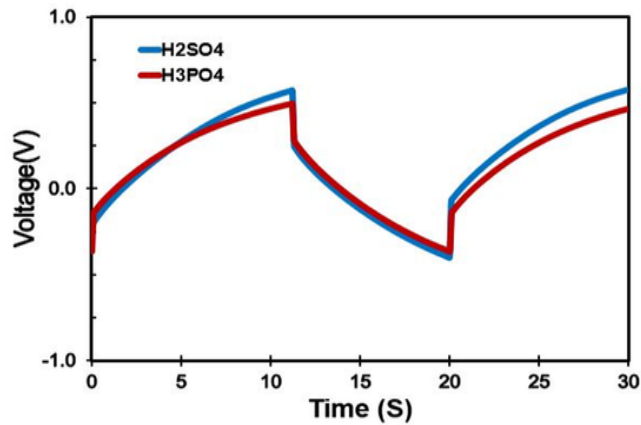


Fig. S3: Constant current charge-discharge of CNT-based supercapacitors with  $\text{H}_2\text{SO}_4$  and  $\text{H}_3\text{PO}_4$  acid electrolyte.

The ESR values were found to be  $161 \Omega$  and  $106 \Omega$  for the CNT based devices with the sulfuric and phosphoric based liquid electrolytes, respectively

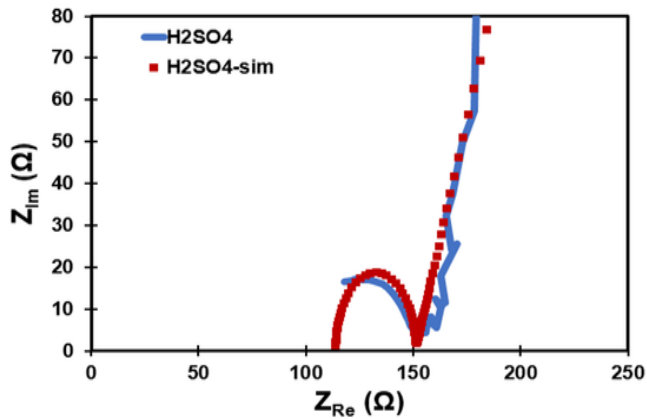


Fig. S4: Nyquist impedance of CNT-based supercapacitors with  $\text{H}_2\text{SO}_4$  electrolyte and its simulation result.

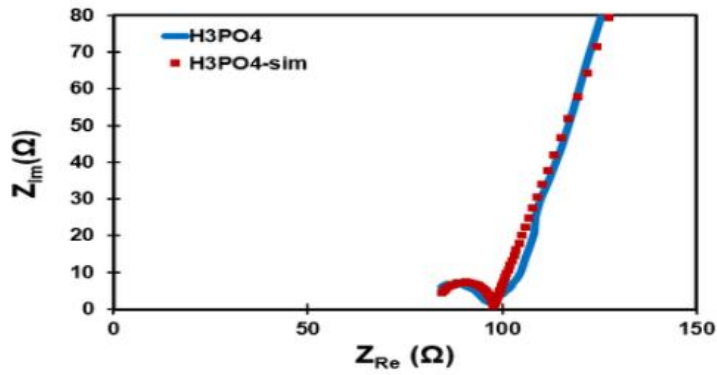


Fig. S5: Nyquist impedance of CNT-based supercapacitors with H<sub>3</sub>PO<sub>4</sub> electrolyte and its simulation result.

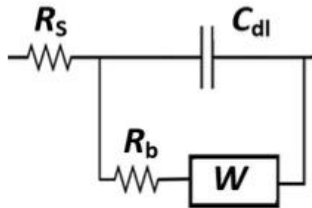


Fig. S6: Electrical equivalent circuit model.

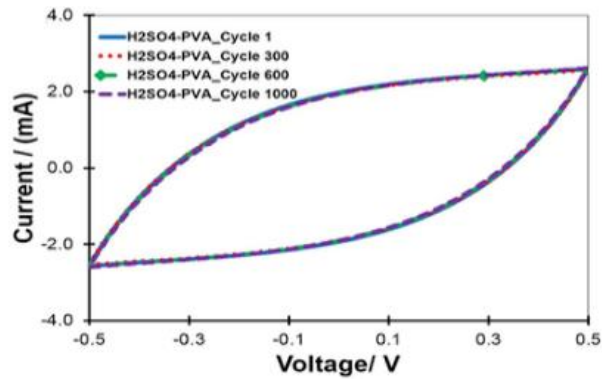


Fig. S7: Cyclic voltammetry of the supercapacitors based on H<sub>2</sub>SO<sub>4</sub>-PVA for cycle 1, 300, 600, and 1000.

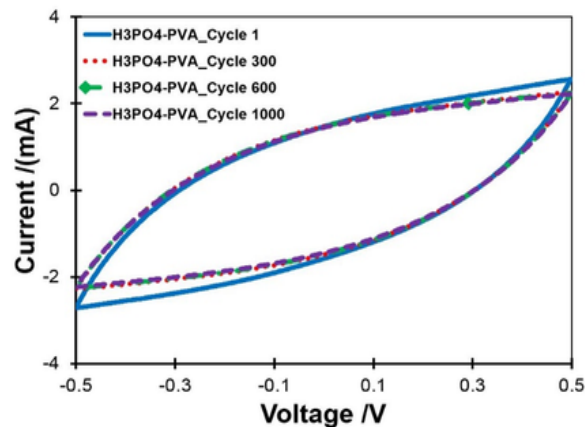


Fig. S8: Cyclic voltammetry of the supercapacitors based on H<sub>3</sub>PO<sub>4</sub>-PVA for cycle 1, 300, 600, and 1000.

Cyclic voltammetry was carried out to observe the stability and mechanical strength for a supercapacitors-based gel electrolyte under different bending conditions. The results showed that there were no significant change in the capacitance values as shown in Table 5 and 6 [3].

#### References:

1. Ma G, Dong M, Sun K, Feng E, Peng H, Lei Z (2015) A redox mediator doped gel polymer as an electrolyte and separator for a high performance solid state supercapacitor. *J. Mater. Chem. A* 3 (7):4035-4041
2. Chen Q, Li X, Zang X, Cao Y, He Y, Li P, Wang K, Wei J, Wu D, Zhu H (2014) Effect of different gel electrolytes on graphene-based solid-state supercapacitors. *RSC Adv.* 4 (68):36253-36256
3. Nam I, Park S, Kim G-P, Park J, Yi J (2013) Transparent and ultra-bendable all-solid-state supercapacitors without percolation problems. *Chem. Sci.* 4 (4):1663-1667

## Appendix C: Supplementary Information for Chapter 8

### A Polyaniline-Based Redox-Active Composite Gel Electrolyte with Photo-Electric and Electrochromic Properties

Belqasem Aljafari<sup>a</sup>, Sharan Kumar Indrakar<sup>a</sup>, Manoj K. Ram<sup>b</sup>, Prasanta Kumar Biswas<sup>a,c</sup>, Elias Stefanakos<sup>a,d</sup>, Arash Takshi<sup>a,d\*</sup>

<sup>a</sup> Department of Electrical Engineering, University of South Florida, Tampa FL 33620, USA

<sup>b</sup> PolyMaterials APP LLC, Tampa, FL 33620, USA

<sup>c</sup> Department of Chemistry, Barasat College (West Bengal State University affiliation), Kolkata 700126, India

<sup>d</sup> Clean Energy Research Center, University of South Florida, Tampa, FL 33620, USA

**Corresponding author\*:** atakshi@usf.edu (Arash Takshi)

[Video 1. The electrochemical device under 0.0 V and 2.0 V bias.](#)

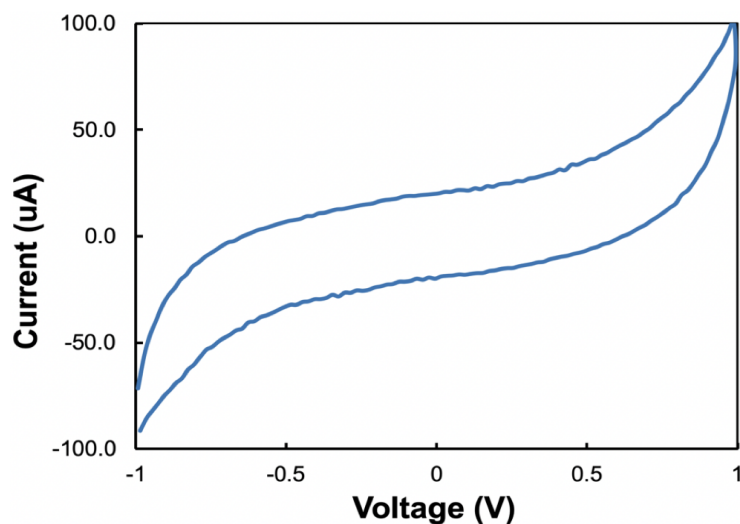


Figure S1. CV result of supercapacitor with PVA gel without conducting polymer electrolyte-based GC electrodes.

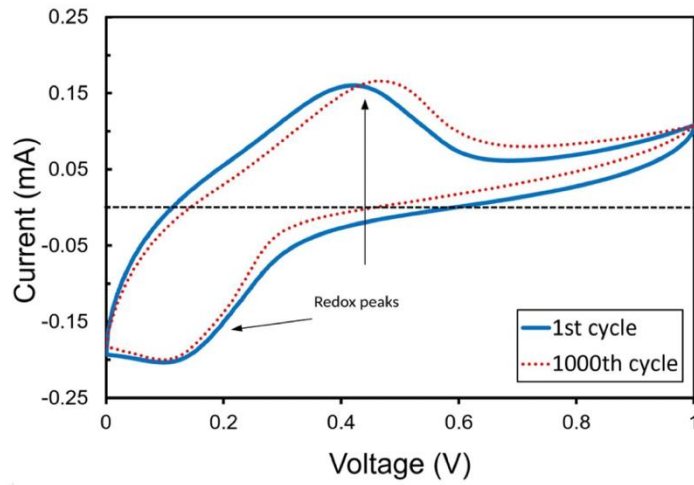


Figure S2. 1000 cycles of the PANI based composite gel electrolyte in the absence of any sealing in the CV.

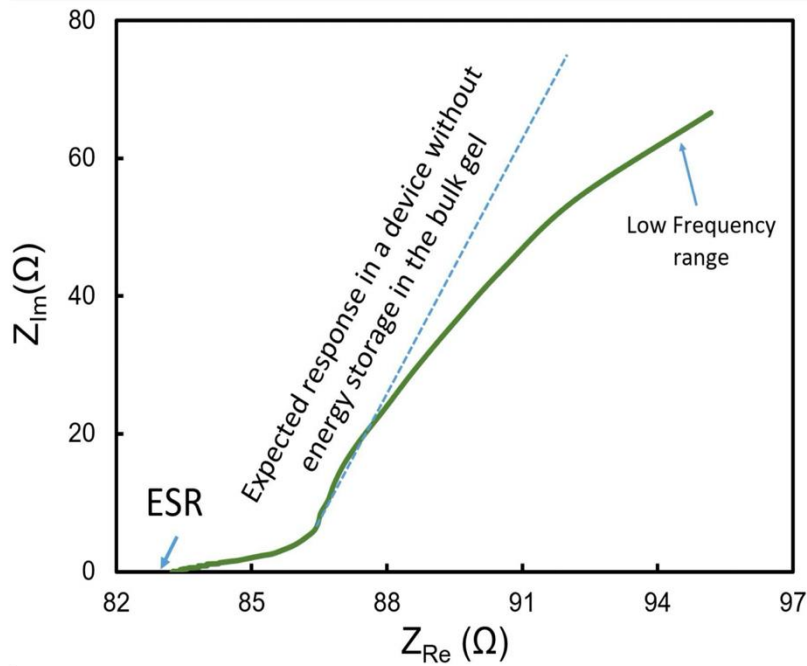


Figure S3. Nyquist impedance result of supercapacitor with CNT based porous electrodes and a thin layer of PANI composite gel electrolyte.

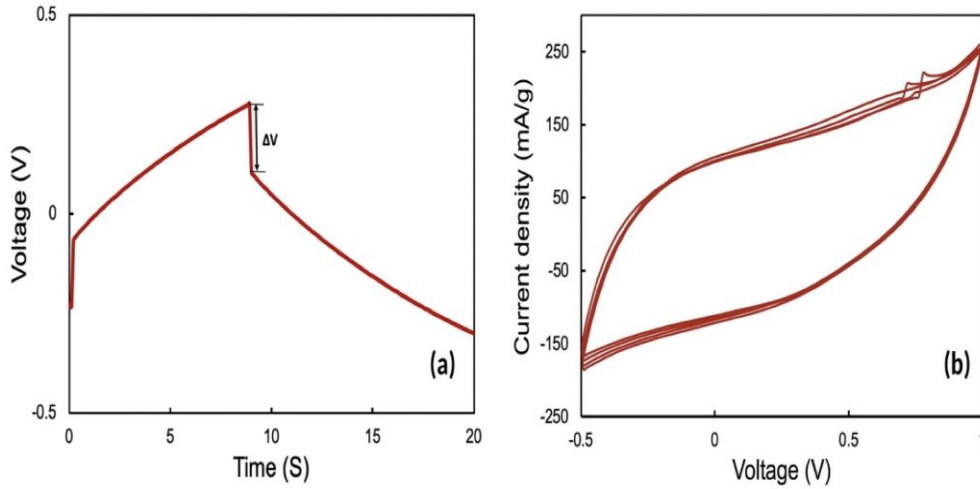


Figure S4. (a) Voltage versus time in response to  $\pm 1$  mA current pulses (galvanostatic experiment) for the supercapacitor device with porous carbon electrodes and the composite gel electrolyte.  $\Delta V$  at the transition suggests equivalent series resistance (ESR) of  $\sim 83 \Omega$ . (b) CV results of the supercapacitor device.

Multiple cycles show the repeatability of the results. Specific capacitance,  $C_s$ , of the device was calculated from:

$$C_s = \frac{\int_{T_1}^{T_2} i(t) dt}{(E_2 - E_1) \times m \times v}$$

where  $m$  is the mass of CNT in the electrodes,  $v$  is the scan rate, and  $\int_{T_1}^{T_2} i(t) dt$  is the integral of the current during the voltage scan from  $E_1$  to  $E_2$  corresponding to the starting time  $T_1$  and end time of  $T_2$  in either scanning up or down the voltage.

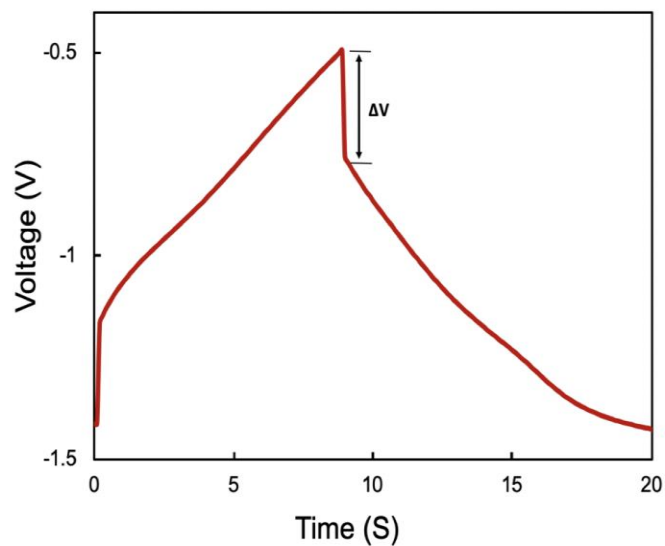


Figure S5. Galvanostatic experiment result for the hybrid photoactive supercapacitor.  $\pm 1$  mA current pulses were applied. ESR of the cell were estimated to be  $\sim 120 \Omega$ .

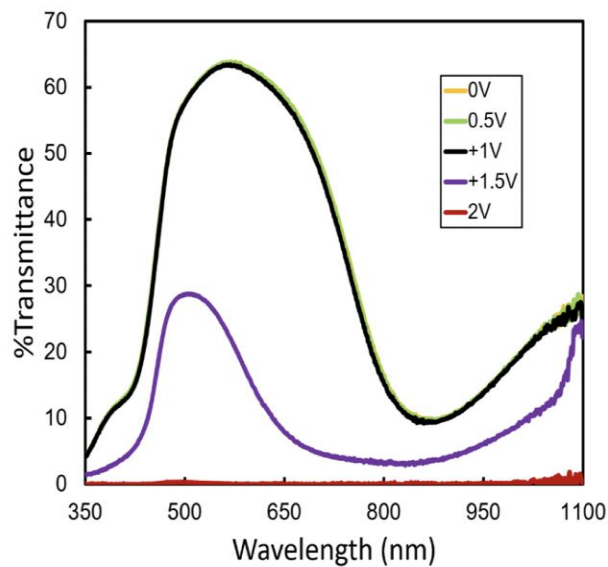


Figure S6. Transmittance spectrum for the electrochromic device at different biasing voltages.

### **About the Author**

Belqasem Aljafari received his B.Sc. in Electrical Engineering in 2011 from Umm Al Qura University. In 2012, he joined Najran University as a teacher assistant in the Electrical Engineering Department. He got a full scholarship to complete his studies from Najran University, and he earned his M.Sc. in Electrical Engineering in 2016 from Northern Illinois University. He began his doctoral studies in Electrical Engineering at the University of South Florida (USF) in 2016 and started working at the Bio-Organic Lab under the guidance of Dr. Arash Takshi. He worked on several research activities on making electrochemical devices such as supercapacitors and DSSCs based on gel electrolytes. Belqasem has received an award from USF by choosing him as the winner of the 9th graduate student research symposium in 2017 at USF. He has been selected by the USF to participate in Statewide Graduate Student Research Symposium.